

# **STABILITY AND CONTROL CHARACTERISTICS OF MODEL HELICOPTERS**

Jonathan Gerhardus Visagie



Thesis presented in partial fulfilment of the requirements for the degree of Master of  
Mechanical Engineering at the University of Stellenbosch.

**Supervisor:** Dr. Dirk Pienaar

**December 2004**

## **Declaration**

I, Jonathan Gerhardus Visagie, the undersigned, hereby declare that the work contained in this thesis is my own original work and has not previously, in entirety or in part, been submitted at any university for a degree.

18 November 2004



## SUMMARY

A need exists for the development of an unmanned rotorcraft capable of autonomous flight, as would be required for the survey of high voltage electricity supply lines. A program was initiated at the University of Stellenbosch in December 2002 in order to develop such an aircraft.

The first goal of this thesis was the development of software that could calculate the stability and control derivatives of a model helicopter. These derivatives could then be used in the formulation of an appropriate helicopter control strategy. The second goal of the thesis was an investigation of the stability and control characteristics of model helicopters.

The trim settings of the helicopter were required in the calculation of the stability and control derivatives. A computer program was developed to determine the trim settings of a helicopter in forward flight. Another program was developed to calculate the stability and control derivatives, using the results of the trim analysis.

The trim analysis was based on the assumption of negligible coupling between the longitudinal and lateral modes of motion. The method proposed by Bramwell (1976) was used to perform the trim analysis. The stability and control derivatives were calculated by obtaining the trim settings from the trim analysis. These derivatives were then used to solve the roots of the characteristic equations of the longitudinal and lateral modes of motion. The stability of the helicopters were investigated firstly by examining the stability derivatives and secondly through root-loci analyses.

The most important results were the following:

- The root-loci analyses indicated that a helicopter without a horizontal stabiliser suffered from instability of the phugoid mode. It was also found that the short-period motion of these helicopters was heavily damped. Fitting a horizontal stabiliser to these helicopters caused the phugoid motion to become stable even at low speeds. This was achieved at the cost of a reduction in short-period motion damping.
- The periods of the lateral and longitudinal motions were smaller than those found on full-scale helicopters. This was attributed to the small mass and inertia properties of the model helicopters.

- An increase in speed is generally accompanied by an increase in the stability of the helicopters. This could be attributed to the effective operation of the tail surfaces at higher speeds.
- The axial climbing speed of a helicopter is influenced by the rotor speed. A low rotor speed allows higher climbing velocities at a given power setting. This was due to lower induced power losses at low rotor speed, assuming that no blade stall occurs.
- The rotor speed does not influence the incremental amount of power ( $\Delta P_c$ ) required to achieve a certain climbing velocity, due to the fact that the profile power losses are constant for a certain rotor speed.
- The simplified horseshoe-vortex theory can be used to analyse the downwash angle at the horizontal stabiliser if the helicopter is in high-speed forward flight.



## OPSOMMING

Daar is tans 'n vraag na die ontwikkeling van onbemande rotor-vlerk vliegtuie wat die vermoë beskik om hulself te beheer. Hierdie tipe vliegtuie sal gebruik word om byvoorbeeld hoë-spannings elektrisiteits-verskaffingsdrade na te gaan. 'n Program is in Desember 2002 by die Universiteit van Stellenbosch begin om sulke vliegtuie te ontwikkel.

Die eerste doel van hierdie tesis was om sagteware te ontwikkel wat die stabiliteit- en beheerafgeleides van 'n model helikopter kon bereken. Hierdie afgeleides kan dan gebruik word om 'n gepaste helikopter beheerstrategie saam te stel. Die tweede doel van die tesis was om die stabiliteit- en beheerseienskappe van model helikopters te ondersoek.

Die berekening van die stabiliteit- en beheerafgeleides van die helikopter berus op die beheerinsette benodig om die helikopter in ewewig te hou (*trim*). 'n Rekenaarprogram is ontwikkel om hierdie beheerinsette vir 'n helikopter in voorwaartse vlug te bereken. 'n Ander program is ontwikkel om die stabiliteit- en beheerafgeleides te bereken met behulp van die ewewig beheerinsette.

Die analise van die helikopter in ewewig berus op die aanname dat die grootte van die koppeling tussen die longitudinale en laterale bewegingsmodusse weglaatbaar klein is. Die beheerinsette van die helikopter in ewewig tydens voorwaartse vlug is bereken deur van Bramwell (1976) se metode te gebruik. Die stabiliteit- en beheerafgeleides is bereken deur van hierdie beheerinsette gebruik te maak. Die afgeleides is gebruik om die wortels van die karakteristieke vergelykings van die longitudinale en laterale bewegingsmodusse te bereken. Die stabiliteit van die helikopters is eerstens beoordeel deur die stabiliteitsafgeleides te ondersoek en tweedens deur middel van 'n wortel-lokus analise.

Die belangrikste resultate is as volg:

- Die wortel-lokus analise toon dat 'n helikopter sonder 'n horisontale stabiliseerder *phugoid*-onstabiliteit (langperiode onstabiliteit) het. Die kort-periode beweging van hierdie helikopters het verder groot hoeveelhede demping aangetoon. Die *phugoid*-beweging kon selfs teen lae snelhede gestabiliseer word deur 'n horisontale stabiliseerder aan te heg. Hierdie stabiliteit is egter bereik ten koste van die demping van die kort-periode beweging wat verminder is.

- Die periodes van die longitudinale en laterale bewegings is kleiner gewees as vir volskaal helikopters. Dit kan toegeskryf word aan die klein massa en inersie van die model helikopters.
- Die stabiliteit van die helikopter is in die algemeen verbeter soos die snelheid verhoog. Dit kan toegeskryf word aan die beter werking van die stert teen die verhoogde snelhede.
- Die klimtempo van die helikopter word beïnvloed deur die hoofrotor snelheid. 'n Laer hoofrotor snelheid laat 'n hoër klimtempo toe teen 'n spesifieke drywinginset. Dit is as gevolg van die laer geïndusseeerde drywingsverliese teen die laer hoofrotor snelheid. Daar word aanvaar dat die lugvloei oor die lem nie staak nie.
- Die hoofrotor snelheid beïnvloed nie die inkrimentele drywing ( $\Delta P_c$ ) wat benodig word om 'n sekere klimtempo te bereik nie. Dit is as gevolg van die konstante drywings verliese teen 'n sekere hoofrotor snelheid.
- Die vereenvoudigde perdeskoenwerwel teorie kan gebruik word om die afspoel hoek by die horisontale stabiliseerder te bereken indien die helikopter in hoë-spoed voorwaartse vlug is.



## ACKNOWLEDGEMENTS

The completion of this thesis was a laborious affair, of which the result hung in the balance a couple of times from birth to death. The author wishes to thank the following people without whom this thesis would never have been possible:

- Surien, for loving me and caring for me whenever this project had me close to breaking point
- Dr. Dirk Pienaar, for excellent guidance, invaluable advice, pleasant demeanour and for not pulling the reigns too tightly, but letting the project go where it wanted to
- The academic staff at the Department of Mechanical Engineering of the University of Stellenbosch, for firstly imparting knowledge, but also for lending a helping hand when possible or asked
- The technical staff, especially Cobus Zietsmann, who helped more than asked and never asked for anything in return.
- Mike Davies for expert knowledge imparted in the field of model helicopters, as well as repairing the helicopter.
- His family and friends who rode the rollercoaster along with him through thick and thin and never got (too) fed up with it.

**List of Symbols**

## Roman Symbols

$A$	Rotor disc area	$m^2$
$a$	Two-dimensional lift-curve slope Inflow factor in momentum theory	1/rad
$a_0$	Main rotor coning angle	rad
$A_1$	Lateral cyclic pitch angle	rad
$a_1$	Longitudinal flapping coefficient	rad
$AR$	Aspect ratio	
$b$	Number of rotor blades	
$B_1$	Longitudinal cyclic pitch angle	rad
$b_1$	Lateral flapping coefficient	rad
$B_{1nt}$	Longitudinal cyclic pitch angle with no contribution from the tail plane	rad
$c$	Rotor blade chord	m
$C_D$	Drag coefficient	
$c_{d0}$	Minimum rotor blade drag coefficient	
$C_L$	Lift coefficient	
$c_{l\alpha}$	Two-dimensional lift-curve slope	1/rad
$C_{mf}$	Fuselage pitching moment coefficient	
$C_{mS}$	Coefficient of centrifugal moment per unit tilt of rotor blades	
$C_P$	Power coefficient = $P / \rho A (\Omega R)^3$	
$C_T$	Thrust coefficient = $T / \rho A (\Omega R)^2$	



$C_Y$	Rotor side-force coefficient	
$D$	Rotor disc diameter Drag	m N
$d_0$	Dimensionless equivalent flat-plate area	
$e$	Dimensionless hinge offset	
$F_X, F_Y, F_Z$	Force in the X-, Y- or Z-direction	N
$f$	Equivalent flat plate drag area of helicopter fuselage	m <sup>2</sup>
$f_1$	Dimensionless offset of helicopter centre of gravity in the x-direction (positive if forward of the rotor shaft)	
$f_2$	Dimensionless offset of helicopter centre of gravity in the y-direction (positive if right of the rotor shaft)	
$g$	Gravitational acceleration constant = 9.81	m/s <sup>2</sup>
$H$	Rotor disc drag	N
$h$	Angular momentum; Fuselage height	kg m <sup>2</sup> /s; m
$h_c$	Rotor disc drag coefficient	
$h_m$	Dimensionless height of main rotor above the helicopter centre of gravity	
$h_T$	Dimensionless height of tail rotor above the helicopter centre of gravity	
$I_B$	Rotor blade flapping moment of inertia	kg m <sup>2</sup>
$I_{XX}, I_{YY}, I_{ZZ}$	Moments of inertia of the helicopter about the x-, y- and z-axes	kg m <sup>2</sup>
$I_{XY}, I_{YZ}$	Products of inertia	kg m <sup>2</sup>
$\vec{i}, \vec{j}, \vec{k}$	Unit vectors in the x-, y- and z-directions	
$L$	Lift; Rolling Moment	N Nm

$l$	Fuselage length	m
$l_T$	Dimensionless distance from the helicopter centre of gravity to the tail rotor	
$M$	Helicopter mass; Pitching moment; Figure of merit	kg Nm
$M_b$	Mass of rotor blade	kg
$M_f$	Fuselage pitching moment	Nm
$M_s$	Centrifugal moment per unit of tilt of the rotor disc plane	Nm/rad
$M_T$	Pitching moment due to the tail plane	Nm
$m$	Mass per unit length of main rotor blade	kg/m
$\dot{m}$	Mass flow-rate	kg/s
$N$	Helicopter rolling moment; number of rotor blades	Nm
$n$	Dimensionless downwash velocity of main rotor	
$P, Q, R$	Angular velocity components in the x-, y- and z-directions.	rad/s
$P$	Power	W
$P_c$	Power required for vertical climbing flight	W
$P_h$	Power required in hover	W
$P_0$	Profile Power	W
$Q$	Rotor torque	Nm
$q_c$	Torque coefficient	
$R$	Rotor radius	m
$r$	Dimensionless radial position along rotor blade	

$r_c$	Equivalent radius of cylindrical fuselage	m
$S$	Equivalent planform area of helicopter fuselage	m <sup>2</sup>
$S_1$	Centrifugal force of the rotor blade	N
$S_f$	Planform area of the vertical stabiliser	m <sup>2</sup>
$S_T$	Planform area of the tail plane	m <sup>2</sup>
$s$	Rotor disc solidity	
$T$	Main rotor thrust	N
$T_D$	Thrust referred to disc-axes	N
$T_T$	Tail rotor thrust	N
$t$	Time	s
$t_{cD}$	Thrust coefficient referred to the disc axes	
$t_{cT}$	Tail rotor thrust coefficient	
$\hat{t}$	Air second (dimensionless time)	
$U, V, W$	Velocity components in the X-, Y- and Z-directions	m/s
$U_T$	Thrust velocity used for the calculation of the induced velocity in forward flight	M/s
$\bar{u}$	Vector of control inputs	
$V$	Speed in the forward direction	m/s
$V_c$	Vertical climbing velocity	m/s
$v_h$	Induced velocity at rotor disc in hover	m/s
$v_i$	Induced velocity at rotor disc in forward flight	m/s
$W$	Weight	N



$w$	Slipstream velocity; width of fuselage	m/s; m
$w_c$	Weight coefficient	
$X, Y, Z$	Resultant aerodynamic force components acting on the helicopter along the x-, y- and z-axes	N
$x, y, z$	Mutually orthogonal directions of the fuselage axes: x forward, y starboard and z down, centred at the helicopter's centre of gravity	
$x_g$	Dimensionless radial distance from hub to the centre of gravity of the rotor blade	
$Y$	Rotor side force	N
<b>Greek Symbols</b>		
$\alpha$	Angle of incidence	rad
$\alpha_D$	Rotor disc incidence angle measured in the disc axes	rad
$\alpha_f$	Incidence of vertical stabiliser under zero side-slip	rad
$\alpha_s$	Zero-lift line of tail plane	rad
$\alpha_T$	Incidence of tail plane	rad
$\beta_e$	Side-slip angle	rad
$\beta_w$	Angle between the x-axes of the wind-axes and hub-wind reference systems	rad
$\delta$	Constant rotor blade drag coefficient	
$\delta_0, \delta_1, \delta_2$	Constants describing rotor blade drag as a function of the incidence angle	
$\varepsilon$	Downwash angle at tail plane	rad
$\gamma$	Lock number	
$\kappa$	Empirical factor used to estimate induced power	

$\lambda$	Inflow velocity ratio	
$\lambda_i$	Induced velocity ratio	
$\lambda_{ih}$	Induced velocity ratio in hover	
$\lambda_D$	Inflow velocity ratio in the disc plane	
$\mu$	Forward speed ratio	
$\eta$	Efficiency of the rotor disc	
$\Theta$	Euler pitch angle	rad
$\theta$	Perturbation of the pitch angle	rad
$\Phi$	Euler roll angle	rad
$\phi$	Perturbation of the roll angle	rad
$\Psi$	Euler yaw angle	rad
$\psi$	Perturbation of the yaw angle	rad
$\theta_{tw}$	Linear twist angle of rotor blade – positive when blade pitch increases from root to tip	rad/m
$\theta_0$	Main rotor collective pitch angle	rad
$\theta_{0T}$	Tail rotor collective pitch angle	rad
$\theta_{1c}$	Lateral cyclic pitch	rad
$\theta_{1s}$	Longitudinal cyclic pitch	rad
$\theta_{.75}$	Collective pitch at 75% of rotor blade radius	
$\phi$	Inflow angle of air at rotor blade section	rad
$\rho$	Air density	kg/m <sup>3</sup>
$\tau$	Flight path angle	rad
$\dot{\Psi}$	Helicopter turning rate	rad/s

$\Omega$	Rotor speed	1/rad
$\omega$	Angular velocity	rad/s

### Subscripts

$D$	Disc- (tip-path) plane
$e$	Trim, equilibrium
$f$	Fuselage
$fn$	Vertical fin
$h$	Hub-axes system
$i$	Induced
$nf$	Plane of no-flapping
$T$	Tail
$TR$	Tail rotor
$w$	Wind-axes system

### Superscripts

-	Component vector
-	Physical vector
$\wedge$	Non-dimensional quantity
•	Time derivative



**TABLE OF CONTENTS**

	<b>Page</b>
Summary	i
Opsomming	iii
Acknowledgements	v
List of Symbols	vi
Table of Contents	xiii
1. INTRODUCTION	1
1.1 Helicopter History and Development	2
1.2 The Helicopter Rotor	5
1.3 The Swashplate	9
1.4 Helicopter Reference Axes	10
1.5 Momentum Theory of Actuator Discs	12
1.6 Blade Element Theory	14
1.7 Induced Velocity in Forward Flight	18
1.8 Concluding Remarks	19
2. EQUATIONS OF MOTION	20
2.1 Newton's Second Law	20
2.2 Inertia Tensor	23
2.3 Euler Angles	24
2.4 Equations of Motion	25
3. HOVER ANALYSIS	27
3.1 Aerodynamics in Hover	28

3.2 Results	30
4. VERTICAL CLIMBING FLIGHT	32
4.1 Flow States of the Rotor in Axial Flight	32
4.2 Governing Equations	34
4.3 Results	36
4.4 Conclusion	38
5. TRIM IN FORWARD FLIGHT	40
5.1 Trim in Straight and Level Flight	41
5.2 General Trim Problem	43
5.3 Calculating the Trim Settings of a Helicopter in Forward Flight	45
5.3.1 Longitudinal Trim	46
5.3.2 Lateral Trim	53
5.4 Verification of Calculated Trim Settings	56
5.4.1 Fuselage Attitude	57
5.4.2 Longitudinal Cyclic Pitch Input	57
5.4.3 Collective Pitch	57
5.4.4 Fuselage Roll Angle	58
5.4.5 Lateral Cyclic Pitch	58
5.4.6 Further Verification	59
5.4.7 Conclusion	61
6. DYNAMIC STABILITY AND CONTROL	62
6.1 Introduction to the Stability Analysis	62
6.1.1 Simplifying Assumptions	63

6.1.2 Physical Interpretation	64
6.2 Longitudinal Dynamic Stability	65
6.2.1 Non-dimensionalization of the Equations	66
6.2.2 Stick-fixed Dynamic Longitudinal Stability	68
6.2.3 Aerodynamic Derivatives	69
6.2.4 Longitudinal Stability in Hover	74
6.3 Lateral Dynamic Stability	74
6.3.1 Stick-fixed Dynamic Lateral Stability	75
6.3.2 The Lateral Stability Derivatives	76
6.3.3 Lateral Stability in Hover	78
6.4 Control Response	79
6.4.1 Control Derivatives	79
6.4.2 Control Response in Forward Flight	80
6.5 Verification of Calculated Stability Characteristics	81
6.5.1 Longitudinal Stability Characteristics	81
6.5.2 Lateral Stability Characteristics	82
<b>7. STABILITY AND CONTROL CHARACTERISTICS OF MODEL HELICOPTERS</b>	<b>83</b>
7.1 Hirobo Shuttle Z	83
7.2 JR Voyager E	85
7.3 General Remarks	86
<b>8. CONCLUSION AND RECOMMENDATIONS</b>	<b>89</b>
8.1 Trim Analysis	89
8.2 Stability and Control Analysis	89
8.3 Root Locus Analysis	91



8.4 Performance Analysis	91
8.5 Recommendations	92
REFERENCES	94
ILLUSTRATIONS AND GRAPHICAL RESULTS	97
TABLE OF NUMERICAL RESULTS	155
APPENDICES	161
A. Computer Programs	162
A.1 Hover Analysis	162
A.2 Vertical Climbing Flight	175
A.3 Combined Trim Analysis and Calculation of the Stability and Control Derivatives of a Helicopter in Forward Flight	181
B. Derivation of the $\partial a_1/\partial \mu$ Derivative	199
C. Helicopter Specifications	200
C.1 Huey Cobra	200
C.2 Bramwell Test Helicopter	201
C.3 Hirobo Shuttle Z	202
C.4 JR Voyager E	203
D. Example of a Full Dynamic Model	204

## 1. INTRODUCTION

The usefulness of the unmanned air vehicle (UAV) is clear. UAV's has been successfully employed in combat roles where manned missions would be too dangerous. These roles include reconnaissance, artillery spotting, battlefield communication relay hubs and as target drones. The usefulness of these aircraft also extends to the civilian role where they are used in coastal patrols and traffic monitoring. UAV's can either be autonomously controlled or remotely controlled by a human operator.

All these roles are performed by fixed-wing UAV's. The existence of rotary wing UAV's would present the mission planner with new capabilities. These capabilities include hovering, slow forward flight, vertical climbing, flying sideways and backwards. Despite all these benefits, there are only a few rotary-wing UAV's in military or civil service at present. Examples of these are the Yamaha range of helicopters (civil) and the Cypher (military).

A need thus exists for the development of such rotary wing UAV's capable of autonomous flight. A program was initiated at the University of Stellenbosch to perform research in this field in November 2002. The program was jointly undertaken by the Mechanical and Electrical Engineering Departments.

The successful development of this UAV was dependent on (among other system elements) the development of a successful and viable stability and control augmentation system (SCAS). In order to develop the SCAS, the helicopter's stability and control derivatives would be required.

Remote controlled model helicopters would be used as the basis for the rotary wing UAV. Two model helicopters representing a broad spectrum of model helicopters currently in service were investigated. The Hirobo Shuttle Z (Figure 1.1) is a methanol engine helicopter in the medium-size class. The JR Voyager E (Figure 1.2) is electronically powered and falls in the small-size class.

The goal of this thesis was to establish the capability to perform the required stability and control analysis of the model helicopters. In order to reach this goal, the following smaller objectives were identified:



- The development of a computer program for performing a trim analysis in hovering flight, vertical climbing flight and forward flight.
- The development of a computer program that performs a stability and control analysis of a model helicopter in forward flight.

The rest of this chapter is dedicated to a discussion of the history of the helicopter as well as a brief review of general aerodynamic and helicopter theory.

### 1.1 Helicopter History and Development

The first successful powered human flight was undertaken by the Wright brothers on 17 December 1903 in a fixed-wing aircraft. The first successful helicopter flight would only be accomplished much later. This paragraph is a summary of the development of the helicopter and relies heavily on Johnson (1980).

Three problems faced the initial development of helicopters:

- a. to find a light and reliable engine
- b. to develop a light and strong structure for the rotor, hub, and blades while maintaining good aerodynamic efficiency
- c. to develop mechanisms for controlling the main rotor and for balancing the rotor torque.

The first recorded suggestion of a rotary wing vehicle was made by Leonardo da Vinci in the late 15<sup>th</sup> century. The first powered working model was demonstrated by M.V. Lomonosov in Russia (1754). He used coiled springs to power his model. More spring-powered models were demonstrated by Launoy and Bienvenu (France, 1784) and Sir George Cayley (England, 1790's).

The next power-plant was the steam engine. The steam engine was plagued by a low power-to-weight ratio. Viscomte Gustave de Ponton d'Amecourt coined the word "helicopter" in 1863 which literally means "helical wing". In 1878 Enrico Forlanini built a 3.5kg flying steam-driven model. Thomas Edison recognized in the 1880's that no helicopter would be able to fly until engines with a weight-to-power ratio below 1 to 2 kg/hp were available.



### ***The early years***

The invention of the internal combustion engine (circa 1900) at last provided the engine that could be used to power man into the air. Around the same time, Renard invented the flapping hinge and used it to build a helicopter with two side-by-side rotors in 1904. In 1907, the Brügget-Richet Gyroplane No.1 completed a one minute tethered flight with a passenger. Paul Cornu constructed a helicopter with two contrarotating rotors in tandem configuration. Control was achieved by adjusting vanes that were placed in the rotor slipstream, but was not very effective. The helicopter had structural and stability problems.

The first helicopter that could fly untethered was built by Emile and Henry Berliner in 1909. Boris N. Yuriev built a helicopter with one main rotor and an anti-torque tail rotor. The helicopter could not achieve flight, but Yuriev went on to supervise helicopter development in Russia. The aerodynamics pioneer von Karman built a tethered helicopter along with Petroczy (Austria, 1916) that achieved an altitude of 50m while carrying a payload.

### ***World War 1***

The First World War expedited the development of more powerful engines. George de Bothezat built a helicopter with four six-bladed rotors (United States, 1922). The rotors were driven by a 180 hp engine at the centre of the helicopter. Control was established by applying different amounts of collective pitch on the four rotors. Successful flights were carried out up to an altitude of 4 to 6m. A similar machine was built by Etienne Oemichen (France, 1924). The machine was complicated by many sets of propellers for attitude control and yawing. It set the first helicopter distance record at 360m.

During the same year in Spain, Marquis Raul Pateras Pescara constructed a helicopter that was controlled by warping the rotor blades. He was the first to demonstrate effective cyclic control of the main rotors. The helicopter improved the distance record to 736m, but had stability problems.

A.G. von Baumhauer (Holland, 1924-1929) developed a helicopter that utilised a single main rotor and a vertical tail rotor. Both were driven by their own engines, as apposed to being linked to the same engine in current helicopters. The main rotor's rotor blades were linked with a cable to form a teetering rotor. Cyclic pitch control was achieved by using a swashplate. The project was ended after a bad crash.



The helicopter was in an advanced state of development by the early 1930's. Successful helicopter flights were still hampered by the lack of adequate stability and control characteristics. The lack of the ability to achieve forward flight and autorotation limited the usefulness of the helicopters of that era. Many of the problems experienced in the early development of the helicopter would be addressed and solved during the design and operation of the autogiro.

### ***The autogiro***

The autogiro was developed mainly by Juan de la Cierva in Spain between 1920 and 1930. The autogiro is an aircraft that produces lift by a windmilling rotor in addition to a fixed wing. In the autogiro, lift is produced by forward velocity, and the autogiro was therefore incapable of hovering flight. Cierva proposed the use of a flapping hinge on his C-3 autogiro (1922). This eliminated the rolling moment created by the asymmetry of the lift over the rotor-disc. The lead-lag hinge was added to his rotors in 1927 after a crash led to an investigation that indicated the high in-plane bending moments at the blade roots of the rotors. The lead-lag hinges caused ground resonance problems that were solved by the introduction of lag dampers. This completed the development of the articulated hub.

Although the autogiro could never compete with fixed-wing aircraft, it was the drive behind most of the early theoretical work that could be applied to helicopters.

Louis Breguet and Rene Dorand built a helicopter that employed an articulated hub (France, 1935). Pitching and rolling was performed by cyclic pitch and directional control by differential torque in the coaxial rotors. This helicopter held the record for speed (44.7 kph), altitude (158m), duration (1 hour and 2 minutes) and closed-circuit distance (44 km). E.H. Heinrich Focke constructed a helicopter in 1936 that improved these records to 122.5 kph, 2440 m and had an endurance of 1 hour and 21 minutes.

### ***World War 2***

During the Second World War, German engineers made large advances in rotary wing development. The Focke-Achgelis Fa-223 was developed in 1941 and had an absolute ceiling of 5000m, a range of 300km and a cruising speed of 120 kph. All of this was accomplished while carrying a useful load of 900kg.



During that same year, Igor Sikorsky built the VS-300, which utilised a single main rotor and a small anti-torque tail rotor. This helicopter was the first to employ the controls as they are used at present (cyclic stick, pedals and a collective stick with a twist grip throttle). A derivative of this helicopter (the R-4) went into production and several hundred were produced during the Second World War.

### ***The post-war years***

Lawrence Bell started building helicopters in 1943. He utilised the gyro stabilising bar developed by Arthur Young on his teetering rotors. This configuration became so well known that the stabilising bar is now referred to as the Bell stabilising bar. Utilising this technology, the Bell Model 47 became the first helicopter to receive the American certificate of airworthiness for helicopters.

Frank N. Piasecki developed the PV-3 tandem rotor helicopter in 1945. Piasecki's company eventually became the Boeing Vertol Company. This company would later build the famous Boeing CH-47 Chinook tandem rotor helicopter (Figure 1.3).

Stanley Hiller developed the Hiller gyro stabiliser bar with aerodynamic surfaces between 1946 and 1948. The pilot controlled these aerodynamic surfaces in order to adjust the rotor orientation. During the same period, Charles Karman developed the servotab control method of rotor pitch control. In this method of control, the rotor blade is twisted rather than rotated about a pitch bearing at the root.

In the Soviet Union, helicopters were built by Mikhaol Mil', Nikolai Kamov and Alexander Yakolev. Kamov's helicopters became well-known for their double rotor coaxial configuration.

Helicopters achieved their current state of development with the introduction of the turboshaft engine. This type of engine was known for its low specific weight and finally solved the weight-to-power ratio problem identified by Thomas Edison. The K-225 helicopter built by the Karman Aircraft Company in 1951 was the first helicopter to utilise this type of engine. In 1954, the HTK-1 (also built by Karman) became the first twin-engine turbine powered helicopter.

## **1.2 The helicopter rotor**

The power source was not the only important requirement for the successful development rotary-winged aircraft. In order to achieve



efficient vertical flight, large diameter rotors were required. To ensure good aerodynamic efficiency, blades with a high aspect-ratio would be required. These two requirements resulted in blades that were much more flexible than those of high disk loading rotors such as propellers. As a result, substantial motion occurred in the blades in response to the aerodynamic forces.

During the early development of the helicopter, flapping hinges were usually employed to connect the rotor-blade root to the hub. In this configuration, no bending moment would be transmitted to the hub.

More recently, the flapping hinge has been eliminated. In this configuration, the structure was submitted to the bending moments generated due to the aerodynamic forces. The root load and hub moment was found to have a significant influence on the design of the helicopter as well as its operating characteristics.

The difference between the rotor dynamics of helicopters with fully articulated rotors and those with hingeless rotors are so substantial that different methods of analysis are required. The motion of a rotor that is attached to the hub by a set of hinges can be described as rigid body rotations about each hinge. For a helicopter with an articulated rotor, the motion consists mainly of flapping and lagging motion. Hingeless rotors can be viewed to be similar to articulated rotors due to the large amount of centrifugal stiffening, except in the blade root where most of the bending takes place.

Control of the helicopter is obtained by changing the pitch of the blade. Changing the pitch of the blade changes the angle of incidence for the rotor blade. This in turn changes the thrust-vector produced by the blade and allows control of the helicopter. Pitch adjustment (also called feathering motion) requires a pitch bearing between the hub and the rotor blade.

Johnson (1980) classified helicopter rotors by mechanical arrangement as follows:

- *Articulated rotor: The blades are attached to the hub with flap and lag hinges. (Examples include the Sea King and the Puma)*
- *Teetering rotor: Two blades forming a continuous structure are attached to the rotor shaft with a single flap hinge in a teetering or seesaw arrangement. The rotor has no lag hinges. Similarly, a gimbaled rotor has three or more blades attached to the hub without hinges, and the hub is attached to the rotor shaft by a*



*gimbal or universal joint arrangement. (Examples include the AH1G Huey Cobra and the UH1 Iroquois)*

- *Hingeless rotor: The blades are attached to the hub without flap or lag hinges, although often with a feathering bearing or hinge. The blade is attached to the hub with cantilever root restraint, so that blade motion occurs through bending at the root. This rotor is also called a rigid rotor. However, the limit of a truly rigid blade, which is so stiff that there is no significant motion, is applicable only to high disk loading rotors. (Examples include the Westland Lynx and the Boeing Comanche)*

### **Basic Rotor Terminology**

The profile of a rotor blade is very similar to that of a normal wing found on fixed-wing aircraft. In the analysis of the helicopter (see Figure 1.4)

- R is the rotor radius and is defined as the distance from the centre of the hub to the tip of the blade.
- r is the radial location on the blade measured from the centre of the hub.
- c is the blade chord, defined as the distance between the leading edge and the trailing edge.
- $\Omega$  is the rotational speed of the hub of the rotor.
- $\psi$  is the azimuth angle of the blade, which is zero at the downstream position (over the tail boom) and  $180^\circ$  at the front of the helicopter. The  $90^\circ$  mark is on the starboard side and the  $270^\circ$  mark is on the port side.
- b is the number of rotor blades
- $I_b$  is the moment of inertia of the blade about the flapping hinge.

$$I_b = \int_0^R m r^2 dr \quad (1.1)$$

For a rectangular blade with uniform mass-distribution, this reduces to

$$I_b = \frac{1}{3} m R^2 \quad (1.2)$$

The following derived quantities are important

- The rotor disk area is the total area which is swept by a rotor blade in one full revolution, or

$$A = \pi R^2 \quad (1.3)$$

- The rotor solidity is the ratio of the total blade area to the rotor disk area, defined as

$$\sigma = Nc / \pi R \quad (1.4)$$

- The Lock number is the ratio of the aerodynamic and inertial forces acting on the blade. It is defined as

$$\gamma = \rho a c R^4 / I_b \quad (1.5)$$

### **Rotor blade forces**

As the rotor blades rotate about the hub, aerodynamic forces are created. If the helicopter is in motion, the velocity vector at any point on the rotor blade will be a function of the azimuth angle as well as radius. The variation in the velocity vector will cause varying aerodynamic forces. These aerodynamic forces results in blade flapping and the various rotor forces results from resolving these force vectors into their components:

- Thrust – defined to be normal to the disc plane and positive when directed upward. The lift produced by the airfoil is usually defined by means of a lift coefficient. The lift coefficient is the non-dimensionalised lift produced by the airfoil. Then the lift produced by the rotor is

$$L = \frac{1}{2} \rho V^2 A_{planform} C_L \quad (1.6)$$

This is sometimes altered by utilising the two-dimensional lift-curve slope. This number describes the linear dependence of the lift coefficient on the angle of incidence. Using this method, the lift coefficient can be expressed as

$$C_L = \frac{\partial C_L}{\partial \alpha} \alpha \quad (1.7)$$

- Rotor drag force (the so-called H-force) – a force that opposes the forward velocity of the helicopter. It is defined to be positive



when directed rearward. The drag is usually defined by means of a non-dimensional drag coefficient.

- Rotor side force (the so-called Y-force) – a force that is defined to be positive when directed to the right, toward the advancing side of the rotor (on a helicopter with anti-clockwise rotating blades)

### 1.3 The Swashplate

It was stated in the section on the development of the helicopter that most flights were at first only tethered hovering flights. These helicopters were thus very similar in its usefulness to the observation balloons that were used during the First World War. To be truly useful, these helicopters would need the ability to be controlled in flight. A form of control over the cyclic pitch would be required.

At first the rotor blades were deformed in order to achieve cyclic pitch control, but this method placed unnecessary strain on an already strained rotor blade. Other attempts included the swivelling of the whole rotor disc (shaft included), but this caused very large unwanted gyroscopic forces and moments.

It was A.G. von Baumhauer who first used the swashplate in his helicopter. The swashplate would become the standard means of employing collective and cyclic pitch variations in all modern helicopters.

The construction of the swashplate is illustrated in Figure 1.5. It consists of mainly two parts: a rotating part and a non-rotating part. The rotating part is attached to the rotors through pitch link rods. Moving these pitch link rods causes the blade feathering (or blade pitching) to change. The non-rotating part is attached to the control actuator inputs.

The rotating part rests on a bed of bearings that allows it to rotate over the non-rotating part. If the pilot applies a control input, the control actuators would move the non-rotating part to conform to the pilot's input. The orientation of the rotating part is moved by the non-rotating part. This pilot command is then transmitted to the rotor blades by means of the pitch link rods.



Adjusting the collective pitch is the primary mechanism for adjusting the amount of thrust produced by the rotor disc. It is applied to all the rotor blades collectively and thus the expression "collective pitch". In order to adjust the collective pitch, the swashplate is moved up or down without tilting it.

Cyclic pitch is the term used to define the one-per-revolution sinusoidal variation in rotor blade pitch. Changing the orientation of the swashplate will cause the rotor blade to experience different amounts of feathering while completing one revolution about the hub. The changes in feathering will cause flapping in the rotor blades. The maximum and minimum flapping angle will occur at the same azimuth as where the maximum and minimum displacement of the swashplate occurs. The rotor disc will assume the same orientation as that of the swashplate if the rotor blades are linked to the swashplate in a 1:1 ratio through the pitch link rods,

#### **1.4 Helicopter reference axes**

The kinematics of rigid body motion can be classified into three categories: pure translation, pure rotation and combined translation and rotation. In order to define these, it is required to have some frame of reference.

##### ***The inertial reference frame***

An inertial reference frame is one that moves at constant velocity and does not rotate compared to the distant stars. An earth-fixed frame is clearly not an inertial frame, but its acceleration and angular velocity is very small compared to that which a helicopter experiences when manoeuvring. This justifies the assumption, for the purpose of helicopter flight mechanics, that an earth-fixed frame is approximately inertial.

##### ***The body axes***

The body axes are centred at the helicopter's centre of gravity and are fixed to the helicopter, as shown in Figure 1.6. It translates and rotates exactly as the helicopter does. The orientation of the body axes of the helicopter is also shown in this figure.



### ***The hub axes system***

The hub axes system is a body-fixed system centred at the main rotor hub. The  $Z_h$ -axis is aligned with the rotor shaft, and its  $X_h$ - and  $Y_h$ -axes are parallel to that of the body-axes, as shown in Figure 1.6.

### ***The hub-wind axes system***

The hub-wind axes system has certain features in common with the hub axes system. The origin of both these systems lies on the centre of the hub and the  $Z_{wa}$ -axis is the same axis as the  $Z_h$ -axis. The  $X_{wa}$ - and  $Y_{wa}$ -axes of the hub-wind system is orientated so that the  $X_{wa}$ -axis faces into the wind. The hub and hub-wind systems are collinear if the helicopter is not sideslipping.

If a helicopter has a forward velocity component of  $U_h$  and a sideward velocity component of  $V_h$  along the  $Y$ -axis, then the  $X_{wa}$ -axis is rotated by

$$\beta_w = \tan^{-1} \frac{V_h}{U_h} \quad (1.8)$$

The velocity in the  $X_{wa}$ -axis ( $V_A$ ) becomes

$$V_A = U_{wa} = \sqrt{U_h^2 + V_h^2} \quad (1.9)$$

The component of velocity along the  $Y_{wa}$ -axis is zero by definition. The orientation of the hub-wind axes can be seen in Figure 1.7.

### ***The no-feathering or control axis***

The no-feathering axis is the axis that is normal to the plane of the swashplate. No cyclic feathering occurs relative to this axis. Due to the fact that the blade pitch is constant in the plane of the swashplate, the only other type of blade motion contributing to the local blade incidence is that due to rotor blade flapping. It is convenient to use this axis to express blade flapping.

### ***The tip-path-plane axis (or disc axis)***

The tip-path-plane is formed by the locus of the positions of the rotor's blade-tips through one revolution. The tip-path-plane axis (or disc axis) is the axis that lies perpendicular to this plane for flapping hinges with zero offset. There will be no flapping relative to this plane, but there will be feathering motion relative to the plane. The amount of feathering in this plane is exactly equal to the flapping relative to the no-



feathering axis. The tip-path-plane is no longer the plane of no flapping in the presence of offset flapping hinges. However, the error in assuming that the tip-path plane is the plane of no flapping is very small if the hinge-offset is small.

### ***The shaft- or hub-plane axis***

Both flapping and feathering motion is present if the rotor is viewed from this axis. It is thus less convenient for the calculation of rotor forces, but it becomes more useful when it is used to analyze helicopters with hingeless rotors.

## **1.5 Momentum theory of actuator discs**

In order to provide a forward propulsive force (also called thrust) it is necessary to increase the rearward momentum of an amount of gas. In the case of helicopters this increase in momentum is performed entirely on atmospheric air.

According to Houghton and Carpenter (1993), Froude proposed a theoretical determination of the amount of thrust produced by a rotor-disc through the so-called momentum theory of propulsion (see Figure 1.8). The theory is based on the concept that a rotor-disc can be replaced with an ideal actuator disc. Thus actuator disc is assumed to be permeable and infinitely thin and it offers no resistance to the air passing through it.

The force exerted by the actuator disc on the air causes the air to flow through the disc, thus adding momentum to the air. This momentum is added uniformly over the whole area of the disc and the pressure distribution over the area of the disc is uniform too. A further consequence of this is that the velocity of the air passing through the disc is also constant over the disc area. The wake of the disc is separated from the static atmosphere by a pronounced slip-surface.

The aim of this paragraph is not to repeat the derivation of Froude's momentum theory. It will however be used to indicate some important and useful results of the theory that will be referred to in later chapters. All the results are from the books of Houghton and Carpenter (1993) and Johnson (1980).

The rotor is analysed as a one-dimensional system. Hence, the velocity only changes in only one dimension. The area of the flow is however



allowed to change. In the derivation of the theory, Froude referred to three velocities: the velocity far upstream of the disc,  $V$ , the velocity far downstream of the disc,  $V_s$  and the velocity at the disc,  $V_0$ . A factor describing the efficiency of momentum transfer could be written in terms of the velocity far upstream of the disc and at the disc:

$$\eta = 1 / (1 + a) = V / V_0 \quad (1.10)$$

In equation (1.10),  $a$  is called the inflow-factor, which is defined such that

$$V_s = V(1 + 2a) \quad (1.11)$$

It can be seen from equation (1.11) that an increase in the slipstream velocity causes an increase in the inflow factor  $a$ . The increase of the inflow factor will cause a decrease in the efficiency of the actuator disc according to equation (1.10). It can thus be seen that the efficiency of the actuator disc decreases as the velocity of the slipstream increases. The efficiency of the actuator disc increases as the slipstream velocity decreases, which is accompanied by a decrease in the amount of momentum transferred to the air. The inflow factor influences the amount of thrust produced according to the equation

$$T = 2\rho A V^2 (1 + a)a \quad (1.12)$$

A disc with ideal efficiency ( $a = 0$ ) thus produces no thrust as no momentum is added to the air passing through the disc. This is representative of a disc that is not in operation. Therefore, an actuator disc always operates at an efficiency of less than 1. The power required to drive the actuator disc is

$$P = \frac{TV}{\eta} = TV_0 \quad (1.13)$$

The velocity in the actuator disc is thus critical in determining the amount of power required to drive the actuator disc.

The above equations still leave us without a clear method of carrying out a performance analysis of the actuator disc. Johnson (1980) modifies these equations to be applied to the helicopter in axial flight. The analysis is based on the value of the induced velocity. The induced velocity is the amount by which the velocity of the air stream exceeds the climbing velocity of the aircraft. The induced velocity in axial flight is based on the induced velocity in hover

$$v_h = \sqrt{T / 2\rho A} \quad (1.14)$$

The thrust produced by the disc is

$$T = 2\rho A(V + v_i)v_i \quad (1.15)$$

where the induced velocity is

$$v_i = -\frac{V}{2} + \sqrt{\left(\frac{V}{2}\right)^2 + v_h^2} \quad (1.16)$$

The power required to move the disc at a velocity of  $V$  is thus

$$P = T \left( \frac{V}{2} + \sqrt{\left(\frac{V}{2}\right)^2 + v_h^2} \right) \quad (1.17)$$

Johnson (1980) states that even simple analyses can be used to obtain important and useful results using the momentum theory. A higher degree of accuracy requires a more complicated analysis. The next section will contain a discussion of a more accurate theory.

## 1.6 Blade Element Theory

Blade element theory is used to perform more accurate calculations of the performance of the rotor disc (or airscrew). The required performance is usually the starting point during the design of these airscrews or rotor discs.

Blade element theory is based on applying lifting-line theory to the rotating wing. It is assumed that each blade section acts as a two-dimensional airfoil to produce the aerodynamic force. This aerodynamic force can then be resolved into lift and drag. The effect of the wake on the rotor is accounted for entirely by calculating the induced angle of attack of the section.

Lifting line theory is based on the assumption that the airfoil has a very high aspect ratio. For helicopters, the aspect ratio is

$$AR = R/c \quad (1.18)$$

The aspect ratio of a wing affects the lift-curve slope. If the airfoil has an infinite aspect ratio, then the two-dimensional lift-curve slope of the airfoil would be at a maximum. It is however a fact that all airfoils do



have a finite aspect ratio and the size of the lift-curve slope reduces with a reduction in the aspect ratio.

Table 1.1 contains the aspect ratios of the rotor blades of some modern full-scale and model helicopters. It can be seen that the aspect ratio is almost always above 10. It can thus be assumed that lifting line theory can be applied to the rotor blades of these helicopters.

**Table 1.1 – Aspect Ratio of some helicopter rotor blades**

Helicopter	AR
AH1-G Huey Cobra	9.78
Westland Lynx	16.37
Aerospatiale Puma	13.89
DLR Bo 105	18.19
Hirobo Shuttle Z	14.05
JR Voyager E	11.28

Blade element theory forms the foundation of almost all analyses of helicopter aerodynamics because it deals with the detailed flow and loading of the blade. The detailed design parameters can thus be used to determine the rotor performance.

The basic assumptions of blade element theory are that

- the rotor blade has a high aspect ratio (AR)
- the disk loading is low
- compressibility and blade stall can be neglected

For the blade section, lift is defined as the force vector perpendicular to the resultant velocity vector on the airfoil, while drag is the force vector parallel to this vector. The pitch angle  $\theta$  is measured from the plane of rotation to the zero-lift line (Figure 1.9). The air stream impinges on the blade section at an incidence angle of  $\alpha$ . The air stream with velocity  $U$  can be resolved into components perpendicular and tangent to the helicopter x-axis, such as

$$U = \sqrt{U_T^2 + U_P^2} \quad (1.19)$$

The inflow angle

$$\phi = \tan^{-1} U_P / U_T \quad (1.20)$$

is defined in terms of the angle of incidence and the section pitch angle

$$\phi = \theta - \alpha \quad (1.21)$$

From basic aerodynamics

$$dL = \frac{1}{2} \rho U^2 c C_L dr \quad (1.22)$$

is the elemental lift and

$$dD = \frac{1}{2} \rho U^2 c C_D dr \quad (1.23)$$

the elemental drag on the differential element. The aerodynamic forces resulting from the integration of equations (1.22) and (1.23) along the length of the rotor blade is resolved into force components in the vertical and horizontal direction ( $F_z$  and  $F_x$ ) respectively as

$$F_z = L \cos \phi - D \sin \phi \quad (1.24)$$

and

$$F_x = L \sin \phi + D \cos \phi \quad (1.25)$$

Using these expressions, the elemental thrust, torque and power on each rotor blade section can be calculated as

$$dT = F_z dr \quad (1.26)$$

$$dQ = F_x r dr \quad (1.27)$$

$$dP = \Omega dQ = F_x \Omega r dr \quad (1.28)$$

respectively. At this point it is necessary to make further assumptions:

- The small angle assumption is appropriate for helicopters
- The effects of stall and compressibility are negligible, hence the lift coefficient is linearly related to the two-dimensional lift-curve slope

Johnson (1980) describes the contribution of the rotor-blade section to the thrust and power in dimensionless form as



$$dC_T = \frac{\sigma a}{2} (\theta r^2 - \lambda r) dr \quad (1.29)$$

and

$$dC_p = \left[ \frac{\sigma a}{2} (\theta r \lambda - \lambda^2) + \frac{\sigma c_d}{2} r^2 \right] r dr \quad (1.30)$$

respectively. In equations (1.29) and (1.30)

$$\lambda = \frac{(V + v_i)}{\Omega R} \quad (1.31)$$

is the inflow velocity ratio.  $V$  is the vertical velocity of the helicopter and can indicate both climbing and descending flight. If the assumption is made that the inflow velocity is uniform and that the blade has linear twist, then

$$\theta = \theta_0 + r \theta_{tw} = \theta_{.75} + (r - 0.75) \theta_{tw} \quad (1.32)$$

and

$$C_T = \frac{\sigma a}{2} \left( \frac{\theta_{.75}}{3} - \frac{\lambda_i}{2} \right) \quad (1.33)$$

where  $\theta_{.75}$  is the pitch of the blade at 75% radius and  $\theta_{tw}$  is the linear twist angle per unit span of the rotor blade. The elemental power coefficient can be written as

$$dC_p = \lambda dC_T + \frac{s c_{d0}}{2} r^3 dr \quad (1.34)$$

The first term in equation (1.34) is the induced power loss. It arises from the in-plane component of the lift due to the induced angle of attack. The second term is the profile power loss and it is assumed to be constant. This profile power loss is due to the viscous drag forces on the rotor blade. Johnson (1980) suggests

$$C_p = \frac{\kappa C_T^{3/2}}{\sqrt{2}} + \frac{s c_{d0}}{8} \quad (1.35)$$

in order to estimate the total power required in hover. The factor  $\kappa$  is used to account for the additional losses of a real rotor due to the varying values of  $\lambda$  over the span of the rotor.

## 1.7 Induced Velocity in Forward Flight

Glauert was the first to suggest a method of calculating the induced velocity of a rotor in forward flight. He applied the lifting line theory to the rotor disc, which he modelled as an elliptically loaded circular wing. He proposed that the induced velocity was

$$v_i = \frac{T}{2 \rho A V'} \quad (1.36)$$

where

$$V' = \sqrt{V^2 + v_i^2} \quad (1.37)$$

Defining the "thrust velocity" as

$$U_T = \sqrt{\frac{T}{2 \rho A}} = v_{ih} \quad (1.38)$$

equation (1.36) can be rewritten as

$$\bar{v}_i^4 + \bar{V}^2 \bar{v}_i^2 - 1 = 0 \quad (1.39)$$

where

$$\bar{v}_i = \frac{v_i}{U_T} \quad (1.40)$$

and

$$\bar{V} = \frac{V}{U_T} \quad (1.41)$$

Figure 1.10 indicates the relationship between  $\bar{v}_i$  and  $\bar{V}$ . It can be seen that the induced velocity in hover is the same as the result obtained from momentum theory. Consider for a moment the induced velocity of an elliptically loaded airfoil according to the lifting line theory:

$$w_i = -\frac{\Gamma_0}{4b} \quad (1.42)$$

The circulation strength of the airfoil is



$$\Gamma_0 = \frac{2L}{\rho V_\infty \pi b} \quad (1.43)$$

Combining equations (1.42) and (1.43) shows that

$$w_i = -\frac{L}{2\rho V(\pi b^2)} \quad (1.44)$$

The area of a circle is of course  $A = \pi b^2$ . It can thus be seen that the induced velocity in forward flight as suggested by Glauert (equation 1.36) is very similar to that of an elliptically loaded wing in forward flight.

## 1.8 Concluding remarks

This chapter started with a brief history of the development of the helicopter. A brief explanation of some of the pertinent factors concerning the dynamics of helicopters then followed in the preceding paragraphs. These paragraphs were not intended to be an exhaustive explanation of helicopter theory, but were intended to serve as a point of departure for the rest of the thesis.

In the next chapter, the equations of motion of a helicopter will be investigated. Then a trim- and performance analysis will be performed on a helicopter in hovering flight. The next step would be the trim analysis of the helicopter in vertical climbing flight. With the knowledge gained, the analysis will be expanded to include forward flight. The trim analysis is followed by the discussion of the stability and control characteristics of the model helicopters. The thesis is concluded with a discussions and recommendations about possible future work.

## 2. EQUATIONS OF MOTION OF THE HELICOPTER

The first chapter contained important information about the basics of helicopter flight and helicopter theory as well as the development of helicopters. This chapter will be dedicated to the derivation of the equations that describe the motion of the helicopter. It is based on the work done by Ashley (1974) and De Waard (1985).

### 2.1 Newton's Second Law

The helicopter consists of infinitesimal mass elements with mass  $dm$ . Each mass element is referenced to the body axes by a position vector  $\vec{r}$ . If the body is rigid, these position vectors will remain constant. This approximation can be used to write

$$M = \int_{\text{Body}} dm \quad (2.1)$$

and

$$\vec{0} = \int_{\text{Body}} \vec{r} dm \quad (2.2)$$

The aircraft body is exposed to external forces and moments where

$\vec{F}(t)$  is the time-dependent resultant of all external forces and

$\vec{G}(t)$  is the time-dependant resultant of all external moments about the aircraft centre of gravity. It is important to include the moment of  $\vec{F}(t)$  about the centre of gravity.

Newton's Second Law describes the resultant force on a body in terms of the change of the momentum vector as

$$\vec{F} = m \frac{d\vec{v}_c}{dt} \quad (2.3)$$

and

$$\vec{G} = m \frac{d\vec{h}}{dt} \quad (2.4)$$

where



$$\vec{h} = \vec{r} \times m\vec{v} = \int_{\text{Bod}} \vec{r} \times [\vec{v}_c + \vec{\omega} \times \vec{r}] dm \quad (2.5)$$

is the angular momentum of the body. In equation (2.5)  $\vec{v}_c$  is constant for all particles of the rigid body and can thus be factored outside the integral. In order to satisfy equation (2.2), this term must be zero.

The angular velocity vector  $\vec{\omega}$  and the linear velocity vector  $\vec{v}_c$  of the centre of gravity are measured relative to the inertial reference frame.

At this point it is necessary to introduce a rectangular coordinate system with the origin at the centre of gravity. Define the unit vectors on the x, y and z axes as  $\vec{i}$ ,  $\vec{j}$  and  $\vec{k}$  respectively (see Figure 2.1). The contribution of the vectors from the X, Y and Z components now become

$$\vec{r} = x\vec{i} + y\vec{j} + z\vec{k} \quad (2.6)$$

$$\vec{v}_c = U\vec{i} + V\vec{j} + W\vec{k} \quad (2.7)$$

$$\vec{\omega} = P\vec{i} + Q\vec{j} + R\vec{k} \quad (2.8)$$

and

$$\vec{h} = h_x\vec{i} + h_y\vec{j} + h_z\vec{k} \quad (2.9)$$

The aircraft will be rotating relative to a non-rotating reference. The Law of Coriolis is used to express this type of motion. For any random vector (say  $\vec{A}$ ) this law states that

$$\frac{d\vec{A}}{dt} = \frac{\partial\vec{A}}{\partial t} + \vec{\omega} \times \vec{A} \quad (2.10)$$

The partial derivative indicates a change in the vector relative to the body axes of the aircraft, while the normal derivative indicates the change in the vector relative to the inertial reference frame. The last term indicates that the aircraft has an angular velocity of  $\vec{\omega}$  relative to the inertial reference frame. Using equation (2.10) to rewrite the force and moment equations yields

$$\vec{F} = m \left( \frac{\partial\vec{v}_c}{\partial t} + \vec{\omega} \times \vec{v}_c \right) \quad (2.11)$$

and

$$\vec{G} = \frac{\partial \vec{h}}{\partial t} + \vec{\omega} \times \vec{h} \quad (2.12)$$

An observer rotating at  $\vec{\omega}$  along with the body axes would only notice time rates of change in  $U$ ,  $V$  and  $W$ , of which the resultant is reflected by

$$\frac{\partial \vec{v}_c}{\partial t} = \dot{U} \vec{i} + \dot{V} \vec{j} + \dot{W} \vec{k} \quad (2.13)$$

The vector cross product of two vectors (for example  $\vec{A}$  and  $\vec{B}$ )

$$\begin{aligned} \vec{A} \times \vec{B} &= \begin{bmatrix} \vec{i} & \vec{j} & \vec{k} \\ A_x & A_y & A_z \\ B_x & B_y & B_z \end{bmatrix} \\ &= (A_y B_z - A_z B_y) \vec{i} + (A_z B_x - A_x B_z) \vec{j} \\ &\quad + (A_x B_y - A_y B_x) \vec{k} \end{aligned} \quad (2.14)$$

Applying equations (2.7), (2.8), (2.13) and (2.14) to equation (2.11) and resolving the force vector into its components yields

$$\begin{aligned} F_x &= m(\dot{U} + QW - VR) \\ F_y &= m(\dot{V} + RU - WP) \\ F_z &= m(\dot{W} + PV - UQ) \end{aligned} \quad (2.15)$$

It is clear from equation (2.15) that each of the force components is influenced by three terms: one linear acceleration term along the direction of the force and two acceleration terms that exist due to rotation around the other two directions. Equation (2.12) can be rewritten similarly to the force equation as

$$\begin{aligned} L &= \dot{h}_x + Qh_z - Rh_y \\ M &= \dot{h}_y + Rh_x - Ph_z \\ N &= \dot{h}_z + Ph_y - Qh_x \end{aligned} \quad (2.16)$$



Equation (2.15) and (2.16) together forms the equations of motion of a body moving with six degrees of freedom.

## 2.2 The Tensor of Inertia

In order to split the inertial angular momentum of equation (2.5) into its Cartesian components, the vector identity

$$\vec{A} \times (\vec{B} \times \vec{C}) = \vec{B}(\vec{A} \cdot \vec{C}) - \vec{C}(\vec{A} \cdot \vec{B}) \quad (2.17)$$

is used. De Waard (1985) calculated this to be

$$\begin{aligned} & \vec{r} \times (\vec{\omega} \times \vec{r}) \\ &= \{P(y^2 + z^2) - Qxy - Rxz\} \vec{i} \\ & \quad \{Q(x^2 + z^2) - Pxy - Ryz\} \vec{j} \\ & \quad \{R(x^2 + y^2) - Pxz - Qyz\} \vec{k} \end{aligned} \quad (2.18)$$

The definition of the moments and products of inertia are

$$I_{XX} = \int_{Body} (y^2 + z^2) dm \quad (2.19a)$$

$$I_{YY} = \int_{Body} (x^2 + z^2) dm \quad (2.19b)$$

$$I_{ZZ} = \int_{Body} (x^2 + y^2) dm \quad (2.19c)$$

$$I_{XY} = \int_{Body} xy \, dm \quad (2.19d)$$

$$I_{YZ} = \int_{Body} yz \, dm \quad (2.19e)$$

$$I_{XZ} = \int_{Body} xz \, dm \quad (2.19f)$$

Using equation (2.19) with equation (2.18) yields the components of the inertial angular momentum as

$$\begin{aligned}
 h_x &= PI_{xx} - QI_{xy} - RI_{xz} \\
 h_y &= -PI_{xy} + QI_{yy} - RI_{yz} \\
 h_z &= PI_{xz} - QI_{yz} + RI_{zz}
 \end{aligned}
 \tag{2.20}$$

The time-derivative of equation (2.20) is

$$\begin{aligned}
 \dot{h}_x &= \dot{P}I_{xx} - \dot{Q}I_{xy} - \dot{R}I_{xz} \\
 \dot{h}_y &= -\dot{P}I_{xy} + \dot{Q}I_{yy} - \dot{R}I_{yz} \\
 \dot{h}_z &= \dot{P}I_{xz} - \dot{Q}I_{yz} + \dot{R}I_{zz}
 \end{aligned}
 \tag{2.21}$$

The equations derived up to this point apply to any rigid body moving through space. The equations will now be applied more specifically to airframes.

### 2.3 Euler Angles

The solution of the equations of motion requires knowledge of the orientation of the helicopter relative to the axes of the inertial reference frame. The most common way of specifying this orientation is by the use of Euler Angles. Ashley (1974) describes the four ordered steps required to define the Euler angles shown in Figure 2.2 as follows:

- Place axes  $Cx_1y_1z_1$  with origin at the instantaneous centre of mass and directions parallel to  $x$ ,  $y$  and  $z$  (*the prime denotes the axes of the inertial reference plane*).
- Rotate the system through angle  $\Psi$  about the vertical direction  $Cz_1$  until the x-axis is in the vertical plane containing vehicle axis  $Cx$ . The new axes are called  $Cx_2y_2z_2$ ;  $z_2$  and  $z_1$  coincide.
- Rotate the system through angle  $\Theta$  about the horizontal direction  $Cy_2$  until the x-axis coincides with  $Cx$ . The new axes are called  $Cx_3y_3z_3$ ;  $y_2$  and  $y_3$  coincide.
- Rotate the system through angle  $\Phi$  about  $Cx_3 = Cx$  until the y- and z-axes coincide with the  $Cy$  and  $Cz$  axes.

Gravitation force components along the body axes are expressed in terms of the Euler angles by



$$\begin{aligned}
 F_{x_g} &= -mg \sin \Theta \\
 F_{y_g} &= mg \cos \Theta \sin \Phi \\
 F_{z_g} &= mg \cos \Theta \cos \Phi
 \end{aligned}
 \tag{2.22}$$

The total force components now become

$$\begin{aligned}
 F_x &= X + F_{x_g} \\
 F_y &= Y + F_{y_g} \\
 F_z &= Z + F_{z_g}
 \end{aligned}
 \tag{2.23}$$

in which  $X$ ,  $Y$  and  $Z$  are the sum of the aerodynamic and propulsive forces on the airframe.

## 2.4 The Equations of Motion

The equations of motion of an aircraft with six degrees of freedom can now be rewritten in its final form as

$$\begin{aligned}
 X - mg \sin \Theta &= m(\dot{U} + QW - RV) \\
 Y + mg \cos \Theta \sin \Phi &= m(\dot{V} + RU - PW) \\
 Z + mg \cos \Theta \cos \Phi &= m(\dot{W} + PV - QU)
 \end{aligned}
 \tag{2.24a}$$

$$\begin{aligned}
 L &= I_{xx} \dot{P} - I_{xz} \dot{R} + (I_{zz} - I_{yy})QR - I_{xz} PQ \\
 M &= I_{yy} \dot{Q} + (I_{xx} - I_{zz})RP - I_{xz}(P^2 - R^2) \\
 N &= I_{zz} \dot{R} + (I_{yy} - I_{xx})PQ - I_{xz} \dot{P} + I_{xz} QR
 \end{aligned}
 \tag{2.24b}$$

Equation (2.24a) and (2.24b) is the non-linear six degrees of freedom equations of motion of an airframe. Note that the last term in each of the subsections of equation (2.24b) is identically zero for a body with an xz-plane of symmetry. The effect of the asymmetry of a helicopter

about its  $xz$ -plane, however, is small enough that it can be assumed that the value of these terms are zero in the study of helicopter dynamics.

The motion can be separated into longitudinal and lateral motion. Each of these modes requires three equations to describe the motion. The  $X$ -force,  $Z$ -force and pitching moment equations describe the longitudinal mode while the  $Y$ -force, rolling moment and the yawing moment equations describe the lateral mode of motion.



### 3. Hover Analysis

The ability of a helicopter to hover gives it certain distinct advantages over fixed-wing aircraft. In hovering flight the helicopter is stationary relative to the inertial reference frame (see chapter 2). A full solution of the equations of motion is thus not necessary. The equations required to provide the information can be solved in closed form (no iteration is needed). The analysis of helicopters in hovering flight is thus less complicated than for helicopters in forward or vertical climbing flight.

Momentum theory is widely used in the analysis of the helicopter in hover. The momentum theory of actuator discs was discussed in paragraph 1.5.

The object of the hover analysis was to obtain information about the effect of the main rotor rotational velocity on the main and tail rotor collective as well as the torque and power required. Two computer programs were developed in order to achieve this goal.

The first of these was a real-time engineering simulator (Figure 3.1). It was used to investigate the effect of the controls on the helicopter's trim. The user can change the main rotor or tail rotor collective pitch as well as the main rotor rotational velocity. The program then computes the thrust produced, the power and torque required by the main rotor as well as the anti-torque generated by the tail rotor for each change in the control settings.

The second program was developed in order to observe the effect of changing the main rotor rotational velocity in graphical format. The change in main rotor and tail rotor collective pitch as well as the power and torque required with the change in main rotor rotational velocity was considered.

It is assumed that

- the rotor blades have a constant chord and constant drag coefficient
- the effect of blade stall and compressibility is negligible
- the lift coefficient is linearly related to the angle of attack (equation 1.2)
- the rotor blades have no twist

### 3.1 Aerodynamics in Hover

The most important characteristics to consider of helicopters in hover are thrust, power and torque required by the main rotor as well as the counter-torque produced by the tail-rotor.

The thrust-coefficient is defined by Johnson (1980) as

$$C_T = \frac{T}{\rho A (\Omega R)^2} \quad (3.1)$$

In order to maintain hover, the thrust produced by the main rotor must equal the weight of the helicopter. It is known that the amount of thrust produced is a function of the velocity of the air through the disc, as indicated by the study of momentum theory (equation 1.12). The velocity of the air through the disc is also called the inflow velocity. The induced inflow ratio is defined in terms of the main rotor speed  $\Omega$  and radius  $R$  as

$$\lambda_{ih} = \frac{v_{ih}}{\Omega R} \quad (3.2)$$

where  $\lambda_{ih}$  is the inflow ratio and  $v_{ih}$  is the inflow velocity in hover. This is the same as equation (1.31), but with the climbing velocity equal to zero. It was stated in the discussion on momentum theory that the induced velocity in hover was

$$v_{ih} = \sqrt{T/2\rho A} \quad (1.14)$$

In order to make equation (1.14) dimensionless, it must be divided by the main rotor tip speed as in equation (3.2). From the definition of the thrust coefficient, it is clear that in hover

$$\lambda_{ih} = \frac{v_{ih}}{\Omega R} = \sqrt{\frac{T}{2\rho A(\Omega R)^2}} = \sqrt{\frac{C_T}{2}} \quad (3.3)$$

According to equation (1.34)

$$dC_{Ph} = \lambda_{ih} dC_T + \frac{sC_{d0}}{2} r^3 dr \quad (1.34)$$

The first term in equation (1.34) is called the induced power loss of the differential element. This is created by the in-plane component of the lift due



to the induced angle of attack. It thus refers to the amount of power required in order to move the air through the actuator disc. This is illustrated by

$$dP_i = v_i dT \quad (3.4)$$

which is the equation of the induced power in hover.

The second term in equation (1.34) is the elemental coefficient of profile power loss. This is due to the viscous drag forces on the rotor blade. This factor is greatly dependent on the rotor profile drag coefficient. It is also a function of the incidence angle of the rotor blade. It is usual to express it as

$$c_d = \delta_0 + \delta_1 \alpha + \delta_2 \alpha^2 \quad (3.5)$$

where  $\delta_0$ ,  $\delta_1$  and  $\delta_2$  are constants.

It is however more common to assume that the drag coefficient is constant for easier analyses. Using this assumption, Johnson (1980) determined the power coefficient to be

$$C_p = \kappa \frac{C_T^{3/2}}{\sqrt{2}} \frac{s c_{d0}}{8} \quad (3.6)$$

where  $\kappa$  was used to estimate the induced losses of the rotor and usually had a value of about 1.15.

The thrust produced by the differential element was indicated by equation (1.29) to be

$$dC_T = \frac{s a}{2} (\theta r^2 - \lambda r) dr \quad (1.29)$$

Johnson (1980) combined momentum theory and blade element theory to show that

$$\lambda_{ih} = \frac{s a}{16} \left[ \sqrt{1 + \frac{32}{s a} \theta r} - 1 \right] \quad (3.7)$$

Substituting equation (3.7) into equation (1.29) yields

$$C_T = \int_0^1 \frac{sa}{2} (\theta r^2) dr - \int_0^1 \left( \frac{sa}{2} \right) \frac{sa}{16} \left[ \sqrt{1 + \frac{32}{sa} \theta r} - 1 \right] r dr \quad (3.8)$$

or

$$C_T = \frac{sa}{6} \theta_0 - \int_0^1 \frac{(sa)^2}{32} \left[ \sqrt{1 + \frac{32 \theta r}{sa}} - 1 \right] r dr \quad (3.9)$$

Equations (3.8) and (3.9) allow the calculation of the rotor thrust in terms of the collective pitch angle and the rotor blade properties.

The amount of torque required by the main rotor is

$$Q = P / \Omega \quad (3.10)$$

The tail rotor produces anti-torque to the amount of

$$Q_T = l_T T_T \quad (3.11)$$

The tail rotor thus requires a thrust of

$$T_T = \frac{P}{\Omega l_T} \quad (3.12)$$

The tail rotor thrust and power is calculated in exactly the same way as that of the main rotor.

### 3.2 Results

The analysis referred to in this paragraph was performed on the Hirobo Shuttle Z. The details of this helicopter are given in Appendix C.3. The following results were obtained from this analysis.

Figure 3.2 indicates that an increase in the main rotor rotational velocity causes a decrease in the figure of merit. The figure of merit is an indication of the rotor hovering efficiency. This figure compares the



actual rotor performance with the performance of an ideal rotor, which has only inescapable induced power loss:

$$M = \frac{P_{ideal}}{P_{actual}} = \frac{T v_h}{P_{actual}} = \frac{T \sqrt{T/2\rho A}}{P} \quad (3.13)$$

It is observed that an increase in the main rotor rotational speed corresponds to a large decrease in the figure of merit. This indicates that the rotor is not very efficient at high rotational velocities.

Figure 3.3 shows that an increase in the power supplied to the main rotor is required if the main rotor rotational speed is increased. Figure 3.4 was included to show the contribution of the tail rotor to the total power. These figures indicate a large increase in the amount of power required to drive the main and tail rotor with an increase in rotor speed. The large increase is due to the increase in the induced power losses (as indicated by the drastic decrease of the figure of merit) as the profile power loss is independent of the rotor speed (equation 3.6).

Although the main rotor power required increases with an increase in rotor speed, the amount of torque required to turn the rotor decreases (Figure 3.5). It is found from equation (3.1) that the thrust coefficient reduces in size as the rotor speed increases. The power coefficient thus decreases with increasing rotor speed, according to equation (3.6). Now, using Johnson's definitions

$$\frac{P}{\rho A (\Omega R)^3} = \frac{Q}{\rho A R (\Omega R)^2} \times \frac{\Omega}{\Omega} \quad (3.14)$$

or

$$C_p = C_q \quad (3.15)$$

Hence, the torque coefficient decreases with an increase in rotor speed as well. The quadratic dependence of  $C_q$  on the rotor speed is not large enough to cause an increase in the amount of torque required with an increase in rotor speed.

It is also observed that the amount of collective pitch required for both the main rotor and tail rotor decreases (Figure 3.6). This can be explained by equations (1.1) and (1.2). An increase in velocity over the rotor blade allows a decrease in the angle of incidence.



#### 4. VERTICAL CLIMBING FLIGHT

The previous chapter was dedicated to the analysis of a helicopter in hovering flight. This chapter is used to perform the analysis of a helicopter in vertical climbing flight. The helicopter is constrained to motion in one degree of freedom in vertical climbing flight. Hence the helicopter can only climb (or descend) without pitching or rolling. The yaw moment due to the action of the main rotor is trimmed out by using the tail rotor. The equation describing this motion is

$$Z + mg \cos\Theta \cos\Phi = m(\dot{W} + PV - QU) \quad (2.24a)$$

The aerodynamics and aeromechanics of a helicopter in vertical climbing flight is quite similar to that of a helicopter in hover. The inflow velocities in both cases are symmetrical with regards to the rotor disc and rotor shaft. The governing equations can also be solved in closed form in both cases. Once again momentum theory can be used to gain understanding of the helicopter in climbing flight.

##### 4.1 Flow States of the Rotor in Axial Flight

The main rotor of a helicopter can be considered to operate in different *states* while in axial flight. The classifications of these states are based on the flow of the air through and around the main rotor disc. This paragraph contains a discussion of the different rotor states that occur and relies heavily on Johnson (1980).

###### ***Normal working state***

The normal working state is valid for both climbing and hovering flight. While in a climb, the velocity throughout the flow field is downward with both  $V$  and  $v$  positive. Applying the conservation of mass theorem leads to the conclusion that the wake contracts downstream of the rotor disk. This is due to the increase in velocity of the air inside the wake. It is thus possible to use a wake model with a definite slipstream to analyse this flow state. Momentum theory yields a good estimate of performance of this state according to Johnson (1980).

It should be noted that hovering flight is the limit of the normal working state. Once again by considering the conservation of mass, it is found that the area of the slipstream becomes infinite upstream of the rotor. Even though there is some recirculation present at the rotor disc, the momentum theory is still quite accurate and produces a good estimate of the performance of the rotor.



**Vortex Ring State**

This flow state only occurs in descending flight. The flow inside and outside the slipstream in the far wake moves in opposite directions while in this state. It is due to this opposing motion of the air that the definite slipstream ceases to exist. Johnson (1980) reports that the power of the main rotor is

$$P = T(V + v_i) > 0 \quad (4.1)$$

This implies that the power extracted from the airstream is less than the induced power. If the descent rate is low in the vortex ring state, recirculation occurs near the disc and unsteady, turbulent flow develops above it. At a descent velocity of about

$$V = -\frac{1}{2} v_{ih} \quad (4.2)$$

the flow near the disc becomes highly unstable and turbulent. At descent velocities above this level, the helicopter experiences high vibration and even loss of control. While flying in this state it is very difficult to control the descent rate due to the fact that the power required is not very sensitive to changes in this rate.

**Turbulent Wake State**

For ideal autorotation

$$V + v_i = 0 \quad (4.3)$$

and hence no power would be required for descent if the rotor blade had no profile power loss. Even though there is nominally no flow through the disc, considerable recirculation and turbulence is present. Johnson describes this flow state to be similar to that of a circular plate of the same area with no flow through the disc, but with a turbulent wake above it.

**Windmill Brake State**

If the descent rates are large enough, the flow is smooth again. This is the so-called windmill brake state. Descent velocities of

$$V < -2v_{ih} \quad (4.4)$$

are classified as forming part of this state. The velocity is now upwards through the disc. The rotor extracts power from the air while

descending at these velocities. The boundary between the windmill brake state and the turbulent wake state is

$$V + 2v_h = 0 \quad \text{or} \quad V = -2v_h \quad (4.5)$$

The flow changes very abruptly at this boundary from a smooth slipstream to one with recirculation and turbulence. Hence, the validity of the momentum theory cease abruptly at the windmill brake state boundary.

## 4.2 Governing Equations

These governing equations apply to the normal working state. It was found from momentum theory that

$$v_i = -\frac{V_c}{2} + \sqrt{\left(\frac{V_c}{2}\right)^2 + v_{ih}^2} \quad (1.16)$$

which could be rewritten as

$$V_c + v_i = \frac{V_c}{2} + \sqrt{\left(\frac{V_c}{2}\right)^2 + v_{ih}^2} \quad (4.6)$$

The induced velocity is reduced by the climbing velocity because of the increased mass flow through the rotor disc. The power required for climbing is

$$P_c = T(V_c + v_i) + P_0 \quad (4.7)$$

where  $P_0 = P_{ih} - Tv_{ih}$  is the profile power. Assuming this to be constant

$$P_c = \Delta P + P_{ih} = T(V_c + v_i - v_{ih}) + P_{ih} \quad (4.8)$$

The power increment between climb and hover is

$$\Delta P = P_c - P_{ih} = T(V_c + v_i - v_{ih}) \quad (4.9)$$

Setting equation (4.6) into equation (4.9) and dividing by the amount of thrust, it is found that

$$\frac{\Delta P}{T} = \frac{V_c}{2} + \sqrt{\left(\frac{V_c}{2}\right)^2 + v_{ih}^2} - v_{ih} \quad (4.10)$$



This increase in power is required to accelerate the air through the rotor disc as well as to increase the rate of change of the potential energy.

There is an increase in thrust required due to vertical drag on the fuselage. To estimate the drag force, it is necessary to consider the downwash velocity in the fully developed rotor wake. This increase can be written in terms of an equivalent drag area,  $f$

$$\Delta T = \frac{1}{2} \rho (V_c^2 + 4v_{ih}^2) f \quad (4.11)$$

The equivalent drag area can be represented as the product of  $S$ , the planform area of the fuselage, and  $C_D$ , the flat-plate drag coefficient, as

$$f = S C_D \quad (4.12)$$

The fuselage is usually quite close to the rotor and it is not accurate to assume that it is in the far wake. Johnson (1980) assumes that the downwash velocity at the fuselage is  $n v_{ih}$  with

$$n = 1 + \frac{z/R}{\sqrt{1 + (z/R)^2}} \quad (4.13)$$

where  $z$  is the vertical distance from the rotor. It is obvious that  $n$  will vary from 1 near the rotor disc to 2 in the far wake. Now

$$\frac{\Delta T}{T} = \frac{n^2 f}{4 A} = \frac{S}{A} \left( \frac{n^2 C_D}{4} \right) \quad (4.14)$$

For climbing flight, this becomes

$$\frac{\Delta T}{T} = \frac{S}{A} C_D \left( \frac{V_c + n v_i}{2 v_h} \right)^2 \quad (4.15)$$

The control settings required to climb at a certain velocity can now be determined. It was seen in the discussion on the blade element theory that

$$C_T = \frac{s a}{2} \left( \frac{\theta_{.75}}{3} - \frac{\lambda_i}{2} \right) \quad (1.33)$$

or alternatively that

$$\theta_{.75} = 3 \left( \frac{2C_T}{sa} + \frac{\lambda_i}{2} \right) \quad (4.16)$$

According to Johnson (1980), the incremental collective pitch required for climbing flight is

$$\Delta\theta = \frac{3}{2} (\lambda_i - \lambda_{ih}) = \frac{3}{2} \frac{V_c + v_i - v_h}{\Omega R} \quad (4.17)$$

In terms of the power and thrust coefficient, equation (4.17) becomes

$$\Delta\theta = \frac{3}{2} \frac{\Delta C_P}{C_T} \quad (4.18)$$

The collective pitch setting for the main rotor can now be found by summing the value obtained from equation (4.18) with the value found in the hovering case

$$\theta = \theta_h + \Delta\theta \quad (4.19)$$

The tail rotor collective setting is determined by calculating the torque required for the main rotor and then determining the thrust required by the tail rotor. This is similar to the method used in the hovering case.

### 4.3 Results

In this paragraph, the Hirobo Shuttle Z (see Appendix C.3) was once again used as the subject for the analysis. The following results were obtained from this analysis.

It can be seen from Figure 4.1 that the incremental power required for climbing flight is independent of the main rotor rotational speed. This can be explained by referring to equation (4.9). None of the terms on the right hand side of the equation is affected by the main rotor rotational velocity.

It is further observed that the incremental power increases almost linearly with increasing climbing velocity. Johnson states that for small climb rates

$$V_c + v_i \approx \frac{V_c}{2} + v_h \quad (4.20)$$



Hence equation (4.9) can be reduced to

$$\frac{\Delta P}{T} \approx \frac{V_c}{2} \quad (4.21)$$

Any climbing velocities

$$V_c < v_h \quad (4.22)$$

are classified as small climbing rates (in the numerical example used,  $v_h = 2.97$  m/s). A sample calculation at a climbing velocity of 1 m/s was made to test this statement.

$$\Delta P = T \frac{V_c}{2} = 26.1204 \times \frac{1}{2} = 13.06 \quad (4.23)$$

The same value was calculated as 14.15 using the numerical analysis. This represented an error of 8.35%. Equation (4.21) thus seems to be reasonably accurate for small climbing velocities.

Figure 4.2 indicates that the required amount of main rotor collective pitch increases with an increase in climbing speed. It is observed that the required amount of incremental collective pitch increases with a reduction in main rotor rotational velocity. Upon the assumption of small climbing velocities, the simplification can be made that

$$\Delta\theta \approx \frac{3}{2} \frac{V_c}{2} \frac{1}{\Omega R} = \frac{3}{4} \lambda_c \quad (4.24)$$

A sample calculation at a climbing velocity of 1 m/s and with a main rotor rotational velocity of 1000 RPM yields

$$\Delta\theta = \frac{3}{4} \times \frac{1}{1000 \times 2\pi / 60 \times 0.618} \times \frac{180}{\pi} = 0.664 \quad (4.25)$$

The analysis predicted a value of 0.72, indicating an error of 8.43% upon comparison with the simplified equation (4.24).

The main rotor collective setting required for climbing flight is shown in Figure 4.3. It can be seen that the amount of collective pitch required for climbing is the highest for the lowest main rotor rotational speed setting. Apart from the reduced increase required for higher main rotor

rotational velocities (Figure 4.2), higher rotational velocities also require lower collective pitch settings in hover (Figure 3.6).

Figure 4.4 illustrates that the tail rotor collective setting follows the same form as the main rotor collective. The increase in tail rotor collective can be attributed mainly to the increase in the torque required to drive the main rotor. This, in turn, increased the amount of thrust required by the tail rotor in order to provide the necessary counter torque.

The total power required for climbing is illustrated in Figure 4.5. It is observed that the increase in main rotor rotational velocity is accompanied by a large increase in the amount of power required. For the model used in the analysis, the ratios of power required for 1000 RPM, 1100 RPM and 1200 RPM was found to be 1:1.06:1.13.

Table 4.1 indicated the increase in power required to increase the climbing rate from 1m/s to 1.5 m/s. That table was constructed with disregard of the fact that engines are limited to the amount of power they can produce. All engines are however limited in the amount of power it can deliver. If the engine in the Hirobo Shuttle Z could produce a maximum of 145 W, the following performance table could be compiled:

#### **4.4 Conclusion**

This section utilised a computer program that was developed to analyse a helicopter in climbing flight. This program is contained in Appendix A.2. The analysis of the helicopter in axial flight focussed on the effect of the main rotor speed on the trim of the helicopter.

It was shown that Johnson's (1980) assumption of small climbing velocities is valid and produced reasonable estimates of the incremental power and collective pitch required in vertical climbing flight.

As with hovering flight, it was shown that higher main rotor rotational velocities allowed lower settings of the main rotor collective pitch required. This came at a considerable cost in power required however. Although the incremental additional amount of power required for climbing flight was independent of the main rotor rotational velocities, the power required in hovering increased with an increase in this figure.



It was shown in Table 4.1 that the amount of additional power required to increase the climbing rate of the helicopter was decreased with an increase in main rotor rotational velocity.

An interesting observation could be made from Table 4.2. Although more main rotor collective pitch would be required, higher climbing velocities could be obtained at a certain power setting using lower main velocity rotational velocities. The reason for this was that less power would be lost to the profile power requirement. If the induced power losses could be minimised, more power would be available for increasing the potential energy of the helicopter. This increase in potential energy would of course be realised as an increase in height.

## 5. TRIM IN FORWARD FLIGHT

In the previous chapters, the trim settings were calculated for helicopters using closed-form equations. In chapter three, the trim settings of a helicopter in hovering flight was analysed and the effect of the main rotor rotational velocity on these settings was observed. In chapter four, this analysis was extended to include vertical climbing flight. Once again, the effect of the main rotor rotational velocity on the trim settings was investigated.

Both hovering and vertical climbing flight have the following in common:

- The inflow velocity distribution is axially symmetrical.
- The only controls required by the pilot are the main rotor and tail rotor collective pitch and the throttle.

In forward flight, however, the shape of the inflow velocity distribution over the rotor disc is no longer symmetrical. The amount of thrust required also increases in forward flight.

This chapter will outline the calculation of the trim settings of a helicopter in forward flight. The trim problem is concerned with the control positions required to hold a specific aircraft in equilibrium. The solution of the trim settings does not necessitate straight and level flight. The aircraft may be turning, diving or climbing, as long as the three translational velocities remain constant with fixed controls. If this condition is met, the aircraft is said to be in trim.

Strictly speaking, an aircraft in climbing and descending flight cannot be considered to be in trim, due to the fact that the changing air-density will require corrections to the control to keep the velocities constant. These changes are negligible however and the aircraft can be considered to be in trim if the analysis is conducted over a short time-span.

Performing a trim analysis is an important step in the analysis of the helicopter. This is mainly because the trim analysis offers answers to questions about the mechanics of the aircraft (both rotary-wing and fixed-wing aircraft). The trim analysis is also a very important step towards determining the stability and control derivatives of the aircraft.



Stability and control derivatives are used to indicate the effect of changing certain parameters on the forces and moments that are acting on the aircraft. The trim settings of the helicopter are required to calculate these derivatives. The work described in this chapter is thus an important step in obtaining the stability and control characteristics of the helicopter.

## 5.1 Trim in Straight and Level Flight

The simplest trim state is straight and level flight. Let us first investigate a very simple model of a helicopter in trim flight. In this model, the helicopter only consists of a main rotor, a tail rotor and a fuselage that only experiences drag. The rotor is assumed to be teetering in flap and that no moments are transmitted to the fuselage via the hub. It is assumed that the centre of mass lies on the rotor shaft below the rotor. It is also assumed that the pitch and roll attitudes are small. Taking a balance of forces in the vertical direction yields

$$T \approx W \quad (5.1)$$

According to Padfield (1996) this assumption is true for most helicopters even up to moderate forward speeds. If a force balance is taken along the waterline of the fuselage (the x-axis), the approximate pitch angle is found to be

$$\vartheta \approx -\frac{D}{T} \quad (5.2)$$

Padfield further states that the thrust can be assumed to remain essentially constant in trimmed straight flight. Hence the pitch varies only with the drag force ( $D$ ) according to equation (5.2). Furthermore, the drag force is usually dependent on the square of the velocity. It should be remembered that this model disregards any pitching moments due to the fuselage or due to the rotor disc.

An estimate of the tail rotor thrust can be made by dividing the main rotor torque required by the tail rotor arm

$$T_T \approx \frac{Q_R}{l_T} \quad (5.3)$$

It can thus be seen that the tail rotor thrust will display the same characteristics as those displayed by the main-rotor torque. A graph of



main rotor torque vs. forward speed will display the characteristic “bucket” at the speed required for minimum-power flight. The tail rotor will thus also require the minimum thrust at this speed.

It is usual for the tail rotor to be vertically offset from the centre of gravity of the helicopter. The tail-rotor thus induces a rolling moment in the helicopter. This rolling moment must be countered by lateral disc-flapping. The value of the lateral disc flapping required is found to be

$$b_1 \approx \frac{h_T T_T}{h_R T} \quad (5.4)$$

Equation (5.4) describes the lateral flapping angle of the rotor disc and should not be confused with the lateral control angle. The height of the tail rotor is represented by  $h_T$  while  $h_R$  is the height of the main rotor above the helicopter centre of gravity

A rotor of a helicopter with a rotor turning in an anti-clockwise direction will tilt to the left (looking forward over the nose of the helicopter). The roll angle of the helicopter can be found by taking a sum of the side forces. The roll angle is the only unknown and can be determined from

$$\phi \approx \frac{T_T}{m_a g} \left( 1 - \frac{h_T}{h_R} \right) \quad (5.5)$$

In equation (5.5),  $m_a$  is the mass of the helicopter. It can further be seen from equation (5.5) that the helicopter must roll in order to cancel out the moment generated by the tail rotor (it is assumed that the tilting of the disc creates no extra rolling moment that has to be counteracted). Table 5.1 indicates the roll angle as a ratio of tail rotor thrust for some helicopters. From this table and equation (5.5) it was observed that the roll angle of the helicopter is influenced by the ratio of  $h_T$  to  $h_R$ .

It is also observed from equation (5.5) that the roll angle is dependent on the tail rotor thrust. The amount of tail rotor thrust required is a function of the torque required by the main rotor and the length of the tail rotor arm. The more torque required by the main-rotor, the more roll angle will occur. The roll angle can thus be written in terms of the main rotor torque required as



$$\phi \approx \frac{Q_R}{I_T m_a g} \left( 1 - \frac{h_T}{h_R} \right) \quad (5.6)$$

Padfield (1996) comments that this model is not a realistic representation of helicopter dynamics. The forces generated in the plane of the rotor-disc (the H- and S-forces) as well as the moments generated by the rotor disk have a significant influence on the resulting rolling angle. The fuselage does not only experience drag, but also generates a pitching moment. This model is however useful in illustrating some of the basic mechanics of helicopter flight.

## 5.2 General Trim Problem

The analysis of a helicopter in straight and level flight was discussed in the previous paragraph. This is however not the most general case of helicopter flight. In the general trim problem, the aircraft may be turning, climbing, descending or sideslipping.

The most general trim condition is a steady rotation around a fixed vertical axis at constant pitch and roll angles. This also causes the gravitational force components to be constant. It must however be remembered that the general condition does still require that the rate of change of the magnitude of the velocity vector be identically zero.

Consider the three force and three momentum equations of motion (equations 2.24a and 2.24b) adjusted for trimmed flight. The subscript e refers to the equilibrium or trim state

$$-(W_e Q_e - V_e R_e) + \frac{X_e}{m_a} - g \sin \Theta_e = 0 \quad (5.7)$$

$$-(U_e R_e - W_e P_e) + \frac{Y_e}{m_a} + g \cos \Theta_e \sin \Phi_e = 0 \quad (5.8)$$

$$-(V_e P_e - U_e Q_e) + \frac{Z}{m_a} + g \cos \Theta_e \cos \Phi_e = 0 \quad (5.9)$$

$$(I_{YY} - I_{ZZ}) Q_e R_e + I_{XZ} P_e Q_e + L_e = 0 \quad (5.10)$$

$$(I_{ZZ} - I_{XX}) R_e P_e + I_{XZ} (P_e^2 - R_e^2) + M_e = 0 \quad (5.11)$$

$$(I_{XX} - I_{YY}) P_e Q_e - I_{XZ} Q_e R_e + N_e = 0 \quad (5.12)$$

The applied forces and moments are, to first order approximation, linear functions of the perturbations of the translational velocities ( $u, v, w$ ), the angular velocities ( $p, q, r$ ) and the rotor controls ( $\theta_0, \theta_{1s}, \theta_{1c}, \theta_{0T}$ ).

The angular velocity components in the x-, y- and z-directions are determined by using the Euler angles as

$$P_e = -\dot{\Psi}_e \sin \Theta_e \quad (5.13)$$

$$Q_e = \dot{\Psi}_e \cos \Theta_e \sin \Phi_e \quad (5.14)$$

$$R_e = \dot{\Psi}_e \cos \Theta_e \cos \Phi_e \quad (5.15)$$

where  $\dot{\Psi}_e$  is the turn rate of the helicopter.

The motion of the helicopter is fully described by equations (5.7) to (5.15). There are thirteen variables present in these nine equations. This system is thus over-determined and any four of these thirteen variables can be prescribed arbitrarily. Some groupings of these four variables are more popular and useful in practice than others. In one such grouping, the following four variables are prescribed:

$V_{fe}$             flight speed

$\gamma_{fe}$             flight path angle (with regards to the horizon)

$\Omega_{ae} = \dot{\Psi}_e$     turning rate of the fuselage (not the main rotor)

$\beta_e$             sideslip

This grouping of prescribed variables is useful, because it allows the engineer to prescribe the flight path and velocity of the helicopter. The movement of the helicopter through the air is thus specified by these four



variables. The rest of the variables that needs to be solved are concerned with the control values and effects of applying these controls. This is similar to a pilot who wants to fly a certain trajectory between two points at a certain speed. After deciding on the trajectory and speed, the pilot applies the required controls in order to obtain this flight path.

### **5.3 Calculating the Trim Settings of a Helicopter in Forward Flight**

The full solution of the trim settings of a helicopter in general flight would require the simultaneous solution of all the equations of motion plus the three auxiliary equations describing the Euler angles. This makes nine equations that have to be solved simultaneously. The solution of these equations implies the selection (or calculation) of the nine unknown variables such that there would be no resultant forces or moments on the helicopter.

It is a well-known fact that a vehicle with an xz symmetry plane does not have inertial coupling between the longitudinal and lateral modes of motion. Helicopters do not possess this symmetry plane in general due to the presence of the tail rotor and the cyclic flapping of the main rotor. Coupling would thus occur between the longitudinal and lateral modes of motion. These couplings would manifest in pitching and yawing moments due angular accelerations in roll or yaw, etc. Complex computational methods must be used in order to find the trim solution for aircraft with coupling between the longitudinal and lateral modes of motion.

According to Bramwell (1976) it is not necessary, for practical purposes, to solve all of these equations simultaneously. The fact that a lot of the aerodynamic data required in these equations are not accurate enough to justify the necessity of the full solution is given as another reason why decoupling can be performed. It was assumed that the amount of coupling between the longitudinal and lateral modes would be negligible in the derivation of the equations of motion set out in the rest of this chapter. This allowed the analysis of the trim characteristics of the helicopter to be split into two smaller analyses: an analysis of the longitudinal mode of motion and an analysis of the lateral mode of motion.

It was assumed that the rotor blades had constant two-dimensional lift-curve slopes and that the lift coefficient would thus be a linear function of the angle of incidence, as explained in equation (1.6). It was also assumed that the rotor blades had constant profile drag coefficients. This



would allow the analysis to make use of lifting line theory as set out in the description of the blade element theory in paragraph 1.8. It was further assumed that blade stall would not occur at any flight speed.

While deciding on the reference plane for the rotor disc, it was decided to choose the reference plane that would allow the most simplification of the equations used in the analyses. One such possible simplification was the reduction of the size of the H-force (see paragraph 1.2) by working in the rotor tip-path plane. The resultant rotor force was found to be nearly perpendicular to this plane. This had the effect that the H-force (or rotor drag force) was rather small in this reference frame.

Using the rotor tip-path plane had further benefits. These included the ease of establishing the rotor disc incidence in this plane, as well as the ease of calculating and using the force coefficients. With the help of these, the unknown variables could be obtained more easily. It was thus decided to perform the analyses of the trim settings of the helicopter in forward flight using the rotor tip-path plane.

### 5.3.1 Longitudinal Trim

Let us observe a helicopter in forward flight making the assumption that the amount of coupling between the longitudinal and lateral modes of motion is negligible (this paragraph is based on the work of Bramwell, 1976). Make the further assumption that the helicopter is experiencing no sideslip. Using the subscript  $D$  to refer to the forces and moments in the tip-path plane and resolving the forces vertically

$$T_D \cos(\alpha_D + \tau) - H_D \sin(\alpha_D + \tau) = W + D \sin \tau \quad (5.16)$$

Resolving the forces horizontally

$$T_D \sin(\alpha_D + \tau) + H_D \cos(\alpha_D + \tau) = -D \cos \tau \quad (5.17)$$

In steady flight, the inclination of the rotor disc plane to the horizontal is usually quite small, and if  $\tau$  is small too, then

$$\sin(\alpha_D + \tau) \approx \alpha_D + \tau \quad \text{and} \quad \cos(\alpha_D + \tau) \approx 1 \quad (5.18)$$



Equations (5.16) and (5.17) then reduces to

$$T_{cD} \approx T = W + D \sin \tau \quad (5.19)$$

$$T(\alpha_D + \tau) + H_D = -D \cos \tau \quad (5.20)$$

It should be remembered, however, that the disc incidence angle and the flight path angle may both be large angles, for example, both are in the region of  $90^\circ$  for vertical flight, in which case equations (5.16) and (5.17) must be used as is.

### **Drag Model**

At this point it becomes necessary to model the drag of the fuselage. One way of doing this is to work with the so-called flat-plate area of the fuselage. In this model, the helicopter is seen (for methods of determining drag) as a two-dimensional flat-plate. The equivalent drag area is calculated in such a manner that the drag-force is equal to the actual drag experienced on the fuselage body. Hence, it is usually necessary to determine the equivalent flat-plate area experimentally. If equivalent flat-plate area  $f$  is known, it can be said that

$$D = \frac{1}{2} \rho V^2 f C_D \quad (5.21)$$

White (1999) reported that the drag coefficient of a two-dimensional flat plate is equal to two.

In the absence of accurate models to represent the change of drag with the change in pitch, two other models were used. The first of these was a rectangular prism. The frontal area (with zero pitching) was approximately equal to that of the helicopter and the length was selected based on the approximate fuselage length. The equivalent flat-plate area is

$$f = w(h|\cos \theta| + l|\sin \theta|) \quad (5.22)$$

In equation (5.22),  $w$  is the width,  $h$  the height and  $l$  the length of the helicopter's fuselage.

The second model was a cylindrical prism. Once again, the frontal area in steady flight was approximately equal to that of the helicopter. The change in equivalent flat-plate area was calculated to be

$$f = 2l r_c |\sin \theta| + \pi r_c^2 |\cos \theta| \quad (5.23)$$

In equation (5.22),  $r_c$  is the radius of the circular flat-plate area of the model and  $l$  is the length of the fuselage. In both of these models, the value of the drag coefficient is still equal to two, although the value of the equivalent flat-plate area changes. The cylindrical prism produced results that represented previously published data more closely.

### **Normalization**

Following Bramwell (1976), equations (5.19) and (5.20) are converted to coefficient form by normalizing with respect to  $\rho s A \Omega^2 R^2$ , which yields

$$t_{cD} = w_c + \frac{1}{2} \hat{V}^2 d_0 \sin \tau \quad (5.24)$$

and

$$t_{cD} (\alpha_D + \tau) + h_{cD} = -\frac{1}{2} \hat{V}^2 d_0 \cos \tau \quad (5.25)$$

In these equations

$$d_0 = f / s A \quad (5.26)$$

is the non-dimensional equivalent flat-plate area and

$$\hat{V} = \frac{V}{\Omega R} \quad (5.27)$$

is the air speed normalized with respect to the tip-speed. From equation (5.25) the disc incidence can be solved as

$$\alpha_D = -\left( \frac{1}{2} \hat{V}^2 d_0 \cos \tau + h_{cD} \right) / t_{cD} - \tau \quad (5.28)$$



Bramwell (1976) states that in cases where the rotor-disc incidence is fairly small (as is the case in normal forward flight conditions), it is usual to assume that

$$t_{cD} = w_c \quad (5.29)$$

### **H-Force coefficient**

The only remaining unknown quantity in equation (5.28) is the H-force coefficient. In the tip-path-plane axis, this coefficient can be written in terms of the longitudinal flapping coefficient and the collective pitch.

$$h_{cD} = \frac{1}{4} \mu \delta + \frac{a \lambda_D}{4} \left[ \frac{1}{2} a_1 - \mu \theta_0 \right] \quad (5.30)$$

According to Bramwell it appears from numerical calculations that the most important term of (5.29) is the first one. This is the term that represents the rotor profile drag. Hence, as a first approximation

$$h_{cD} \approx \frac{1}{4} \mu \delta \quad (5.31)$$

In equation (5.30) the speed ratio  $\mu$  is introduced is defined as

$$\mu = \frac{V}{\Omega R} \cos \alpha_{nf} = \hat{V} \cos \alpha_{nf} \quad (5.32)$$

The no-flapping incidence angle  $\alpha_{nf}$  is usually quite small so that it is acceptable to assume that

$$\mu \approx \hat{V} \quad (5.33)$$

The inflow ratio can be calculated from the equation

$$\lambda_D = \mu_D \tan \alpha_D - \lambda_i \approx \mu_D \alpha_D - \lambda_i \quad (5.34)$$

### **Inflow velocity and inflow ratio**

It can be seen from equation (5.34) that the inflow velocity ratio is required next. Glauert's method was used to determine the inflow velocity. The reason for this was that the less complicated  $1/V$  approximation was

not very accurate at low speeds. The so-called “thrust-velocity” is defined as

$$U_T = \sqrt{\frac{T}{2 \rho A}} \quad (5.35)$$

which is the same as the induced velocity  $v_{ih}$  in hovering flight at the same rotor thrust. Further, a normalized velocity is defined as

$$\bar{V} = V / U_T \quad (5.36)$$

The inflow velocity can be determined by first calculating

$$\bar{v}_i = \sqrt{\frac{-\bar{V}^2 + \sqrt{\bar{V}^4 + 4}}{2}} \quad (5.37)$$

and then

$$v_i = \bar{v}_i U_T \quad (5.38)$$

The inflow velocity ratio is

$$\lambda_i = \frac{v_i}{\Omega R} \quad (5.39)$$

The inflow velocity referenced to the tip-path-plane is found from equation (5.34).

### ***Longitudinal control to trim***

To perform the trim calculations, the governing equations had to be referenced to a certain set of axes. These trim calculations were referenced to the body axes (see paragraph 1.4). This was done in accordance with the work of Bramwell (1976) on which this paragraph is based. Heights and distances were written as fractions of the main rotor diameter. Hence the height of the rotor above the centre of gravity was written as  $hR$  and the distance to the centre of gravity from the rotor shaft was written as  $fR$ . The origin of moments is defined as the point on the shaft that is met by the perpendicular from the center of gravity. Taking



moments about the origin of moments and making the small-angle assumption, Bramwell (1976) arrived at the equation

$$-W fR - T hR B_{1nt} + H hR + M_f - M_s (B_{1nt} - a_1) = 0 \quad (5.40)$$

In equation (5.40)  $M_f$  is the fuselage pitching moment.  $M_s$  is the centrifugal moment per unit tilt of the blades and can be calculated as

$$M_s = \frac{1}{2} b S_1 e R \quad (5.41)$$

where  $S_1$  is the centrifugal force of a rotor blade. The longitudinal control input was determined from equation (5.40) by assuming that  $T_D = W$  and solving for  $B_{1nt}$ . Bramwell (1976) solved this in non-dimensional form as

$$B_{1nt} = a_1 + \frac{C_{mf} + h_{cD} h - w_c f}{w_c h + C_{mS}} \quad (5.42)$$

where the subscript  $nt$  refers to the longitudinal control input for a helicopter with no tail. In equation (5.42)

$$C_{mf} = M_f / \rho s A \Omega^2 R^3 \quad (5.43)$$

and

$$C_{mS} = \frac{b M_b x_g e}{2 \rho s A R} \quad (5.44)$$

It is obvious from equation (5.44) that  $C_{mS}$  will be zero if there is no hinge offset. The value of the longitudinal control input  $B_{1nt}$  is related to the amount of longitudinal flapping. It was thus necessary to know the amount of longitudinal flapping that the rotors experienced in order to determine the longitudinal control input.

The longitudinal flapping in the tip-path-plane is a function of the main rotor collective pitch, the velocity ratio and the induced velocity ratio. It is found by firstly assuming that the flapping can be expressed in the form of a Fourier series. The flapping values are entered into the flapping differential equation and the coefficients are collected. Bramwell (1976) determined the longitudinal flapping angle in disc axes to be

$$a_1 = \frac{2\mu \left( \frac{4}{3} \theta_0 + \lambda_D \right)}{1 + \frac{3}{2} \mu^2} \quad (5.45)$$

The thrust produced by a helicopter's rotor could be found by integrating the average value of the differential thrust coefficient over the azimuth range. The elemental thrust coefficient was in turn determined by integrating the elemental thrust coefficient over the length of the rotor blade. Bramwell (1976) derived an expression for the thrust coefficient as

$$t_{cD} = \frac{a}{4} \left[ \frac{2}{3} \theta_0 \frac{1 - \mu^2 + \frac{9}{4} \mu^4}{1 + \frac{3}{2} \mu^2} + \lambda_D \frac{1 - \frac{\mu^2}{2}}{1 + \frac{3}{2} \mu^2} \right] \quad (5.46)$$

This expression can now be solved in order to obtain a first estimate for the required main rotor collective pitch setting by writing it in terms of  $\theta_0$ .

### **The tail plane**

It is assumed that the effect of the tail plane can be isolated from the rest of the fuselage. The lift produced by the tail plane is dependent on the incidence angle of the air at the tail plane. The incidence angle is influenced by the zero-lift line of the tail plane,  $\alpha_s$ , as well as the downwash angle  $\varepsilon$ . The downwash angle is usually found by empirical methods. The incidence angle of the tail plane is

$$\alpha_T = \theta - \tau + \alpha_s - \varepsilon \quad (5.47)$$

Bramwell (1976) reported that Heyson and Katzoff measured and calculated values for the downwash downwind of the main rotor. This data was published in the form of empirical equations. Unfortunately, the lack of analytical means of determining the downwash downstream of the rotor makes it very difficult to calculate the downwash angle. A first approximation of this angle was taken as

$$\varepsilon = v_{ih} / V = \varepsilon_0 \quad (5.48)$$



The tail plane generates an aerodynamic force. A pitching moment exists due to the distance between the centre of gravity and the centre of pressure of the tail plane. This pitching moment is derived by Bramwell (1976) as

$$M_T = -\frac{1}{2} \rho V^2 S_T l_T R a_T (\alpha_D - B_1 + a_1 + \alpha_s - \varepsilon) \quad (5.49)$$

in which  $S_T$  is the area of the tail plane,  $a_T$  the lift slope of the tail plane and  $l_T$  is the distance between the centre of gravity and the centre of pressure of the tail plane. The value of the longitudinal control input is now different from that reported in equation (5.42) as it includes the presence of a tail. The contribution of the tail can be added to the value that was calculated without the tail plane as  $B_1 = B_{1nt} + \Delta B_{1t}$ . Bramwell (1976) derived the value of the longitudinal control input as

$$B_1 = a_1 + \frac{C_{mf} + h_{cD}h - w_c f - \frac{1}{2} \mu^2 \bar{V}_T a_T (\alpha_D + B_1 - a_1 + \alpha_s - \varepsilon)}{w_c h + C_{ms}} \quad (5.50)$$

in which the tail volume ratio is defined by

$$\bar{V}_T = \frac{S_T l_T}{s A} \quad (5.51)$$

In some helicopters (like the AH1-G Huey Cobra), the tail plane is linked to the longitudinal cyclic pitch, so that the angle of the zero-lift line relative to the free stream changes with a change in the longitudinal control input. In order to account for this implicit relationship between the angle of the zero-lift line and the longitudinal control input, it was necessary to utilize iterative algorithms.

At this point, one is able to perform the trim analysis for the longitudinal case. The next paragraph discusses the lateral trim characteristics.

### 5.3.2 Lateral Trim

The amount of thrust produced by the tail rotor is a very important variable to consider in the lateral trim case. Under normal flying operations, the

main rotor torque is balanced by the counter torque produced by the tail rotor as well as the vertical fin, or

$$T_{TR} + T_{vf} = Q / l_T R \quad (5.52)$$

If the contribution of the vertical fin is zero, the torque must be balanced by the tail rotor alone. This situation may occur if the incidence angle on the vertical fin is zero, or if no vertical fin is fitted to the helicopter.

The torque  $Q$  required in equation (5.52) is expressed in terms of the torque coefficient  $q_c$  by

$$Q = q_c \rho s A \Omega^2 R^3 \quad (5.53)$$

in which  $q_c$  is the torque coefficient. The torque coefficient was determined by integrating the elemental torque on a blade element. It was found that there was torque required to overcome the profile drag as well as the induced torque. Bramwell (1976) calculated the torque coefficient as

$$q_c = \frac{\delta}{8} (1 + 3\mu^2) - \lambda_D t_{cD} - \mu h_{cD} \quad (5.54)$$

### **Lateral flapping**

In order to calculate the amount of lateral flapping, the coning angle must be determined first. The coning angle was derived by Bramwell (1976) to be

$$a_0 = \frac{\gamma}{8} \left[ \theta_0 \frac{1 - 19\mu^2/18 + 3\mu^4/2}{1 + 3\mu^2/2} \right] + \frac{\gamma}{8} \left[ \frac{4}{3} \lambda_D \frac{1 - \mu^2/2}{1 + 3\mu^2/2} \right] \quad (5.55)$$

Mil' et al (1966) calculated the lateral flapping coefficient as

$$b_1 = \frac{4\mu a_0 / 3}{\left(1 + \frac{1}{2}\mu^2\right)} \quad (5.56)$$



Mil' and Nekrasov (1966) based this equation on the assumption that the induced velocity is nearly constant over the blade. It is this assumption that causes differences with the values reported by Bramwell (1976). This equation can be adjusted with empirical factors to account for the variation in the induced velocity. Equation (5.56) was favoured in the absence of such empirical information.

The lateral cyclic pitch control angle and roll angle could be determined by taking the sum of moments and the sum of forces about the centre of gravity and solving for either in turn. Bramwell (1976) determined these to be

$$A_1 = - \frac{(W f_1 R + M_S b_1 + T_{TR} h_{TR} R)}{(W hR + M_S)} \quad (5.57)$$

and

$$\phi = \frac{-T_{TR} + Y_S + F_{fn}}{W} - A_1 \quad (5.58)$$

The side force generated by the main rotor in forward flight  $Y_S$  in equation (5.58) is defined by

$$Y_S = \frac{1}{2} \rho_s R^4 \Omega^2 a C_Y \quad (5.59)$$

in which  $C_Y$  has been shown by Johnson (1980) to be

$$C_Y = b_1 \left( \theta_0 \left( \frac{1}{3} + \frac{1}{2} \mu^2 \right) + \frac{3}{4} \left( \lambda_i + \frac{1}{3} a_1 \mu \right) \right) - \frac{3}{2} a_0 \mu \left( \lambda_i + \frac{1}{2} \theta_0 \right) + a_0 a_1 \left( \frac{1}{3} - \mu^2 \right) \quad (5.60)$$

Bramwell (1976) excluded this force from his model. Numerical analyses however showed that the force due to the vertical fin was not negligible upon comparison with the tail rotor force. The force generated by the vertical fin is calculated as

$$F_{f_n} = \frac{1}{2} \rho V^2 S_{f_n} \alpha_{f_n} a_{f_n} \quad (5.61)$$

In equation (5.61),  $S_f$  is the area and  $a_f$  the two-dimensional lift curve slope of the vertical fin while the incidence with no sideslip is  $\alpha_f$ .

### **Tail rotor control angle**

The collective pitch of the tail rotor can be adjusted on helicopters, but the cyclic pitch of the tail rotor can usually not.

The tail-rotor collective setting is required for a specific set of flight parameters. Let the solidity, rotor area and tip speed of the tail-rotor be denoted by  $S_{TR}$ ,  $A_{TR}$  and  $\Omega_{TR} R_{TR}$ . Define the tail-rotor thrust coefficient as

$$t_{cT} = T_T / \rho S_{TR} A_{TR} \Omega_{TR}^2 R_{TR}^2 \quad (5.62)$$

The inflow velocity through the tail-rotor disc can be determined in exactly the same fashion as for the main-rotor. The calculation of this is similar to calculating the inflow velocity of the main rotor. Hence equations (5.35) to (5.39) are applied to the tail rotor in the analysis. It must however be remembered that in these equations, the thrust, rotor radius, area and rotational speed must be those of the tail-rotor. Padfield (1996) calculated the tail-rotor collective pitch control angle as

$$\theta_T = \frac{3(2 t_{cT} / a + \lambda_{iT} / 2)}{\left(1 + \frac{3}{2} \mu^2\right)} \quad (5.63)$$

After the tail rotor collective pitch have been calculated, the thrust produced by the tail rotor can be calculated by merely using a straight forward variation of equation (5.46).

## **5.4 Verification of Calculated Trim Settings**

The aim of this paragraph was to verify the computer program that performed the trim analysis. The results from the program are compared



to those of Siepker (1990) and Heffley (1979), both of whom performed the trim analysis of the AH1-G Huey Cobra.

#### **5.4.1 Fuselage Attitude**

Figure 5.1 shows that the fuselage pitch angle predicted by the current analysis closely resembles the results of Siepker. The rather unusual curve is due to the connection of the moveable tail to the longitudinal cyclic control input. It is not known whether Heffley accounted for this occurrence.

The largest discrepancy is seen to occur at a forward speed of 10 knots. At this point, the error was found to be 8.68%. The rest of the graph was very similar to Siepker's results. It can thus be assumed that the current analysis is accurate enough in predicting the pitch angle of the fuselage for the purpose of calculating the stability and control derivatives.

#### **5.4.2 Longitudinal Cyclic Pitch Input**

The contribution of the horizontal stabilizer must be known in order to calculate the value of the longitudinal cyclic pitch input. The contribution of the horizontal stabilizer is however dependent on the value of the longitudinal cyclic pitch input, as indicated in equation (5.49). This implicit relationship requires an iterative solution method in order to solve both these equations.

The current computer program yields results very similar to those predicted by Siepker. The largest discrepancy in the comparison was 12.4% and occurred at a forward speed of 10 knots. The errors at the other points of comparison were quite small and the graph can be seen to follow the values as calculated by Siepker. From this, it can be accepted that the computer program calculated the longitudinal cyclic pitch correctly. The results of the analysis are shown graphically as Figure 5.2.

#### **5.4.3 Collective Pitch**

The collective pitch values obtained from the analysis was compared to the results of Siepker and Heffley in Figure 5.3 in which the abbreviation MR refers to the main rotor, while TR refers to the tail rotor. The largest discrepancy found in the calculation of the main rotor collective pitch was less than 4% at 120 knots.



The tail-rotor collective pitch was calculated and compared with the published data. The largest discrepancy was 27% and occurred at 120 knots. This seemingly large error was mainly due to the small value of the tail-rotor collective at that point.

Based on this evidence, it is reasonable to accept that the computer program is accurate enough in predicting both the main rotor and tail-rotor collective settings.

#### **5.4.4 Fuselage Roll Angle**

Figure 5.4 compares the roll angle obtained from the analysis with the results of Siepker and Heffley. The predicted results can be seen to follow the same form as the published data. However, it was found to be offset to the more negative side over the low-speed range. This could be due either to a center of gravity placement slightly off centre (a displacement of even only 0.01R to either side caused a large change in the prediction of the roll angle), or to the fact that coupling between the longitudinal and lateral modes were ignored in the present analysis.

The largest discrepancy was found to be 33% and occurred at 120 knots. Compared to Heffley, this discrepancy was found to be only about 1.5%. It is thus difficult to comment on the accuracy of the estimation of the rolling angle due to the lack of more information. There is better agreement between the predicted values of the roll angle and those reported by Siepker in the low-speed range, but better agreement with Heffley's results were found in the high speed range.

#### **5.4.5 Lateral Cyclic Pitch Input**

The lateral cyclic pitch prediction was found to have a maximum discrepancy of 56% at a forward speed of 40 knots. Upon comparison with Heffley, this discrepancy was found to be smaller than 2% (Figure 5.5). The next largest discrepancy was then found to be 33% at 20 knots, but was only 6.3% relative to Heffley.

It was observed from the previous analyses that the largest discrepancies usually occurred at a speed of 120 knots. As such, it was worth noting the discrepancies found between the reported and predicted lateral cyclic pitch. The value reported by Siepker was about 11% larger than the value predicted by the current analysis while Heffley reported a value that was 8.4%.



### 5.4.6 Further Verification

Bramwell (1976) calculated the required trim settings for an example helicopter (see Appendix C.2 for details of this helicopter) in forward flight at non-dimensional velocity of  $\mu = 0.3$ . The trim settings of this helicopter were calculated and compared to the values published by Bramwell in an attempt to provide further verification that the current analysis could predict the trim settings of a helicopter. The results of this comparison are shown in Table 5.2 and Table 5.3.

It should be noted that it appears that Bramwell reported some of the trim settings incorrectly. Discrepancies in  $P$ ,  $b_1$ ,  $a_0$ ,  $B_1$  and  $A_1$  were found. These discrepancies were removed if these values were recalculated by hand.

Bramwell reported that the difference between the values of the H-force coefficient is not too serious as a large error in this coefficient results in only a small change in the important values. The current analysis was used to calculate all the trim settings very accurately apart from the value of the longitudinal cyclic control setting. It can be seen from Table 5.1 that there was a discrepancy of almost 7% between the values reported by Bramwell and those calculated by the current analysis. It is shown below that this is mainly due to the difference in the downwash angle at the tail plane.

Glauert (1926) suggested that at sufficient forward velocity the helicopter rotor would act like an elliptically loaded round wing. This assumption allowed the use of lifting-line theory to analyse the "wing", which had a span equal to the diameter of the main rotor. The horseshoe vortex model can thus be used to analyze the downwash velocity at the tail plane. Houghton and Carpenter (1993) describe the use of the simplified horseshoe-vortex model. A brief summary of the use of this theory follows.

Using the horseshoe-vortex model requires the use of an equivalent wingspan. This wingspan is equal to the distance between the two trailing vortices and is calculated as

$$s' = \frac{\pi}{4} R \quad (5.64)$$

The circulation of a vortex is an indication of its strength. The circulation of the equivalent simplified loading is now constant along the span. Houghton et al. (1993) calculated the circulation of the horseshoe vortex as

$$K_0 = \frac{L}{\rho V 2s'} = \frac{W}{\rho V 2s'} \quad (5.65)$$

If

$$x_{ip} = \sqrt{(l_H R)^2 + (h_M - h_H)^2} \quad (5.66)$$

is the distance from the centre of gravity to the horizontal stabilizer,

$$y_{ip} = \sqrt{(h_M - h_H)^2 + (s')^2} \quad (5.67)$$

is the distance from the semi-infinite vortex to the horizontal stabilizer and

$$\beta = \tan^{-1} \left( \frac{s'}{l_T R} \right) \quad (5.68)$$

is the angle between the end of the bound vortex and the tail plane (see Figure 5.6) then the downwash velocity at the tail plane is

$$w_{ip} = \frac{K_0}{4\pi x} 2 \cos \beta + 2 \frac{K_0}{4\pi y} (\cos \beta + 1) \quad (5.69)$$

The downwash angle is then

$$\varepsilon = \tan^{-1} \frac{w_{ip}}{V} \quad (5.70)$$

The simplified horseshoe-vortex model

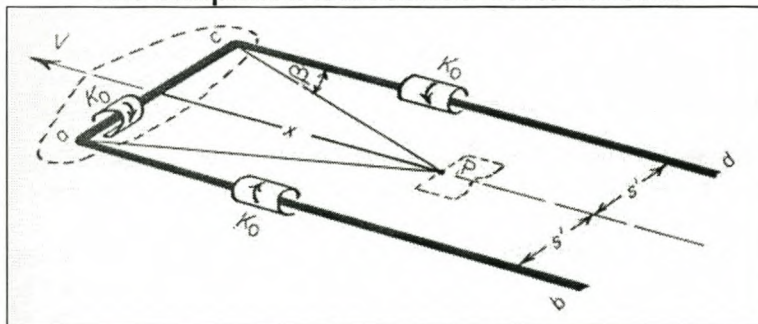


Figure 5.6

Bramwell (1976) reported this angle to be  $2.62^\circ$ . Entering the values for the test helicopter used by Bramwell resulted in a downwash angle of  $2.547^\circ$ , a



discrepancy of only 1.79%. Using this value of the downwash angle led to a longitudinal control angle of  $5.8^\circ$ . Bramwell calculated this angle to be  $5.71^\circ$ . This shows that the horseshoe-vortex model applied to the main rotor of a helicopter at high speed yields a reliable estimate of the downwash at the horizontal stabilizer.

#### **5.4.7 Conclusion**

It was shown that the current analysis was successful in accurately predicting the trim characteristics of a helicopter by verification with published data. The level of accuracy is such that the data gained from the trim analysis can be used in a study of helicopter dynamics.

It appeared, however, that the simulation was less accurate at the highest and lowest simulation speeds. These inaccuracies were probably due to the lack of a proper drag model. It was observed that even a slight change in the drag model greatly influenced the calculated trim settings. The results gained from the analysis were also shown to sometimes approximate Heffley better than Siepker, or vice versa.

The analysis was further validated by the investigation of a helicopter at high forward speed, as analysed by Bramwell (1976). It was shown that the current analysis produced results that closely resembled those published by Bramwell.

## 6. DYNAMIC STABILITY AND CONTROL

In this section, the calculation of the stability and control characteristics of the helicopter in flight will be detailed. The complexity of the solution can be reduced by assuming that the coupling between the longitudinal and lateral modes of motion is negligible. Making this assumption will reduce the accuracy of the analysis, but Bramwell (1976) determined that this reduction of accuracy is negligible in most cases. Padfield (1996) further justified this assumption by stating that the essential understanding of the aerodynamics and dynamics of aircraft still comes from simple theory.

### 6.1 Introduction to the Stability Analysis

The equations of motion for a helicopter could be described in non-linear form as follows (see chapter 2):

$$\dot{\bar{x}} = \bar{F}(\bar{x}, \bar{u}, t) \quad (6.1)$$

In this equation,  $\bar{x}$  is the state vector and is defined as:

$$\bar{x} = \{u, w, q, \theta, v, p, \phi, r, \psi\} \quad (6.2)$$

To control the helicopter, the pilot must be able to adjust the collective pitch, the longitudinal and lateral cyclic pitch and the tail-rotor collective pitch. Hence, the control vector can be described as

$$\bar{u} = \{\theta_0, \theta_{1S}, \theta_{1C}, \theta_{0T}\} \quad (6.3)$$

The basis of the stability analysis is the assumption that helicopter motion can be described as a small perturbation from trim. These perturbations can be written in the form

$$\bar{x} = \bar{x}_e + \delta\bar{x} \quad (6.4)$$

This process of defining the motion of a vehicle as a small perturbation from trim is called the linearization of the equations of motion. This process rests on the assumption that the external forces and moments can be represented as analytic functions of the motion variables and their derivatives. This assumption is valid as long as the disturbances occurring



in the motion and control variables are small. The linearized equations of motion for the full six degrees of freedom, describing perturbed motion about a general trim condition, can then be written as

$$\dot{\bar{x}} - \bar{A} \bar{x} = \bar{B} \bar{u}(t) \quad (6.5)$$

in which  $\bar{A}$  and  $\bar{B}$  are the system and control matrices respectively. These two matrices can be written as

$$\bar{A} = \left( \frac{\partial \bar{F}}{\partial \bar{x}} \right) \bigg|_{\bar{x} = \bar{x}_e} \quad (6.6)$$

and

$$\bar{B} = \left( \frac{\partial \bar{F}}{\partial \bar{u}} \right) \bigg|_{\bar{x} = \bar{x}_e} \quad (6.7)$$

where  $\bar{F}$  is the nonlinear function describing aircraft motion. The system matrix is a 9x9 matrix and the control matrix is a 9x4 matrix. The coefficients in  $\bar{A}$  are called stability derivatives, while the coefficients in  $\bar{B}$  are called the control derivatives. The solution of equation (6.5) depends on the calculation of all these stability and control variables.

The first step of the stability analysis is the calculation of the trim settings of the helicopter. This was discussed in chapter five. The stability and control derivatives are determined after this, at which point some comment can be made about the dynamic behavior of the helicopter. The final step of the stability analysis is a root-locus analysis of the characteristic equation of the longitudinal and lateral modes of motion.

### 6.1.1 Simplifying Assumptions

The stability and control of helicopters can become very complex to analyse if no simplification is made. Such cases require the analysis of the individual motion of the rotor blades as well as the vibration of the fuselage.



Fortunately, only some cases (like that of air resonance) require full modeling of individual blades. However, if the helicopter is operating under normal flying conditions, a lot of simplifying assumptions can be made in order to aid in the stability and control analysis. These assumptions are (directly quoted from Bramwell (1976), pp. 186 - 187):

1. In disturbed flight the rotor behaves as if the motion were a sequence of steady conditions, i.e. the accelerations of the helicopter are small enough to have a negligible effect on the rotor response. This assumption can be justified by showing that the rotating blade can be represented by a second order system having a natural frequency that is the same as the rotor angular frequency; typical disturbed motion corresponds to forcing the blade at a very low frequency ratio so that the rotor responds as if the instantaneous disturbance were being applied steadily. The rotor can thus be regarded as responding instantaneously to speed and angular rates, just as is generally assumed for the fixed-wing aircraft.
2. The rotor speed remains constant. This assumption is justified because not only does the engine control the rotor speed, but also the changes of torque under normal helicopter conditions are quite small [this is however not the case in Nap-Of-Earth flight]. In autogyro flight neither of these two conditions applies, and the rotor angular-velocity variations may be quite considerable.
3. Lateral and longitudinal motions are uncoupled and can be treated independently of one another, as is normally the case with the fixed-wing aircraft. Now, [it is known] that the rotor tilts sideways with forward speed, and there are other examples in which the lateral and longitudinal responses are coupled. Nevertheless, it is believed that the effects of coupling are quite small.

### **6.1.2 Physical Interpretation**

The physical description of the effects of disturbances refers to what happens to the helicopter (and especially the rotor disc) when disturbed. These effects include the forward-speed disturbance, the sideslip disturbance and the yawing disturbance, among others. Understanding these physical occurrences aids in the understanding of the stability and control characteristics of the helicopter. Performing the stability and control analysis provides the basis for making an analytical evaluation of these occurrences.



## 6.2 Longitudinal dynamic stability

In the following section, the wind axes were chosen as the set of reference axes. This was done, because it removed the  $qW_0$  and  $pW_0$  terms from the force equations. A further reason for the choice of this set of axes was that it usually served as the set of reference axes for the analysis of fixed-wing aircraft. This paragraph relies heavily on Bramwell (1976) as the main source of information.

The equations of motion were derived in chapter two. These equations are then linearized around the helicopter motion can be described as a small perturbation from trim (equation 6.4). It is further assumed that second order effects can be ignored. The linearized equations of longitudinal motion referenced to the wind axes are then

$$(W/g)\dot{u} = -W\theta \cos\tau + \Delta X \quad (6.8)$$

$$(W/g)\dot{w} - (W/g)v\dot{\theta} = -W\theta \sin\tau + \Delta Z \quad (6.9)$$

$$I_{yy}\ddot{\theta} = \Delta M \quad (6.10)$$

$\Delta X, \Delta Z$  and  $\Delta M$  are the aerodynamic force and moment increments.

One of the assumptions made in the derivation of the dynamic stability theory, is that the disturbances in  $u$ ,  $w$  and  $q$  are small. The force and moment increments can then be written as only the first terms of a Taylor series. In order to illustrate this, the aerodynamic force in the x-direction is expressed as

$$\Delta X = \frac{\partial X}{\partial u}u + \frac{\partial X}{\partial w}w + \frac{\partial X}{\partial q}q + \frac{\partial X}{\partial B_1}B_1 + \frac{\partial X}{\partial \theta_0}\theta_0 \quad (6.11)$$

$$= X_u u + X_w w + X_q q + X_{B_1} B_1 + X_{\theta_0} \theta_0 \quad (6.12)$$

where  $X_u, X_w, \dots, X_{\theta_0}$  are called the derivatives.

The aerodynamic derivatives are considered to remain constants even if the motion of the helicopter is not. If the helicopter is fitted with a tail-

plane, a new term is introduced to the moment equation. This term is due to the so-called “downwash lag” and is expressed as

$$M_{\dot{w}} \dot{w} = \frac{\partial M}{\partial \dot{w}} \dot{w} \quad (6.13)$$

It is used to account for the time it takes for the downwash from the rotor to reach the horizontal stabilizer.

### 6.2.1 Non-dimensionalization of the equations

De Waard (1985) reported that different arguments could be made for and against the non-dimensionalization of the equations of motion. One of the reasons cited for the non-dimensionalisation to be done is that this allows the comparison of the dynamic behavior of different airframes. One can also observe the effect of changing a design more easily. The strongest reason for keeping the equations in a dimensional form is that no transformations are necessary in order to obtain specific data for the airframe in question.

It was decided to use the equations in non-dimensional form in this analysis because it would allow the direct comparison of different model helicopters. The following reference quantities are used to non-dimensionalise the equations:

1. the rotor-blade radius  $R$  is the reference length,
2. the rotor tip speed  $\Omega R$  is the reference speed,
3. the total rotor blade area  $sA$  is the reference area.

Define the following non-dimensional quantities:

$$\hat{u} = u / \Omega R \quad (6.14)$$

$$\hat{w} = w / \Omega R \quad (6.15)$$

$$\hat{q} = q / \Omega \quad (6.16)$$

As with fixed-wing aircraft, it is customary to define a non-dimensional aerodynamic unit of time, the so-called air-second, which is defined as

$$\tau = t / \hat{t} \quad (6.17)$$



where

$$\hat{t} = W / (g \rho_s A \Omega R) \quad (6.18)$$

(Note that the symbol for the air-second is the same as that of the flight path angle. Care should therefore be taken not to confuse these symbols in the equations!)

It is useful to define a mass ratio (Bramwell calls this the relative-density parameter) for the helicopter. This parameter aids with the derivation of the characteristic equation and is defined as

$$\mu^* = W / (g \rho_s A R) = \Omega \hat{t} \quad (6.19)$$

In equation (6.19),  $W/g$  is the mass of the helicopter and  $\rho_s A R$  is the total mass of the air column of height  $R$  above the rotor blades ( $\mu^*$  can therefore be expected to be quite large).

The non-dimensional moment of inertia is defined as

$$i_B = I_{YY} / (W R^2 / g) \quad (6.20)$$

These non-dimensional factors were used to non-dimensionalise the equations of motion. Bramwell (1976) derived the non-dimensional equations of motion as

$$\frac{du}{d\tau} - x_u u - x_w w - x_q \frac{d\theta}{d\tau} + w_c \theta \cos \tau = x_{B_1} B_1 + x_{\theta_0} \theta_0 \quad (6.21)$$

$$-z_u u + \frac{dw}{d\tau} - z_w w - (\hat{V} + z_q) \frac{d\theta}{d\tau} + w_c \theta \sin \tau = z_{B_1} B_1 + z_{\theta_0} \theta_0 \quad (6.22)$$

$$-m_u u - m_w w - m_{\dot{w}} \frac{dw}{d\tau} + \frac{d^2 \theta}{d\tau^2} - m_q \frac{d\theta}{d\tau} = m_{B_1} B_1 + m_{\theta_0} \theta_0 \quad (6.23)$$

The non-dimensional aerodynamic and control derivatives in equations (6.21) to (6.23) are shown later in this chapter.

### 6.2.2 Stick-fixed dynamic longitudinal stability

Stability analyses can be classified as “stick-fixed” or “stick-free”. When stability calculations are performed while keeping the value of the control inputs constant, it is referred to as “stick-fixed stability”. In longitudinal helicopter flight, this refers to a situation where the main rotor collective pitch and longitudinal cyclic pitch is kept constant. The values of these control derivatives are thus equal to zero.

It is usual to solve the equations of motion of a system by prescribing the form of the solution and then calculating the remaining unknown values. It was thus assumed that the solution of the equations of motion would be of the form

$$u = u_0 e^{\lambda\tau}, \quad w = w_0 e^{\lambda\tau}, \quad \theta = \theta_0 e^{\lambda\tau} \quad (6.24)$$

The value of  $\lambda$  is the only unknown in equation (6.24). Solving  $\lambda$  requires the substitution of the values of  $u$ ,  $w$  and  $\theta_0$  into equations (6.21) to (6.23). The determinant of the coefficients of these equations is then found by canceling  $e^{\lambda\tau}$  throughout. The value of this determinant must be zero for  $u_0, w_0$  and  $\theta_0$  to be non-trivial. Thus

$$\begin{vmatrix} \lambda - x_u & -x_w & w_c \cos \tau \\ -z_u & \lambda - z_w & -(\hat{V}\lambda - w_c \sin \tau) \\ -m_u & -(\lambda m_{\dot{w}} + m_w) & \lambda^2 - m_q \lambda \end{vmatrix} = 0 \quad (6.25)$$

Expanding the determinant in equation (6.25) leads to the characteristic equation that has the form

$$\lambda^4 + B_1 \lambda^3 + C_1 \lambda^2 + D_1 \lambda + E_1 = 0 \quad (6.26)$$

where

$$B_1 = N_1 - m_q - \hat{V}m_{\dot{w}} \quad (6.27)$$

$$C_1 = P_1 - N_1 m_q - Q_1 m_{\dot{w}} - \hat{V}m_w \quad (6.28)$$

$$D_1 = S_1 m_u - P_1 m_q - R_1 m_{\dot{w}} - Q m_w \quad (6.29)$$

$$E_1 = T_1 m_u - R_1 m_w \quad (6.30)$$



with

$$N_1 = -x_u - z_w \quad (6.31)$$

$$P_1 = x_u z_w - x_w z_u \quad (6.32)$$

$$Q_1 = -\hat{V} x_u - w_c \sin \tau \quad (6.33)$$

$$R_1 = -w_c (z_u \cos \tau - x_u \sin \tau) \quad (6.34)$$

$$S_1 = w_c \cos \tau - \hat{V} x_w \quad (6.35)$$

$$T_1 = -w_c (z_u \cos \tau - x_u \sin \tau) \quad (6.36)$$

In equations (6.26) to (6.36), the subscript 1 refers to coefficients of the longitudinal mode of motion equations.

The characteristic equation has four roots, which can be either real or complex. If the values of  $\lambda$  are real and positive, the motion is known as a divergence. If the values are real and negative, the motion is known as a subsidence. Complex roots can be written as

$$\lambda = r \pm is \quad (6.37)$$

The motion is a diverging oscillation if  $r$  is real and positive and a converging oscillation if it is real and negative.

### 6.2.3 Aerodynamic derivatives

It is assumed that the rotor forces and moments depend only on the instantaneous values of speed, incidence and rate of pitch. The calculation of the derivatives thus firstly requires resolving the rotor forces into the required components. The force and flapping equations are then differentiated. Bramwell (1976) derived the aerodynamic force and moment derivatives in the tip-path plane. The  $u$ -,  $w$ - and  $q$ -derivatives of the dimensionless  $x$ - and  $z$ -forces are

$$x_u = -t_c \frac{\partial a_1}{\partial \mu} - \alpha_D \frac{\partial t_c}{\partial \mu} - \frac{\partial h_{cD}}{\partial \mu} \quad (6.38)$$

$$z_u = -\frac{\partial t_c}{\partial \mu} \quad (6.39)$$

$$x_w = -t_c \frac{\partial a_1}{\partial \hat{w}} - \alpha_D \frac{\partial t_c}{\partial \hat{w}} - \frac{\partial h_{cD}}{\partial \hat{w}} \quad (6.40)$$

$$z_w = -\frac{\partial t_c}{\partial \hat{w}} \quad (6.41)$$

$$x_q = -t_c \frac{\partial a_1}{\partial \hat{q}} - \alpha_D \frac{\partial t_c}{\partial \hat{q}} - \frac{\partial h_{cD}}{\partial \hat{q}} \quad (6.42)$$

$$\text{and } z_q = -\frac{\partial t_c}{\partial \hat{q}} \quad (6.43)$$

The position of the rotor forces changes relative to the center of gravity if the helicopter pitches. It is thus necessary to define a new height and length from the center of gravity to the rotor hub if the moments are to be calculated. If  $l$  is the length and  $h$  is the height between the center of gravity and the hub in measured in the body axis, then define

$$h_1 = h \cos \alpha_s - l \sin \alpha_s \quad (6.44)$$

$$l_1 = l \cos \alpha_s - h \sin \alpha_s \quad (6.45)$$

where  $\alpha_s$  is the incidence of the rotor hub axis in trimmed flight. This is equal to the pitch-angle of the helicopter if the rotor shaft is perpendicular to the helicopter longitudinal axis. The subscript 1 is added to distinguish between the values of used in the longitudinal case and the values used in the lateral case (indicated with a subscript 2).

Bryant and Gates used a system of non-dimensionalization that was intended to display the equations of motion in terms of the mass and inertia parameters, according to Bramwell (1976). This system of notation was however cumbersome to use. That is why Bramwell proposed to define moment derivatives that already accounted for the mass and inertia properties. The moment derivatives in the system used by Bryant and Gates are indicated with a prime while the moment derivatives in Bramwell's system have no prime in order to distinguish between the two



systems. The moment derivatives written in the system of Bryant and Gates are:

$$m'_u = -h_1 x_u + l_1 z_u + C_{mS} \frac{\partial a_1}{\partial \mu} + (m'_u)_f \quad (6.46)$$

$$m'_w = -h_1 x_w + l_1 z_w + C_{mS} \frac{\partial a_1}{\partial \hat{w}} + (m'_w)_f \quad (6.47)$$

$$m'_q = -h_1 x_q + l_1 z_q + C_{mS} \frac{\partial a_1}{\partial \hat{q}} + (m'_q)_f \quad (6.48)$$

where the subscript  $f$  refers to the contribution of the fuselage. The final forms of these moment derivatives in the system of Bramwell are:

$$m_u = \frac{\mu^*}{i_B} m'_u, \quad m_w = \frac{\mu^*}{i_B} m'_w, \quad m_q = \frac{\mu^*}{i_B} m'_q \quad (6.49)$$

The  $\mu$ - derivatives of  $\lambda_i$ ,  $t_c$ ,  $a_1$ ,  $\lambda$  and  $h_{cD}$  are given by Bramwell (1976) in the form

$$\frac{\partial \lambda_i}{\partial \mu} = \frac{2\mu\theta_0 + \alpha_{nf} - (4t_c/a\lambda_i)\bar{V}\bar{v}_i^3}{1 + (4t_c/a\lambda_i)(1 + \bar{v}_i^4)} \quad (6.50)$$

$$\frac{\partial t_c}{\partial \mu} = \frac{2\mu\theta_0 + \alpha_D - a_1 + \bar{V}\bar{v}_i^3 / (1 + \bar{v}_i^4)}{4/a + (\lambda_i/t_c) / (1 + \bar{v}_i^4)} \quad (6.51)$$

$$\frac{\partial a_1}{\partial \mu} = \frac{a_1}{\mu} + \frac{2\mu}{1 - \mu^2/2} \times \frac{\partial \lambda}{\partial \mu} + \frac{\mu a_1}{\left(1 - \frac{1}{2}\mu^2\right)} \quad (6.52)$$

$$\frac{\partial \lambda}{\partial \mu} = \alpha_{nf} - \frac{\partial \lambda_i}{\partial \mu} \quad (6.53)$$

$$\text{and } \frac{\partial h_{cD}}{\partial \mu} = \frac{1}{4} \delta \quad (6.54)$$

It will be noted that equation (6.52) is reported differently in Bramwell (1976). The equation is derived in Appendix D. It will further be noted that equation (6.53) is only valid for cases where  $\alpha_{nf}$  is small, such as in forward flight. The  $\hat{w}$ -derivatives of  $\lambda_i$ ,  $t_c$ ,  $a_1$ ,  $\lambda$ ,  $\lambda_D$  and  $h_{cD}$  are listed in Bramwell (1976) as

$$\frac{\partial \lambda_i}{\partial \hat{w}} = \frac{(a/4)\lambda_i/t_c + \bar{v}_i^4}{1 + (a/4)\lambda_i/t_c + \bar{v}_i^4} \quad (6.55)$$

$$\frac{\partial \lambda}{\partial \hat{w}} \approx 1 - \frac{\partial \lambda_i}{\partial \hat{w}} \quad (6.56)$$

$$\frac{\partial t_c}{\partial \hat{w}} = \frac{a}{4} \left( 1 - \frac{\partial \lambda_i}{\partial \hat{w}} \right) \quad (6.57)$$

$$\frac{\partial a_1}{\partial \hat{w}} = \left( \frac{2\mu}{1 - \mu^2/2} \right) \frac{\partial \lambda}{\partial \hat{w}} \quad (6.58)$$

$$\frac{\partial \lambda_D}{\partial \hat{w}} = \frac{1}{1 + (a/4)(\lambda_i/t_c) + \bar{v}_i^4} \times \frac{1 + 3\mu^2/2}{1 - \mu^2/2} \quad (6.59)$$

$$\text{and } \frac{\partial h_{cD}}{\partial \hat{w}} = \frac{a \left( \frac{1}{2} a_1 - \mu \theta_0 + \frac{\mu \lambda_D}{1 - \mu^2/2} \right)}{4 \left[ 1 + (a/4)(\lambda_i/t_c) + \bar{v}_i^4 \right]} \quad (6.60)$$

The  $\hat{q}$ -derivatives of  $a_1$ ,  $b_1$ ,  $a_0$  and  $h_{cD}$  are

$$\frac{\partial a_1}{\partial \hat{q}} = -\frac{16}{\gamma} \cdot \frac{1}{1 - \mu^2/2} \quad (6.61)$$

$$\frac{\partial b_1}{\partial \hat{q}} = -\frac{1}{1 + \mu^2/2} \quad (6.62)$$



$$\frac{\partial a_0}{\partial \hat{q}} = 0 \quad (6.63)$$

$$\begin{aligned} \frac{\partial h_{cD}}{\partial \hat{q}} = & -\frac{a}{4} \left[ \frac{-a_0/3}{1 + \mu^2/2} + \frac{1}{3} a_0 - \frac{1}{2} \lambda \frac{\partial a_1}{\partial \hat{q}} \right] \\ & - \frac{a}{4} \left[ -\mu a_1 \frac{\partial a_1}{\partial \hat{q}} + \mu^2 \theta_0 \frac{\partial a_1}{\partial \hat{q}} + \frac{1}{8} \mu b_1 \right] \end{aligned} \quad (6.64)$$

The effect that the tail-plane has on the helicopter stability is to be included. The pitching moment due to the tail-plane was reported to be

$$M_T = -\frac{1}{2} \rho V^2 S_T l_T R C_{LT} \quad (6.65)$$

Then the contributions of the tail plane to the pitching moment derivatives are written using the system of Bryant and Gates as

$$(m_u)_T' = -\mu \bar{V}_i \left[ C_{LT} + \frac{1}{2} a_T \left( \frac{\partial \lambda_i}{\partial \mu} - \frac{\lambda_i}{\mu} \right) \right] \quad (6.66)$$

$$(m_w)_T' = -\frac{1}{2} \mu \bar{V}_T a_T \left( 1 - \frac{\partial \lambda_i}{\partial \hat{w}} \right) \quad (6.67)$$

$$(m_q)_T' = -\frac{1}{2} \mu \bar{V}_T a_T l_T \quad (6.68)$$

$$(m_{\dot{w}})_T' = -\frac{1}{2} \bar{V}_T a_T l_T \frac{\partial \lambda_i}{\partial \hat{w}} \quad (6.69)$$

These moments due to the tail-plane can be added independently to the other fuselage pitching moments in equations (6.46) to (6.48). This concludes the section on the stability derivatives.

### 6.2.4 Longitudinal Stability in Hover

In hovering flight, the vertical motion is uncoupled from the pitching and fore-and-aft motion. The value of the  $z_u$  derivative can be determined from equations (6.39) and (6.51). The value of  $\mu$  and  $\bar{V}$  is by definition zero in hover. It can be seen from equation (5.45) that  $a_1$ , and from equation (5.28) that  $\alpha_D$  is also zero in hover. The value of  $z_u$  is thus also zero in hover. It must also be remembered that the flight-path angle is undefined in hover.

If the middle line of the determinant in equation (6.25) is now observed for the hovering case, it can be seen that only the  $(\lambda - z_w)$  term remains. Hence, the first root describing the motion of a hovering helicopter was found to be

$$\lambda = z_w \quad (6.70)$$

The remaining three roots that describe the motion of the hovering helicopter could be found from the equation

$$\lambda^3 - (x_u + x_q)\lambda^2 + x_u m_q \lambda + m_u w_c = 0 \quad (6.71)$$

Of these three roots, one is usually real and the other two form a complex pair.

### 6.3 Lateral dynamic stability

The lateral dynamic stability can be established in much the same way as the longitudinal stability, starting with the equations of motion that were derived in chapter two. The linearization depends on the assumptions that the helicopter motion can be described as a small perturbation from trim (equation 6.4) and that second order effects can be ignored. These linearized lateral equations of motion was reported by Bramwell (1976) to be

$$\begin{aligned} \frac{W}{g} \dot{v} - Y_v v - Y_p p + \frac{W}{g} Vr - Y_r r - W\phi \cos\tau - W\psi \sin\tau \\ = Y_{A1} A_1 + Y_{\theta T} \theta_T \end{aligned} \quad (6.72)$$



$$-L_v v + I_{XX} \dot{p} - L_p p - I_{XZ} \dot{r} - L_r r = L_{A_1} A_1 + L_{\theta_T} \theta_T \quad (6.73)$$

$$-N_v v - I_{XZ} \dot{p} - N_p p + I_{ZZ} \dot{r} - N_r r = N_{A_1} A_1 + N_{\theta_T} \theta_T \quad (6.74)$$

The non-dimensional moments of inertia are defined as

$$i_A = I_{XX} / mR^2, i_C = I_{ZZ} / mR^2, i_E = I_{XZ} / mR^2 \quad (6.75)$$

### 6.3.1 Stick-fixed dynamic lateral stability

Lateral stick-fixed stability refers to the scenario where the perturbations of the lateral cyclic and tail-rotor collective are both zero,

$$A_1 = \theta_T = 0 \quad (6.76)$$

Then, as with the longitudinal stability, it is assumed that the solutions have the form

$$v = v_0 e^{\lambda\tau}, \phi = \phi_0 e^{\lambda\tau}, r = r_0 e^{\lambda\tau} \text{ and } \psi = \psi_0 e^{\lambda\tau} \quad (6.77)$$

The determinant of coefficients of the lateral equations of motion is found by substituting the values of equation (6.77) into equations (6.72) to (6.74). The value of this determinant has to be zero in order for  $v$ ,  $\phi$  and  $\psi$  to be non-trivial. Hence,

$$\begin{vmatrix} \lambda - y_v & -w_c \cos \tau & \hat{V}\lambda - w_c \sin \tau \\ -l_v & \lambda^2 - l_p \lambda & -(i_E/i_C)\lambda^2 - l_r \lambda \\ -n_v & -(i_E/i_C)\lambda^2 - n_p \lambda & \lambda^2 - n_r \lambda \end{vmatrix} = 0 \quad (6.78)$$

It can be seen from the main diagonal that resolving the determinant will lead to an equation with five roots. This equation is called the characteristic equation and has the form (where the subscript 2 refers to equations describing the lateral mode of motion)

$$\lambda (A_2 \lambda^4 + B_2 \lambda^3 + C_2 \lambda^2 + D_2 \lambda + E_2) = 0 \quad (6.79)$$

It is obvious from equation (6.79) that the value of one root would always be equal to zero. This zero root confirms that helicopters have no preference for a particular heading, as one would expect intuitively.

Following Bramwell (1976), the coefficients in equation (6.79) can be written as

$$A_2 = 1 - i_E^2 / i_A i_C \quad (6.80)$$

$$B_2 = -y_v \left( 1 - i_E^2 / i_A i_C \right) - N_2 \quad (6.81)$$

$$C_2 = y_v N_2 + P_2 + l_v \left( i_E / i_C \right) \hat{V} + n_v \hat{V} \quad (6.82)$$

$$D_2 = y_v P_2 + l_v Q_2 - n_v R_2 \quad (6.83)$$

$$E_2 = l_v S_2 - n_v T_2 \quad (6.84)$$

and

$$N_2 = l_p + n_r + \left( i_E / i_C \right) l_r + \left( i_E / i_A \right) n_p \quad (6.85)$$

$$P_2 = l_p n_r - l_r n_p \quad (6.86)$$

$$Q_2 = n_p \hat{V} - w_c \cos \tau \quad (6.87)$$

$$R_2 = l_p \hat{V} - w_c \sin \tau \quad (6.88)$$

$$S_2 = n_p w_c \sin \tau + n_r w_c \cos \tau \quad (6.89)$$

$$T_2 = l_p w_c \sin \tau + l_r w_c \cos \tau \quad (6.90)$$

### 6.3.2 Lateral stability derivatives

The effective tail-rotor height and the effective distance rearward from the helicopter center of gravity to the tail-rotor are defined respectively as

$$h'_T R = \left( h_T \cos \alpha_s - l_T \sin \alpha_s \right) R \quad (6.91)$$



and

$$l'_T R = (l_T \cos \alpha_s + h_T \sin \alpha_s) R \quad (6.92)$$

Bramwell (1976) reports the lateral derivatives using the system of Bryant and Gates (where moment derivatives are indicated with a prime, see paragraph 6.2.3) as

$$y'_v = -t_c \frac{a_1}{\mu} - \frac{1}{4} \delta - \bar{s}_T \frac{\partial t_c}{\partial \hat{w}} - 0.3 \mu \frac{S_B}{sA} \quad (6.93)$$

$$l'_v = -(h t_c + C_{mS}) \frac{a_1}{\mu} - h'_T \bar{s}_T \frac{\partial t_c}{\partial \hat{w}} \quad (6.94)$$

$$l'_p = -\frac{16}{\gamma} \left[ \frac{h(t_c + a \lambda_D / 8) + C_{mS}}{1 + \mu^2 / 2} \right] - h'^2_T \bar{s}_T \frac{\partial t_c}{\partial \hat{w}} \quad (6.95)$$

$$l'_r = h'_T l'_T \bar{s}_T \frac{\partial t_c}{\partial \hat{w}} \quad (6.96)$$

$$n'_v = l'_T \bar{s}_T \frac{\partial t_c}{\partial \hat{w}} + (n_v)'_f \quad (6.97)$$

$$n'_p = h'_T l'_T \bar{s}_T \frac{\partial t_c}{\partial \hat{w}} + (n_p)'_f \quad (6.98)$$

$$n'_v = l'^2_T \bar{s}_T \frac{\partial t_c}{\partial \hat{w}} + (n_v)'_f \quad (6.99)$$

It appears that  $\bar{s}_T$  found in equation (6.96) had been omitted by Bramwell. In equation (6.93),  $S_B$  is the projected side-area of the fuselage. The solidity of the tail rotor is defined as

$$\bar{s}_T = s_T A_T (\Omega R)_T / s A (\Omega R) \quad (6.100)$$

The moment derivatives are written in the system used by Bramwell (see paragraph 6.2.3) by performing the following calculations:

$$l_v = \mu^* l'_v / i_A, \quad l_p = \mu^* l'_p / i_A, \quad \dots, \quad n_p = \mu^* n'_p / i_C \quad (6.101)$$

It is usually very difficult to analyse the effect of the fuselage on the moment derivatives (except for the contribution of the horizontal tail and the vertical fin). It was thus decided to ignore the external moments due to the fuselage in this analysis. Bramwell (1976) stated that the errors incurred due to this assumption were small.

### 6.3.3 Lateral Stability in Hover

In the longitudinal hovering case it was found that the value of some of the derivatives in the determinant were zero in hover. This led to great simplification and insight into the behavior of the helicopter in hovering flight. The same is not true in the lateral case. Upon inspection of equation (6.78) it is found that none of the derivatives in the determinant are equal to zero.

If it could be assumed, however, that  $I_r$  was negligible, as is the case of a helicopter where the tail rotor lies close to the rolling axis, then the motion would be analogous to the longitudinal case. In this case, the helicopter can be thought of as consisting of just a rotor. The same motions that could occur in the longitudinal mode could also occur in the lateral mode. If  $I_r$  is negligible, the hovering characteristic equation is

$$(\lambda - n_r) [\lambda^3 - (y_v + I_p) \lambda^2 + y_v I_p \lambda - I_v w_c] = 0 \quad (6.102)$$

It can be seen from equation (6.102) that the characteristic equation of lateral motion in hover is split into two factors. The one factor contains information about the yawing motion and the other contains information about the sideways and rolling motions. It would thus appear as if the yawing motion is independent of the sideways and rolling motion. Such a conclusion can however only be made by considering the equations of motion, and the extent of the coupling between them.

In forward flight, equation (6.79) must be solved in order to investigate the stability characteristics. The time of oscillation of the "Dutch roll" oscillation was found by Bramwell (1976) to be approximately

$$T = 2\pi \hat{t} / \sqrt{(\mu n_v)} \quad (6.103)$$



The “Dutch Roll” is a mixture of yawing and rolling motion. This mode has a negative effect on the flying qualities of a certain helicopter, as it can become very uncomfortable for the pilot. The severity of the effect is not only dependent on the period of the motion, but also on the amplitude.

## 6.4 Control Response

Control response refers to the behaviour of the helicopter in response to the pilot’s control input. Following Bramwell (1976), this paragraph contains a discussion of

1. the normal acceleration in response to a cyclic-pitch control input
2. the pitching and rolling response to cyclic-pitch displacements

Bramwell also considers the effect of vertical gusts in his discussion on the control response of helicopters. This behaviour is not a response to a pilot control input, but will still be considered here as it indicates the response of the helicopter due to an external influence.

### 6.4.1 Control Derivatives

The important force and moment derivatives with regards to changes in cyclic- and collective pitch applications are discussed in this paragraph. The  $B_1$ -derivatives are

$$\frac{\partial t_c}{\partial B_1} = -\mu \frac{\partial t_c}{\partial \hat{w}} \quad (6.104)$$

$$\frac{\partial h_{cD}}{\partial B_1} = -\mu \frac{\partial h_{cD}}{\partial \hat{w}} \quad (6.105)$$

$$\frac{\partial a_1}{\partial B_1} = -\mu \frac{\partial a_1}{\partial \hat{w}} \quad (6.106)$$

$$x_{B_1} = \frac{\partial t_c}{\partial B_1} \alpha_D + t_c \left( 1 + \mu \frac{\partial a_1}{\partial \hat{w}} \right) - \frac{\partial h_{cD}}{\partial B_1} \quad (6.107)$$

$$z_{B_1} = -\frac{\partial t_c}{\partial B_1} \quad (6.108)$$

$$\text{and } m'_{B_1} = -(l - ha_1) \frac{\partial t_c}{\partial B_1} - (t_c + C_{ms}) \left( 1 + \mu \frac{\partial a_1}{\partial \hat{w}} \right) + h \frac{\partial h_{cD}}{\partial B_1} \quad (6.109)$$

The derivatives with respect to an adjustment of the collective pitch input are

$$\frac{\partial t_c}{\partial \theta_0} = \frac{a}{6} \frac{1 + 3\mu^2/2}{1 + (a\lambda_i / 4t_c) / (1 + \bar{v}_i^4)} \quad (6.110)$$

$$\frac{\partial a_1}{\partial \theta_0} = \frac{8\mu/3}{1 - \mu^2/2} \left[ 1 - \frac{\frac{1}{2}as(1 + 3\mu^2/2)}{8\mu + as} \right] \quad (6.111)$$

$$\frac{\partial h_{cD}}{\partial \theta_0} = \frac{a}{8} \left( a_1 \frac{\partial \lambda_D}{\partial \theta_0} + \lambda_D \frac{\partial a_1}{\partial \theta_0} \right) - \frac{a}{4} \mu \left( \lambda_D + \theta_0 \frac{\partial \lambda_D}{\partial \theta_0} \right) \quad (6.112)$$

$$x_{\theta_0} = -t_c \frac{\partial a_1}{\partial \theta_0} - \alpha_D \frac{\partial t_c}{\partial \theta_0} - \frac{\partial h_{cD}}{\partial \theta_0} \quad (6.113)$$

$$z_{\theta_0} = -\frac{\partial t_c}{\partial \theta_0} \quad (6.114)$$

$$\text{and } m'_{\theta_0} = -h_1 x_{\theta_0} + l_1 z_{\theta_0} - C_{ms} \frac{\partial a_1}{\partial \theta_0} \quad (6.115)$$

#### 6.4.2 Control response in forward flight

Sometimes it is useful to have an indication of the initial acceleration that occurs in the helicopter. For this project, two such cases were investigated: the initial accelerations due to a cyclic pitch input and due to



the helicopter entering a sharp upward vertical gust. In both these cases, the initial acceleration was measured in number of "g's". These equations were obtained by performing Laplace transformations on the equations of motion. These transformed equations are then expressed as "transfer functions". Bramwell (1976) reported the initial acceleration (measured in g's) for these two cases as

$$n = -\frac{1}{w_c} (z_{B_1} B_1 + z_w w) \quad (6.116)$$

and

$$n = -\frac{z_w}{w_c} (w_g + w) \quad (6.117)$$

respectively. In equation (6.117),  $w_g$  is the vertical velocity of the gust.

## 6.5 Verification of calculated stability characteristics

The ability of the present computer code to calculate the stability characteristics of a helicopter needs to be verified. The method of verification will be by the comparison of calculated data with published results. Bramwell (1976) published stability derivatives for an example helicopter (described in chapter 6 of the reference). The helicopter specification can be viewed in Appendix C.2.

### 6.5.1 Longitudinal stability derivatives

The comparison of the calculated and published longitudinal stability characteristics can be seen in Figures 6.1 to 6.7. It can be seen that there is excellent agreement between most of the derivatives. Discrepancies were observed in the  $x_u$  and the  $m'_q$  derivatives (Figures 6.4 and 6.6).

After investigation, it is believed that the discrepancy in the  $x_u$ -derivative was probably due to the rearwards flapping of the main rotor per unit of incremental velocity,  $\Delta u$ . The discrepancy in the  $m'_q$ -derivative might be due to the size of the contribution of the tail plane. It might also be due to the forward pitching of the main rotor per unit of incremental pitching,  $\Delta q$ .

The root loci of the longitudinal mode of motion are shown in Figures 6.8 and 6.9 for the cases with no tail and with a tail of solidity equal to 0.1 respectively. The configuration with no tail is seen to suffer from instability in the phugoid mode. The instability becomes worse with increasing speed as shown by the increase in the real parts of the complex conjugate roots. The configuration with the tail is seen to be unstable at low forward speeds and then becoming stable at moderate forward speed. The configuration with the tail is observed to display the short period vibration. Detail of the root loci is shown in Figures 6.10 to 6.14.

These results indicate that the current program is successful in calculating the longitudinal stability derivatives and solving the characteristic equation of motion.

### 6.5.2 Lateral stability derivatives

The graphical comparisons between the calculated and published values of the lateral stability derivatives are shown in Figures 6.15 to 6.20. It can be seen from these graphs that there are excellent agreement between the predicted values and the published data.

The root locus of the lateral modes of motion of the helicopter is shown in Figure 6.21. Only four of the five roots are shown as the fifth root was shown to always be equal to zero. The root-locus is shown to contain the so-called "Dutch-roll" mode, the "spiral root" and a large negative root, as predicted by Bramwell.

The approximate period of the "Dutch roll" oscillation of the helicopter as described by equation (6.101) is presented graphically as Figure 6.25. It can be seen that this mode has a long period at slow speed that reduces quickly with forward speed.

From the above statements, it can be argued that the current program is able to accurately predict the lateral stability derivatives and solve the characteristic equation of lateral motion.



## 7. STABILITY AND CONTROL CHARACTERISTICS OF MODEL HELICOPTERS

The method of performing the trim analysis was detailed in chapter five. The computer program that was written to perform the analysis was also verified. Chapter six contained the discussion of the method of determining the stability and control characteristics of a helicopter. The computer program written to perform the stability analysis was also verified. This chapter will utilise both the trim analysis as well as the stability analysis programs. These programs will be applied to two model helicopters in the non-dimensional velocity range from 0.015 to 0.12.

In this chapter, the phrase "stability characteristics" refers to the collection of stability and control derivatives, as well as a physical interpretation of what these imply. A stabilising force or moment is one that causes the helicopter to counteract the source of the disturbance and to return to trim. A destabilising force or moment will remove the helicopter from a state of trim.

### 7.1 Hirobo Shuttle Z

An estimate of the helicopter's inertia matrix was required in order to calculate the stability characteristics. Specific data about the helicopter's moments- and products of inertia could not be found. As such, it was estimated that the fuselage was a rectangular prism with evenly distributed mass. An investigation of the helicopter's stability characteristics was performed subsequent to the calculation of the force and moment derivatives.

The stability derivatives of the helicopter are indicated in Figures 7.1 to 7.13. These figures are in non-dimensional terms in order to allow the reader to observe similarities and differences between the different types of helicopters.

It is necessary to analyse the root-locus of the characteristic equation in order to assess the stability of the helicopter. The longitudinal- and lateral root-locus of the Shuttle Z is indicated in Figure 7.14 and Figure 7.15 respectively. It is obvious from both of these graphs that an increase in speed causes an increase in stability.

The long-period motion of the helicopter (also called the *phugoid* mode) is the dominant mode of motion in the longitudinal case. For the Shuttle Z, the phugoid-mode is unstable at low speed. The motion of the phugoid mode has a period of 3.83 seconds at the lowest testing speed



of 5.2 kph. The motion is unstable and lightly damped (the damping ratio has a value of 0.11).

The motion of the phugoid mode becomes stable at a velocity of 21 kph. At this speed, the motion has a period of 5.28 seconds and is almost undamped. At the maximum forward test velocity of 42 kph, the period becomes 8.8 seconds. The period of the phugoid motion is thus found to become larger with an increase in forward velocity.

The short period mode is heavily damped at low speeds. This is illustrated by the presence of the roots on the real axis. The amount of damping in the short-period mode starts to reduce around a speed of 18-20 kph. At the maximum testing speed, the period of this mode is found to be about 0.95 seconds and has a damping ratio of 0.725. The frequency of the short period mode is thus almost ten times faster than the phugoid mode at the maximum speed. The phugoid- and short-period modes are displayed in more detail in Figures 7.16 and 7.17.

The dominant (or at least the most recognisable) mode of lateral motion is the so-called "Dutch-roll". McCormick (1979) described the "Dutch Roll" as follows:



*Imagine that the airplane begins to yaw to the right. As it does so, it slips to the left, so that the path remains nearly a straight line. As it yaws to the right, it begins to roll in that direction. While still rolled to the right, the airplane begins to yaw to the left and slip to the right.*

This mode is usually very uncomfortable for the pilot. Coupling between sideslip and roll causes the "Dutch-roll" mode, during which the energy of the aircraft is exchanged between yawing, sideslip and rolling. Higher directional stability will usually be more effective in damping the motion associated with this mode.

The Shuttle Z has a Dutch-roll period of 3.4 seconds at a speed of 5.2 kph, becoming 1.01 seconds at a speed of 42 kph. The amount of damping increases and the period of the Dutch roll becomes smaller as the velocity of the helicopter increases.



There are two more roots visible in Figure 7.15. Bramwell (1976) called the root closest to the imaginary axis the “spiral root”. Consider an aircraft in straight and level flight in order to explain the physical nature of this mode. A disturbance causes the aircraft to start rolling. As it rolls, the aircraft develops a small sideslip velocity. The horizontal stabiliser now creates a yawing moment and this increases the amount of sideslip. This motion will continue to grow if the pilot does not correct it. The aircraft is thus in a spiralling dive towards the ground. The detail of the lateral root-locus can be seen in Figures 7.18, 7.19 and 7.20.

The control derivatives are shown in Figures 7.21 – 7.27.

An important measure of a helicopter’s stability is the initial normal acceleration response to a sharp-edged vertical gust (Figure 7.27). It was observed that even in a large vertical gust of 10.5m/s, the Shuttle Z responded with an initial normal acceleration of below 2g throughout the speed range.

## 7.2 JR Voyager E

The JR Voyager E represented the smaller size model helicopters available at present. As with Hirobo Shuttle Z, no data was available for the moments and products of inertia. As such, the fuselage was modelled as a rectangular prism in order to estimate this data. It was assumed for this estimate that the fuselage was the only component with mass. It was also assumed that the mass was evenly distributed over the fuselage. The helicopter used by the Department of Electronic Engineering of the University of Stellenbosch was not fitted with a tail plane. The stability derivatives of the helicopters are indicated in Figures 7.1 to 7.13 along with the stability derivatives of the Shuttle Z.

The stability derivatives of the Voyager are seen to closely resemble those of the Shuttle Z. The  $m'_w$ -derivative was recalculated for a Voyager E that was fitted with a modestly sized tail plane with an area of 0.01m<sup>2</sup>. These values closely approximated those of the Shuttle Z (Figure 7.5).

It can be seen from Figure 7.6 and Figure 7.7 that the presence of a tail plane has a great influence on the value of the  $m'_q$ - and  $m'_u$ -derivatives respectively.



The longitudinal root-locus is indicated in Figure 7.28 and the lateral root-locus in Figure 7.29. It is obvious from both of these graphs that an increase in speed causes an increase in stability.

The helicopter has a phugoid motion (Figure 7.30) with a period of 5.56 seconds at a non-dimensional speed of 0.015. This mode became stable only at non-dimensional speeds greater than 0.09 (26.3 kph). The period of the phugoid motion was found to be 6.79 seconds at this speed. At the maximum non-dimensional forward velocity of 0.12, the period was 6.85 seconds. It can be observed that the short period motion is heavily damped for this configuration (Figures 7.31 and 7.32).

The Voyager E was observed to have a "Dutch Roll" mode (Figure 7.33) with a period of 3.4 seconds at low speed (4.4 kph). This period became 1.07 seconds at the maximum test speed of 35.1 kph. It is thus observed that the amount of damping increases and the period of the Dutch roll decreases with an increase in forward speed. This can also be seen from equation (6.103) and Figure 7.11. The  $n_v$ -derivative is seen to increase in size over the speed range. The size of the square root in equation (6.103) thus increases and causes a decrease of the period of the oscillation. The so-called "spiral root" is shown in Figure 7.34.

It was decided to investigate the effect of fitting a modestly sized horizontal tail of  $0.01\text{m}^2$  on this helicopter. Figure 7.36 shows the longitudinal root-loci for this configuration.

Adding the tail plane decreases the period of the phugoid motion from 5.56 seconds to 3.46 seconds at 4.4 kph and causes an increase from 6.85 seconds to 6.9 seconds at 35.1 kph. The damping of the alpha mode is observed to become smaller as the velocity increases. The short period motion has a period of 0.88 seconds at the maximum forward speed.

### 7.3 General Remarks

The following information was obtained from an investigation of the stability derivatives of the two test helicopters. Figure 7.1 indicates that an increase in downwards velocity causes an increase in the size of the lift (Z-force) that is produced. This can be explained by observing the rotor blade. An increase in downward velocity will increase the value of the incidence angle, which causes a reduction in the lift produced.



A stabilising force in the negative x-direction is found to accompany an increase in forward velocity (Figure 7.4). This is caused partially due to the rearwards flapping of the rotor and partially due to an increase in the drag force.

The main rotor can be viewed as a gyroscope if the helicopter is busy pitching. This "gyroscope" is subjected to a moment that wants to tilt it sideways. There is a  $90^\circ$  phase-lag, however, which causes the response of the rotor to be in the longitudinal plane. It is thus seen that a positive pitch rate is stabilised by a negative pitching moment (Figure 7.6).

The main rotor of a helicopter responds to changes in the relative wind direction by tilting away from the wind. Motion in the positive y-direction is thus observed to cause a stabilising force in the negative y-direction (Figure 7.8).

If the helicopter experiences yaw, it changes the incidence at the tail rotor and produces a favourable fin effect. This can be seen from Figure 7.12, which shows that the helicopter experiences a yaw moment that opposes the direction of yawing.

The derivative illustrated in Figure 7.2 shows that an increase in forward velocity is accompanied by a decrease in the lift force. This is due to a reduction in the incidence angle, as well as the rearwards tilting of the thrust vector.

A positive pitch moment (rearward flapping of the rotor disc) is found to occur due to an increase in upwards (negative) velocity (Figure 7.5). This happens because a given increase in upward velocity causes a larger decrease in incidence angle on the retreating side than the advancing side, but the same decrease for and aft. This causes the rearward flapping due to the  $90^\circ$  lag.

It is observed that a positive pitching moment occurs due to the rearwards flapping of the rotor disc that takes place when the forward velocity is increased (Figure 7.7). A negative roll moment accompanied an increase in velocity in the positive y-direction due to the same mechanics (Figure 7.9).

If the helicopter experienced an increase of velocity in the positive y-direction, it would be accompanied by a positive yawing moment

(Figure 7.11). This is due to the effect of the wind on the vertical fin and is called "weathercock stability".

The investigation now turns to the root-loci for further information regarding the stability of the helicopters. Both helicopters were seen to display the phugoid mode of motion as well as the Dutch roll and the so-called "spiral root". In the configuration without the horizontal stabiliser, the phugoid mode only became stable at high speeds. The short period was however more heavily damped than the configuration with the horizontal tail. Fitting the tail plane to the Voyager E had the effect of increasing the stability of the phugoid mode. This occurred at the cost of decreasing the amount of damping in the short period mode.

In both configurations, it is observed that an increase in forward speed is usually accompanied by an increase in the stability of the helicopter. This is mainly due to the effect of the tail surfaces. The forces generated due to the action of the air on these tail surfaces increases as the wind-speed increases. This causes moments that oppose disturbances from trim.

It is observed for both configurations that the periods of motion are smaller than for full-scale helicopters. This can partially be attributed to the small mass and moments of inertia of model helicopters.



## **8. CONCLUSION AND RECOMMENDATIONS**

This primary goal of this thesis was the development of computer software for the calculation of the stability and control derivatives of model helicopters.

### **8.1 Trim Analysis**

The calculation of the stability and control derivatives required the trim settings of the helicopter. A computer program was written in order to obtain these trim settings for a helicopter in forward flight. The analysis was validated by comparison with published data of Siepker (1990) and Heffley (1979). The comparison revealed the following:

- The fuselage attitude was modelled to an accuracy of at least 8.68%.
- The largest discrepancy in the longitudinal cyclic input was 12.4%.
- The main rotor collective pitch was accurate to within 4%, but the tail rotor collective pitch had a maximum discrepancy of 27%. The actual values of the predicted and published tail rotor collective pitch however differed only by about 0.5° at this point.
- The predicted roll angle had a maximum discrepancy of 33% if compared to Siepker (1990). The discrepancy compared to Heffley (1979) was only 1.5% at the same point.
- Comparison with Siepker (1990) revealed that the lateral cyclic input had a maximum discrepancy of 56%. Comparison with Heffley (1979) at the same point indicated a discrepancy of less than 2%.

An analysis of the helicopter specified in Appendix C.2 was compared with the results published by Bramwell (1976). The comparison showed excellent agreement between published and calculated results. It was also shown that the downwash angle at the tail plane could be estimated using the simplified horseshoe-vortex model provided that the helicopter was flying at high speed.

### **8.2 Stability and Control Analysis**

A computer program was developed in order to calculate the stability and control derivatives. The stability derivatives were calculated for the helicopter detailed in Appendix C.2 and compared to the results published by Bramwell (1976). This comparison revealed the following:

- The calculation of the  $z_w$ -derivative was more accurate above a non-dimensional speed of 0.1. A maximum discrepancy of 14.3% was observed below this speed. The accuracy above  $\mu = 0.1$  increased dramatically.
- The  $x_w$ -derivative was seen to have excellent agreement with the published results.
- The  $z_u$ -derivative closely resembled the published results. A maximum discrepancy of about 10% was observed.
- There was less agreement between the calculated and published results of the  $x_u$ -derivative. This error might be due to the rearwards flapping of the main rotor per unit of incremental velocity in the x-direction.
- The  $m'_w$ -derivative shows good agreement with published data. The results diverge from the published results over the high speed range, where the maximum discrepancy of 7.1% occurred.
- It is believed that the disparity between the calculated and published values of the  $m'_q$ -derivative was caused by either the size of the contribution of the tail plane, or by the forward flapping of the rotor per unit of incremental helicopter pitching.
- The  $m'_u$ -derivative was seen to have excellent agreement with the published results.
- The  $y_v$ -derivative was seen to have good agreement with the published results. The agreement increased with an increase in forward speed.
- The  $l'_v$ -derivative was seen to have excellent agreement with the published results.
- The  $l'_r$ - and  $n'_p$ -derivatives was seen to have excellent agreement with the published results. The maximum discrepancy of about 5% was observed at  $\mu = 0.05$ .
- The  $n'_r$ -derivative displayed excellent agreement with published data at non-dimensional speeds greater than 0.1. The maximum discrepancy of 16% occurred at  $\mu = 0.05$ .



- The  $n'_v$ -derivative also displayed excellent agreement with published data at non-dimensional speeds greater than 0.1. The maximum discrepancy of 17% occurred at  $\mu=0.05$ .
- Good agreement was observed for the  $l'_p$ -derivative.

The secondary goal of this thesis was an investigation of the stability and control characteristics of model helicopters.

### 8.3 Root-Locus analysis

The root locus analysis was performed by solving the roots of the characteristic equations of the longitudinal and lateral modes of motion. The characteristic equations were determined in chapter six.

It was observed that the presence of a horizontal stabiliser increased the stability of the phugoid mode. This was achieved at the cost of a reduction in the amount of short period damping.

The stability of the helicopters generally increased with an increase in speed. This could be attributed to the effect of the tail surfaces at higher speeds.

The time-periods of the modes of motion of small helicopters were seen to be substantially smaller than those of full-scale helicopters. This was attributed to the small mass and inertia properties of the helicopter.

### 8.4 Performance Analysis

A performance analysis of model helicopters in hovering and axial climbing flight was conducted. It was observed from this analysis that the main rotor speed had an effect on the climbing rate of the helicopter at a certain power setting. This was due to the lower induced power losses of a lower rotor speed. More energy could thus be employed to increase the potential energy of the helicopter.

The main rotor speed did not affect the excess amount of energy required to obtain a certain climbing rate. This was due to the assumption that the induced power losses remained constant for a certain rotor speed, regardless of the climbing speed. The increase in



power was thus only required to increase the potential energy of the helicopter.

As expected, it was found that an increase in main rotor speed required the use of less collective pitch input to maintain trim. Less counter-torque from the tail rotor would also be required, because the required main rotor torque decreased with increasing rotor speed. An increase in main rotor speed would decrease the figure of merit, however, indicating lower rotor efficiency.

In order to maintain trim in a climb required an increase in the main rotor and tail rotor collective input settings.

## **8.5 Recommendations**

Several tasks requiring improvement or investigation were identified during the execution of this thesis. These aspects will be shortly discussed in this paragraph.

The accuracy of the simulation was decreased due to the assumption that the amount of coupling between the longitudinal and lateral modes was negligible. It would be very informative and useful if the analysis on the model helicopters could be performed without making this assumption. A comparison of those results with the results reported in this thesis would be useful and interesting.

An experimental analysis of the two model helicopters could be used as verification of the computer programs developed in this thesis. Several difficulties might be encountered in achieving this goal. The most severe of these difficulties could be measuring the rotor blade angles (the collective and cyclic pitch angles) as well as determining when the helicopter is in a state of trim. The repeatability of the process might also be low due to the nature of the proposed testing facility (the inlet to the large wind tunnel at the Mechanical Engineering Department of the University of Stellenbosch).

It was seen that the presence of the horizontal stabiliser linked to the longitudinal cyclic pitch input (as in the AH1-G Huey Cobra) kept the fuselage pitch angle within a band of less than 1°. The design of such a tail could be very useful for helicopters used to inspect high-voltage electricity supply lines, as the camera would always be pointing at nearly the same angle. This could increase the ease and accuracy of the inspection.



It was reported that the stability of the phugoid mode could be improved by the addition of a horizontal stabiliser. This would however cause a decrease in the damping of the short-period mode. The design of tail plane that provided phugoid stability at low speeds, while still providing good short-period damping would be useful for observation helicopters travelling at medium to low speeds.

The design of an optimally sized horizontal stabiliser could allow for adequate phugoid stability while still providing adequate short-period damping.

One of the difficulties in the analysis of the helicopters was the absence of accurate data about the inertial properties. The accuracy of the analyses conducted in this thesis would be greatly improved if the inertia matrix could be determined accurately. A device that would allow the measurement of the inertial properties of the actual model would be very useful.

## References

Arnold, J, A, 1992, Discrete Vortex Model for the Production of Lift of a N-bladed Rotor, University of Stellenbosch, M.Sc. Thesis

Ashley, H, 1974, Engineering Analysis of Flight Vehicles, Addison-Wesley Publishing Company, Reading

Baruh, H, 1999, Analytical Dynamics, Mcgraw Hill, Singapore

Bramwell, A.R.S., 1976, Helicopter Dynamics, Edward Arnold (Publishers) Ltd, London

Davies, M. 2003. Personal Interview, August, Bellville

De Waard, P.G., 1985, Die Longitudinale en Laterale Dinamiese Gedrag van die AH-1G (Huey-Cobra) in Gelykvlug by Seevlak, University of Stellenbosch, Final Year Project

Finney, R.L., and Thomas, G.B., 1994, Calculus 2<sup>nd</sup> edition, Addison-Wesley Publishing Company, New York

Gerald, C.F. and Wheatley, P.O., 1997, Applied Numerical Analysis, 6<sup>th</sup> edition, Addison-Wesley, New York

Glauert, H.A., 1926, A General Theory of the Autogyro, R&M No.1111, British A.R.C.

Greenberg, M.D., 1998, Advanced Engineering Mathematics, 2<sup>nd</sup> edition, Prentice-Hall, New Jersey

Heffly, R K, 1979, A Compilation and Analysis of Helicopter Handling Qualities Data, Volume Two: Data Analysis, NASA Contractor Report 3145

Hanselman, D. and Littlefield, B., 1997, The Student Edition of Matlab® Version 5 User's Guide, Prentice Hall, Upper Saddle River



Houghton, E.L. and Carpenter, P.W., 1993, Aerodynamics for Engineering Students, 4<sup>th</sup> Edition, Butterworth-Heinemann, Oxford

Inman, D.J., 1996, Engineering Vibration, Prentice Hall, Upper Saddle River

Johnson, W., 1980, Helicopter Theory, Princeton University Press, Princeton

Kuo, B.C., 1995, Automatic Control Systems, 7<sup>th</sup> edition, John Wiley & Sons, New York

Loubser, N.W., 1993, Aspects in the Design of a Real-Time Helicopter Flight Simulator, University of Stellenbosch, M.Sc. Thesis

McCormick, B.W., 1979, Aerodynamics, Aeronautics, and Flight Mechanics, John Wiley & Sons, New York

McCormick, B.W., 1985, The Development of Microcomputer Codes for Studying the Flight Dynamics and Performance of Helicopters, Presented at the International Conference on Rotorcraft Basic Research

McGrath, M., 2001, Java 2 in Easy Steps, Computer Step, Warwickshire

Mil', M.L. et al, 1966, Helicopters: Calculation and Design, Volume 1 – Aerodynamics, National Aeronautics and Space Administration, Washington D.C.

Mil', M.L. et al, 1966, Helicopters: Calculation and Design, Volume 2 – Vibrations and dynamic stability, National Aeronautics and Space Administration, Washington D.C.

Padfield, G.D., 1996, Helicopter Flight Dynamics: The Theory and Application of Flying Qualities and Simulation Modelling, AIAA Education Series, Washington

Padfield, G.D., 1980, On the Use of Approximate Models in Helicopter flight Mechanics, Presented at the Sixth European Rotorcraft and Powered Lift Aircraft Forum

Payne, P.R., 1959, Helicopter Dynamics and Aerodynamics, Sir Isaac Pitman &, Ltd Sons, London

Pienaar, D.vV, 2000, Longitudinal Stability and Control Analysis and Parameter Sensitivity Investigation of Fixed Wing Aircraft In Ground Proximity Using Various Aerodynamic Approaches, University of Cape Town, Ph.D. Dissertation

Schluter, D., 1981, Schluter's Radio Controlled Helicopter Manual, Model & Allied Publications, Herts, England

Siepkers, E.B.J., 1990, The Mathematical Modelling and Simulation of a Conventional Single Main Rotor Helicopter and the Identification of its Linear Models, University of Stellenbosch, M.Eng. Thesis

Uys, J, 1990, Dinamika van Starre Liggame, University of Stellenbosch, Course Notes: Applied Mathematics B224

Visagie, J.G., 2001, Propeller Design Project, University of Stellenbosch, Aerodynamics A 414 Project

White, F.M., 1999, Fluid Mechanics, 4<sup>th</sup> edition, McGraw-Hill, Singapore



**ILLUSTRATIONS AND GRAPHICAL RESULTS**



**Figure 1.1 – Hirobo Shuttle Z**



**Fig 1.2 – JR Voyager E**





**Fig 1.3 – Boeing Vertol CH47 Chinook**

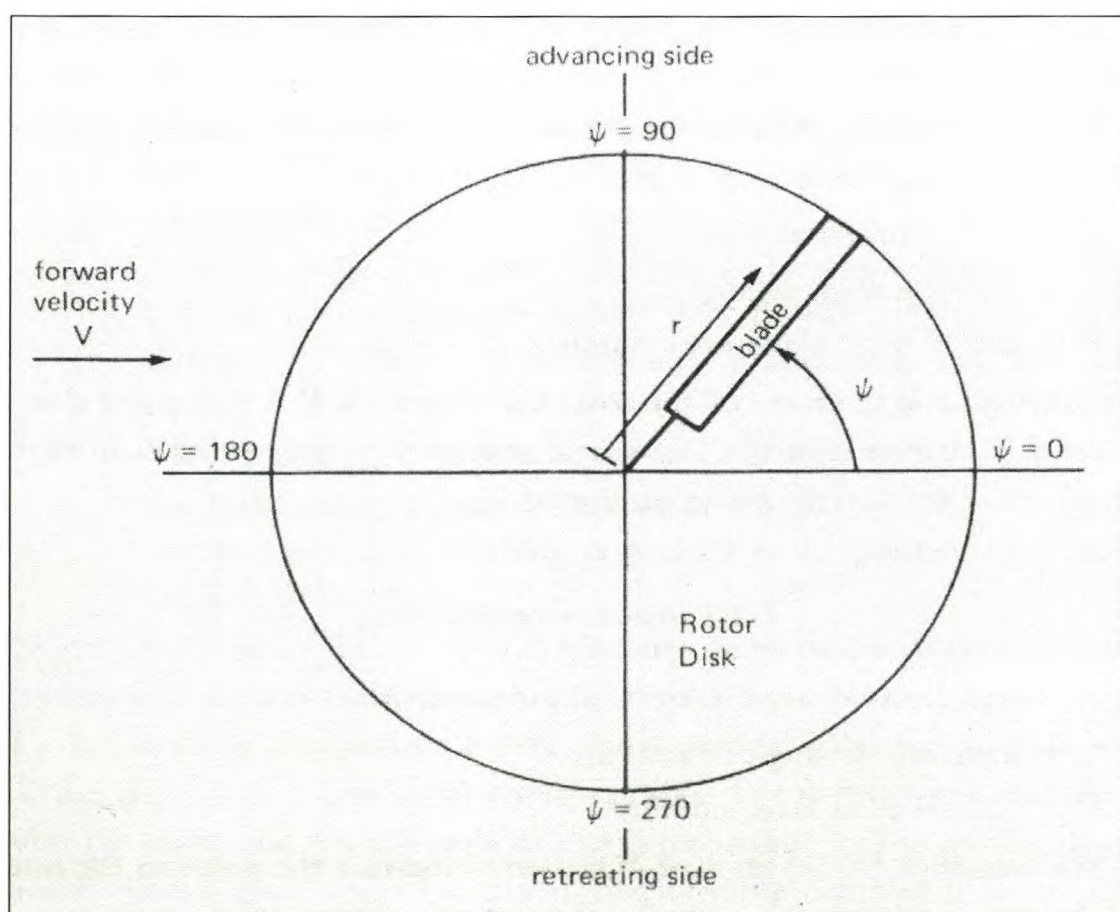


**Fig 1.4 – The helicopter rotor**



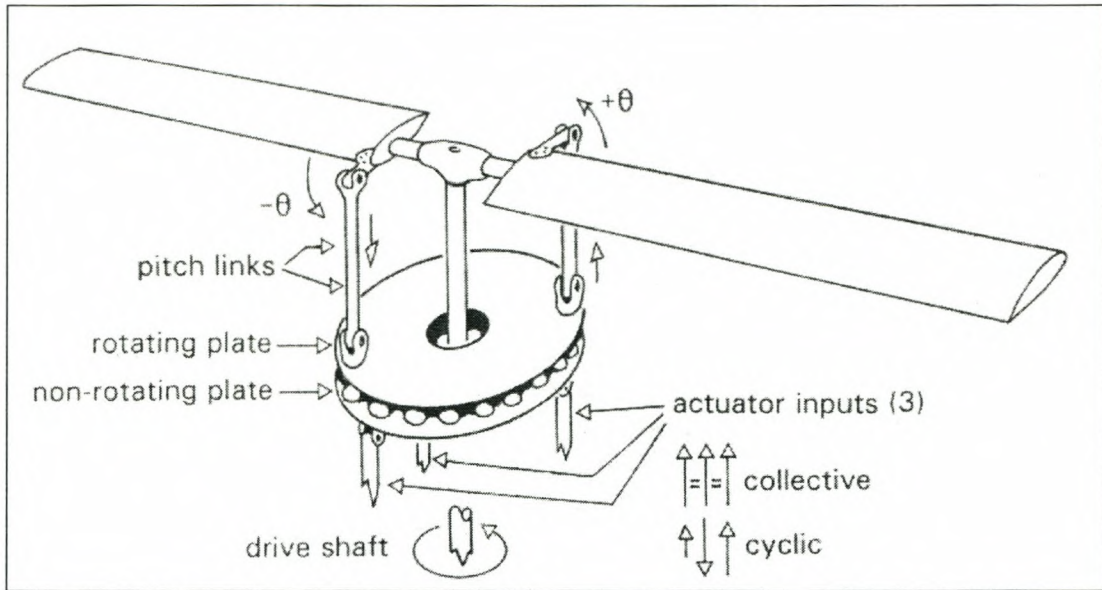


**Fig 1.5 – The swash plate**

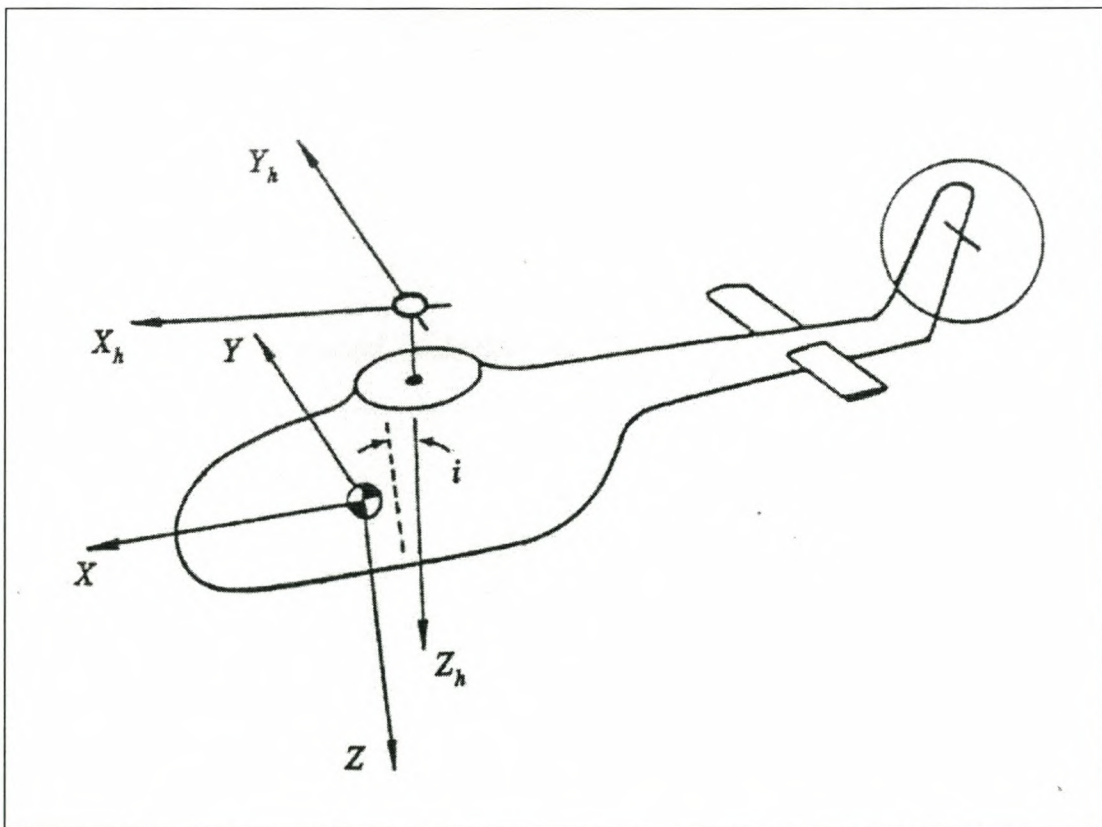


**Fig 1.6 – Helicopter body and hub axes**

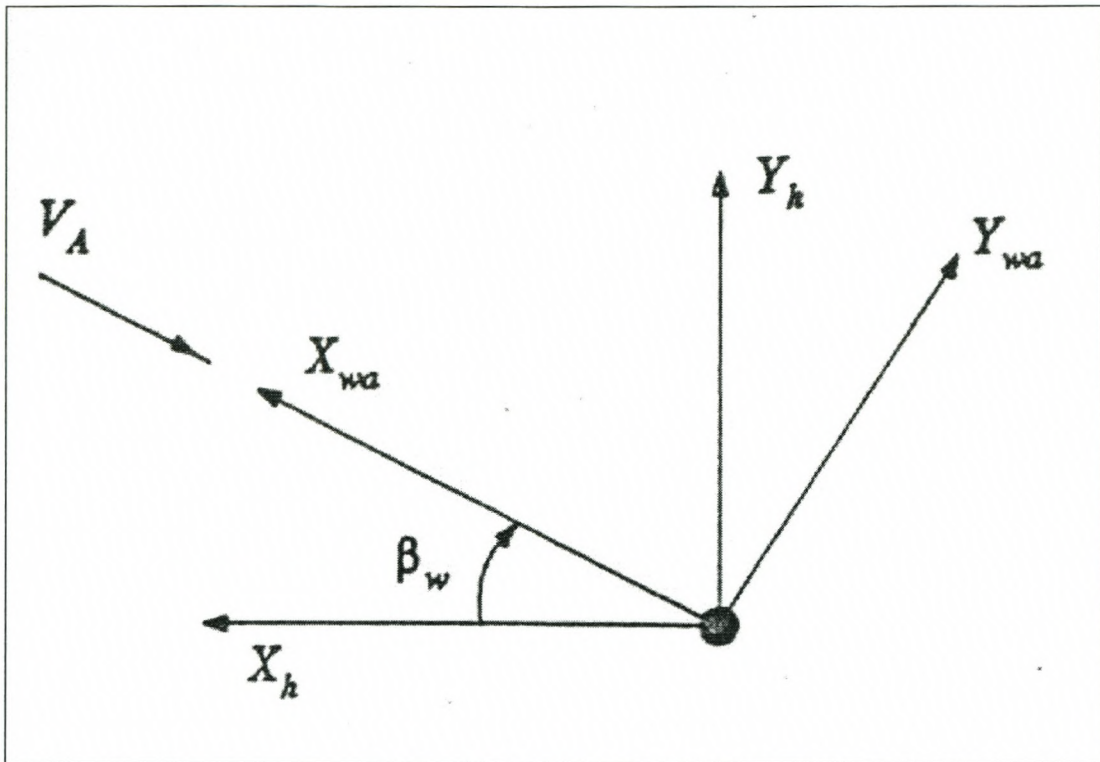


Fig 1.7 – Hub-wind axis

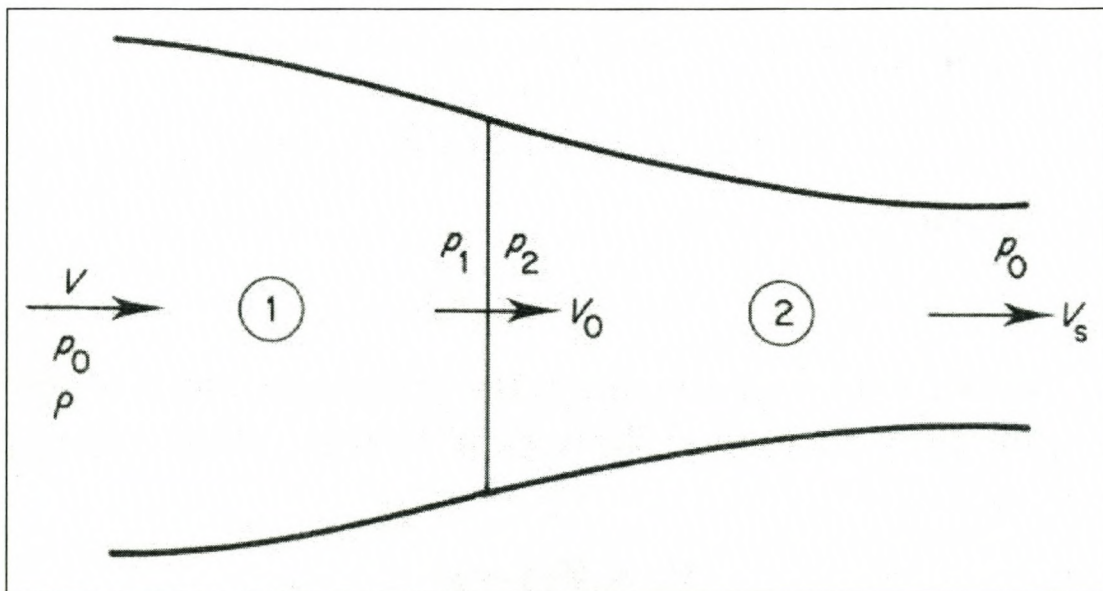
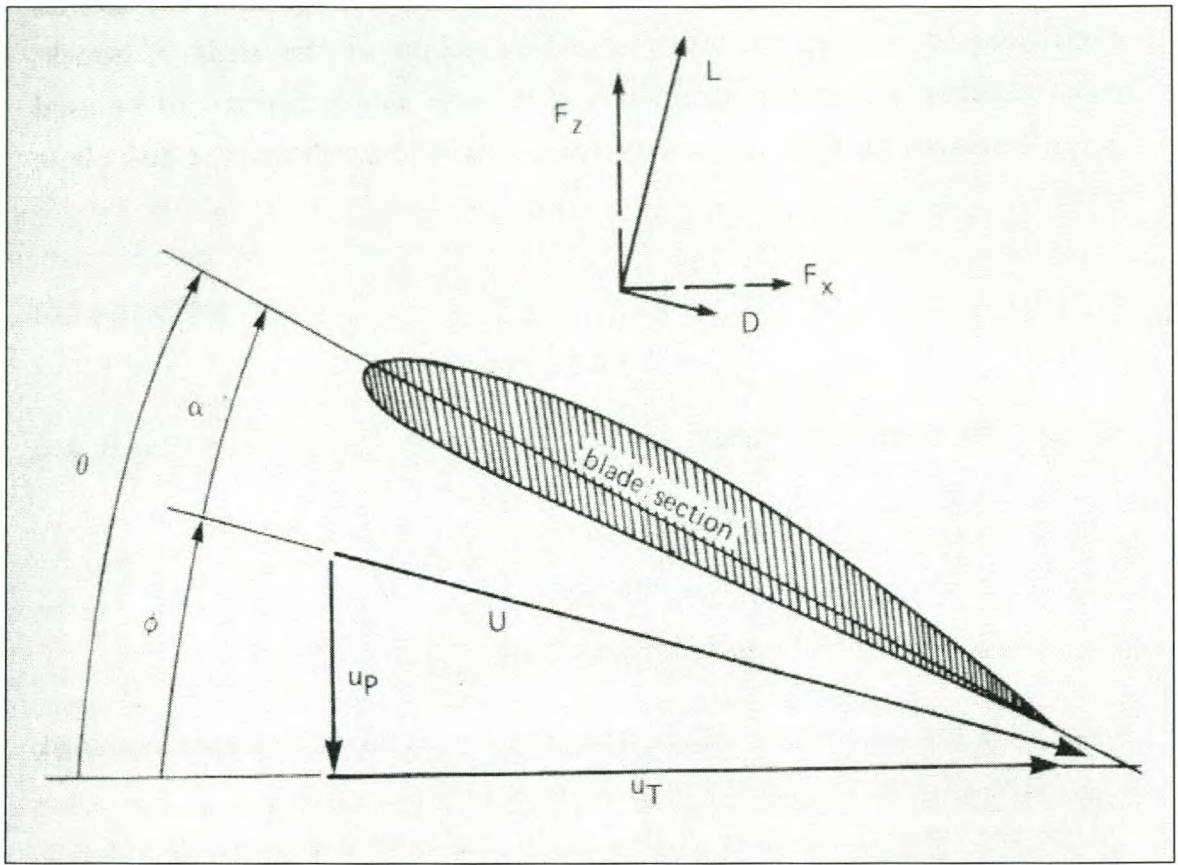
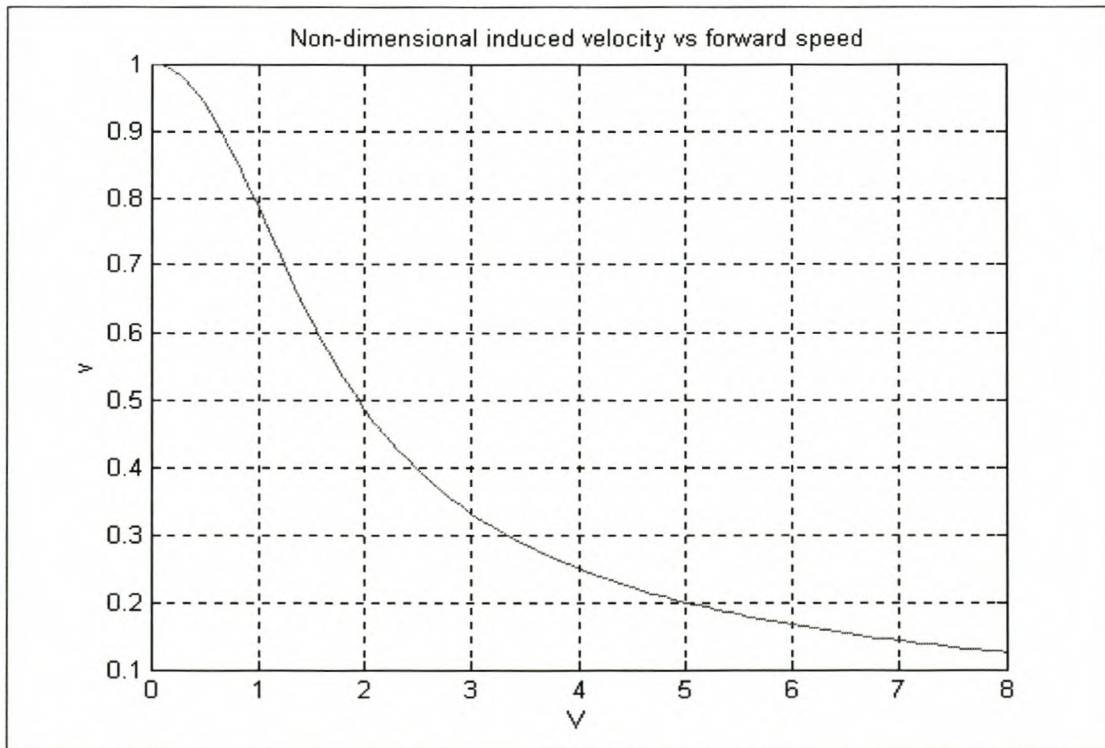


Fig 1.8 – Momentum theory





**Fig 1.9 – Blade Element Theory**



**Fig 1.10 – Induced velocity in forward flight**

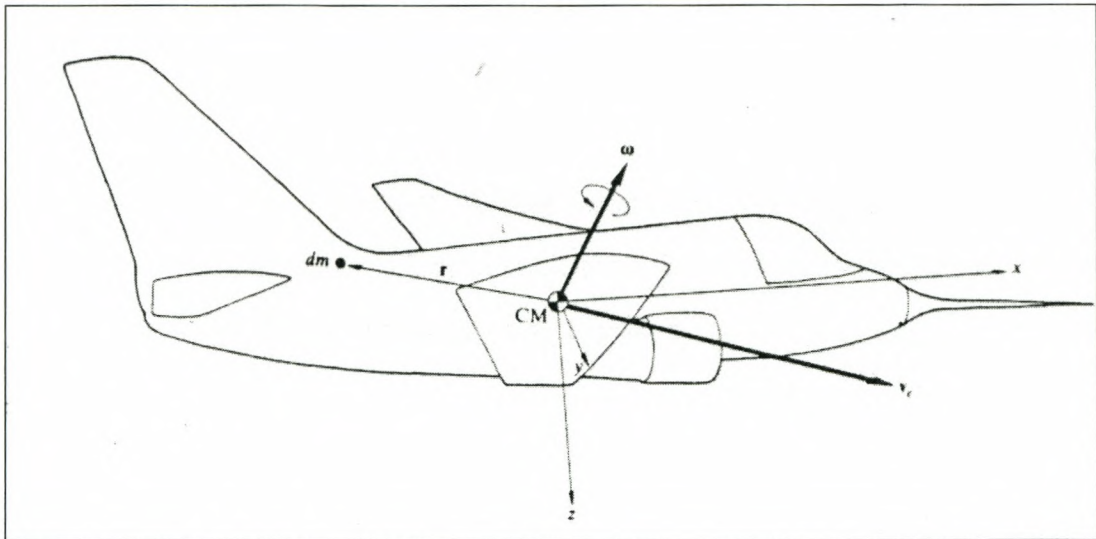


Fig 2.1 – Aircraft reference axes<sup>1</sup>

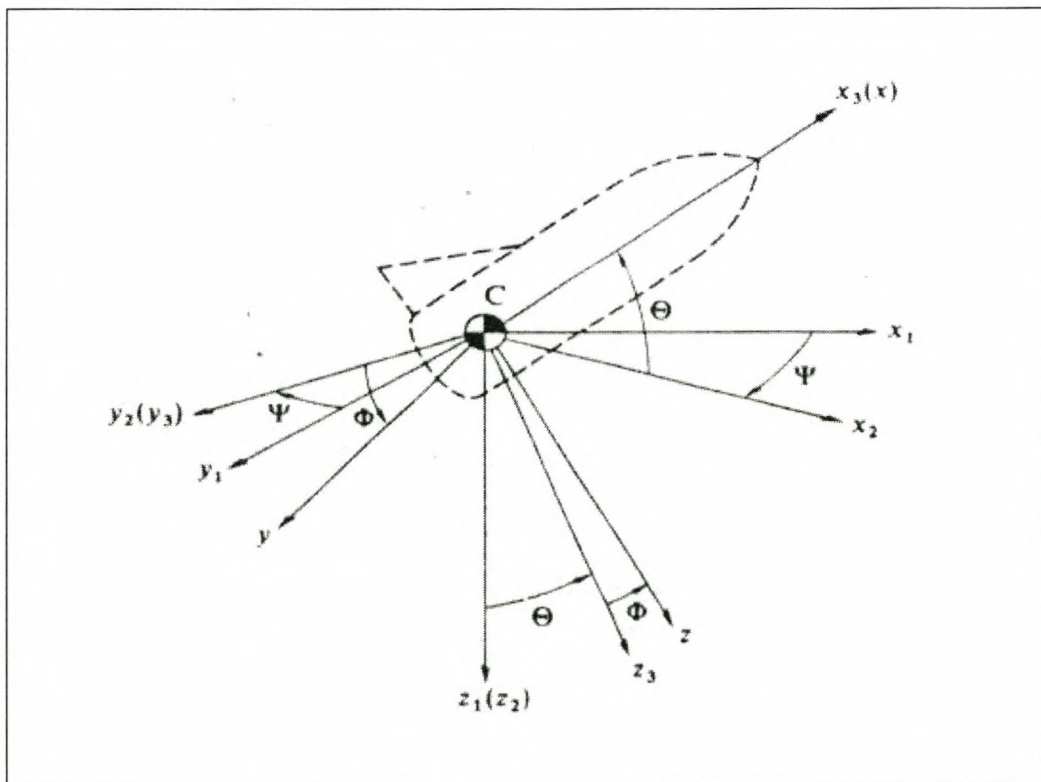
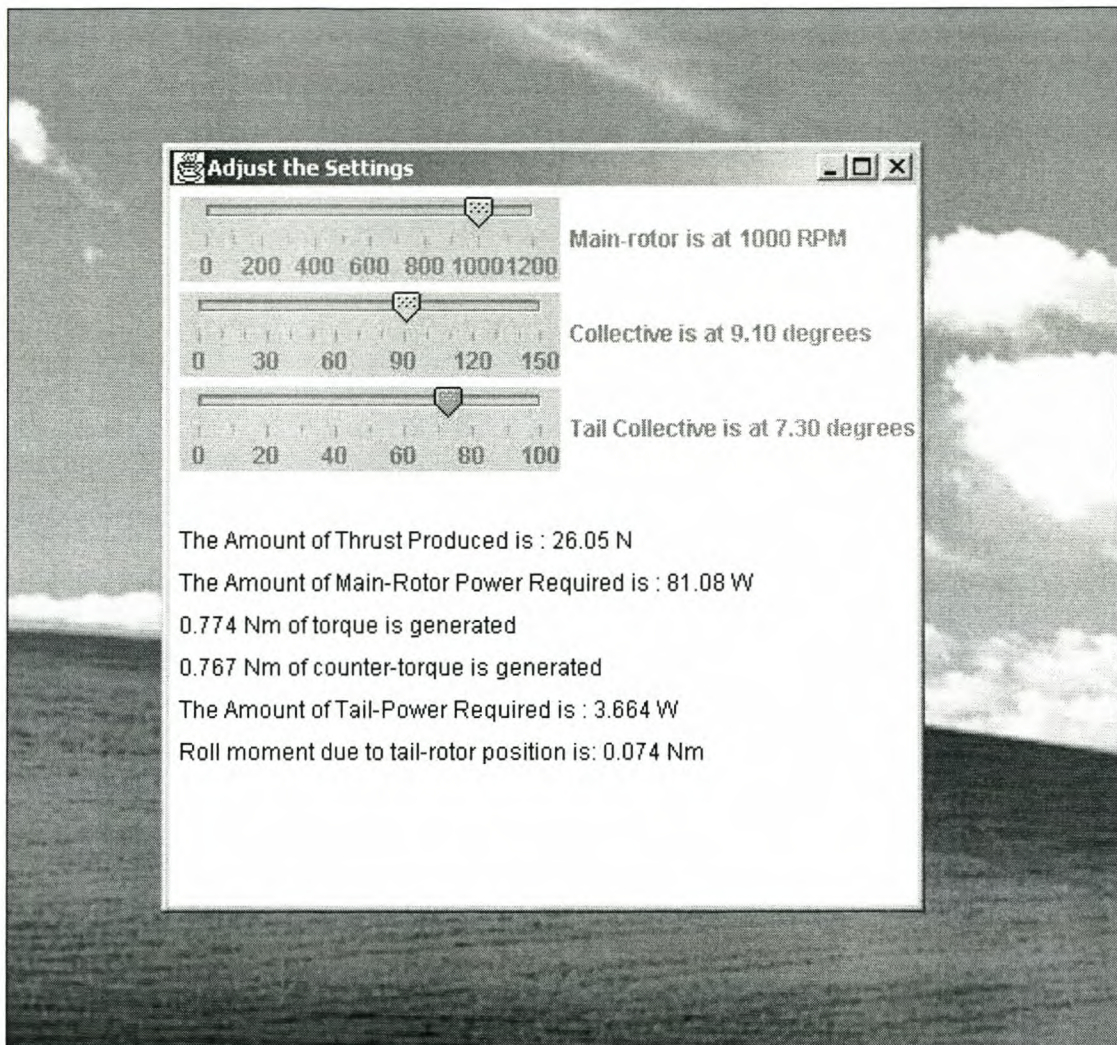


Fig 2.2 – Euler angles<sup>1</sup>

<sup>1</sup> Ashley, Holt Engineering Analysis of Flight Vehicles, Addison – Wesley Publishing Company, Reading, Massachusetts, 1974





**Fig 3.1 – The Hover Analysis Program Interface**

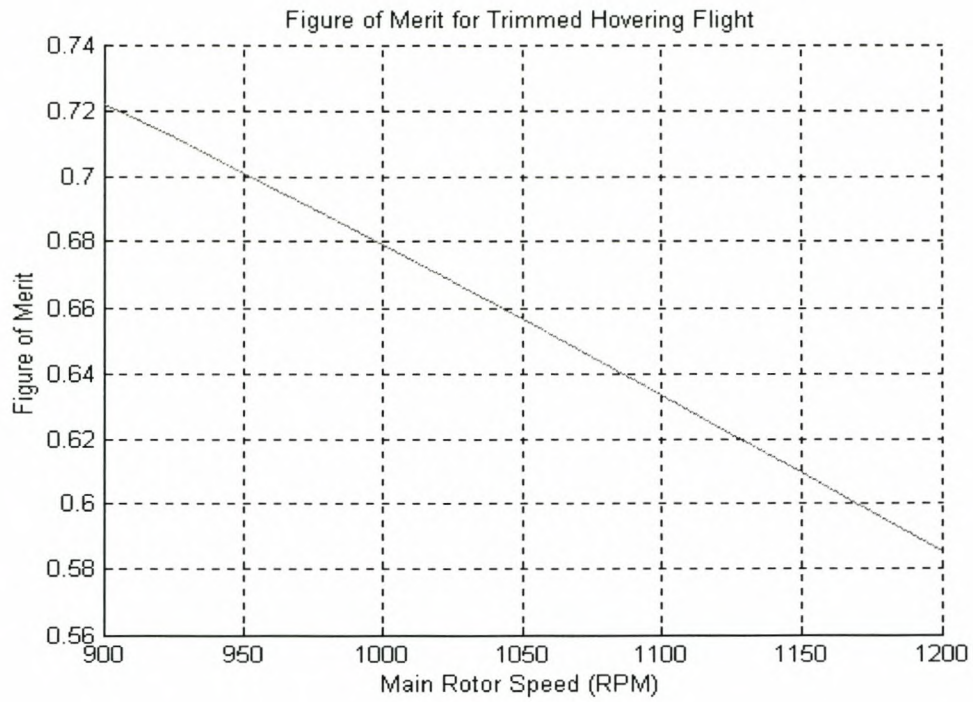


**Figure 3.2**

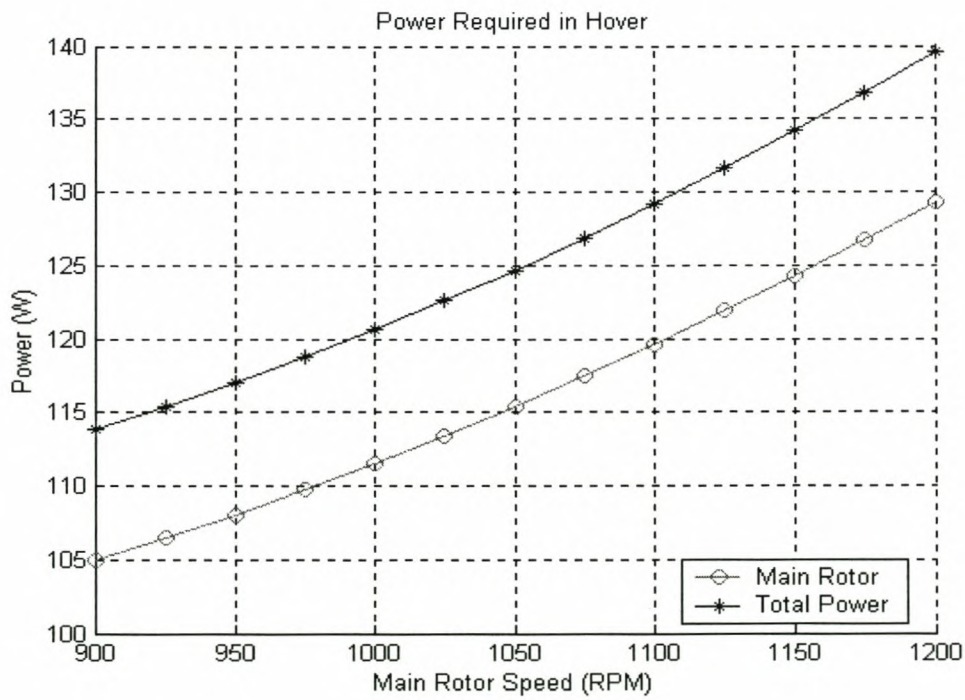


**Figure 3.3**



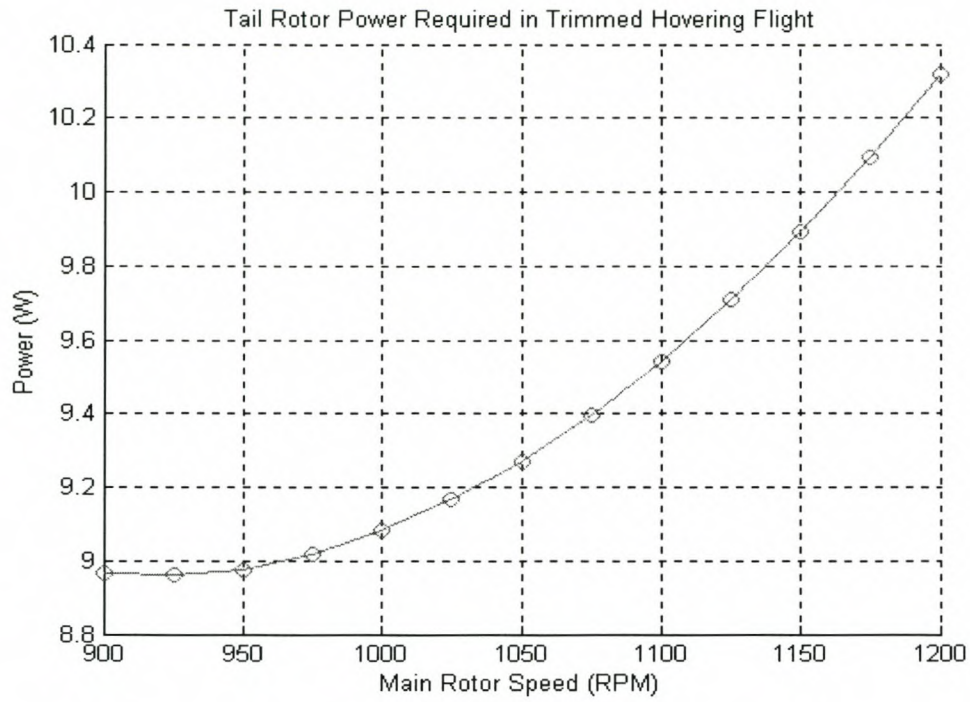


**Figure 3.4**

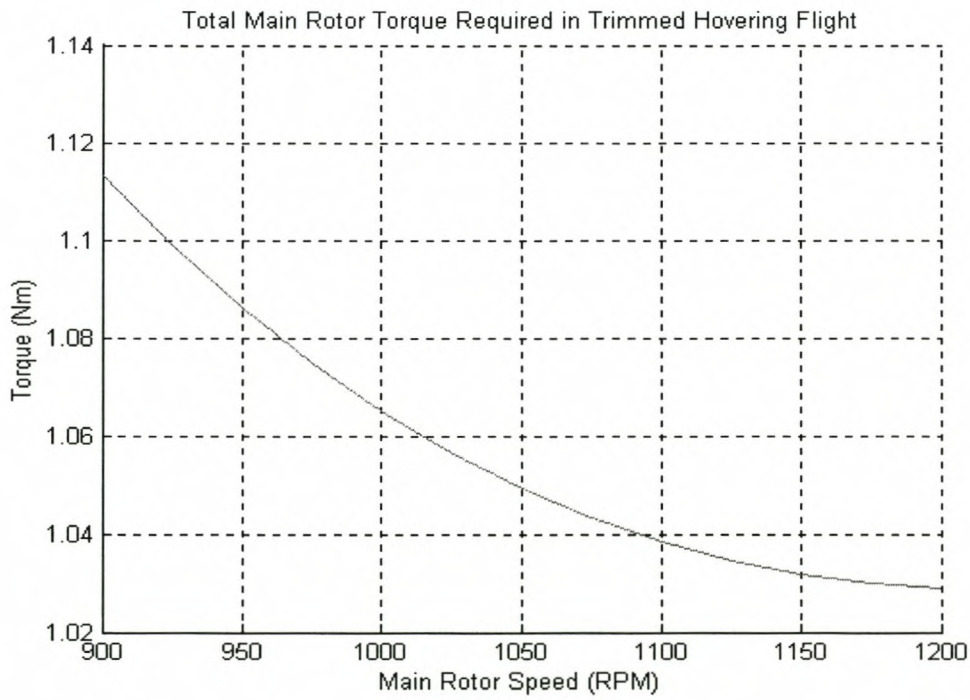


**Figure 3.5**

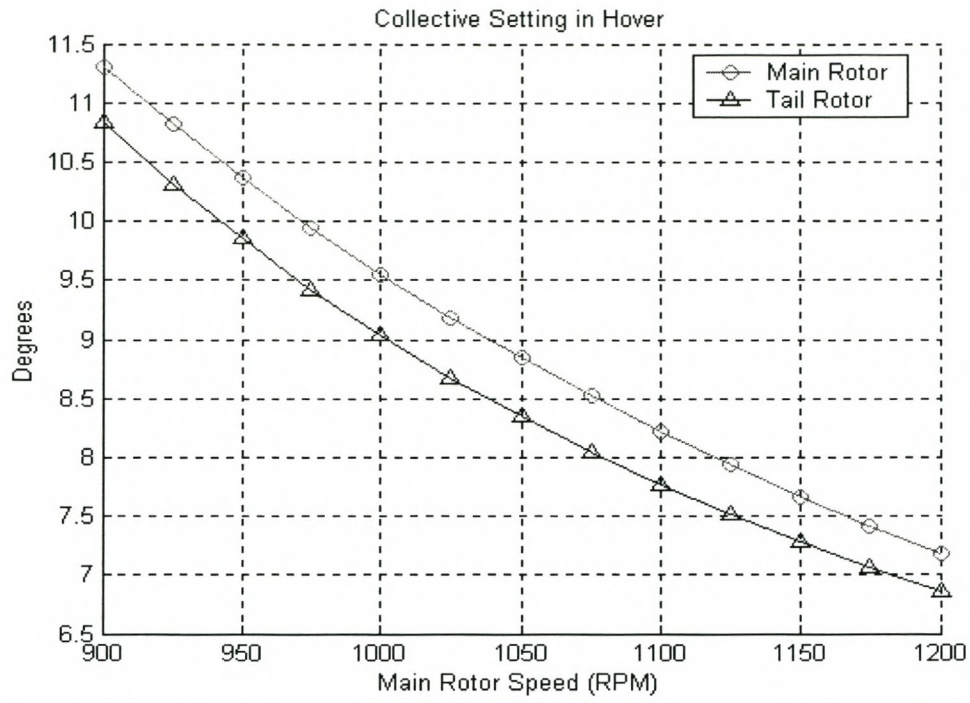


**Figure 3.6**



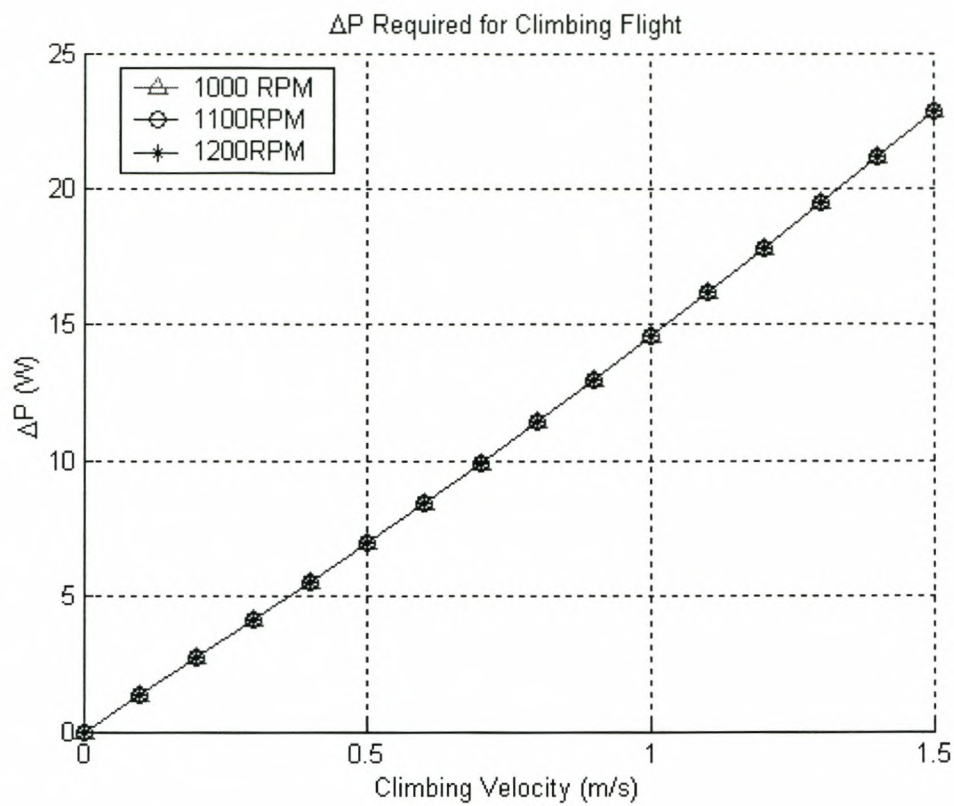


**Figure 4.1**

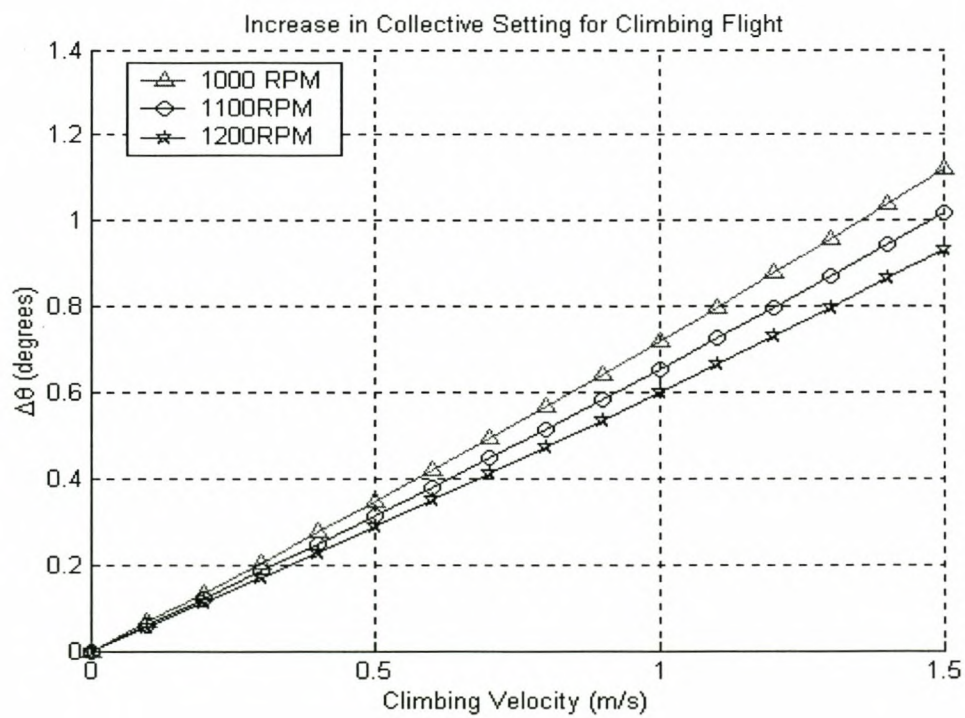


**Figure 4.2**



**Figure 4.3**

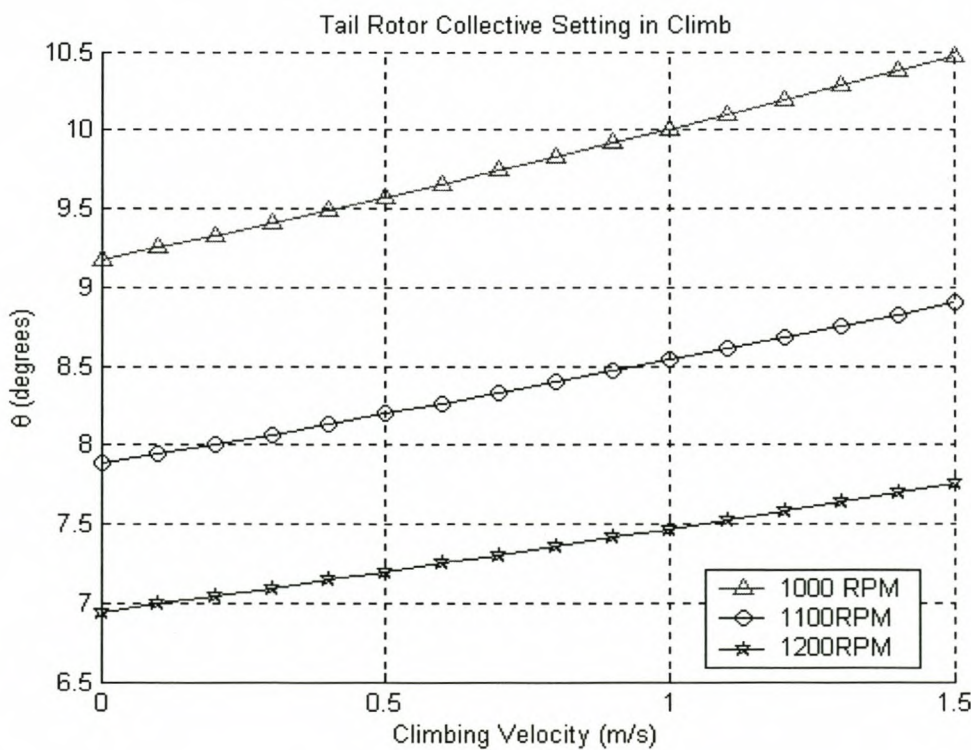




**Figure 4.4**

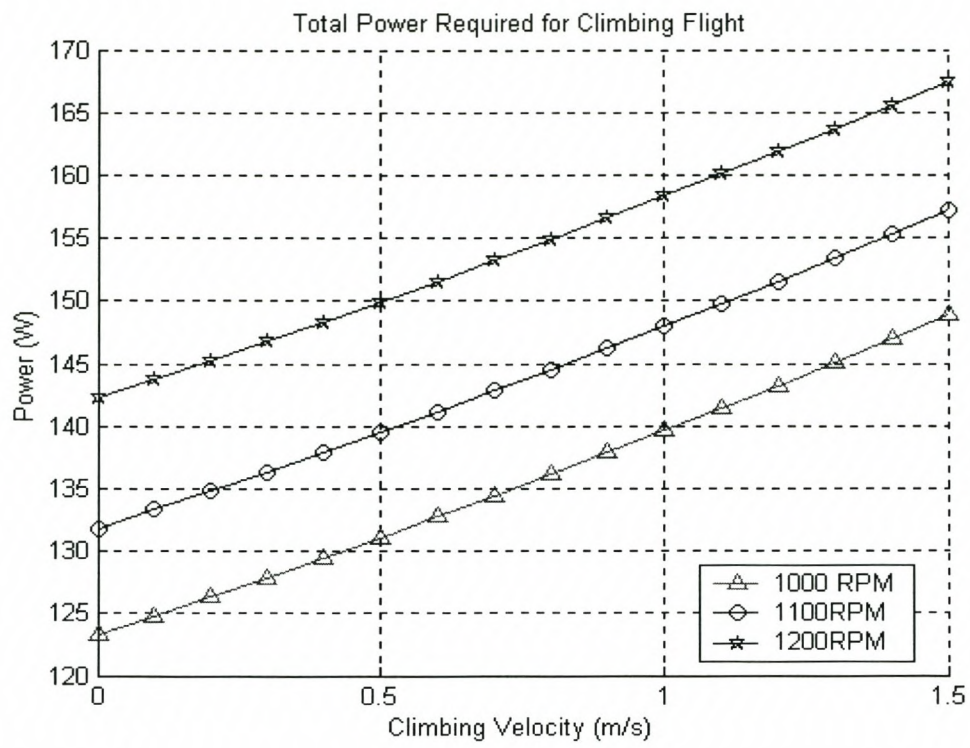


**Figure 4.5**

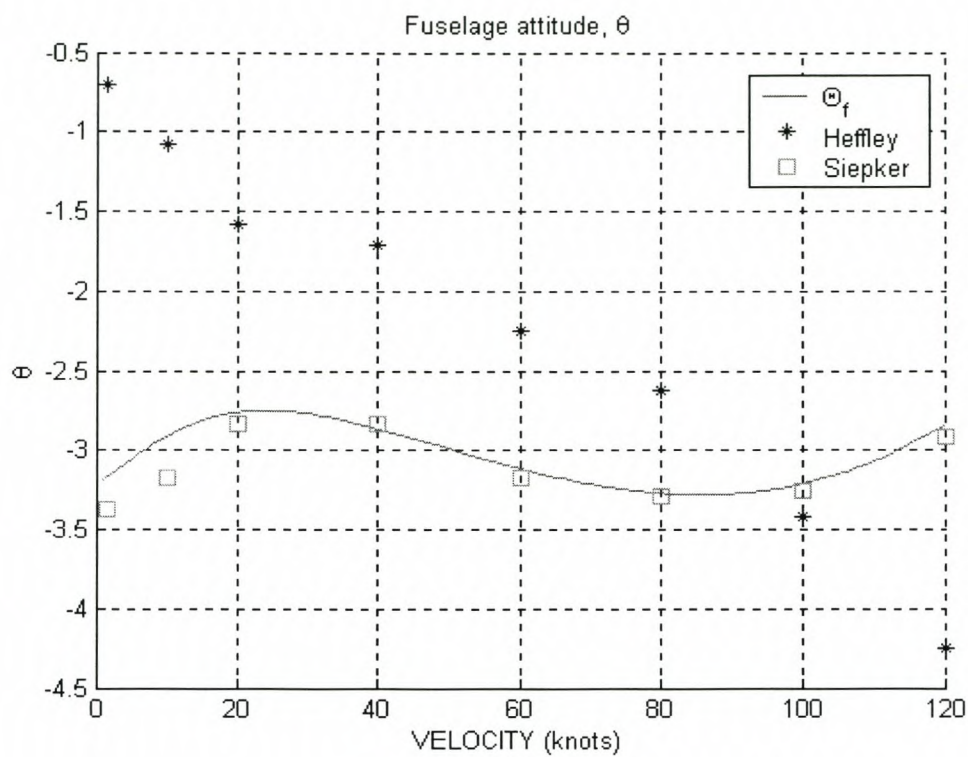


**Figure 5.1**

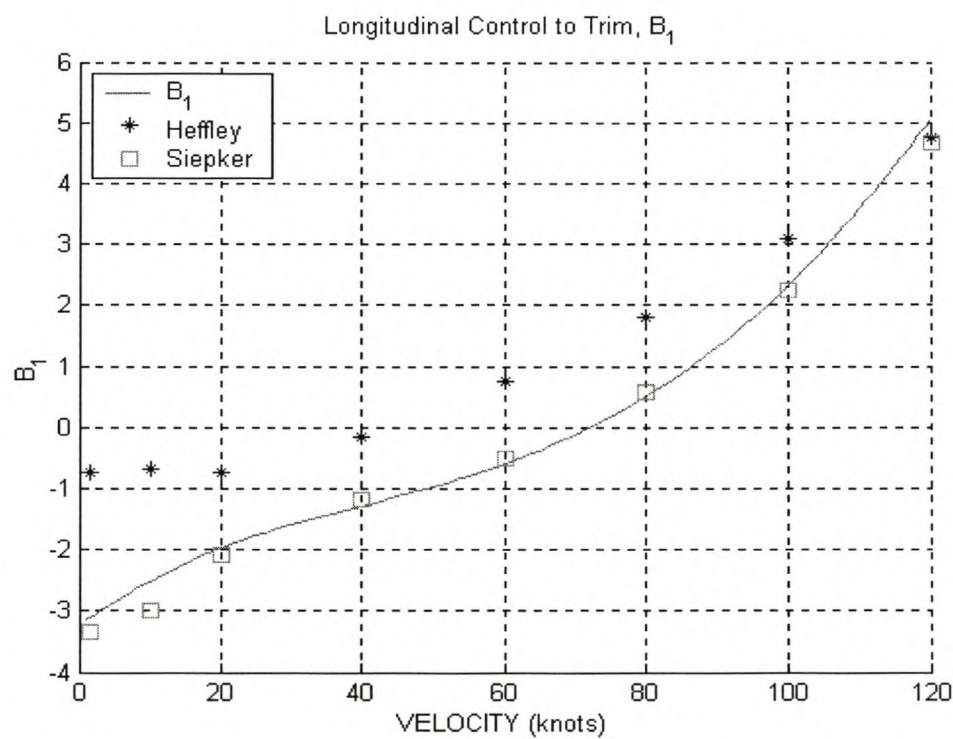


**Figure 5.2**



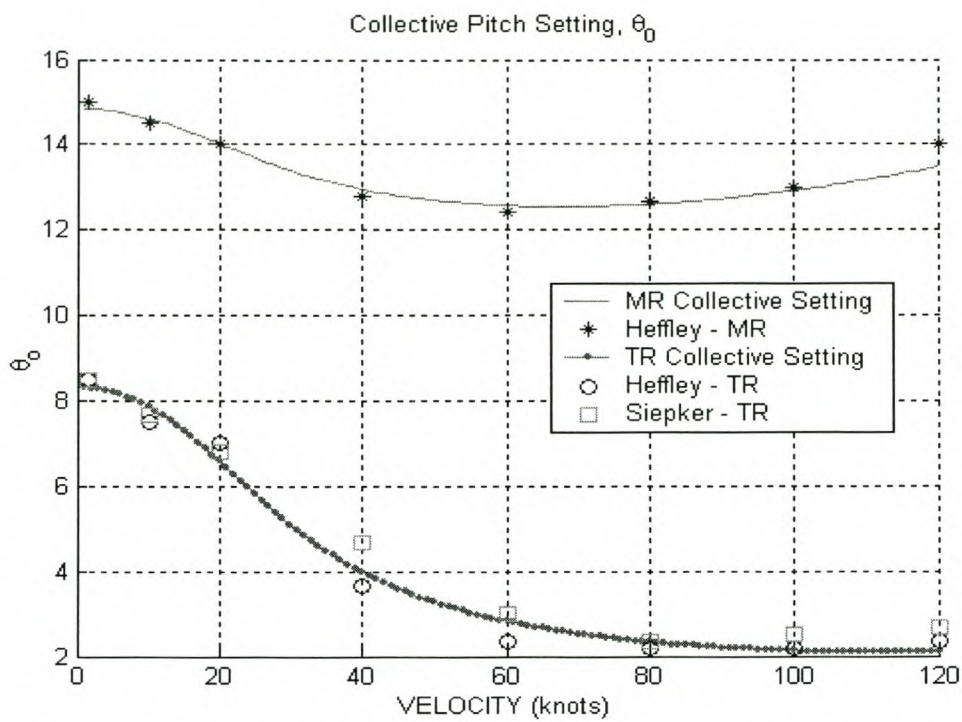


**Figure 5.3**

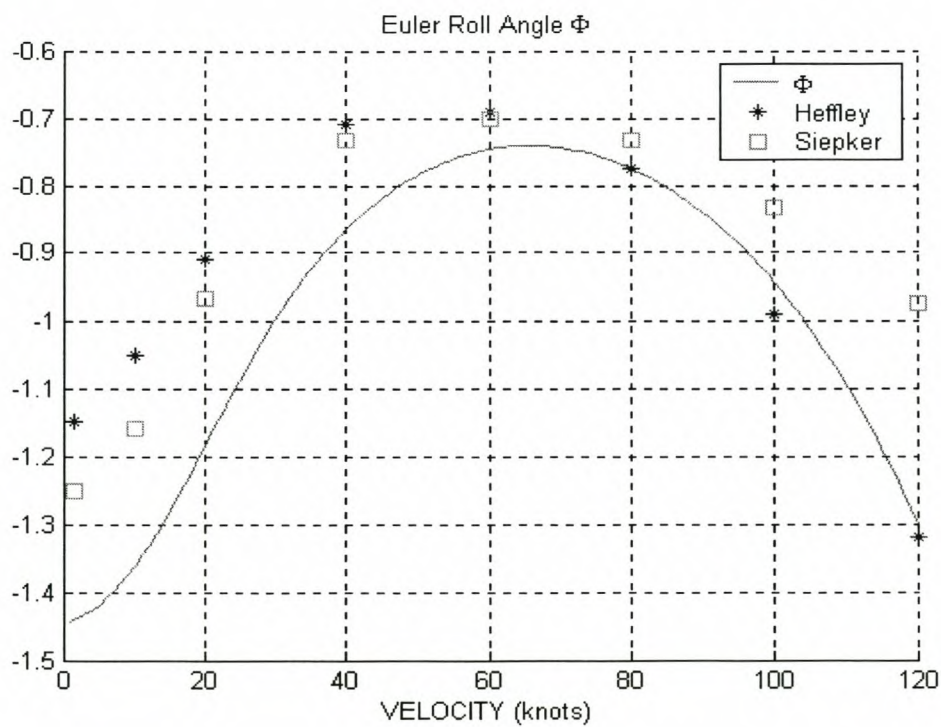


**Figure 5.4**

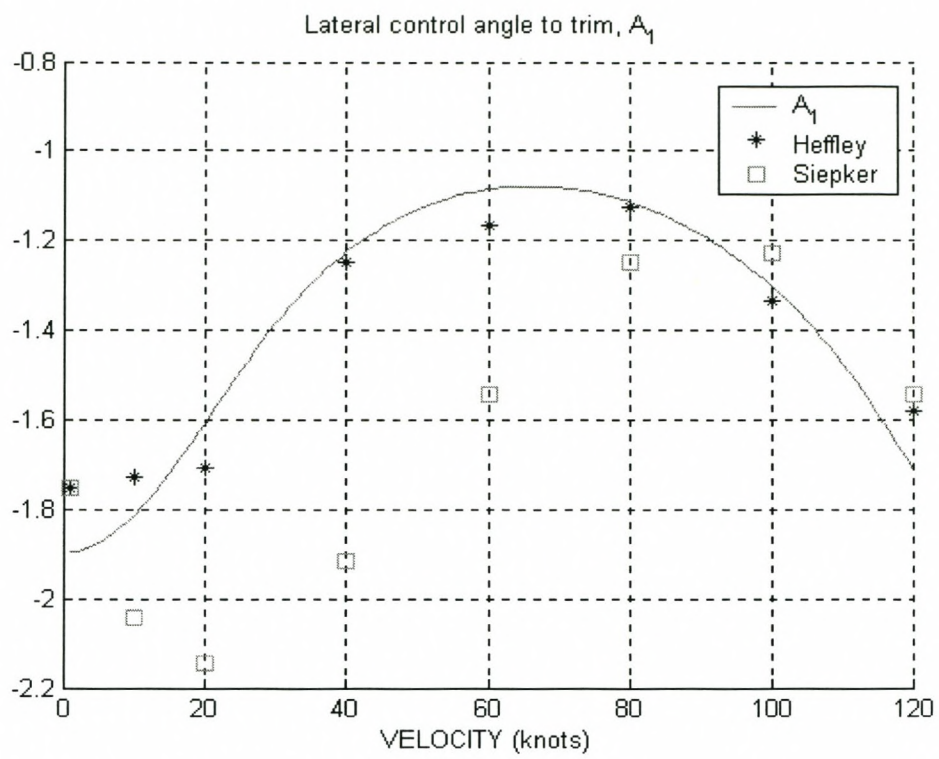


**Figure 5.5**



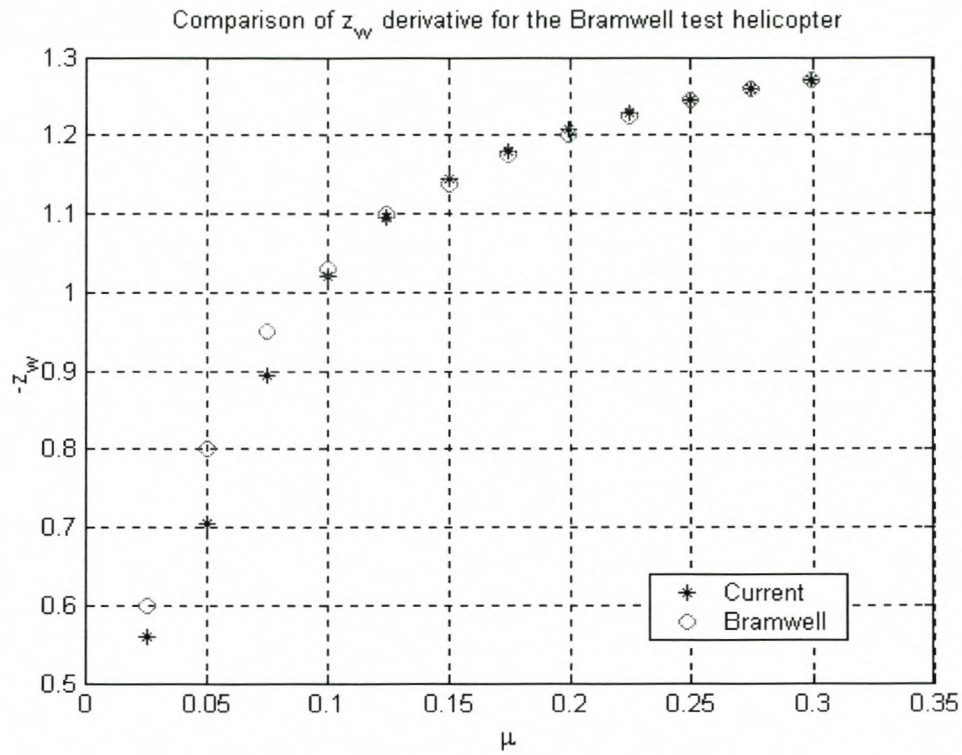


Figure 6.1

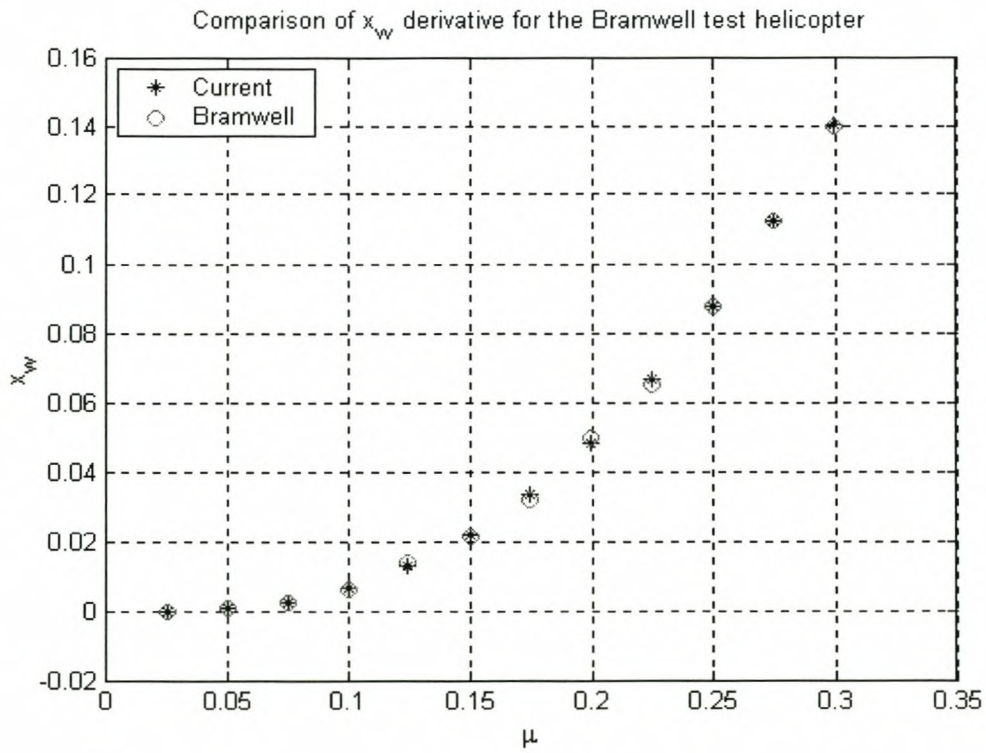


Figure 6.2

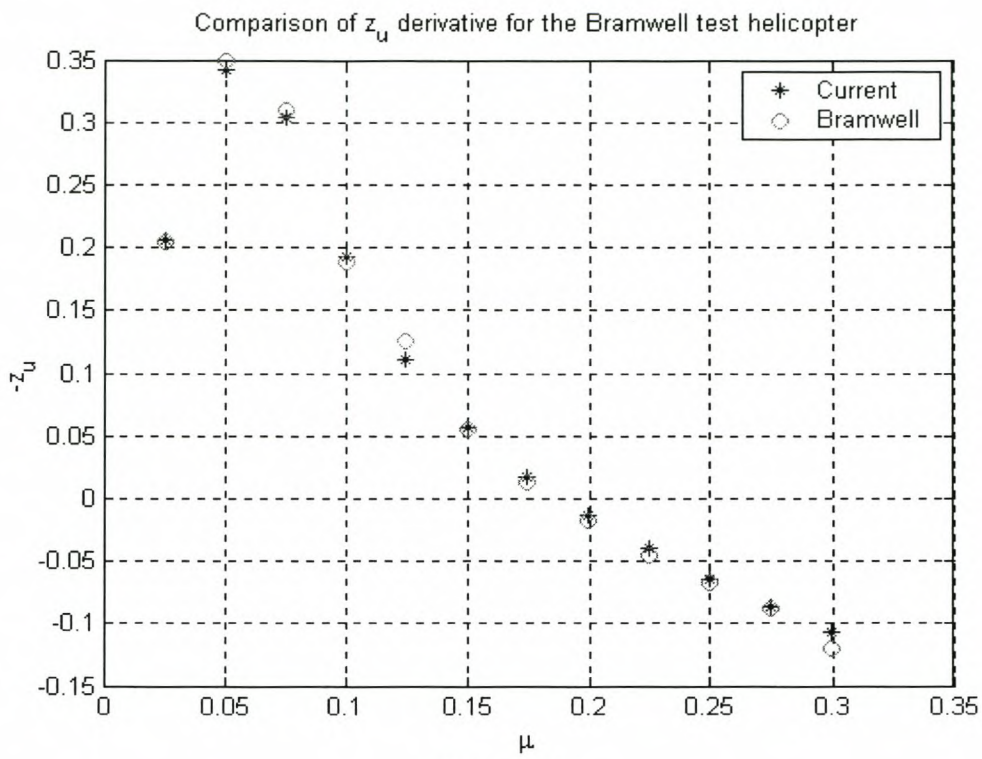


Figure 6.3

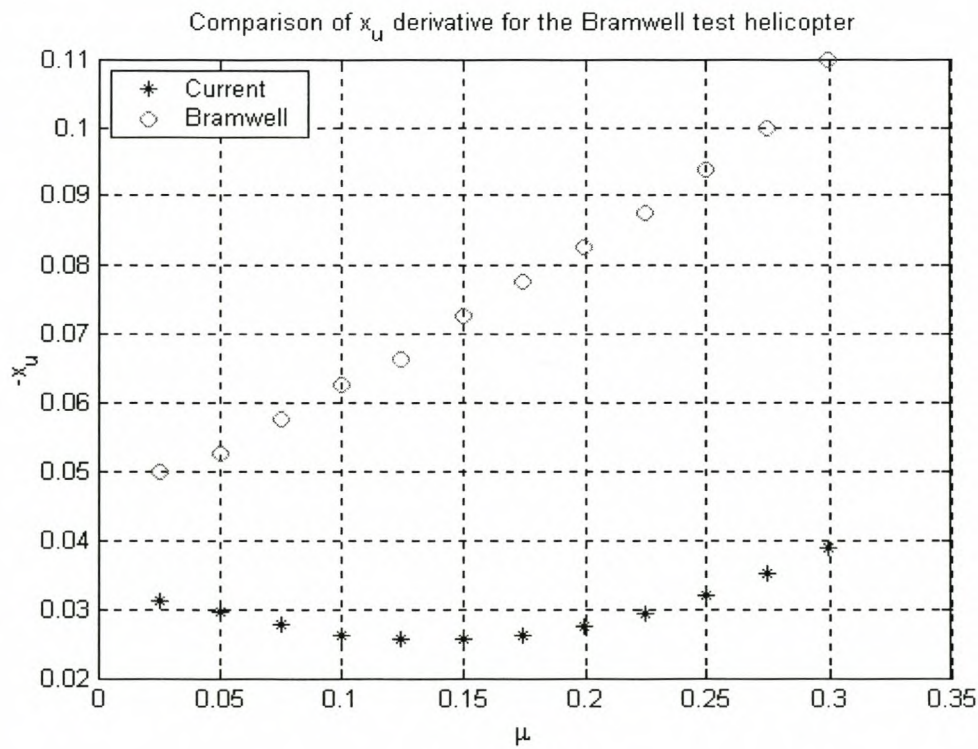


Figure 6.4



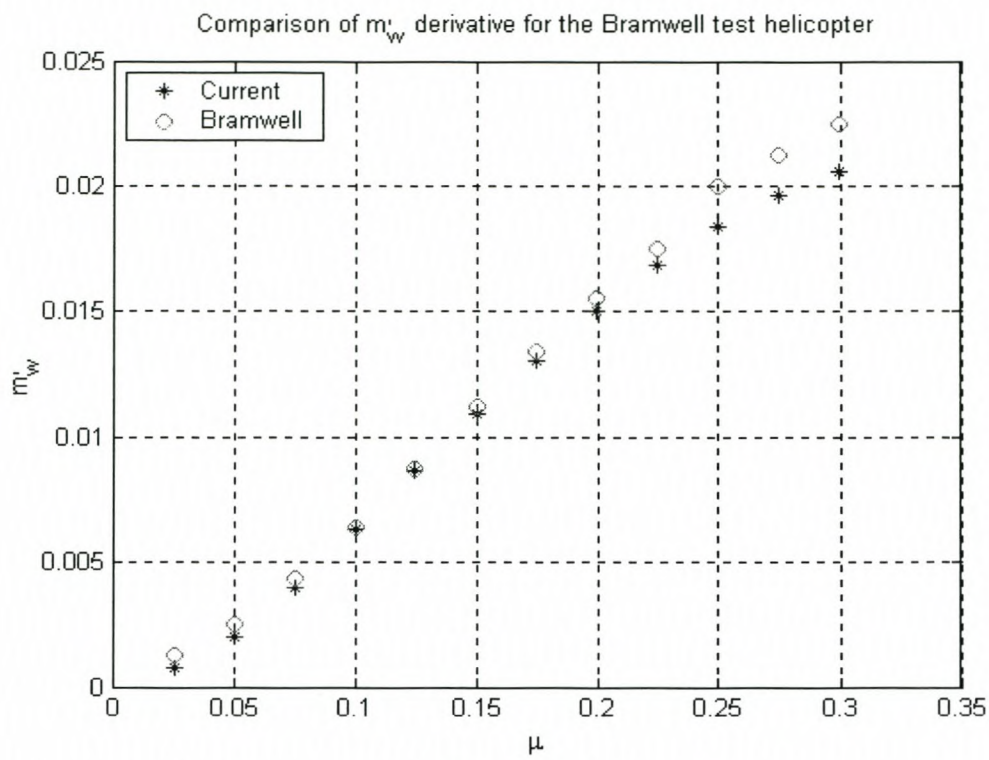


Figure 6.5

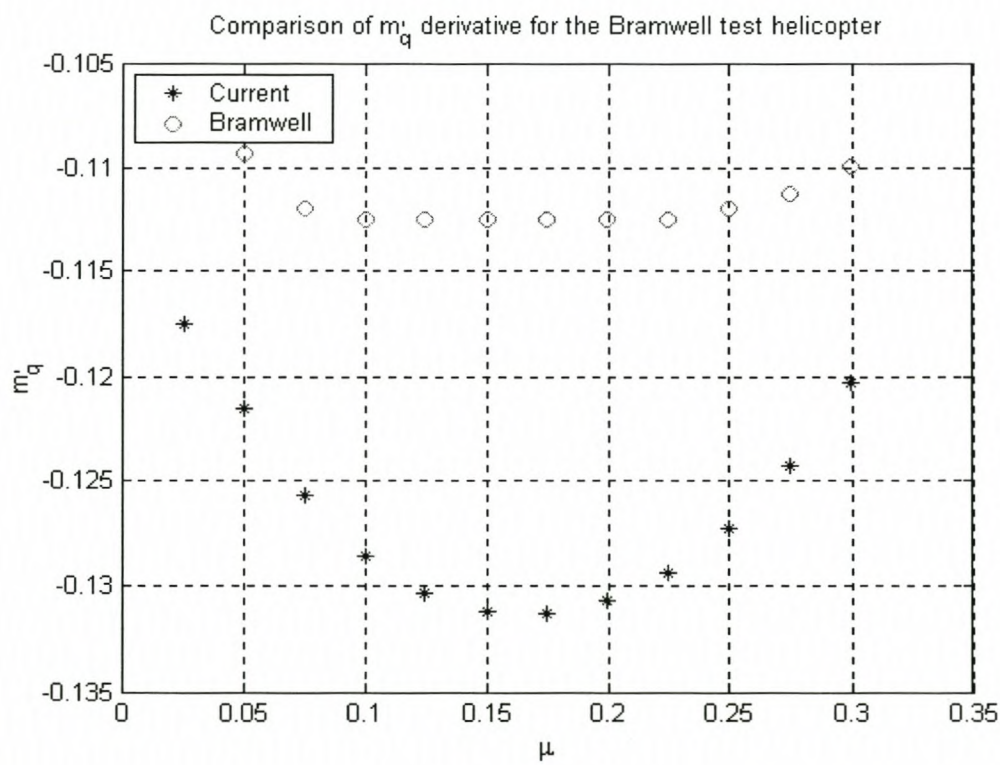


Figure 6.6

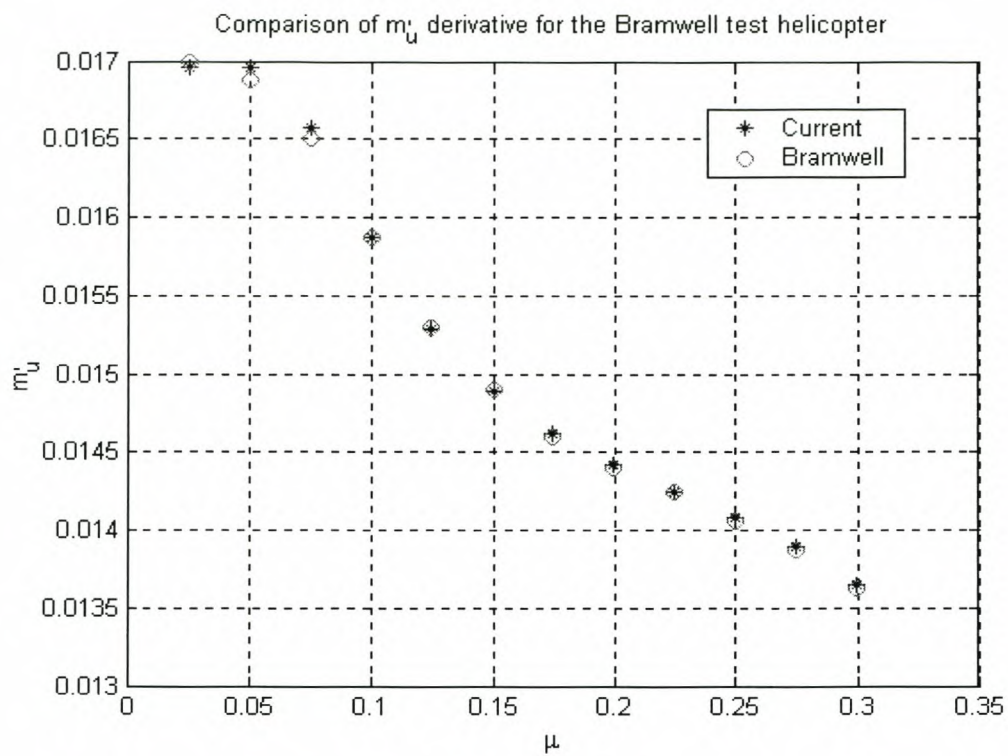


Figure 6.7

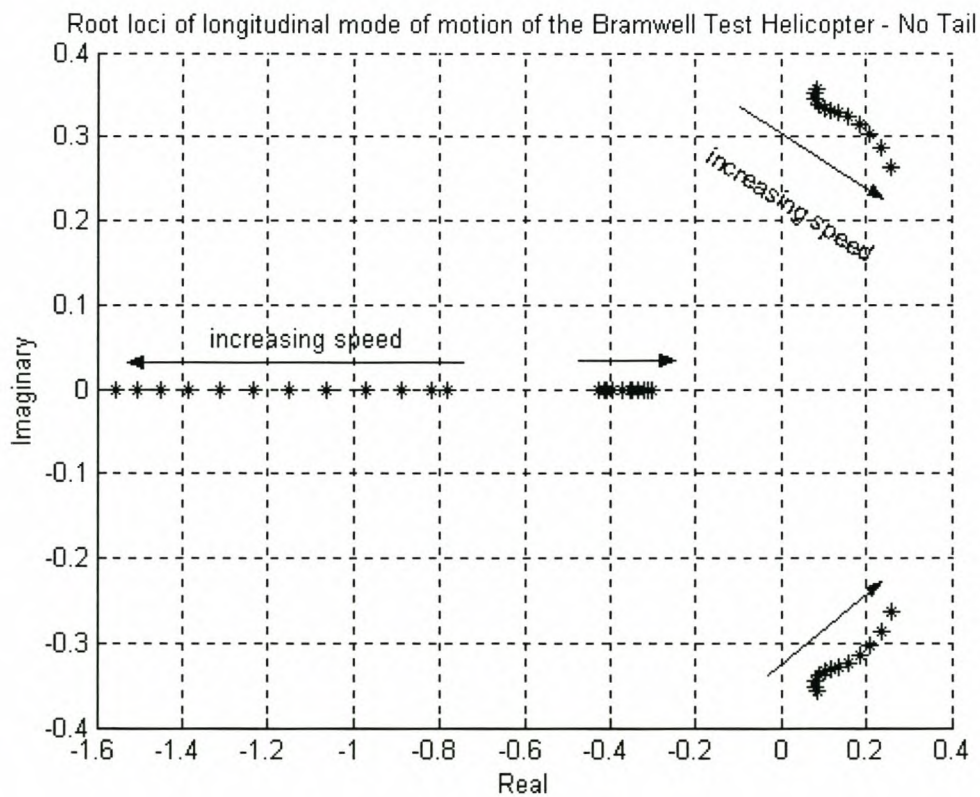


Figure 6.8



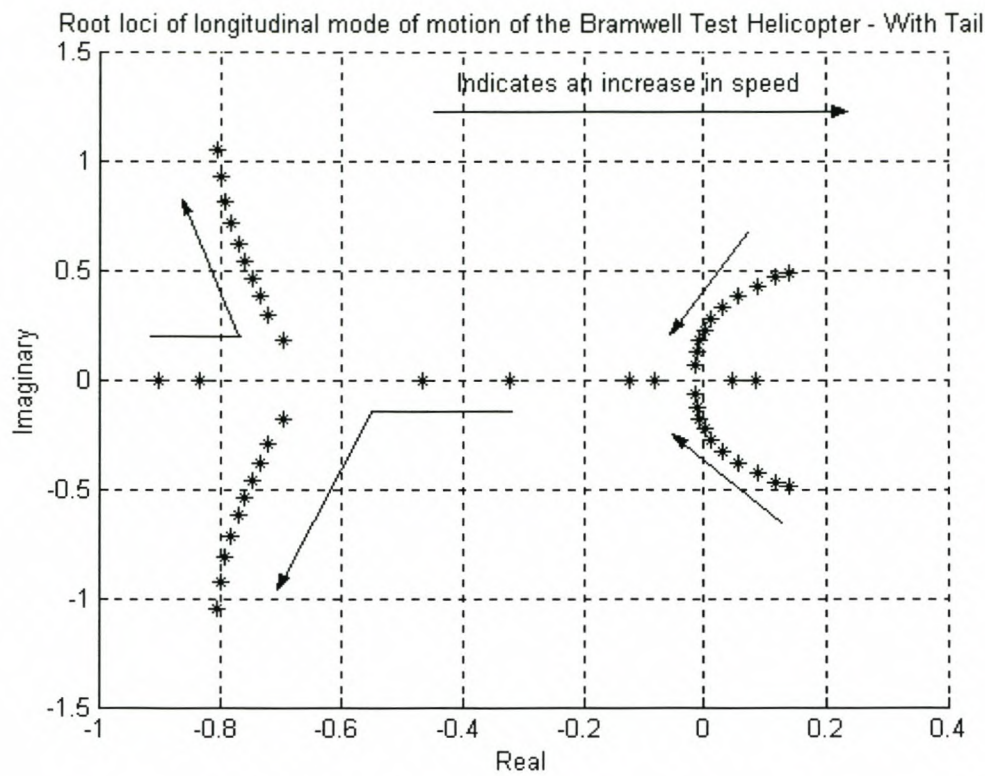


Figure 6.9

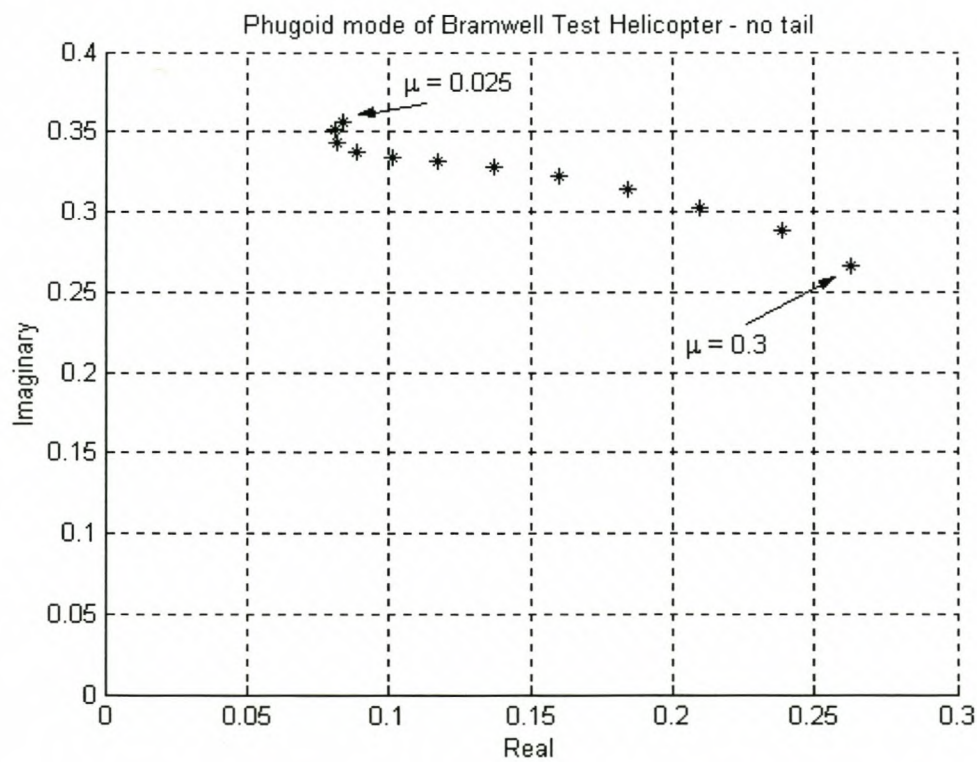


Figure 6.10

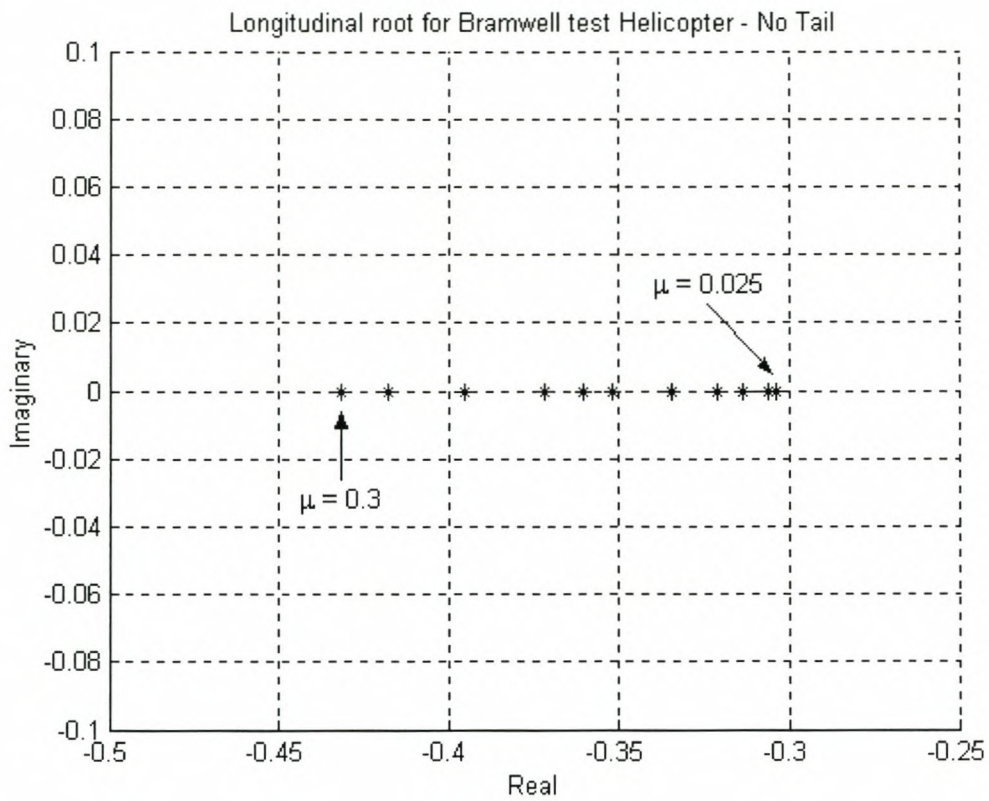


Figure 6.11

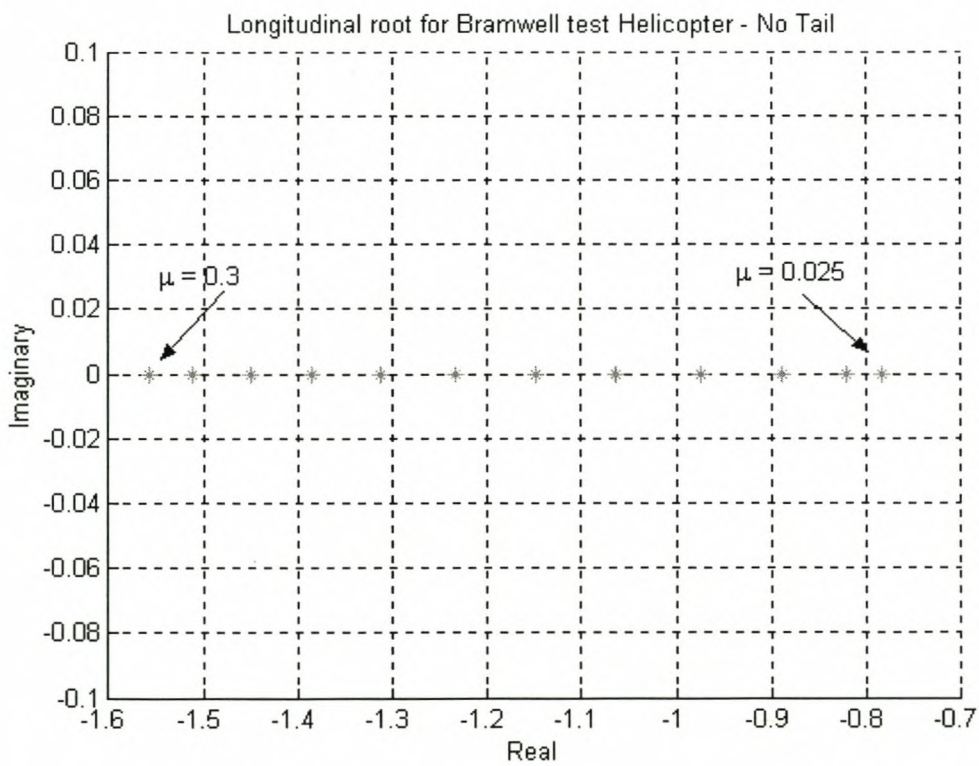
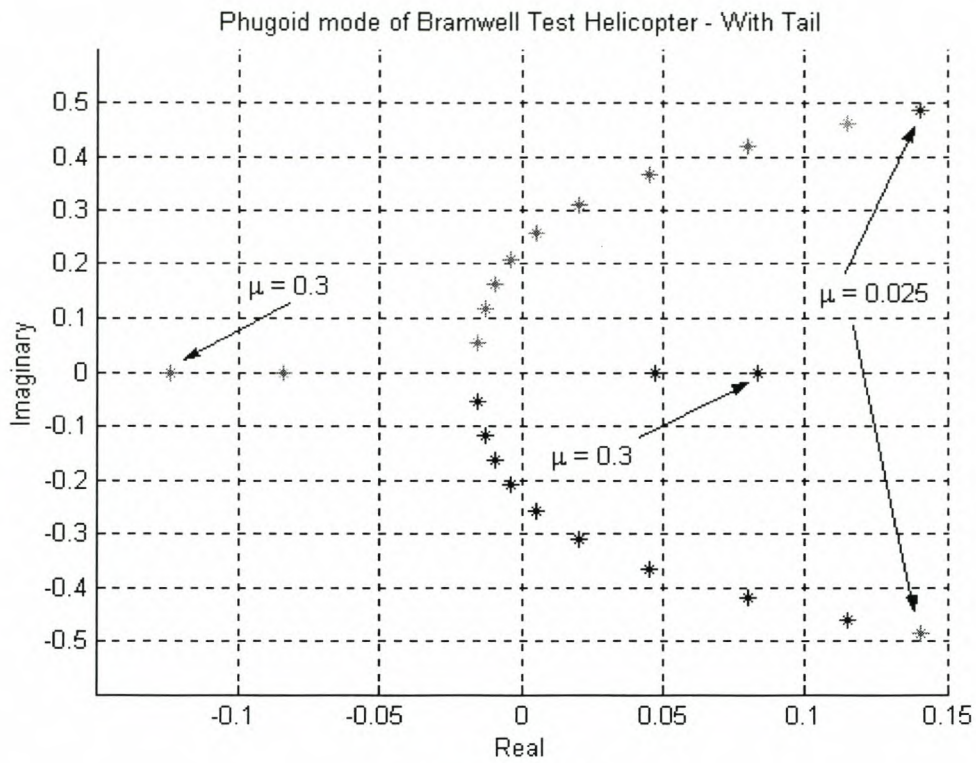
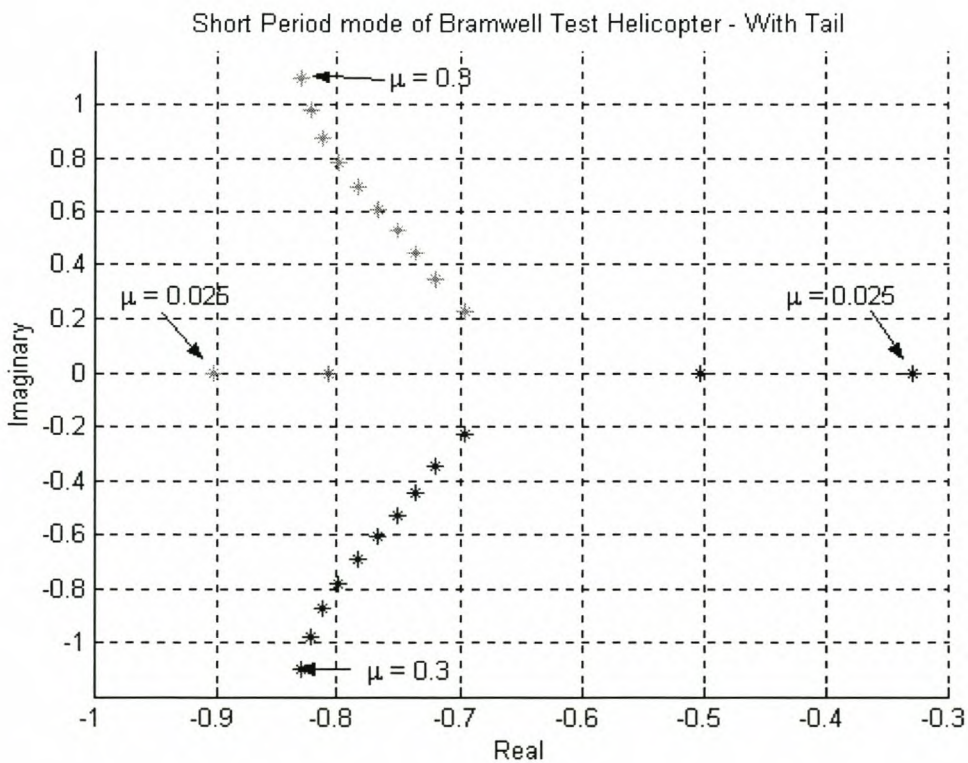


Figure 6.12





**Figure 6.13**



**Figure 6.14**

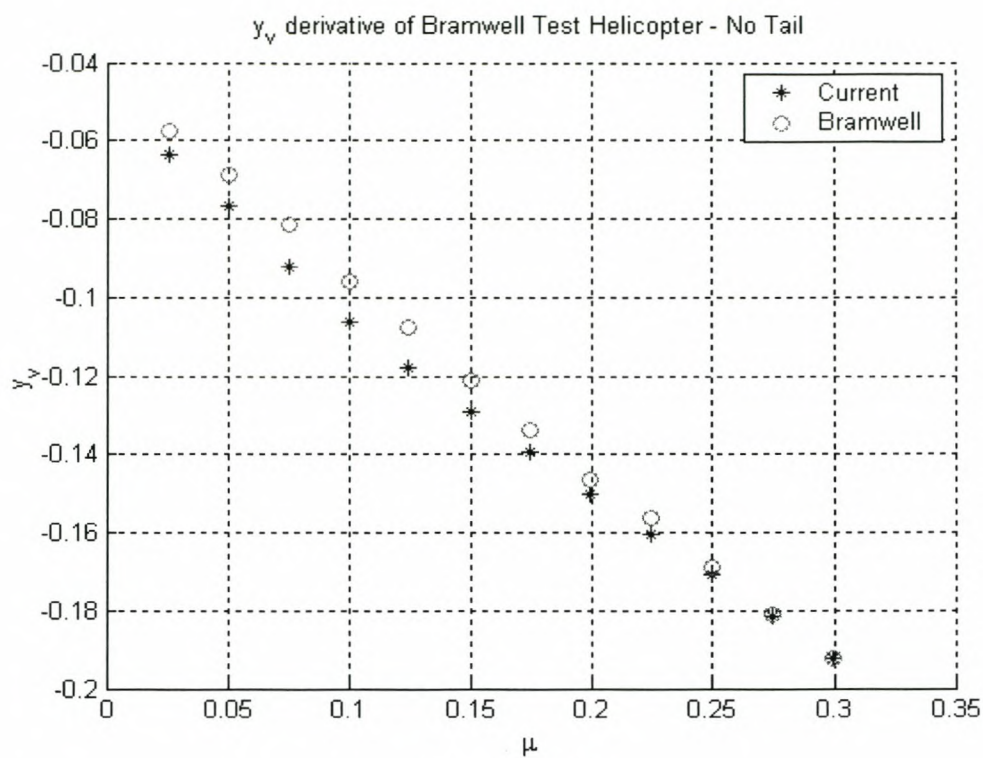


**Figure 6.15**

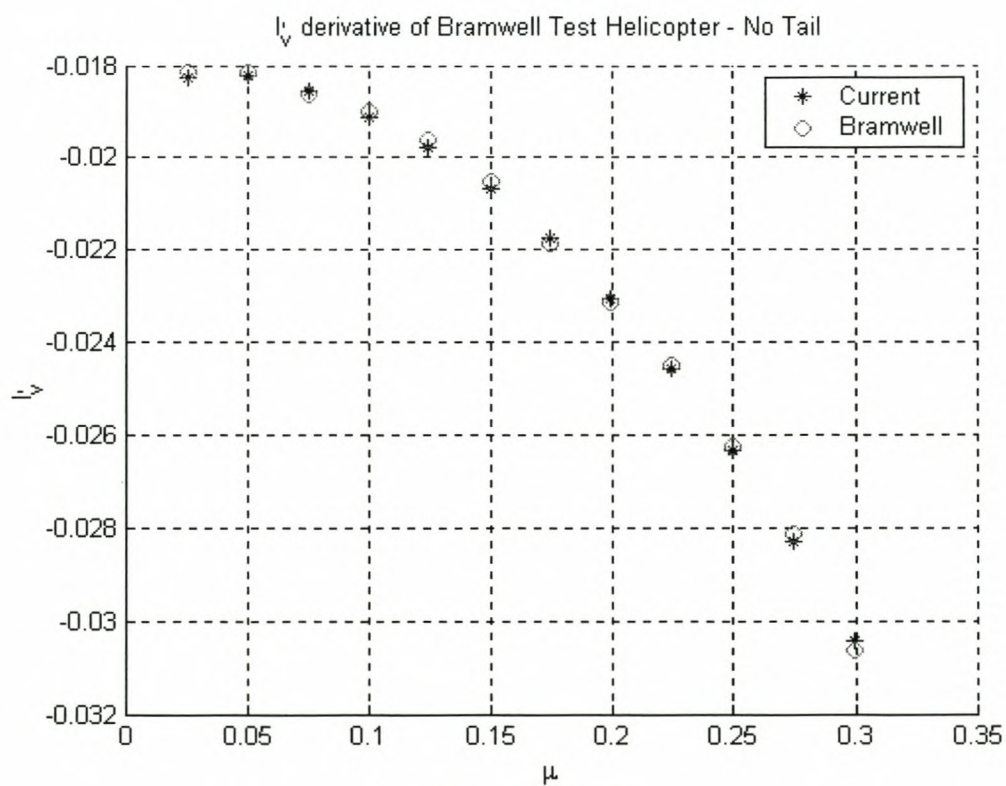


**Figure 6.16**



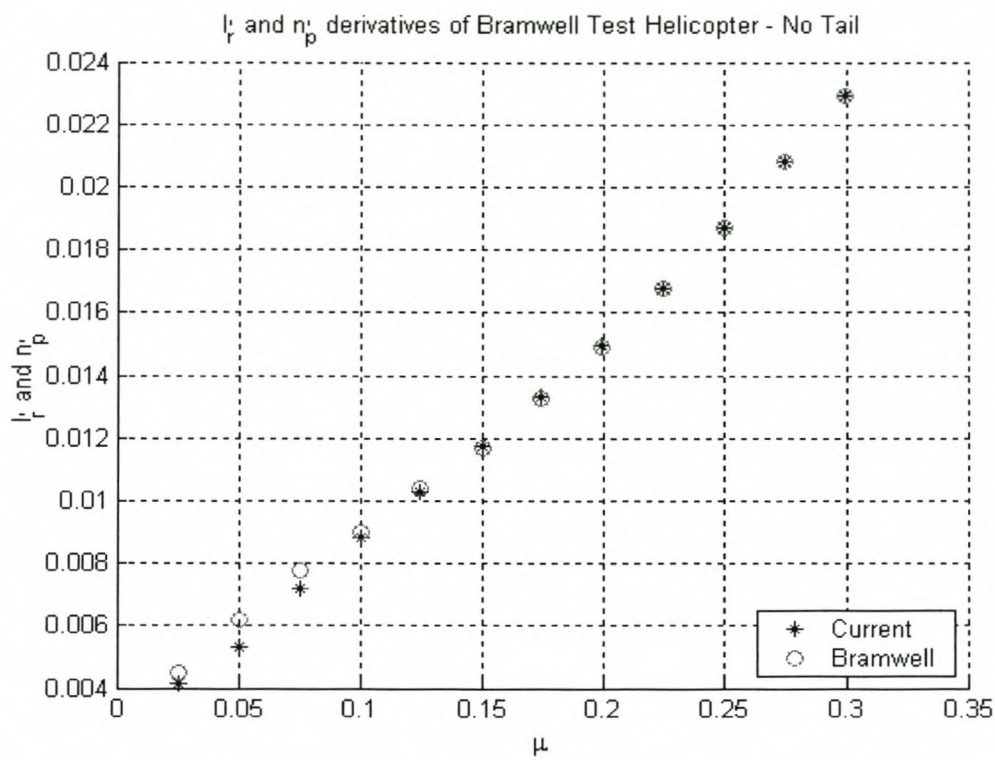


Figure 6.17

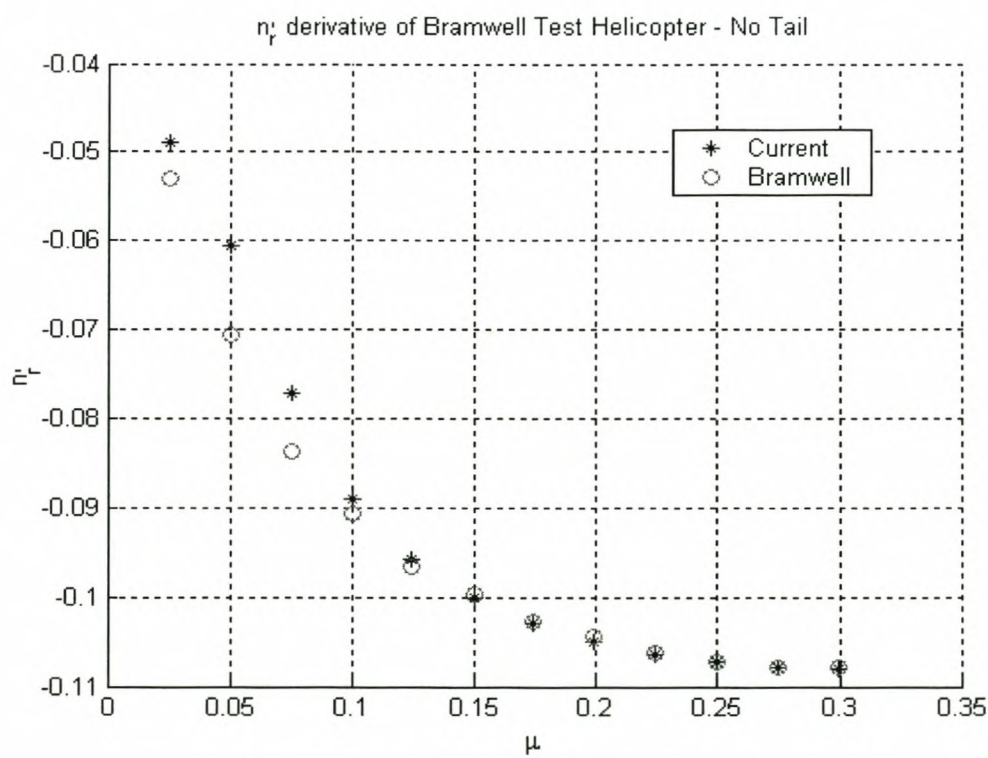
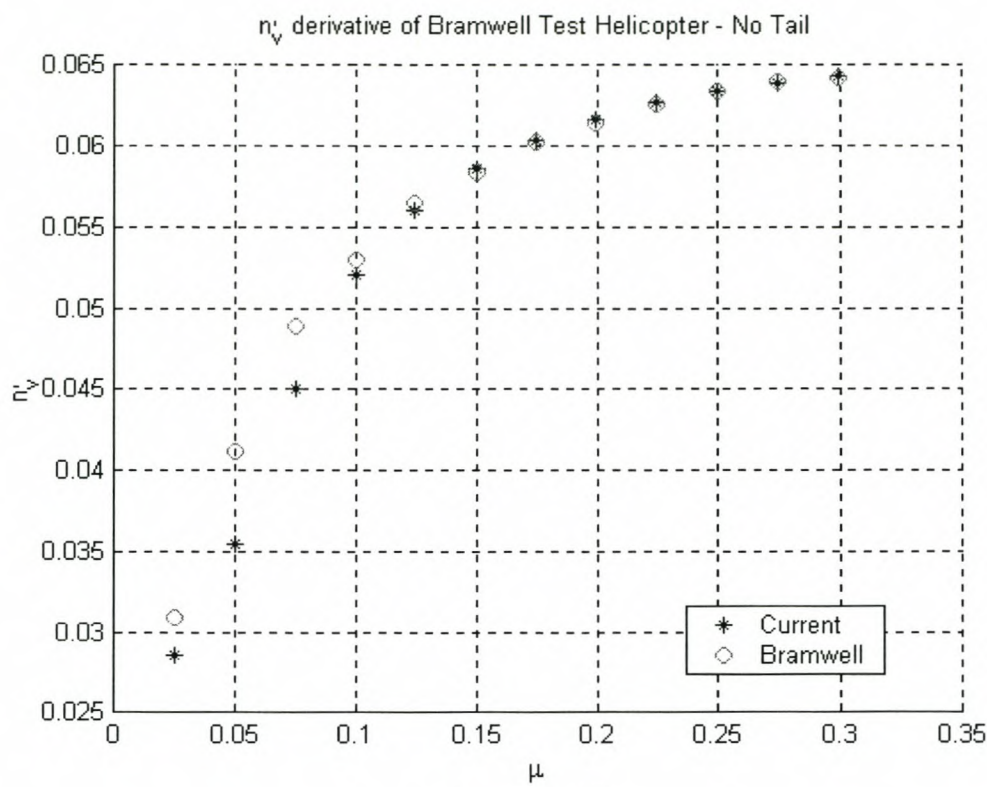
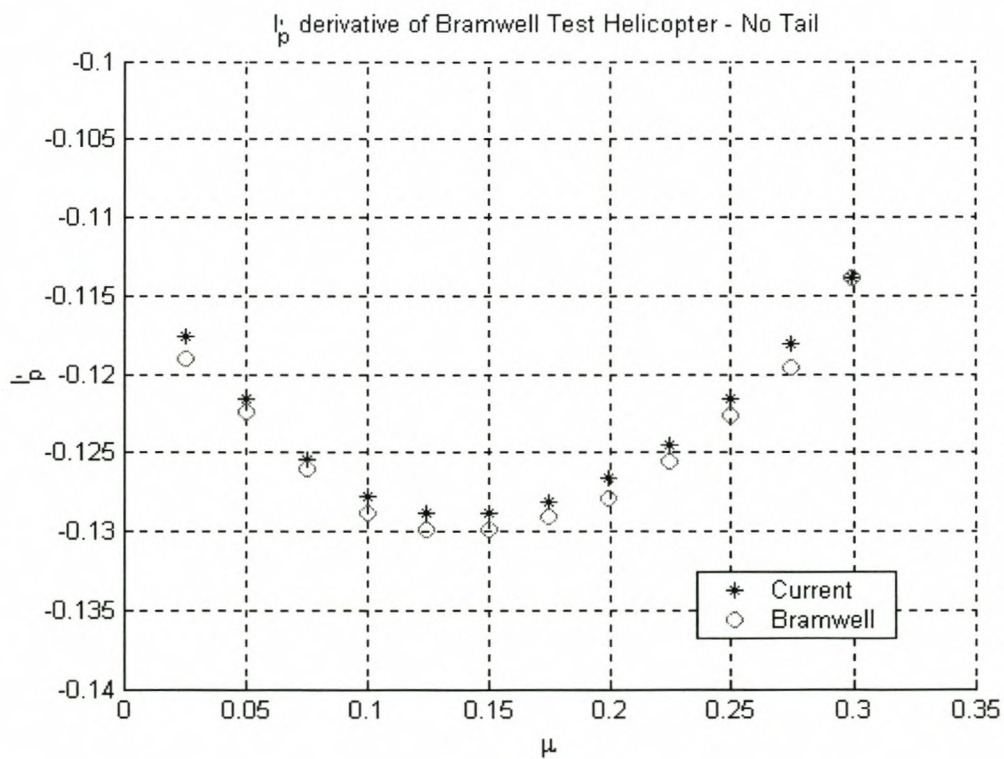


Figure 6.18



**Figure 6.19**



**Figure 6.20**



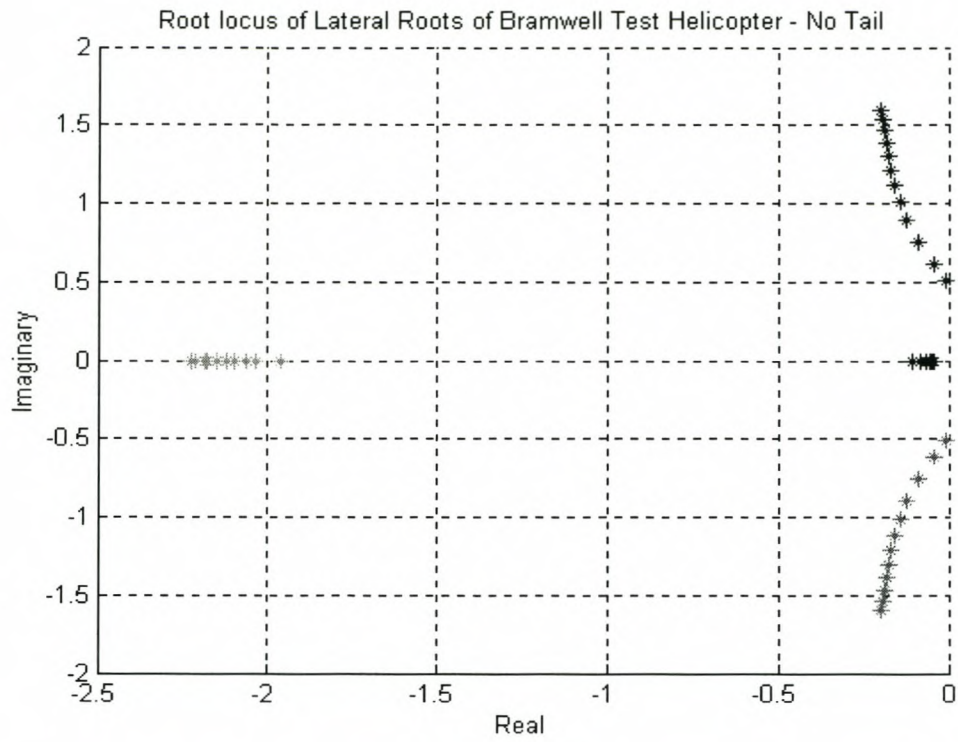


Figure 6.21

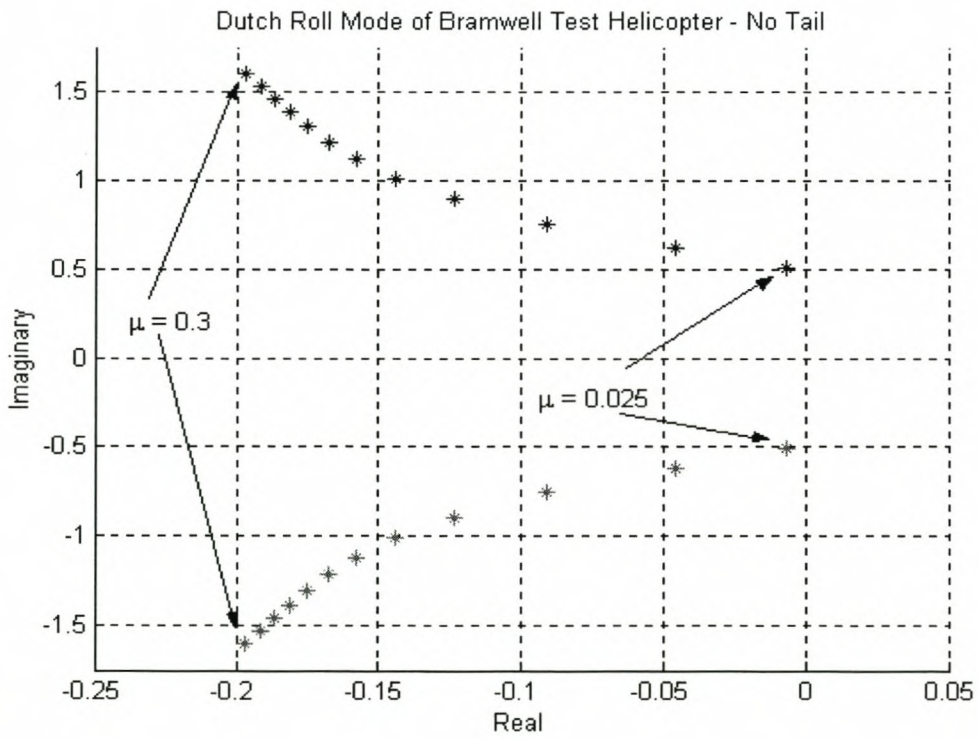
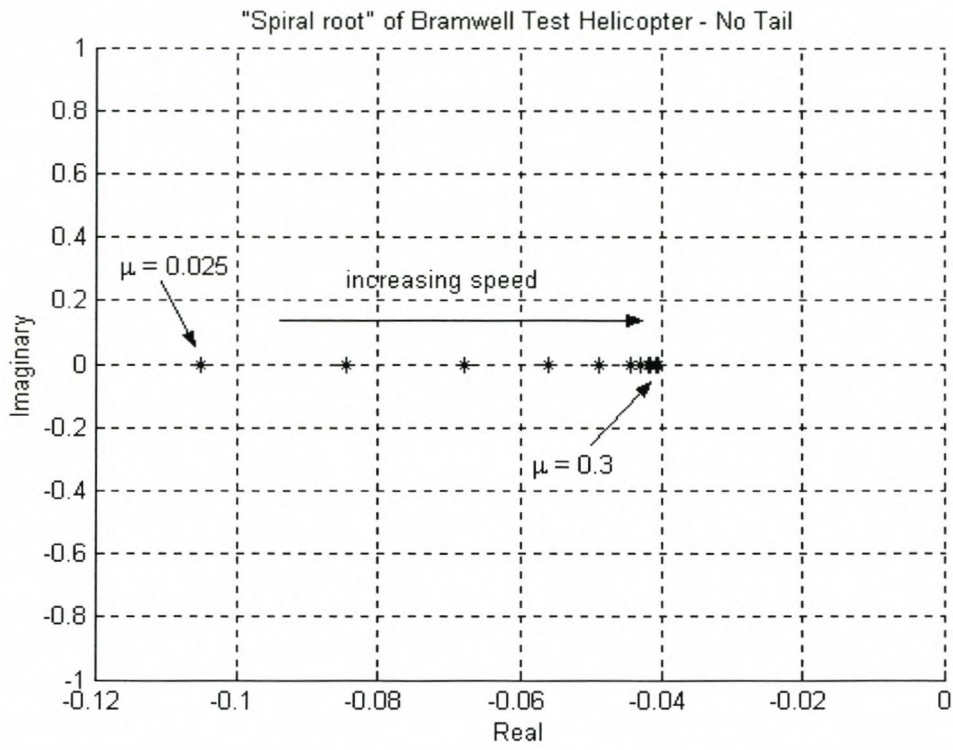
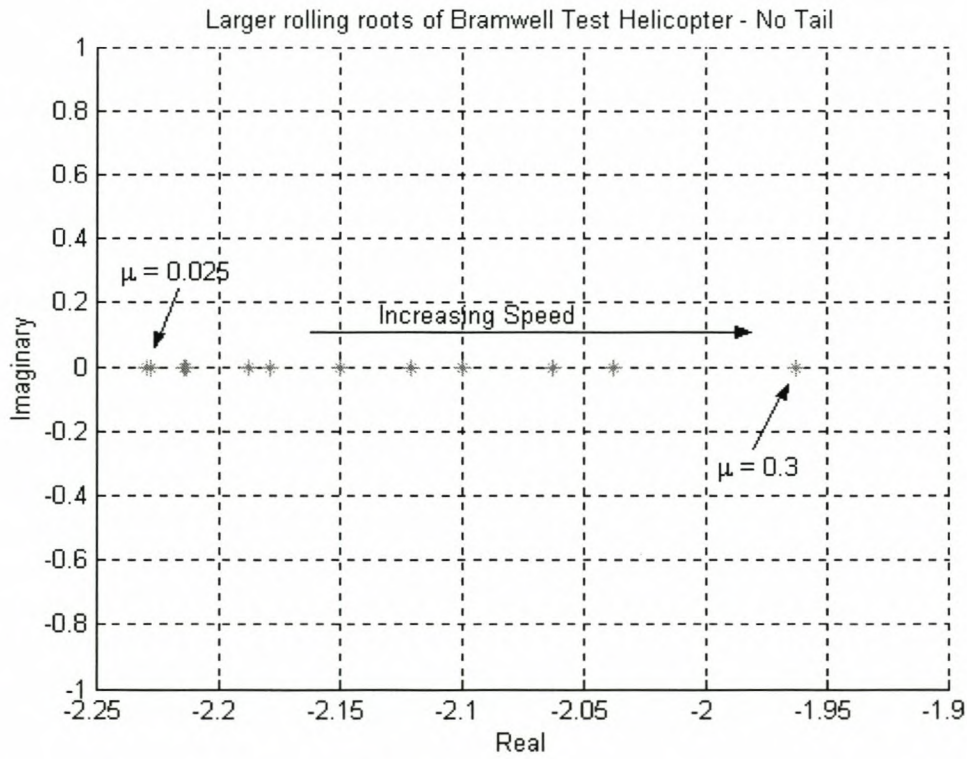


Figure 6.22



**Figure 6.23**



**Figure 6.24**



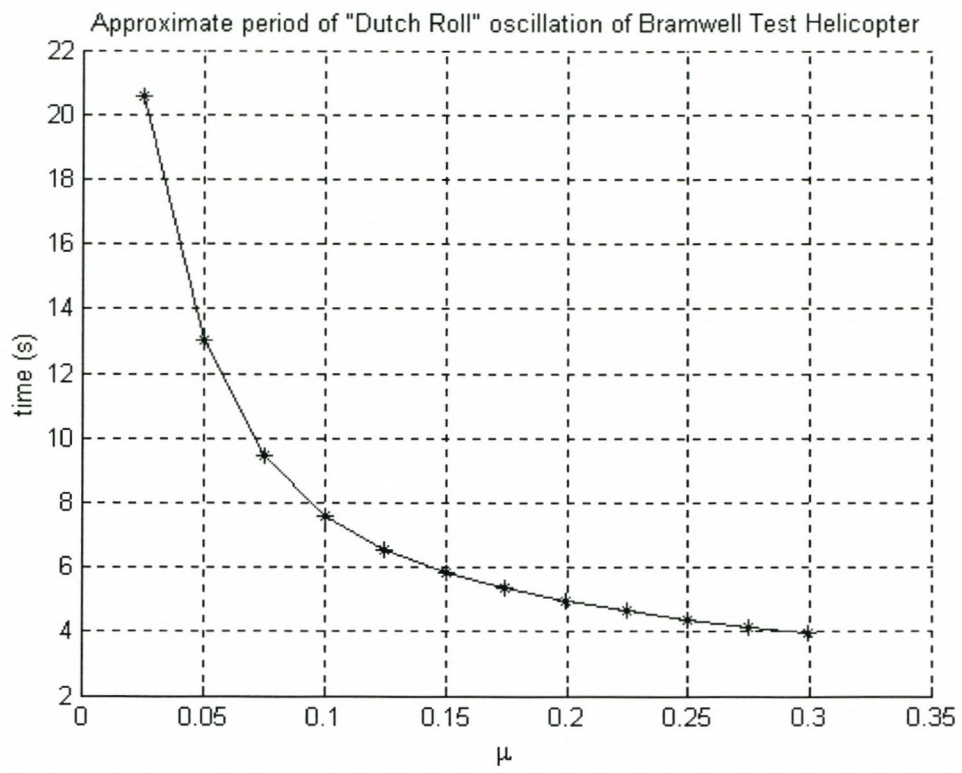


Figure 6.25

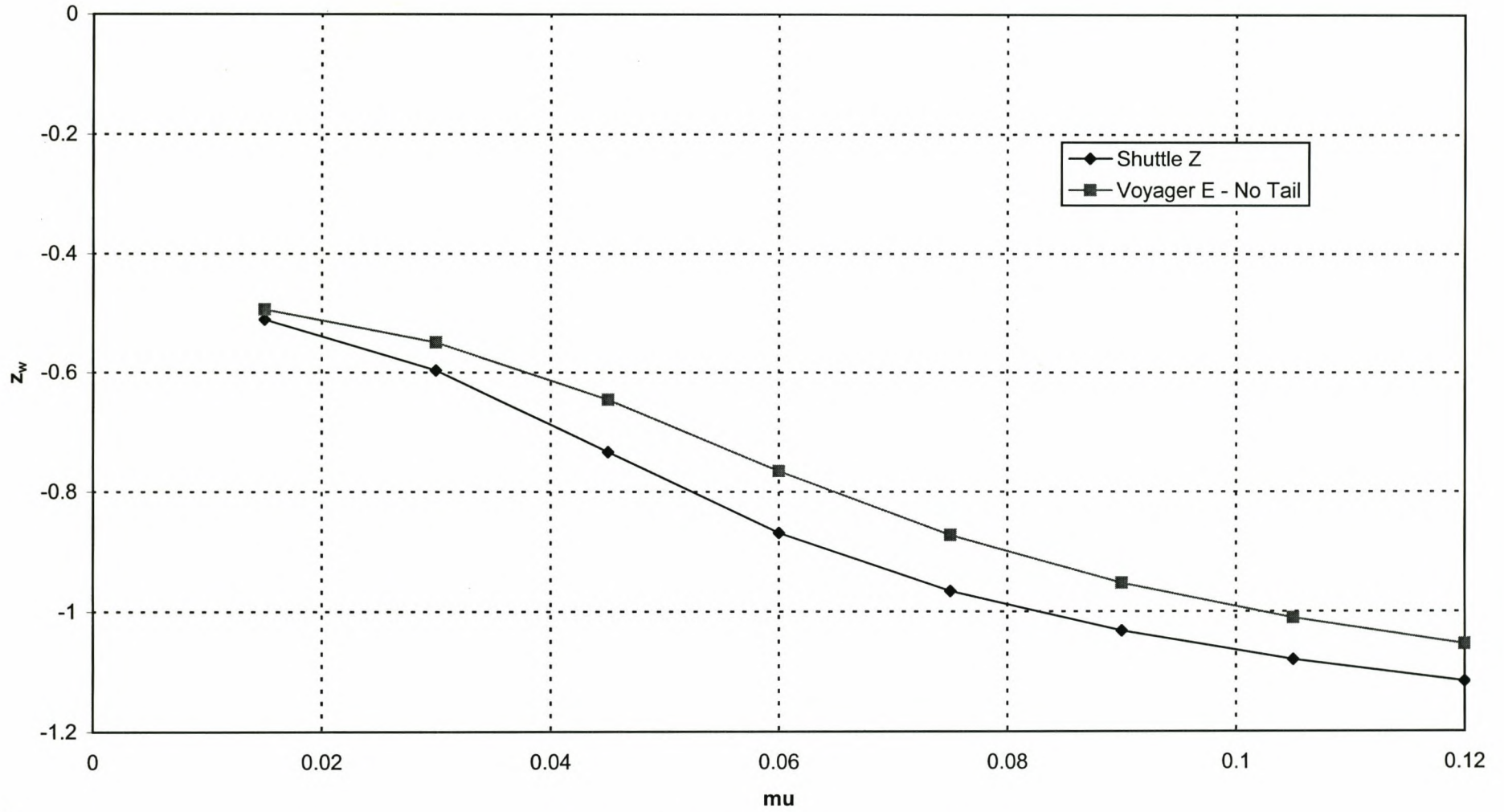


Figure 7.1 - Comparison of the  $z_w$  derivative



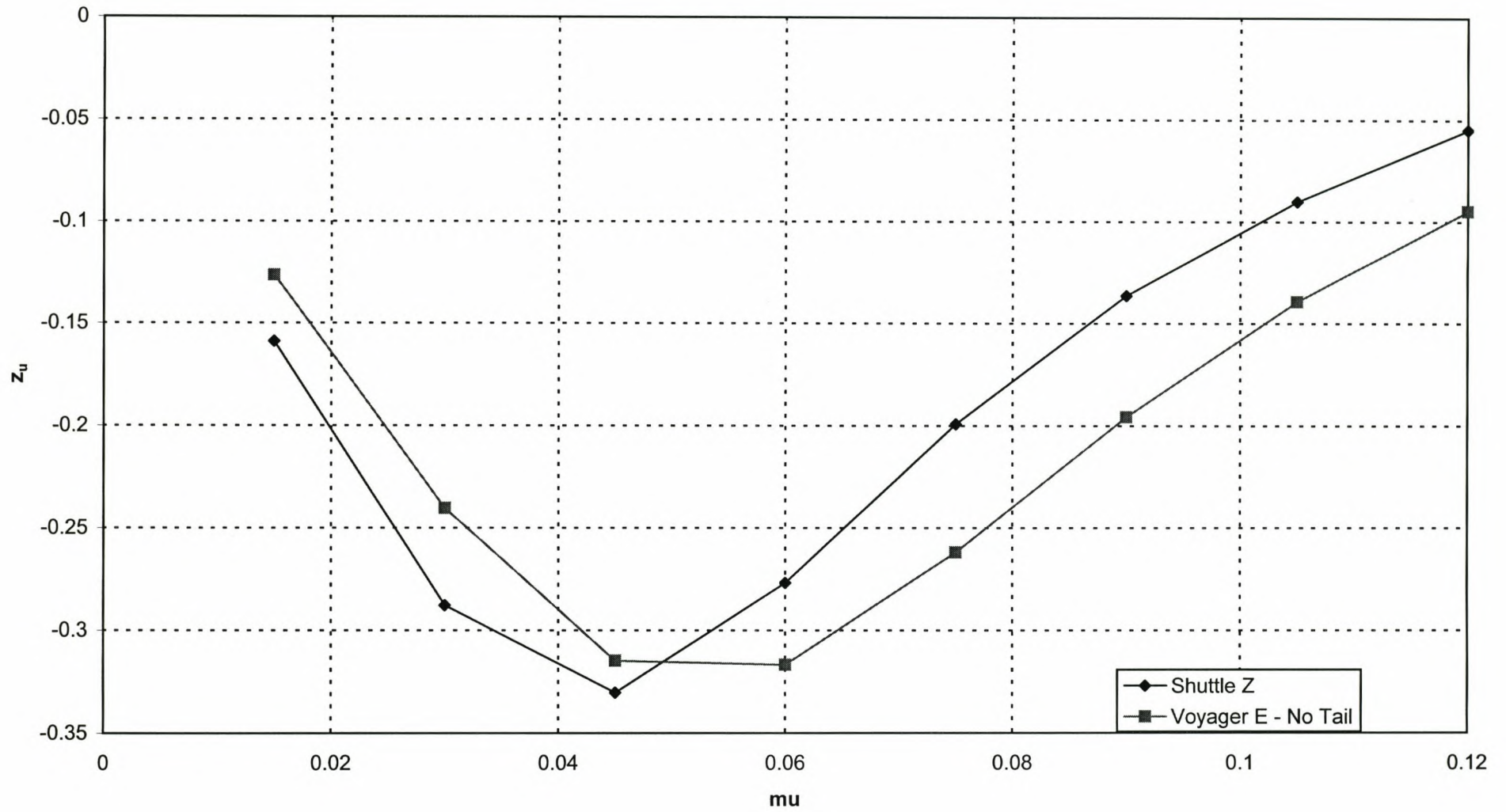


Figure 7.2 - Comparison of the  $z_u$  derivative

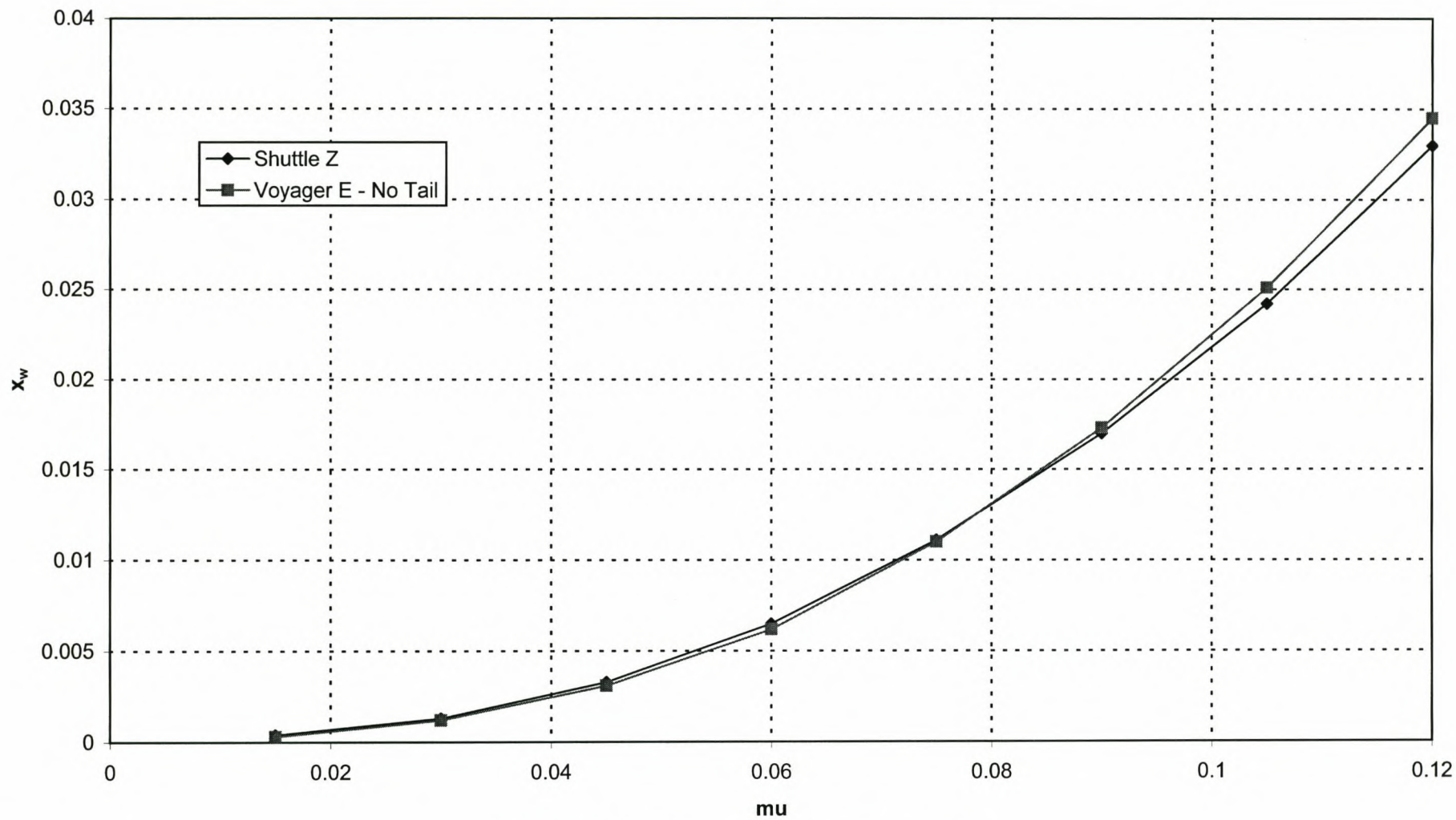


Figure 7.3 - Comparison of the  $x_w$  derivative



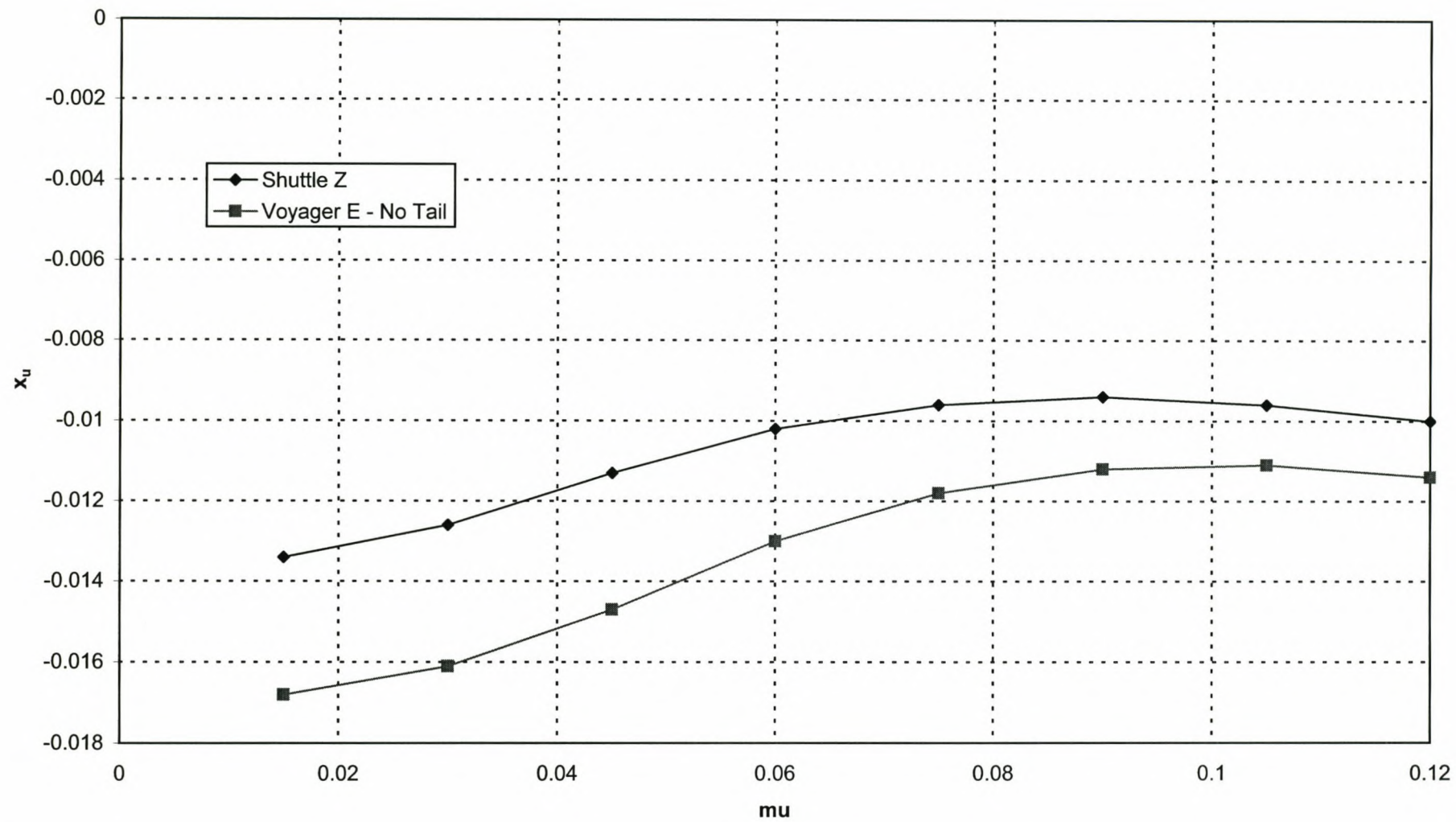


Figure 7.4 - Comparison of the  $x_u$  derivative

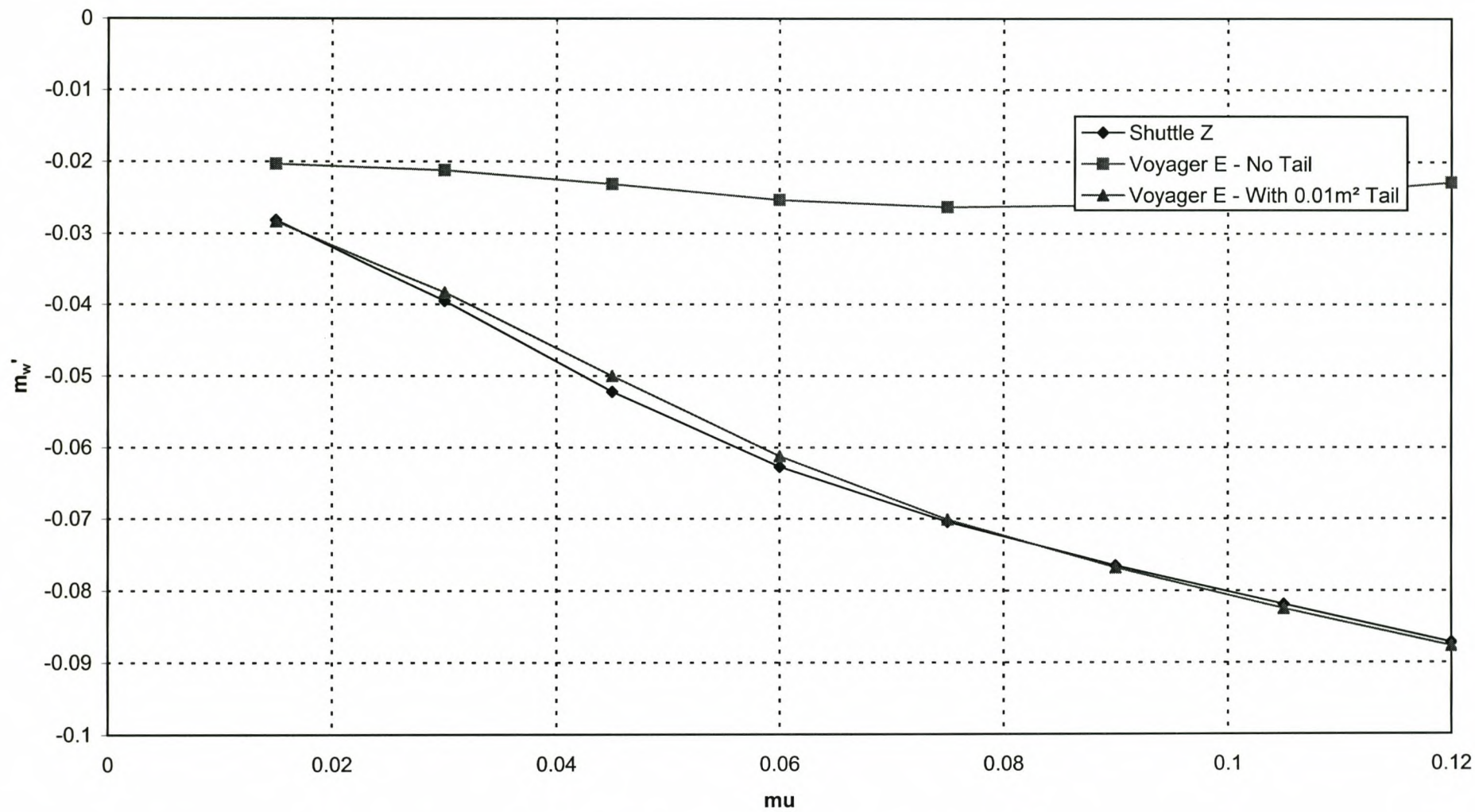


Figure 7.5 - Comparison of the  $m_w'$  derivative



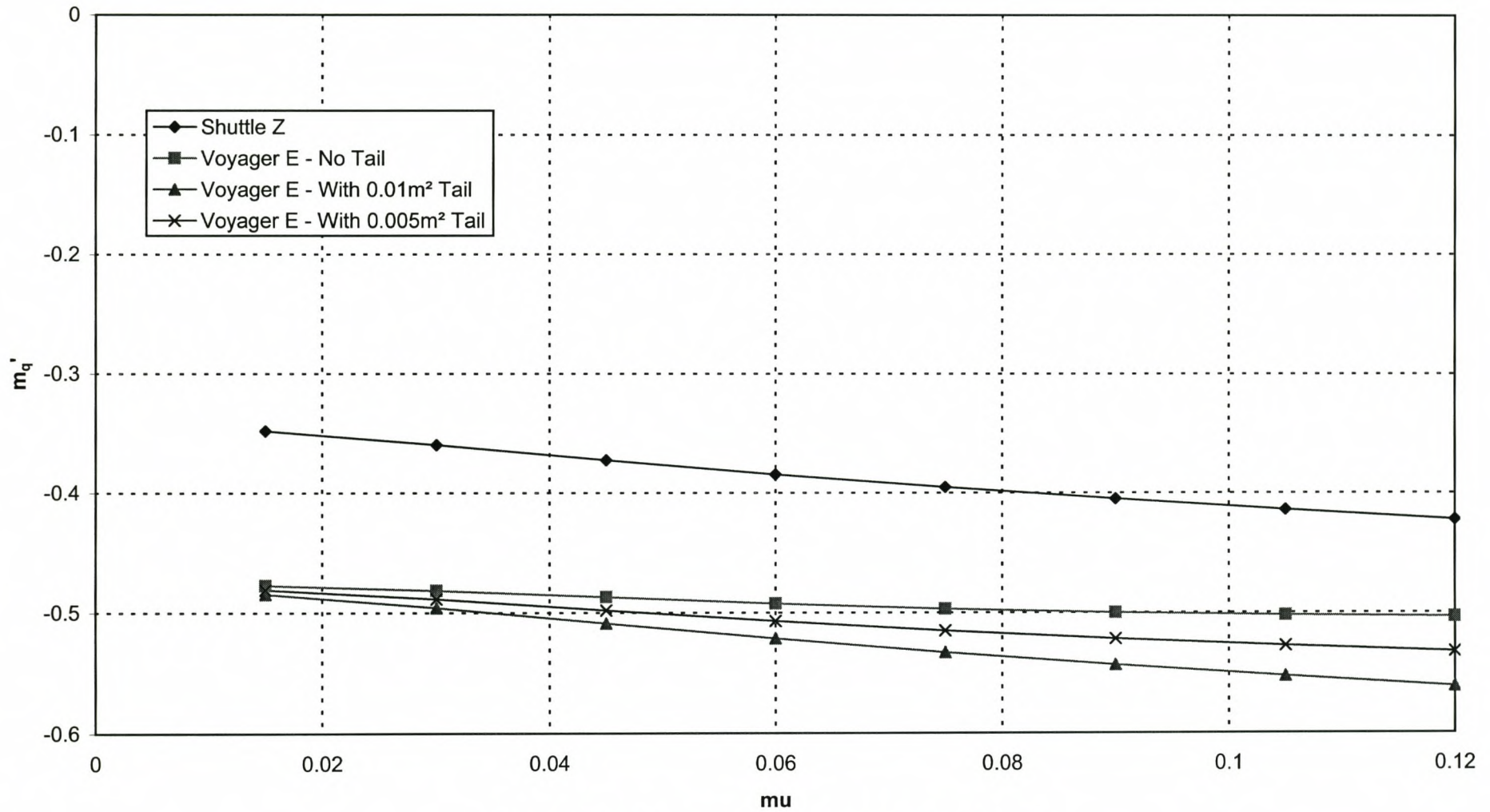


Figure 7.6 - Comparison of the  $m_q'$  derivative

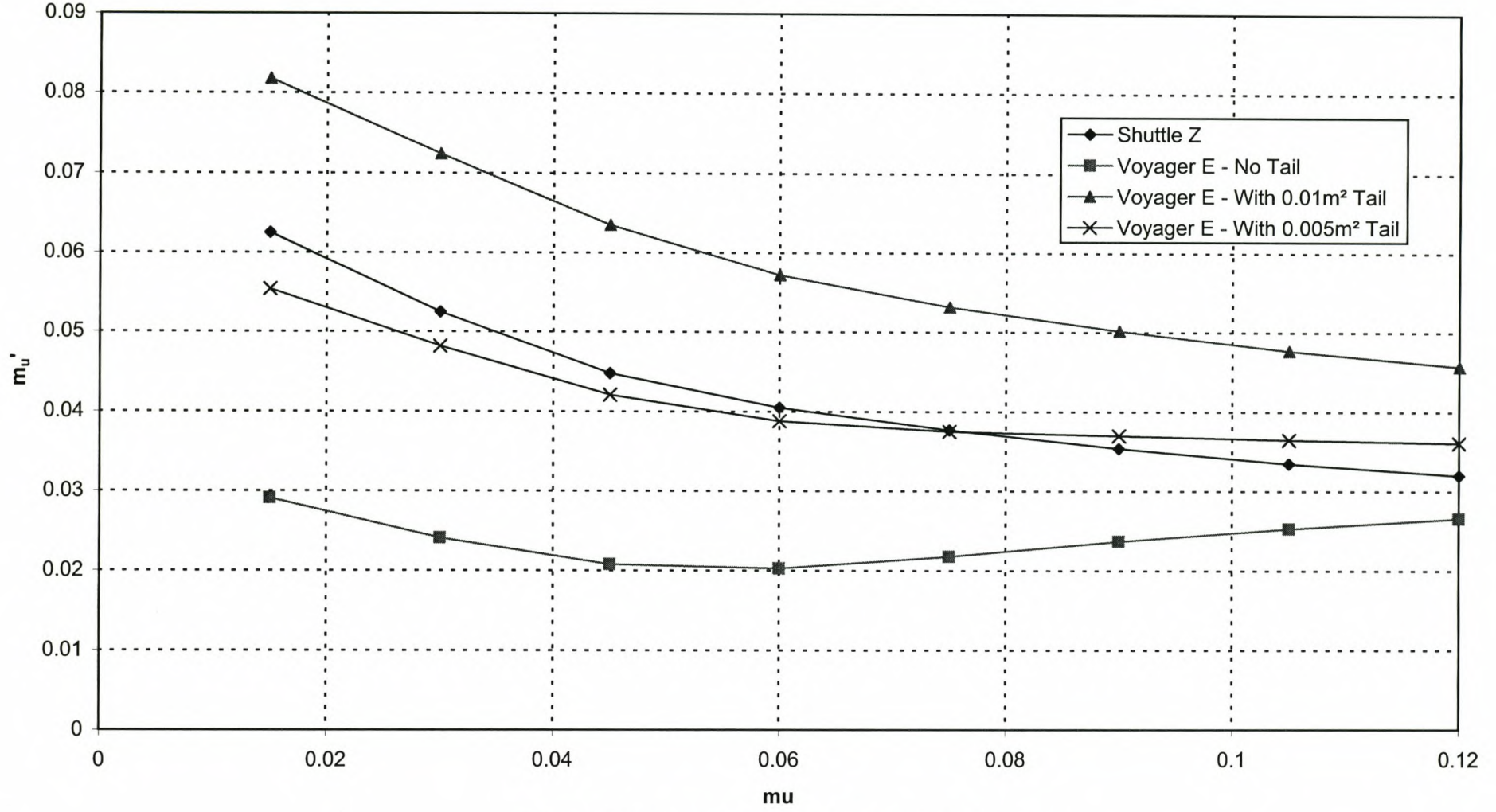


Figure 7.7 - Comparison of the  $m_u'$  derivative



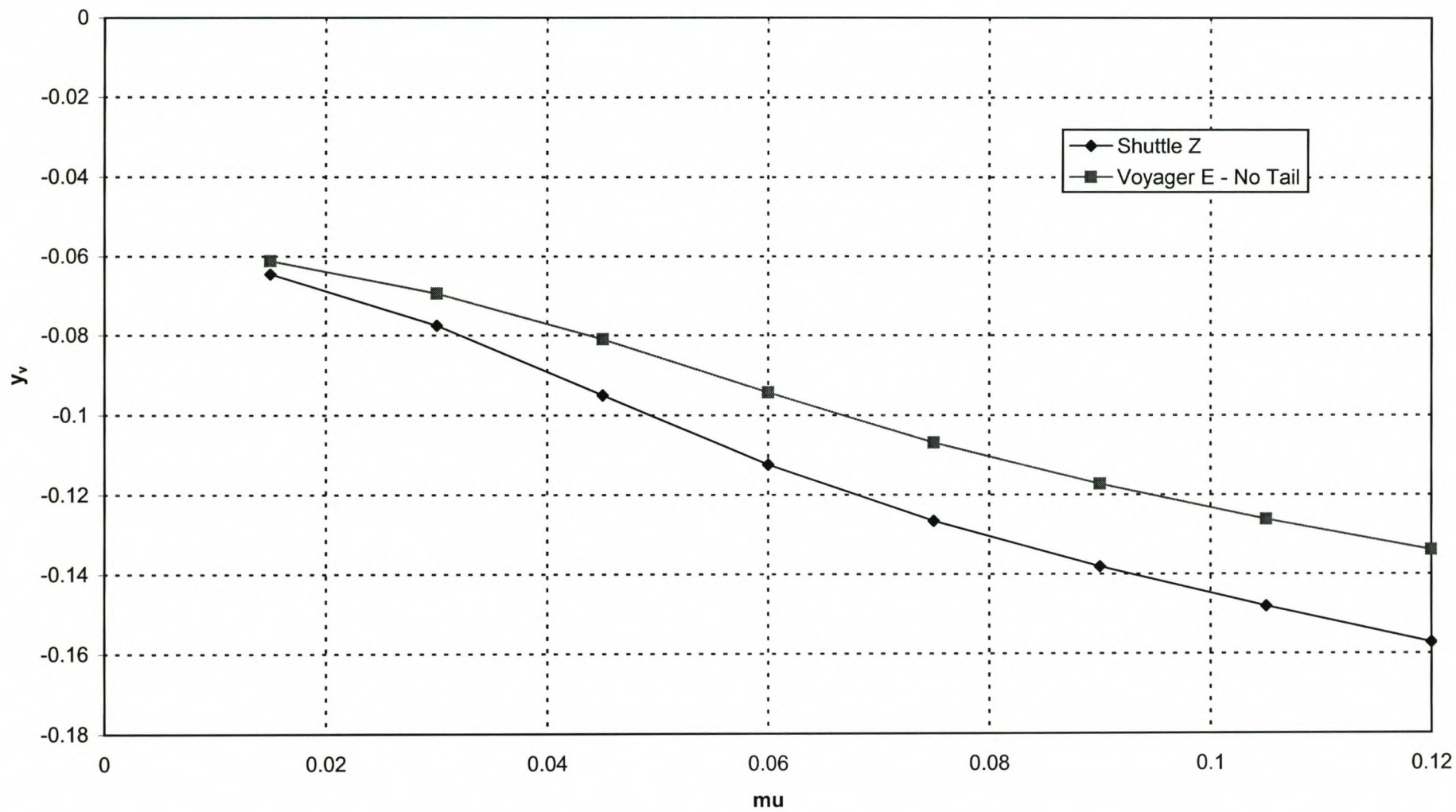


Figure 7.8 - Comparison of the  $y_v$  derivative

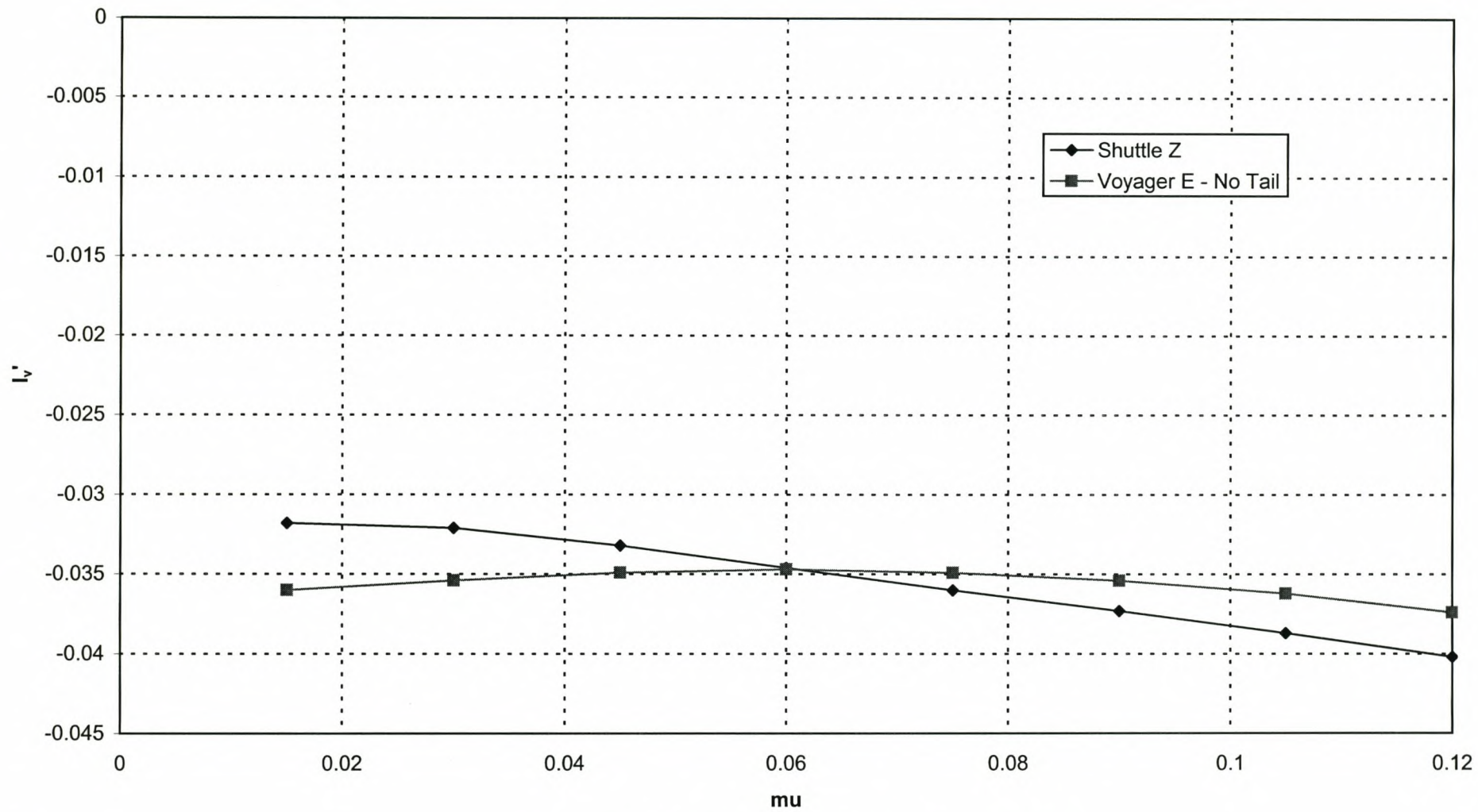


Figure 7.9 - Comparison of the  $l_v'$  derivative



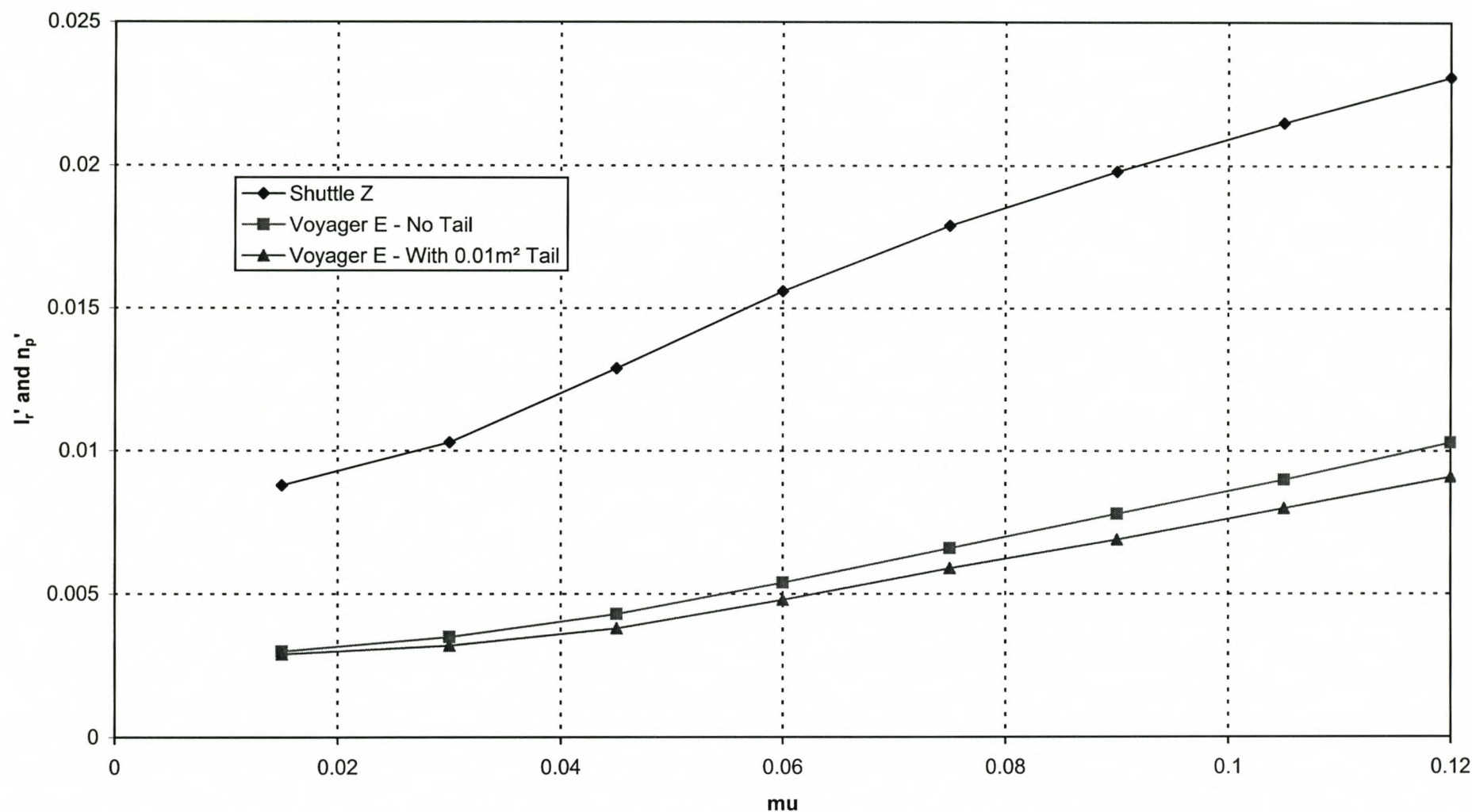


Figure 7.10 - Comparison of the  $I_r'$  and  $n_p'$  derivatives

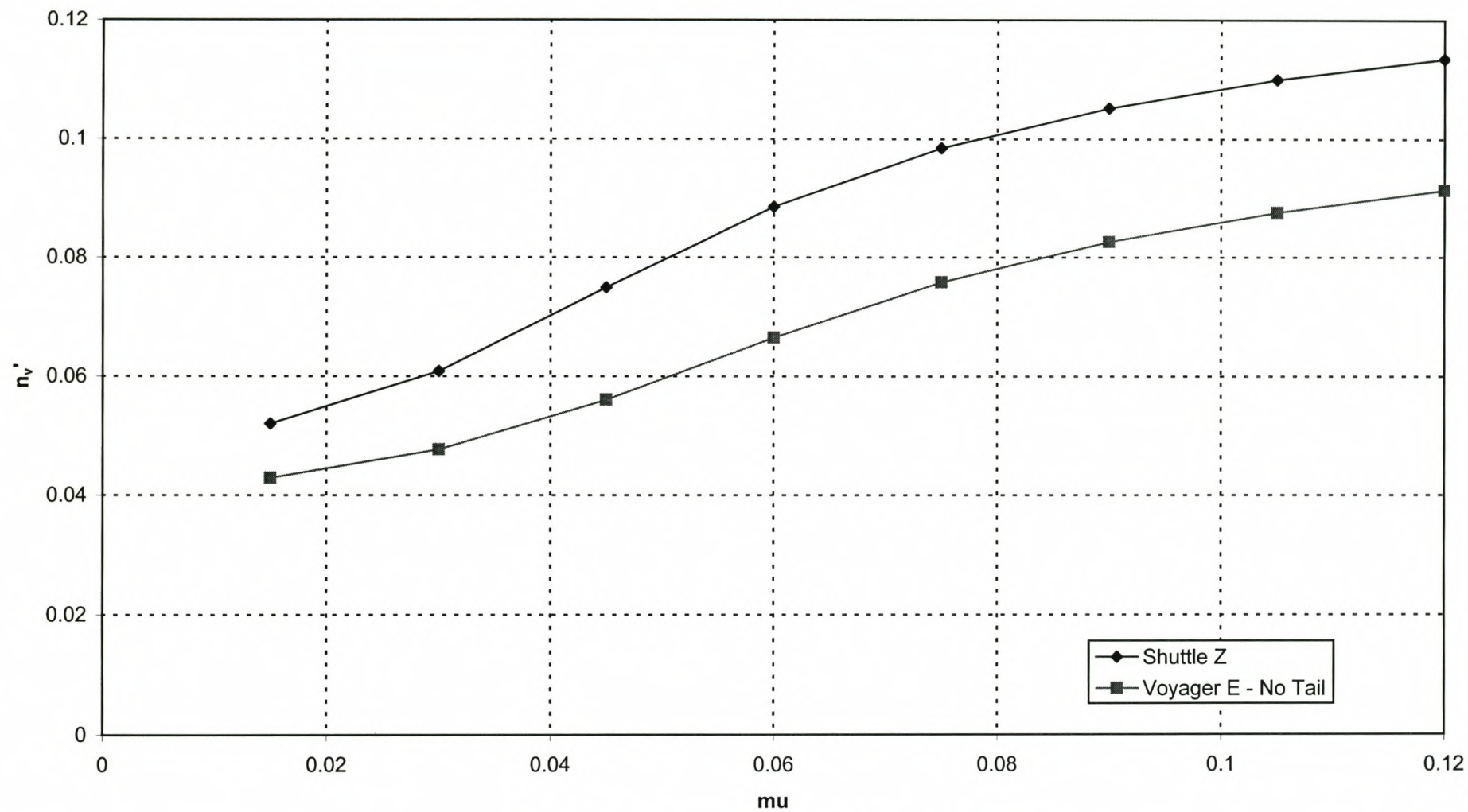


Figure 7.11 - Comparison of the  $n_v'$  derivative



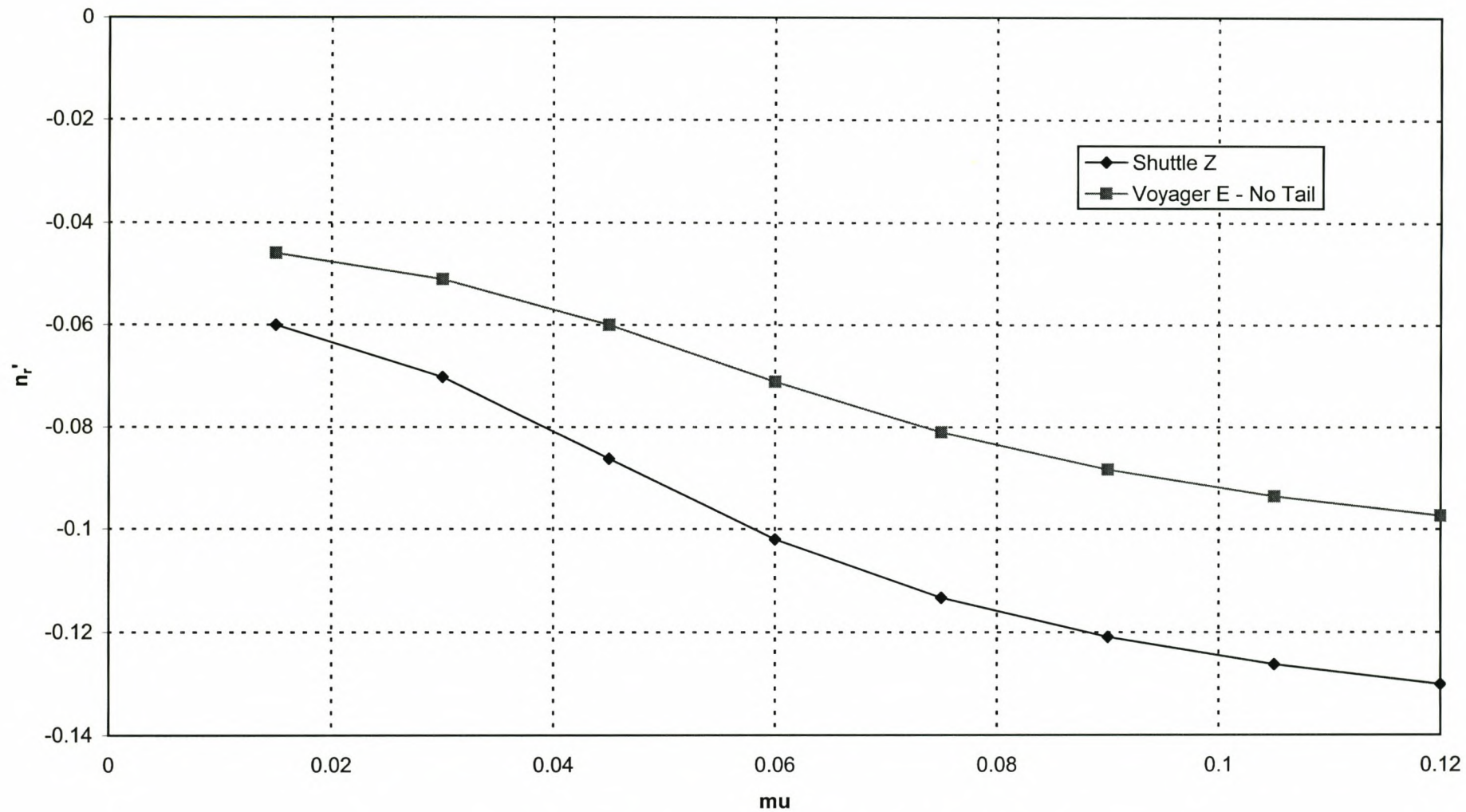


Figure 7.12 - Comparison of the  $n_r'$  derivative

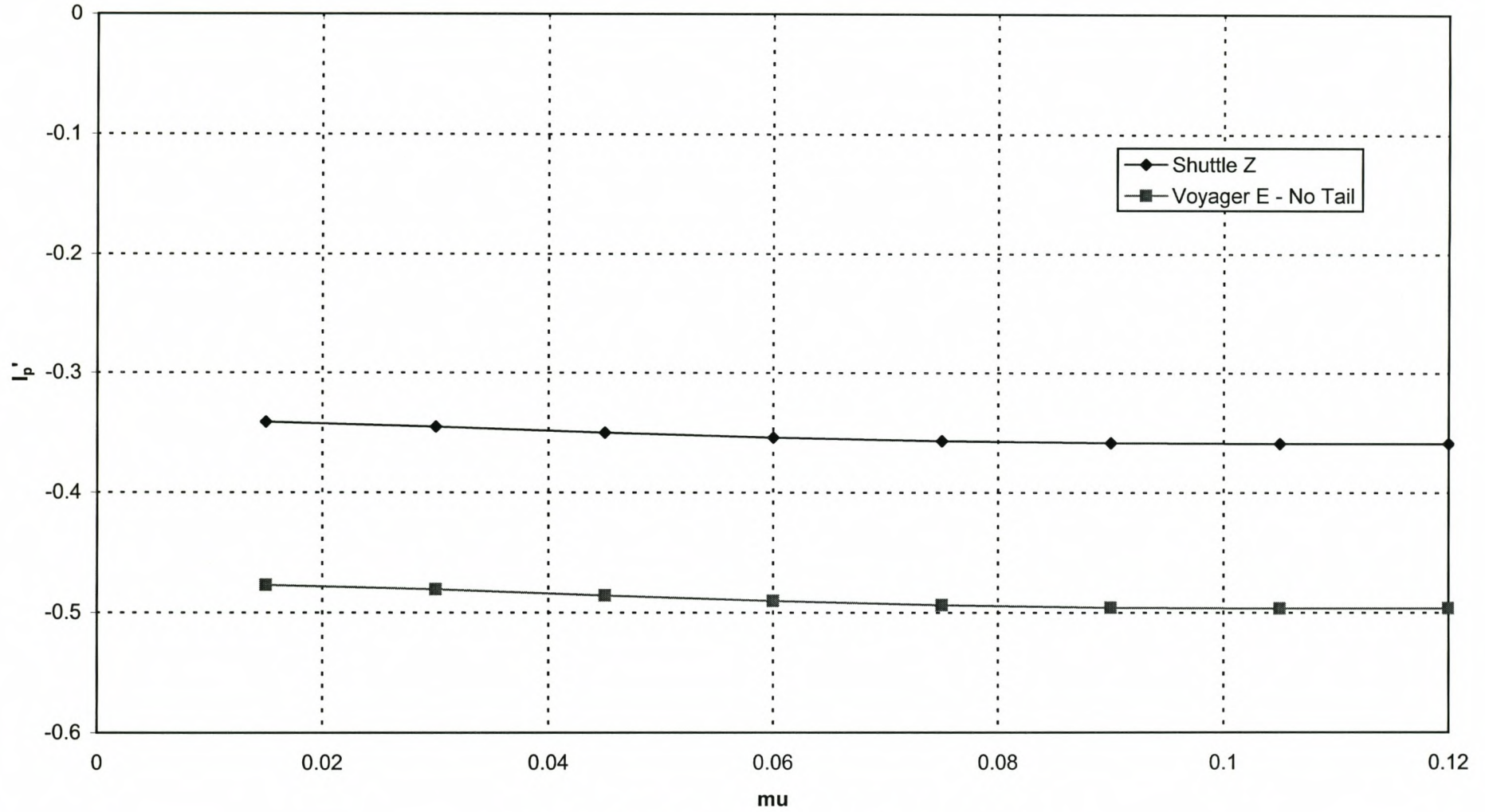


Figure 7.13 - Comparison of the  $I_p'$  derivative



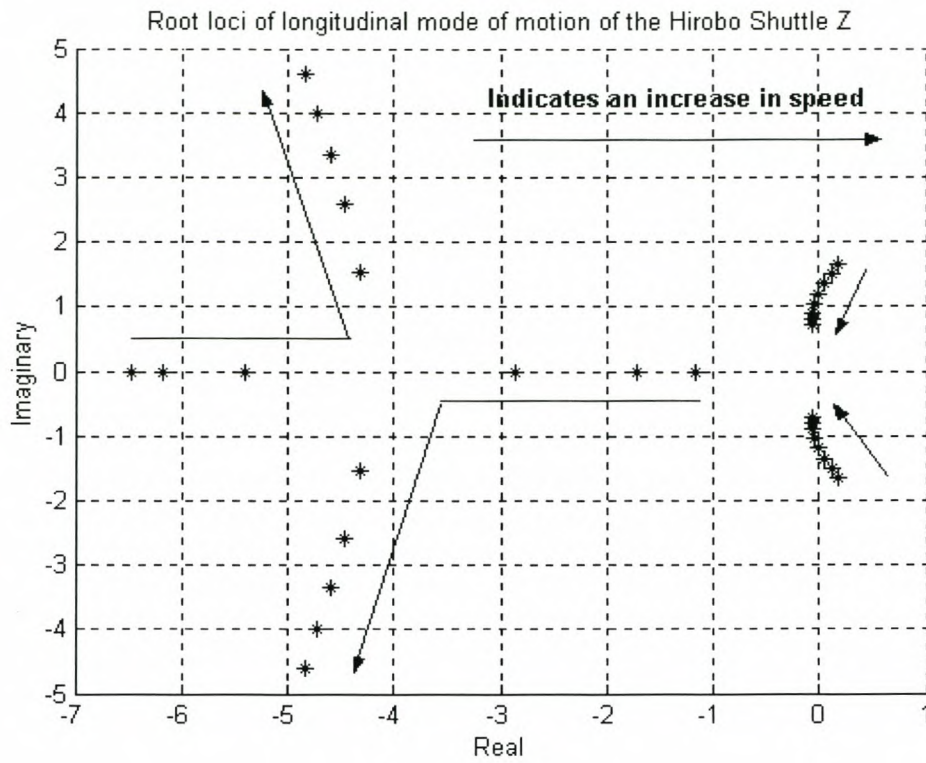


Figure 7.14

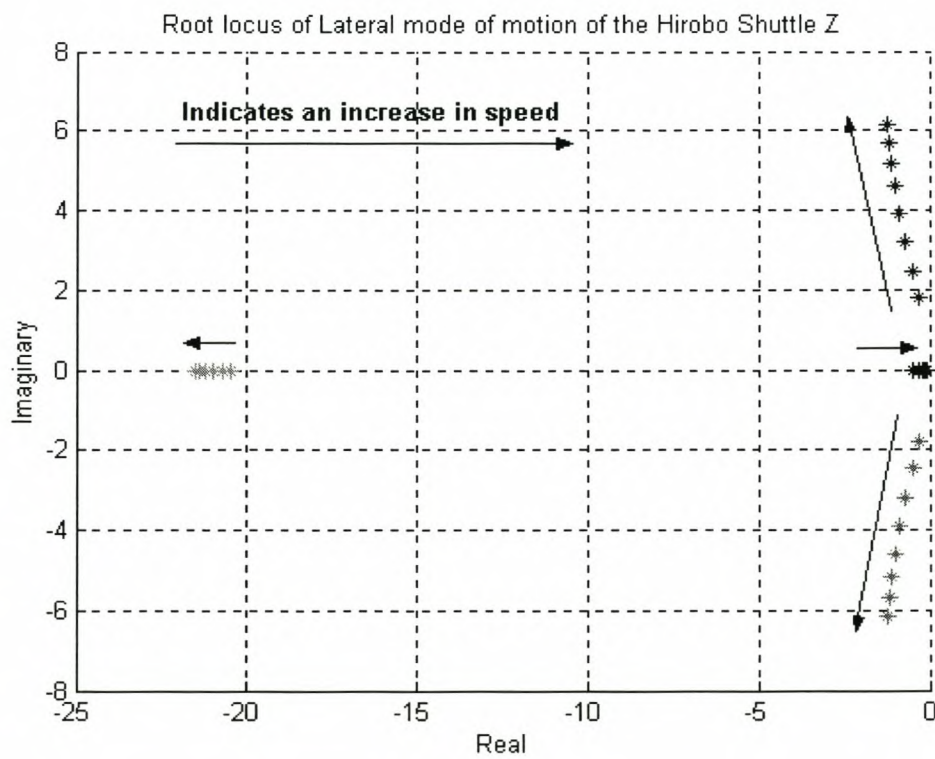
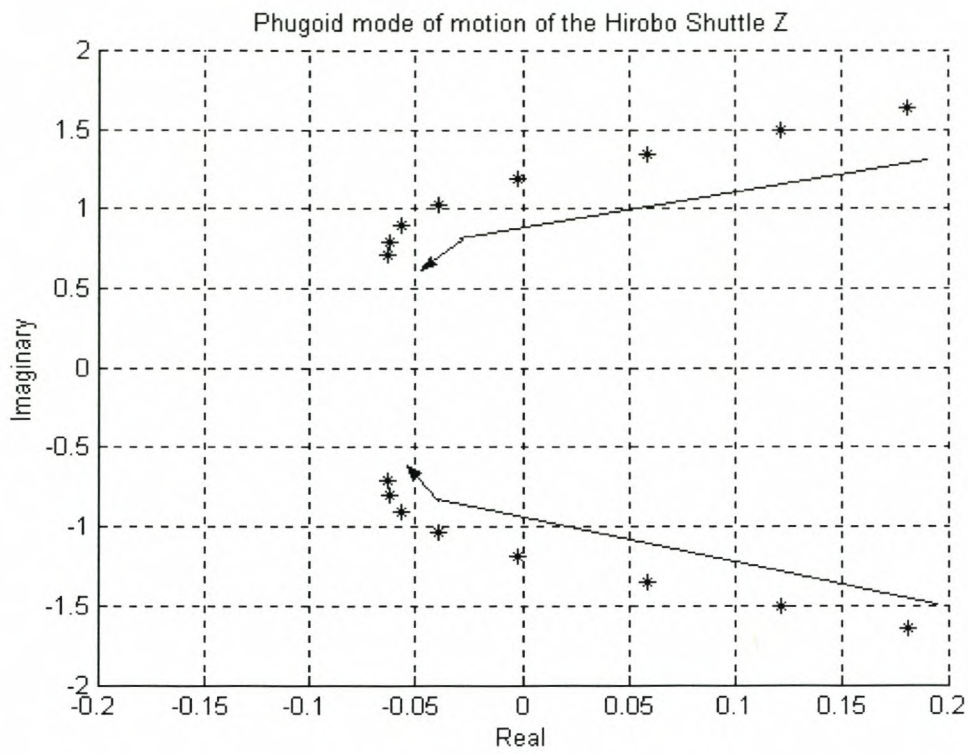
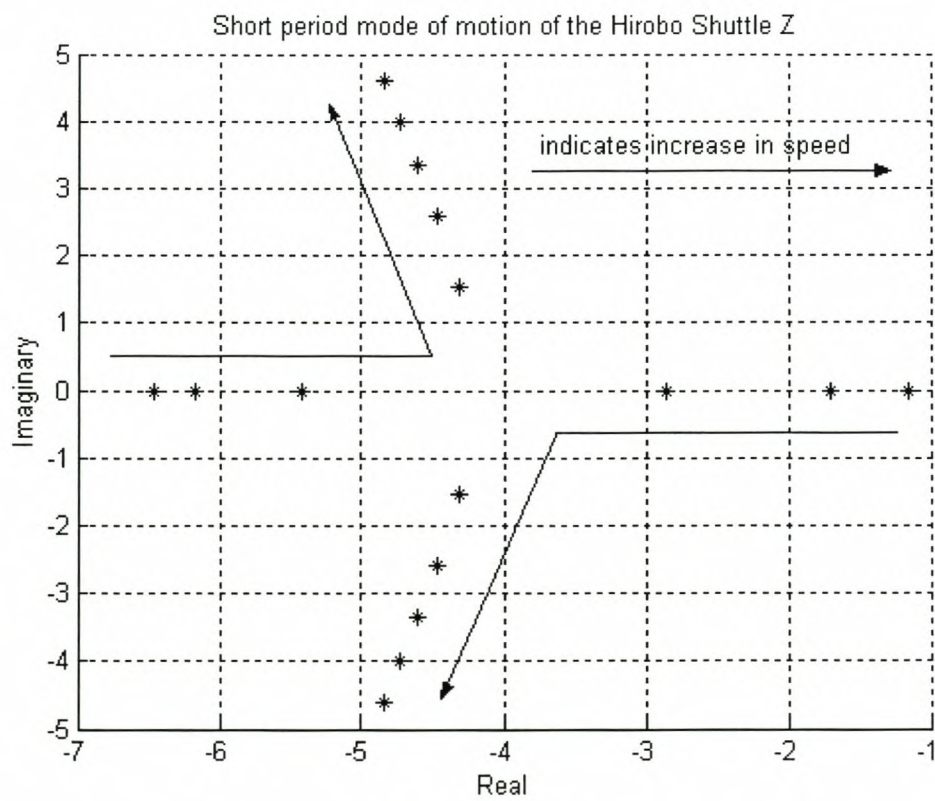


Figure 7.15



**Figure 7.16**



**Figure 7.17**



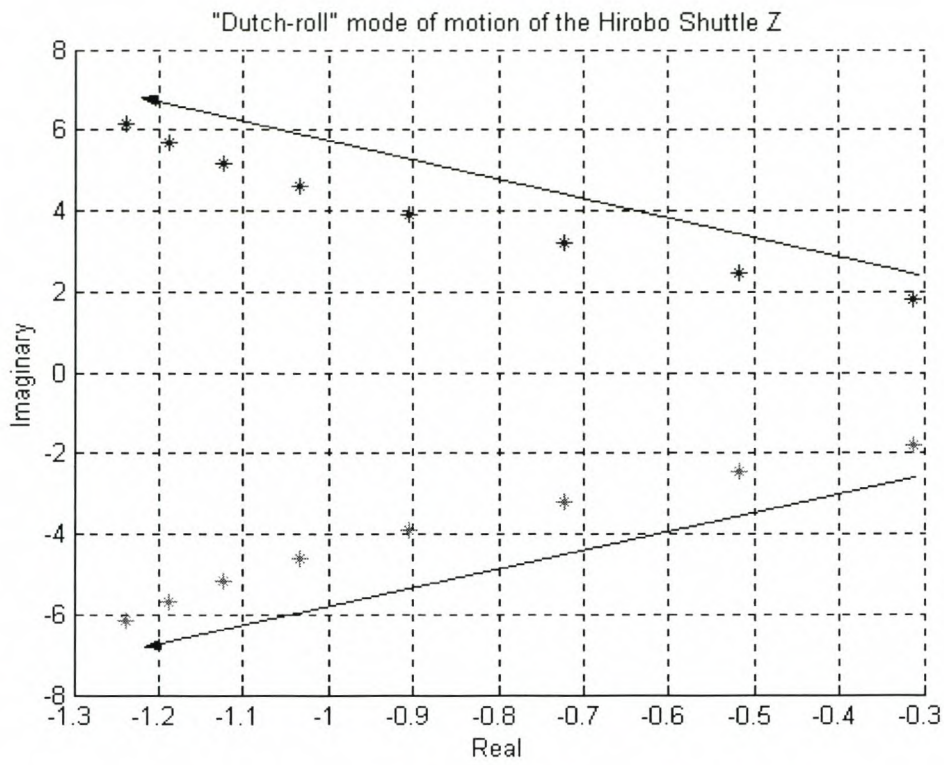


Figure 7.18

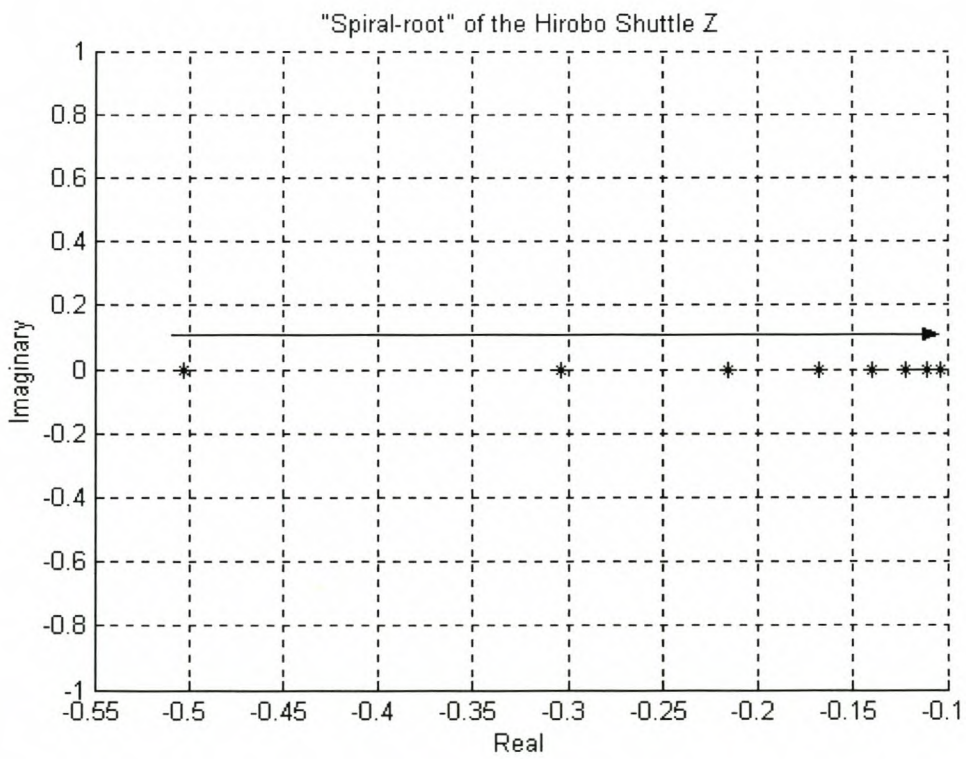


Figure 7.19

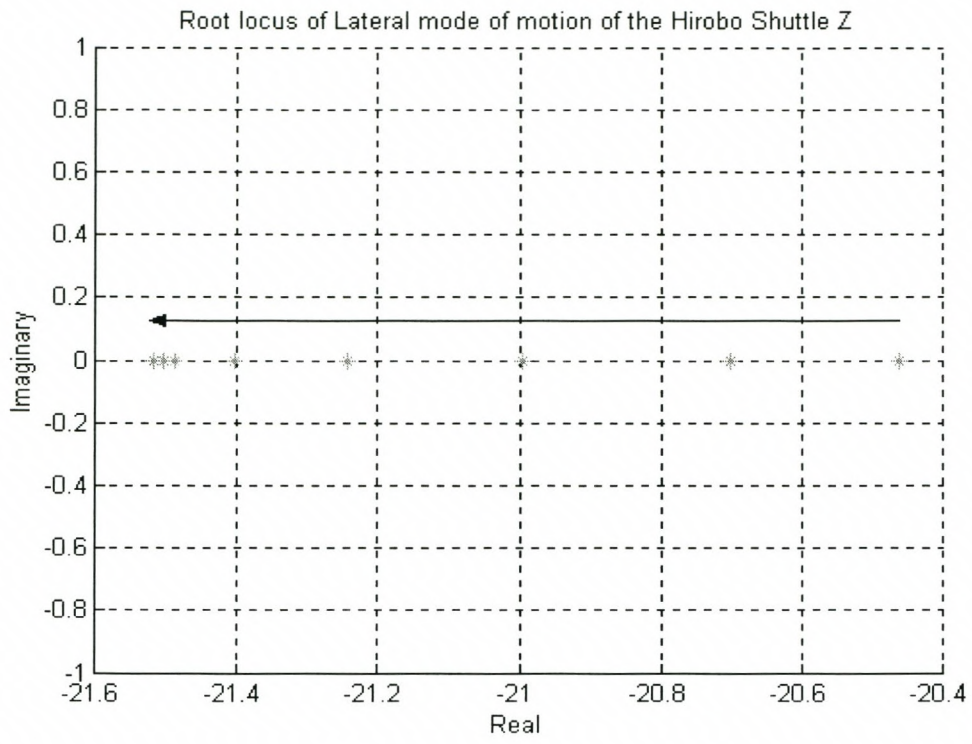


Figure 7.20



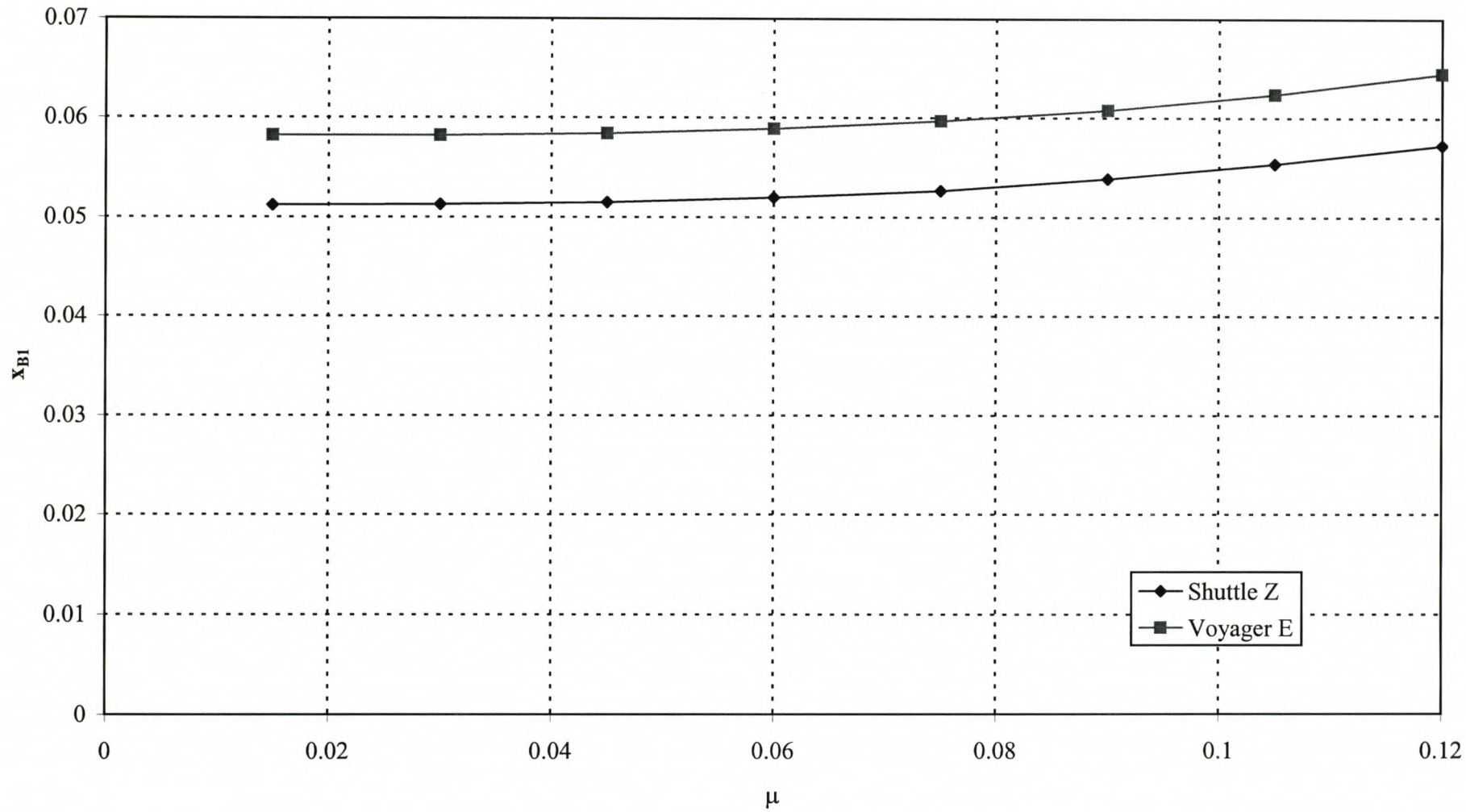


Figure 7.21 - Comparison of the  $x_{B1}$  derivative

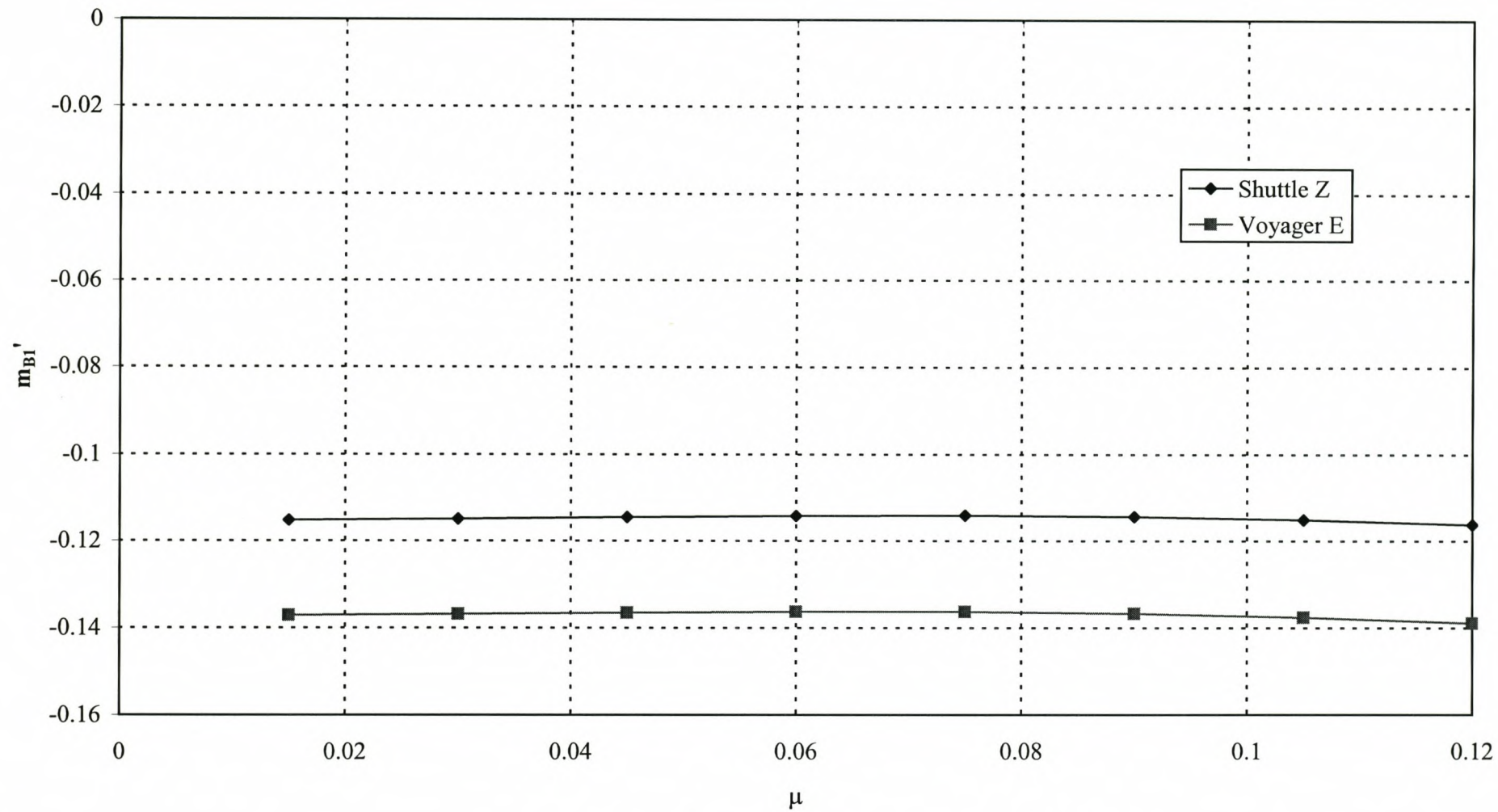


Figure 7.22 - Comparison of the  $m_{B1}'$  derivative



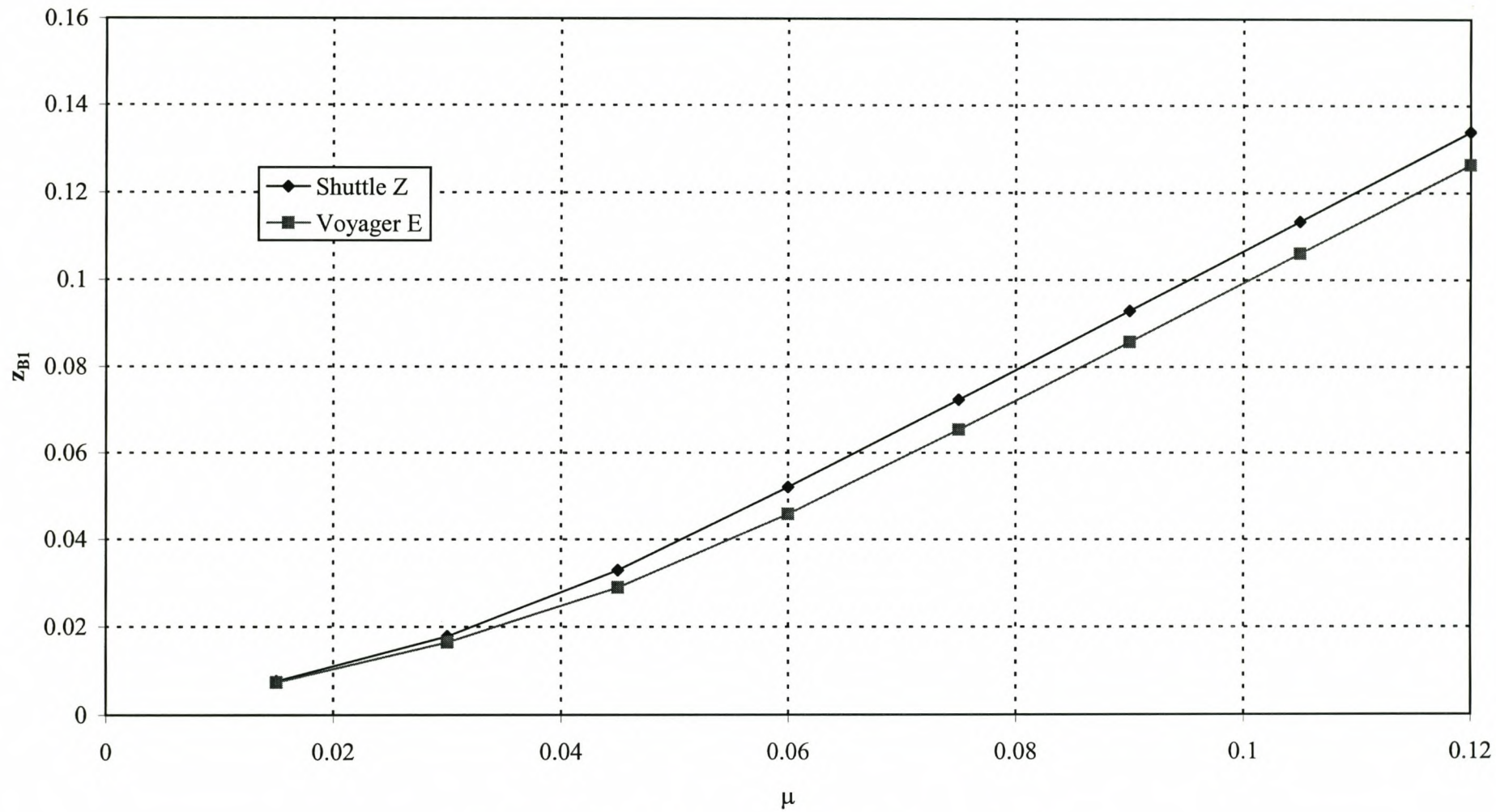


Figure 7.23 - Comparison of the  $z_{B1}$  derivative

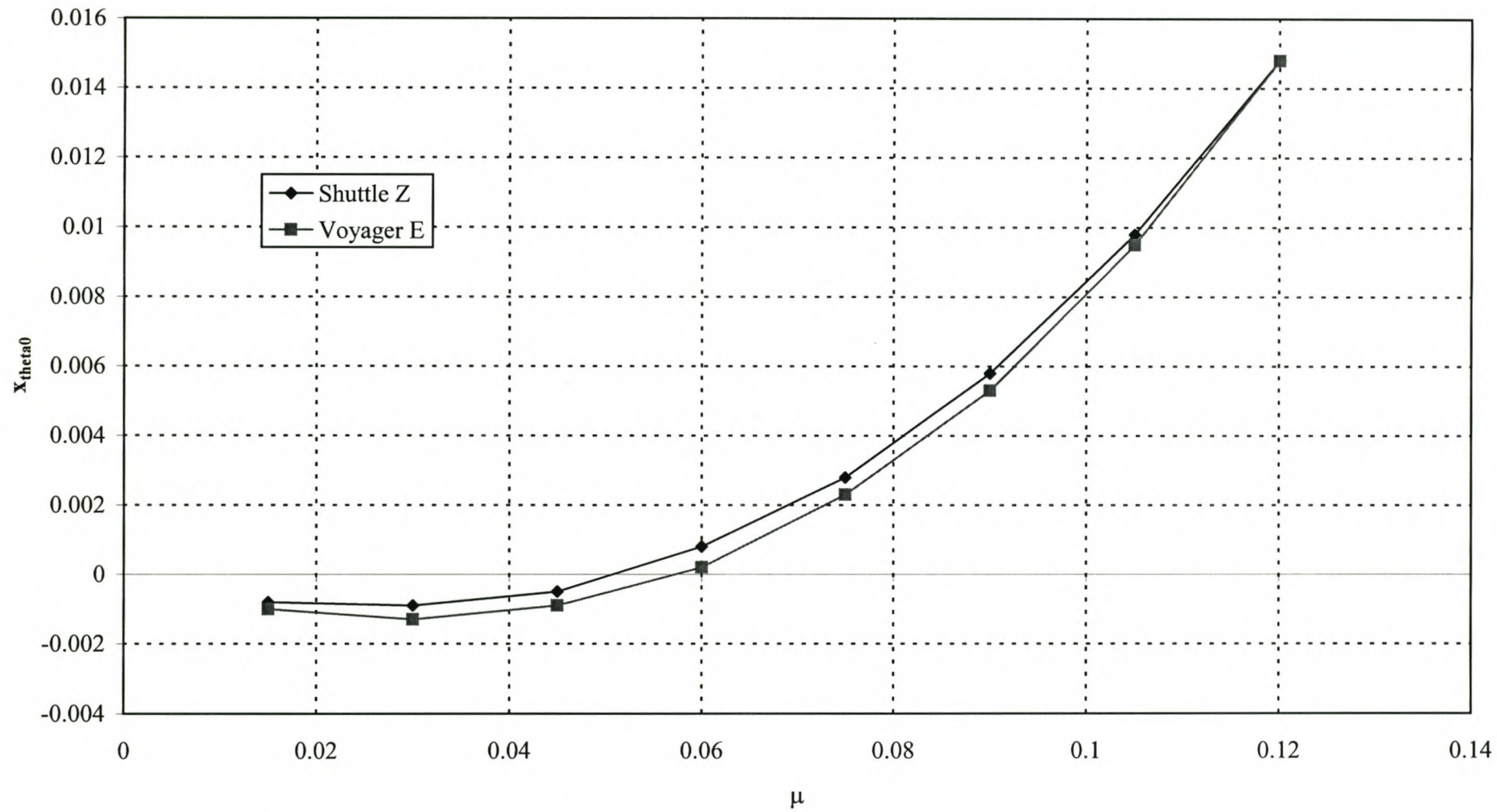


Figure 7.24 - Comparison of the  $x_{\theta_0}$  derivative



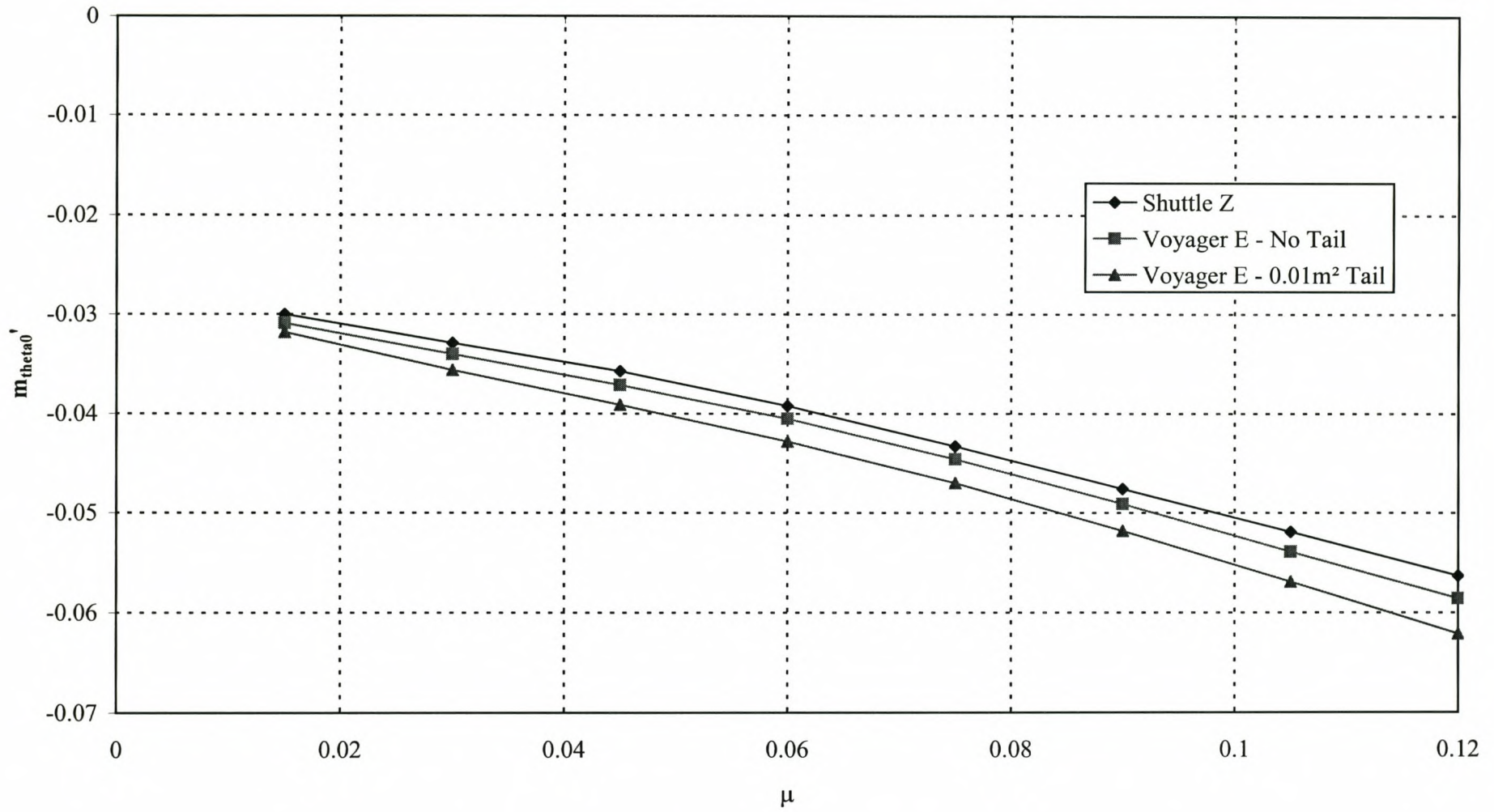


Figure 7.25 - Comparison of the  $m_{\theta_0}'$  derivative

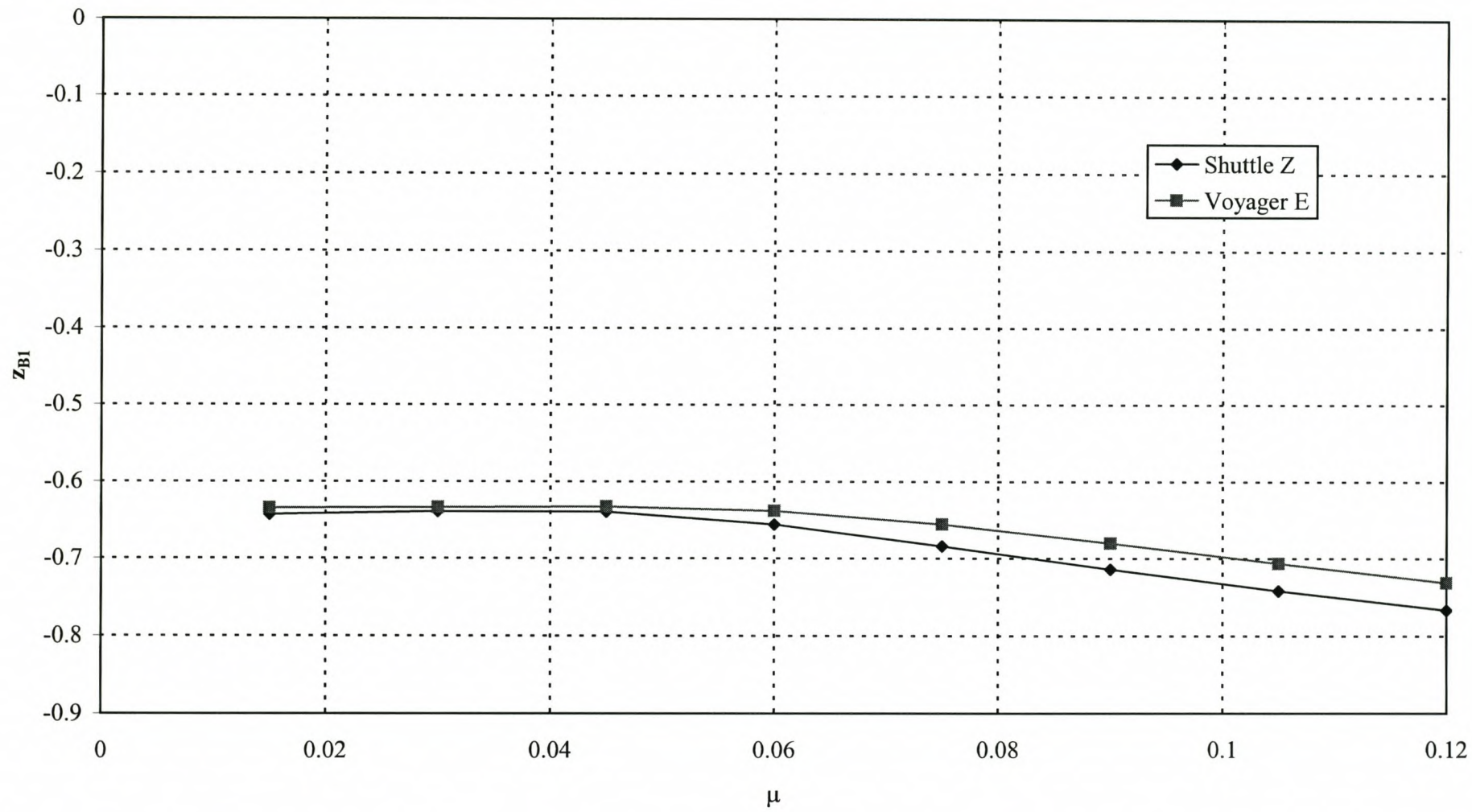


Figure 7.26 - Comparison of the  $z_{BI}$  derivative



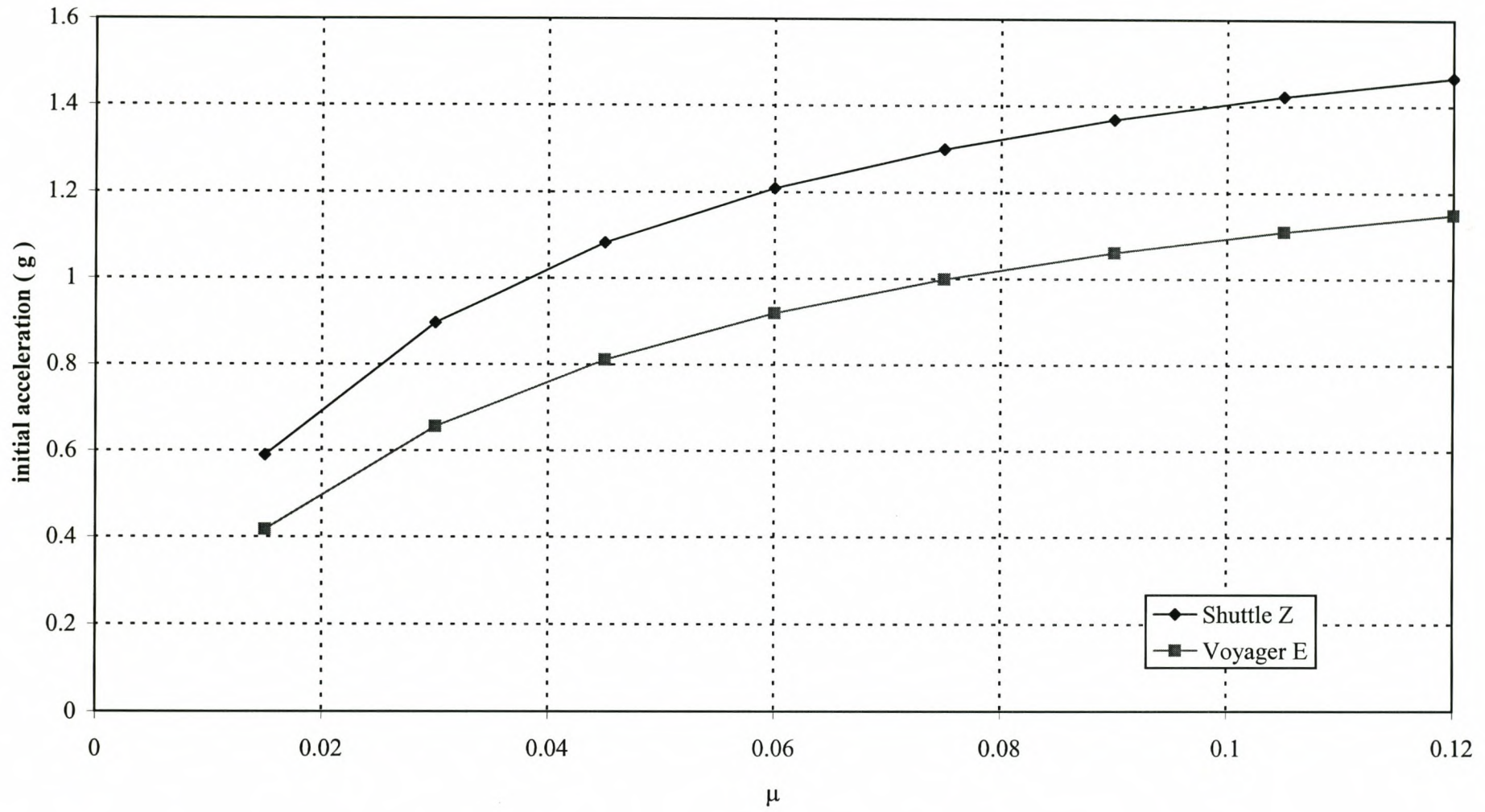
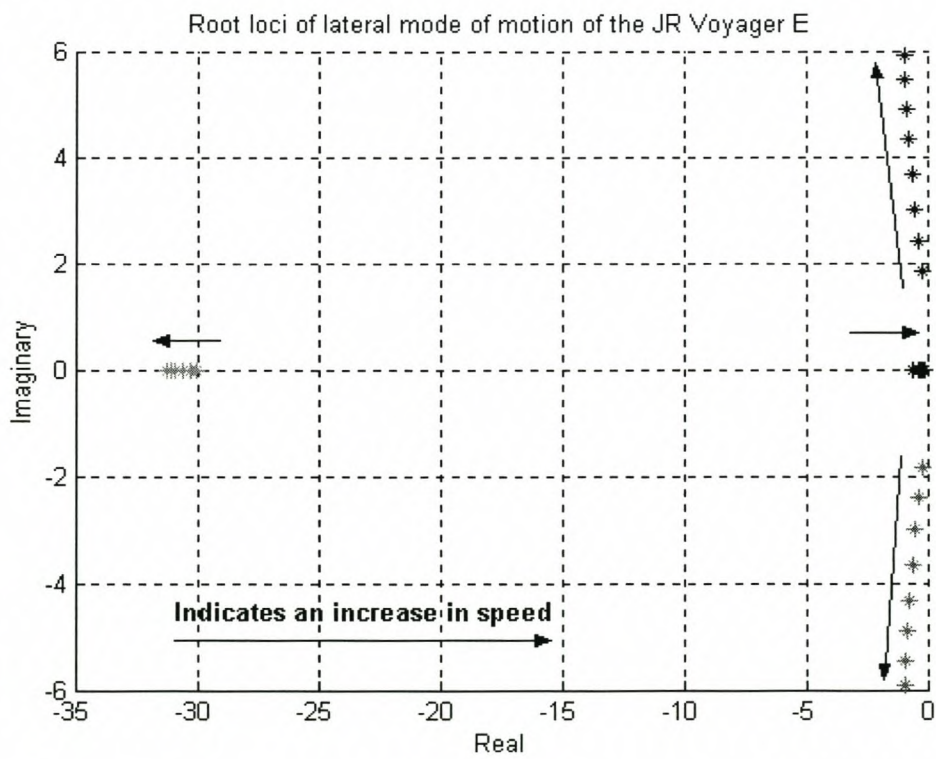
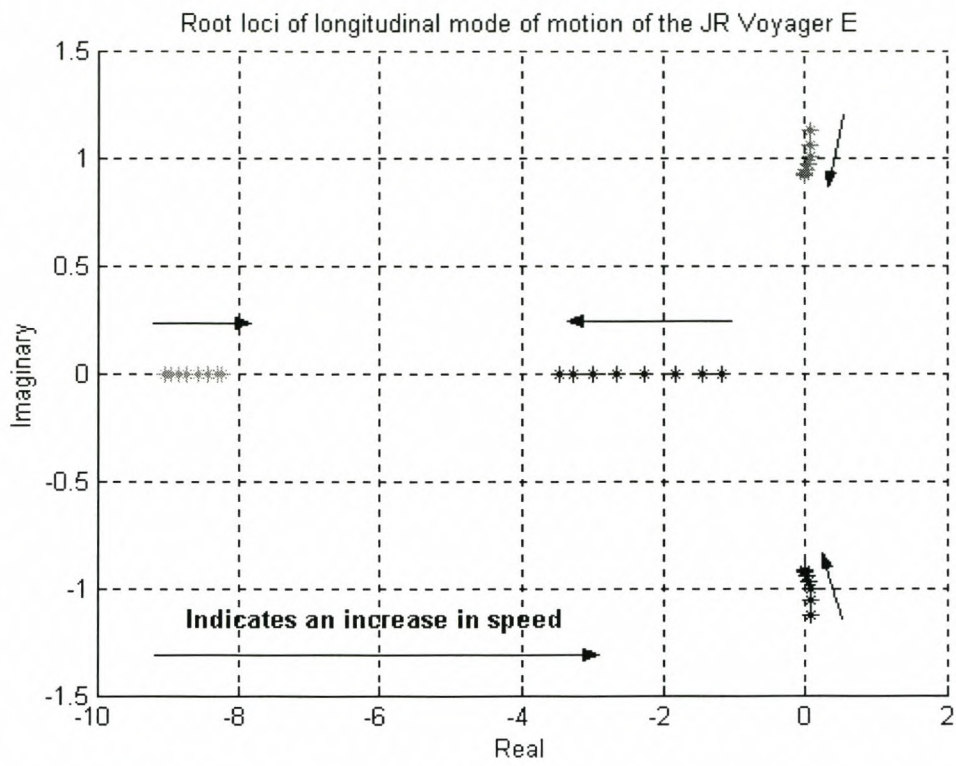


Figure 7.27 - Comparison of the initial gust response





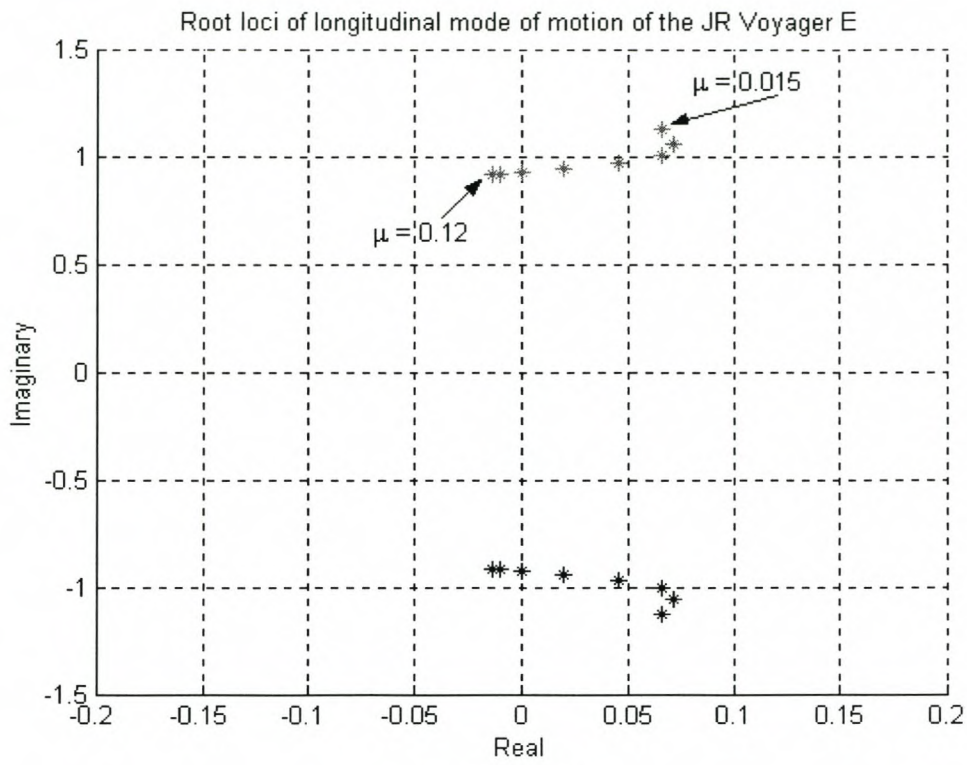


Figure 7.30

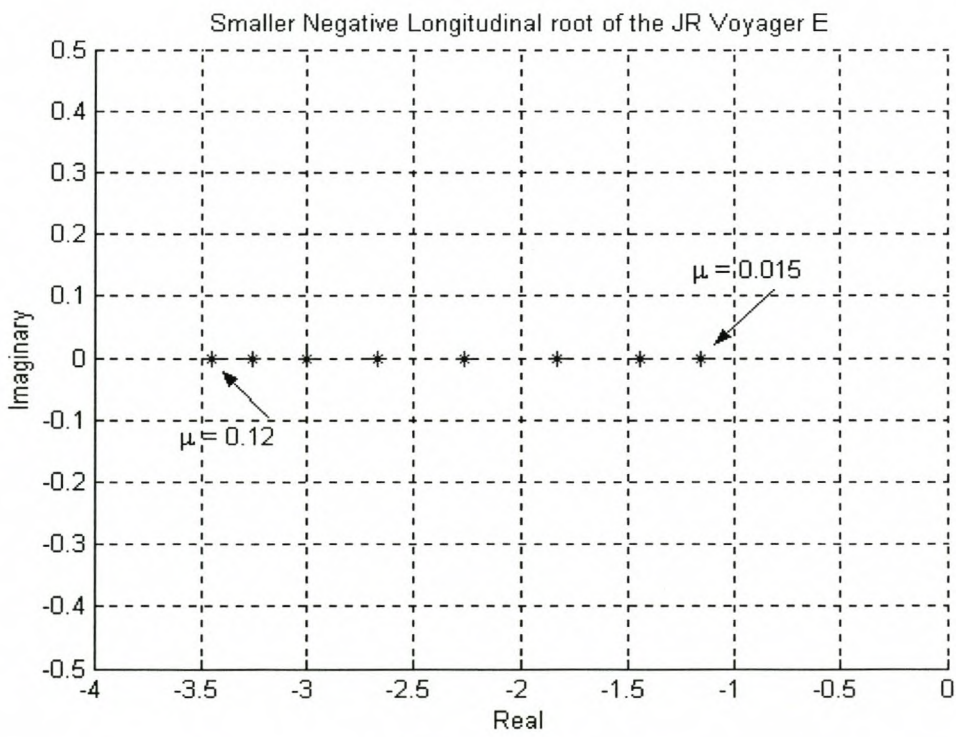
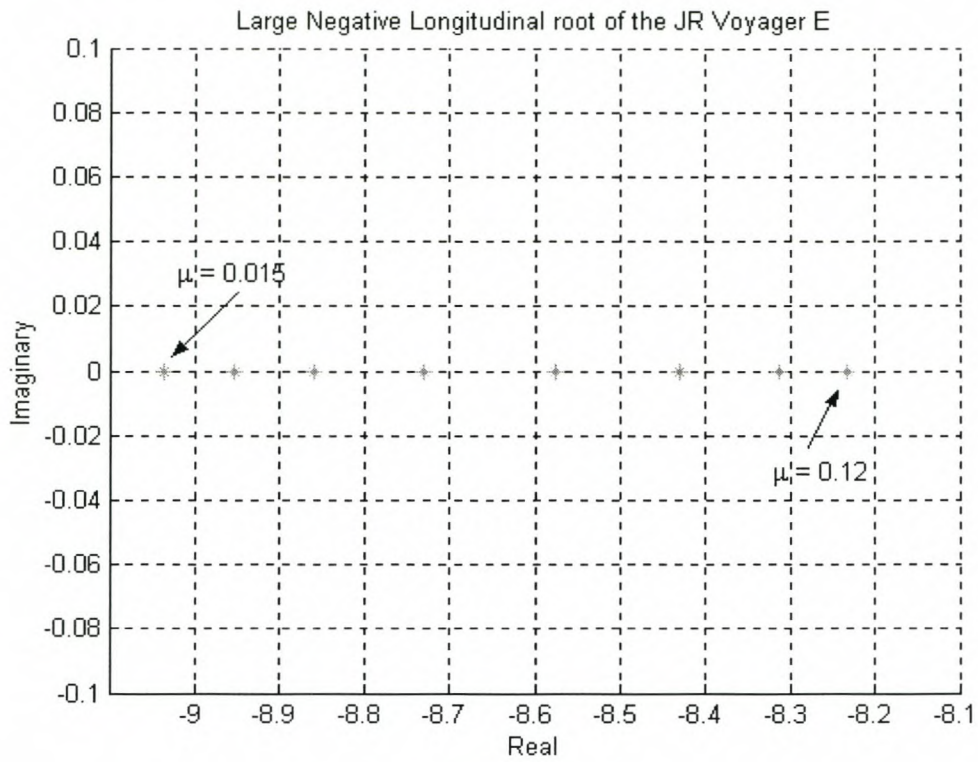
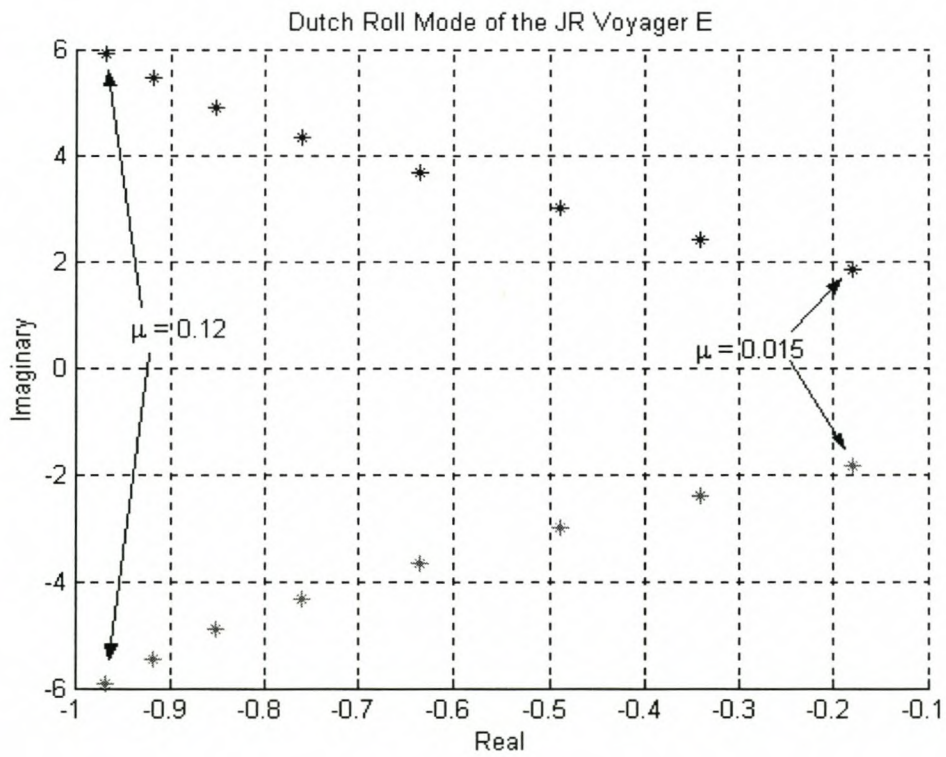


Figure 7.31



**Figure 7.32**



**Figure 7.33**



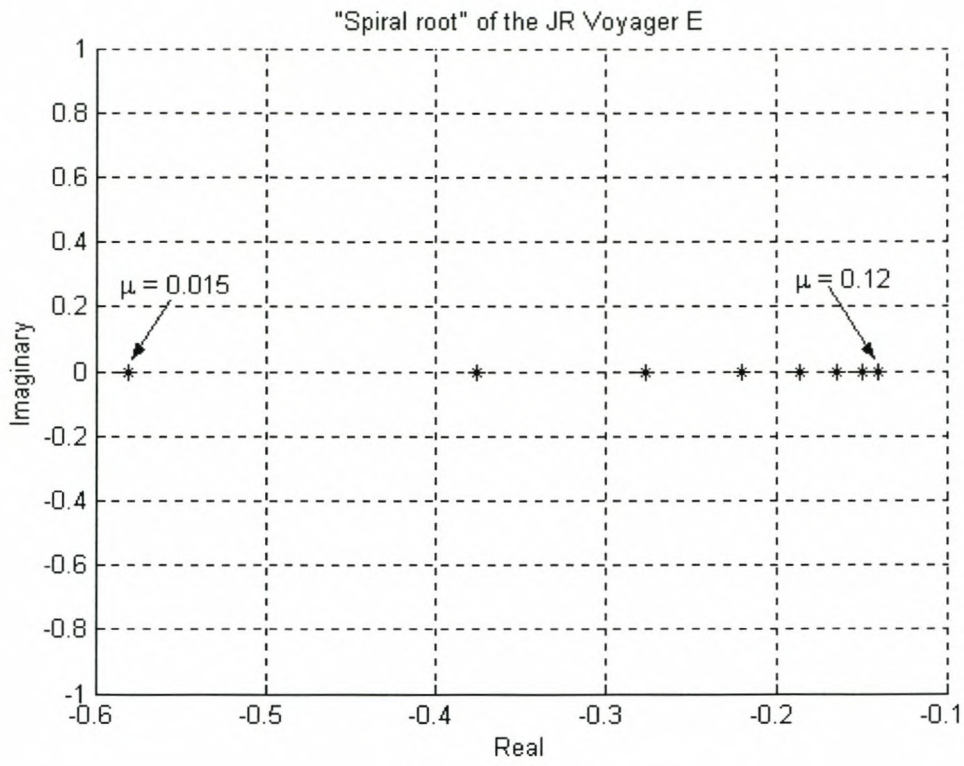


**Figure 7.34**

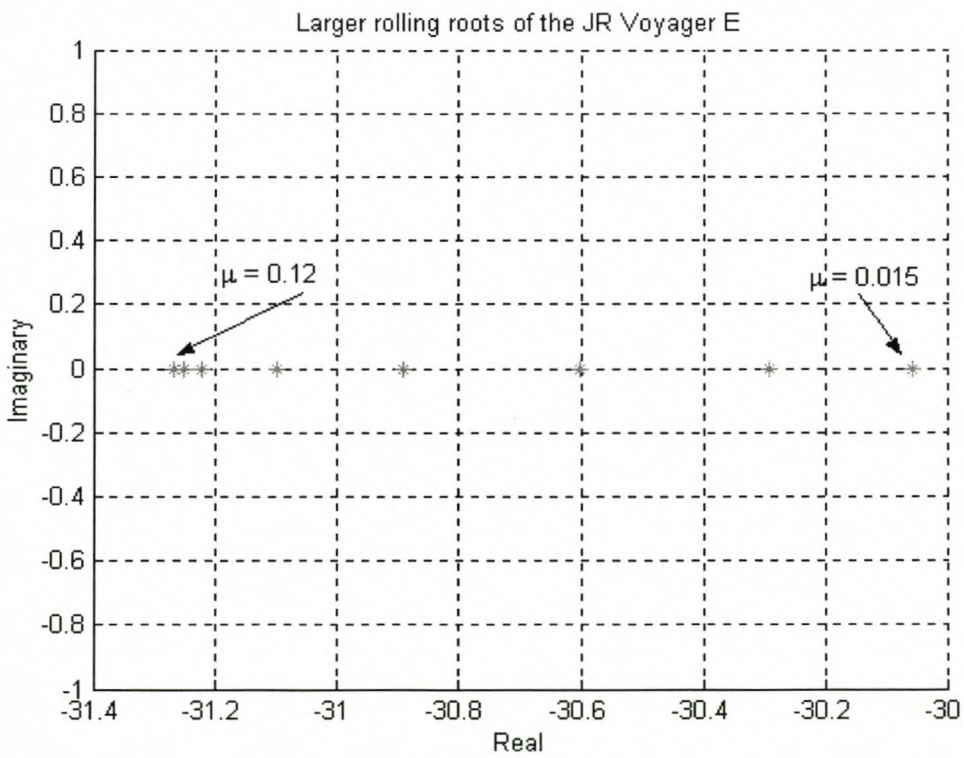


**Figure 7.35**





## TABLES OF NUMERICAL RESULTS

**Table 4.1 – Increase in power required**

<b>RPM</b>	<b>1000</b>	<b>1100</b>	<b>1200</b>
% increase in power required	6.62	6.18	5.75

**Table 4.2 – Performance at  $P_{max}$**

<b>Main Rotor RPM</b>	<b>1000</b>	<b>1100</b>	<b>1200</b>
Maximum climbing velocity (m/s)	1.296	0.828	0.183
Main rotor collective pitch setting ( $^{\circ}$ )	10.7	8.9	7.39

**Table 5.1 – Rolling of Selected Helicopters**

<b>Helicopter</b>	<b>Mass [kg]</b>	<b><math>h_T</math> [m]</b>	<b><math>h_R</math> [m]</b>	<b><math>\phi / T_{TR}</math> [<math>^{\circ}</math> / N]</b>
Lynx	4313.7	1.146	1.274	0.00136
Bo 105	2200	1.72	1.48	-0.00043
Puma	5805	1.587	2.157	0.000266
AH1-G	3628.74	1.15	2.026	0.000696
JR Voyager E	1.6	0.01	0.19	3.458
Shuttle Z	2.6	0.08	0.255	1.542

**Table 5.2 – Verification of Longitudinal Trim Settings**

	Current Analysis	Bramwell	Error (%)
$\theta_0$	10.418°	10.5°	0.79
$a_1$	5.926°	5.95°	0.4
$q_c$	0.006139	0.00613	0.15
$\lambda_D$	-0.0468	-0.0470	0.43
$\lambda_i$	0.0071	0.0071	0
$h_{cD}$	0.000786	0.000731	7.5
$\alpha_D$	-7.4558°	-7.73°	3.68
$C_{MS}$	0.0274	0.0274	0
$P$	674.74 kW	670.23 kW	0.67
$B_1$ no tail	6.143°	6.26°	1.9
$B_1$ with tail	5.352°	5.71°	6.68
$B_1$ with tail and eps*	5.7995°	5.71°	1.57
$b_1$	1.785°	1.80°	0.9
$a_0$	3.7818°	3.824°	1.12
$\theta_f$	-7.2388°	-7.296°	0.79

\* Indicates an adjustment of the downwash at the horizontal stabiliser

**Table 5.3 – Verification of Lateral Trim Settings**

	Current Analysis	Bramwell	Error (%)
$Q$	25951 Nm	25778.25 Nm	0.67
$T_T$	2359.2	2343.5	0.67
$A_1$	-2.836°	-2.848°	0.44
$\phi$	-1.953°	-1.937°	0.83
$\theta_{0T}$	2.954°	2.934°	0.68
$t_{ct}$	0.0729	0.0724	0.68
$\lambda_{iT}$	0.01214	0.01207	0.59



**Table 7.1 – Longitudinal stability derivatives of the Hirobo Shuttle Z**

mu	LONGITUDINAL DERIVATIVES						
	zw	zu	xw	xu	mw'	mq'	mu'
0.015	-0.5103	-0.1588	0.0004	-0.0134	-0.0281	-0.3476	0.0625
0.03	-0.5963	-0.2878	0.0013	-0.0126	-0.0395	-0.3594	0.0525
0.045	-0.7333	-0.3302	0.0033	-0.0113	-0.0522	-0.3722	0.0448
0.06	-0.8684	-0.2768	0.0065	-0.0102	-0.0627	-0.3842	0.0405
0.075	-0.9658	-0.1992	0.0111	-0.0096	-0.0704	-0.395	0.0377
0.09	-1.0322	-0.1363	0.017	-0.0094	-0.0765	-0.4048	0.0354
0.105	-1.08	-0.09	0.0242	-0.0096	-0.0819	-0.4139	0.0335
0.12	-1.1165	-0.0548	0.033	-0.01	-0.0872	-0.4223	0.032

**Table 7.2 – Lateral stability derivatives of the Hirobo Shuttle Z**

mu	LATERAL DERIVATIVES					
	yv	lv'	lr' & nr'	nv'	nr'	lp'
0.015	-0.0645	-0.0318	0.0088	0.0521	-0.06	-0.3409
0.03	-0.0775	-0.0321	0.0103	0.0609	-0.0702	-0.3449
0.045	-0.095	-0.0332	0.0129	0.0749	-0.0862	-0.3498
0.06	-0.1124	-0.0346	0.0156	0.0886	-0.102	-0.3539
0.075	-0.1266	-0.036	0.0179	0.0985	-0.1133	-0.3566
0.09	-0.1381	-0.0373	0.0198	0.1052	-0.1209	-0.3581
0.105	-0.1481	-0.0387	0.0215	0.11	-0.1262	-0.3587
0.12	-0.1572	-0.0402	0.0231	0.1135	-0.1301	-0.3585

**Table 7.3 – Longitudinal stability derivatives of the JR Voyager E**

mu	LONGITUDINAL DERIVATIVES						
	zw	zu	xw	xu	mw'	mq'	mu'
0.015	-0.4935	-0.1263	0.0003	-0.0168	-0.0203	-0.4773	0.0291
0.03	-0.549	-0.2404	0.0012	-0.0161	-0.0212	-0.4814	0.0241
0.045	-0.6455	-0.3147	0.0031	-0.0147	-0.0231	-0.4869	0.0208
0.06	-0.7652	-0.3167	0.0062	-0.013	-0.0253	-0.4924	0.0203
0.075	-0.8725	-0.262	0.011	-0.0118	-0.0263	-0.4967	0.0218
0.09	-0.9525	-0.1957	0.0173	-0.0112	-0.026	-0.4999	0.0237
0.105	-1.0107	-0.1393	0.0251	-0.0111	-0.0247	-0.5021	0.0253
0.12	-1.0545	-0.0946	0.0345	-0.0114	-0.0228	-0.5034	0.0266



**Table 7.4 – Lateral stability derivatives of the JR Voyager E**

mu	LATERAL DERIVATIVES					
	yv	lv'	lr' & nr'	nv'	nr'	lp'
0.015	-0.0611	-0.036	0.003	0.0429	-0.0459	-0.4771
0.03	-0.0694	-0.0354	0.0035	0.0477	-0.0511	-0.4808
0.045	-0.0809	-0.0349	0.0043	0.0561	-0.06	-0.4858
0.06	-0.0943	-0.0347	0.0054	0.0665	-0.0711	-0.4904
0.075	-0.1069	-0.0349	0.0066	0.0758	-0.081	-0.4938
0.09	-0.1173	-0.0354	0.0078	0.0827	-0.0883	-0.4958
0.105	-0.1262	-0.0362	0.009	0.0876	-0.0936	-0.4965
0.12	-0.1339	-0.0374	0.0103	0.0914	-0.0974	-0.4962

**Table 7.5 – Longitudinal stability derivatives of the JR Voyager E with a 0.01m<sup>2</sup> tail plane**

mu	LONGITUDINAL DERIVATIVES						
	zw	zu	xw	xu	mw'	mq'	mu'
0.015	-0.4935	-0.1263	0.0003	-0.0168	-0.0283	-0.4845	0.0818
0.03	-0.549	-0.2404	0.0012	-0.0161	-0.0383	-0.4958	0.0724
0.045	-0.6455	-0.3147	0.0031	-0.0147	-0.05	-0.5086	0.0635
0.06	-0.7652	-0.3167	0.0062	-0.013	-0.0612	-0.5212	0.0572
0.075	-0.8725	-0.262	0.011	-0.0118	-0.0701	-0.5328	0.0532
0.09	-0.9525	-0.1957	0.0173	-0.0112	-0.0768	-0.5433	0.0502
0.105	-1.0107	-0.1393	0.0251	-0.0111	-0.0825	-0.5527	0.0477
0.12	-1.0545	-0.0946	0.0345	-0.0114	-0.0877	-0.5612	0.0457

**Table 7.6 – Lateral stability derivatives of the JR Voyager E with a 0.01m<sup>2</sup> tail plane**

mu	LATERAL DERIVATIVES					
	yv	lv'	lr' & nr'	nv'	nr'	lp'
0.015	-0.0611	-0.0359	0.0029	0.0429	-0.0459	-0.4771
0.03	-0.0694	-0.0351	0.0032	0.0477	-0.0511	-0.4808
0.045	-0.0809	-0.0344	0.0038	0.0561	-0.0601	-0.4857
0.06	-0.0943	-0.0341	0.0048	0.0665	-0.0712	-0.4903
0.075	-0.1069	-0.0341	0.0059	0.0758	-0.0811	-0.4937
0.09	-0.1173	-0.0346	0.0069	0.0827	-0.0884	-0.4956
0.105	-0.1262	-0.0353	0.008	0.0877	-0.0937	-0.4963
0.12	-0.1339	-0.0363	0.0091	0.0915	-0.0977	-0.496



**Table 7.7 – Control derivatives of the Hirobo Shuttle Z**

mu	CONTROL DERIVATIVES						
	x_B1	m_b1'	z_B1	x_thet0	m_thet0'	z_thet0	n_init
0.015	0.0512	-0.1152	0.0077	-0.0008	-0.03	-0.6429	0.59
0.03	0.0513	-0.1149	0.0179	-0.0009	-0.0329	-0.639	0.8959
0.045	0.0515	-0.1145	0.033	-0.0005	-0.0357	-0.6395	1.0831
0.06	0.052	-0.1142	0.0521	0.0008	-0.0392	-0.6557	1.2094
0.075	0.0527	-0.1141	0.0724	0.0028	-0.0433	-0.684	1.3004
0.09	0.0539	-0.1144	0.0929	0.0058	-0.0476	-0.7141	1.3691
0.105	0.0554	-0.1151	0.1134	0.0098	-0.0519	-0.7418	1.4228
0.12	0.0573	-0.1162	0.134	0.0148	-0.0563	-0.7665	1.4659

**Table 7.8 – Control derivatives of the JR Voyager E**

mu	CONTROL DERIVATIVES						
	x_B1	m_b1'	z_B1	x_thet0	m_thet0'	z_thet0	n_init
0.015	0.0582	-0.1371	0.0074	-0.001	-0.0309	-0.6346	0.4171
0.03	0.0582	-0.1368	0.0165	-0.0013	-0.034	-0.6336	0.656
0.045	0.0584	-0.1365	0.029	-0.0009	-0.0371	-0.6328	0.8108
0.06	0.0589	-0.1363	0.0459	0.0002	-0.0405	-0.6382	0.9192
0.075	0.0597	-0.1363	0.0654	0.0023	-0.0446	-0.6552	0.9994
0.09	0.0608	-0.1367	0.0857	0.0053	-0.0491	-0.6799	1.0612
0.105	0.0624	-0.1376	0.1061	0.0095	-0.0539	-0.7062	1.1102
0.12	0.0645	-0.1389	0.1265	0.0148	-0.0586	-0.7314	1.15

**Table 7.9 – Control derivatives of the JR Voyager E  
with a 0.01m<sup>2</sup> tail plane**

mu	CONTROL DERIVATIVES						
	x_B1	m_b1'	z_B1	x_thet0	m_thet0'	z_thet0	n_init
0.015	0.0582	-0.137	0.0074	-0.001	-0.0318	-0.6346	0.4171
0.03	0.0582	-0.1367	0.0165	-0.0013	-0.0356	-0.6336	0.656
0.045	0.0584	-0.1364	0.029	-0.0009	-0.0391	-0.6328	0.8108
0.06	0.0589	-0.1361	0.0459	0.0002	-0.0428	-0.6382	0.9192
0.075	0.0597	-0.1361	0.0654	0.0023	-0.047	-0.6552	0.9994
0.09	0.0608	-0.1364	0.0857	0.0053	-0.0518	-0.6799	1.0612
0.105	0.0624	-0.1371	0.1061	0.0095	-0.0569	-0.7062	1.1102
0.12	0.0645	-0.1382	0.1265	0.0148	-0.0621	-0.7314	1.15



## APPENDICES

## APPENDIX A.1 – HOVER ANALYSIS COMPUTER PROGRAM

### Description

Two computer programs were written to perform the analysis of the helicopter in flight.

The first computer program was written in Java to provide a real-time simulation of the effect of changing the three controls. Three sliders are provided, one each for the main-rotor angular velocity, the main-rotor collective setting and the tail-rotor collective setting

The outputs are the thrust produced, the power required to drive the main-rotor, the torque generated by the main-rotor, the counter-torque produced, the power required to drive the tail-rotor and the rolling moment due to the tail-rotor.

Any of the three sliders can be drawn to a new value with the resulting change in output displayed immediately. This makes the program convenient to investigate the interaction between the three controls.

The program interface is illustrated in Figure 3.1.

The second program was written in Matlab. This program was written mainly to observe the changes required to maintain hover upon changing the main rotor RPM.

The main rotor rotational velocity was selected as values between 900 RPM and 1200 RPM in steps of 25 RPM. The main and tail rotor collective pitch as well as the torque and power required were then calculated.



## The Matlab Program

```
% Johnny Visagie
%
% Hover analysis - NEW
%
% 28 July 2003
%
% Program to analyze a hovering helicopter with certain inputs.
```

```
clear all;
close all;
clc;
```

```
disp('HELICOPTER IN HOVER');
disp('');
disp(' ');
disp(' ');
disp(' ');
disp(' ');
```

```
% inputs
W = 2.6*9.81;
R = 0.618;
N = 2;
c = 0.044;
a = 5.7;
T0 = 6*pi/180;
Tt = T0;
Cd0 = 0.011;
rho = 1.205;
```

```
% Tail Rotor Characteristics
```

```
lt = 0.715; % Distance from cg to tail rotor [m]
Rt = 0.110;
ct = 0.022; % tail rotor chord
At = pi*Rt*Rt; % Tail rotor area
Nt = 2;
SRt = Nt*ct/(pi*Rt);
at = 5.7;
```

```

A = pi*R*R; % Disk Area
SR = N*c/(pi*R); % Solidity Ratio
teller = 0;
for Omega_R = 900:25:1200 % RPM
    Omega_T = (Omega_R*R)/Rt; % To keep mu_MR = mu_TR

    teller = teller + 1;

    w_R = Omega_R * (2*pi)/60;
    w_Rt = Omega_T * (2*pi)/60;

    % Calculate Main Rotor Collective
    C_T = W / (rho * A * (w_R*R)^2);
    MRCol(teller) = 6*C_T/(SR*a) + 1.5*sqrt(C_T/2);

    % Calculate Main Rotor Power
    K = 1.15; % See Johnson, p.54
    CP = K * (C_T^1.5)/sqrt(2) + 0.125*SR*Cd0;
    PowMR(teller) = CP*rho*A*(w_R*R)^3; % Main Rotor Power

    % Calculate the Main Rotor Torque
    Q(teller) = PowMR(teller) / w_R; % Main Rotor Torque

    % Calculate Tail Rotor Collective Setting
    Tt = Q(teller) / It % Tail Rotor Thrust
    C_Tt = Tt / (rho*At*(w_Rt*Rt)^2); % Tail Rotor Thrust Coefficient
    % Tail Rotor Collective Setting

```



```

TRCol(teller) = 6*C_Tt/(SRt*at) + 1.5*sqrt(C_Tt/2);

% Calculate Tail Rotor Power Required

% Tail Rotor Power Coeff
CPT = K * (C_Tt ^ 1.5)/sqrt(2) + 0.125*SRt*Cd0;

PowTR(teller) = CPT*rho*At*(w_Rt*Rt)^3;          % Tail Rotor Power

%Calculate Total Power
PowTot(teller) = PowTR(teller) + PowMR(teller);

% Calculate the Figure of Merit
FOM(teller) = W*sqrt(W/(2*rho*A))/PowMR(teller);

end %Omega_R = 900:25:1200

Omega_R = 900:25:1200;

figure(1); hold on; grid on;
H = plot(Omega_R, MRCol*180/pi,'bo-',Omega_R, TRCol*180/pi,'r^-');
title('Collective Setting in Hover');
xlabel('Main Rotor Speed (RPM)');
ylabel('Degrees');
Legend('Main Rotor','Tail Rotor',0);

figure(2); hold on; grid on;
H = plot(Omega_R, PowMR,'bo-',Omega_R, PowTot,'r*-');
title('Power Required in Hover');
xlabel('Main Rotor Speed (RPM)');
ylabel('Power (W)');
Legend('Main Rotor', 'Total Power',0);

figure(3); hold on; grid on;
H = plot(Omega_R, PowTR,'bo-');
title('Tail Rotor Power Required in Trimmed Hovering Flight');
xlabel('Main Rotor Speed (RPM)');
ylabel('Power (W)');

```

```

figure(4); hold on; grid on;
H = plot(Omega_R, Q,'b-');
title('Total Main Rotor Torque Required in Trimmed Hovering Flight');
xlabel('Main Rotor Speed (RPM)');
ylabel('Torque (Nm)');

```

```

figure(5); hold on; grid on;
H = plot(Omega_R, FOM,'b-');
title('Figure of Merit for Trimmed Hovering Flight');
xlabel('Main Rotor Speed (RPM)');
ylabel('Figure of Merit');

```

---

## The Java Program

```

// Program to calculate required thrust and power for certain
// helicopter settings

//add rolling moment due to tail rotor position

import javax.swing.*;
import java.awt.*;
import javax.swing.event.*;
import java.applet.*;

class Changes4 extends JFrame implements ChangeListener
{

    //create the components

    //create the sliders
    JSlider scale = new JSlider (0, 1200, 1);
    JLabel position = new JLabel ("Set Main-rotor RPM");

    JSlider cyclic = new JSlider (0, 150, 0);
    JLabel cycpos = new JLabel ("Set Collective Position");

    JSlider tail = new JSlider (0, 100, 20);
    JLabel tailpos = new JLabel ("Set Tail Collective Position");

```



```

//create the text areas
JTextArea thrusttext = new JTextArea (1, 25);
JTextArea powertext = new JTextArea (1, 25);
JTextArea torquetext = new JTextArea (1, 25);
JTextArea tailtorque = new JTextArea (1, 25);
JTextArea tailpower = new JTextArea (1, 25);
JTextArea tailroll = new JTextArea (1, 25);
JTextArea spacer = new JTextArea (1, 25);

//global static variables
static int rpm;
static int cycVal;
static int tailCycVal;

public Changes4 ()
{
    super ("Adjust the Settings");
    setSize (400, 400);
    setDefaultCloseOperation (JFrame.EXIT_ON_CLOSE);
    setVisible (true);

    Container content = getContentPane ();
    content.setBackground (Color.white);

    FlowLayout lay = new FlowLayout (FlowLayout.LEFT);
    content.setLayout (lay);

    scale.setMajorTickSpacing (200);
    scale.setMinorTickSpacing (100);
    scale.setPaintTicks (true);
    scale.setPaintLabels (true);

    scale.addChangeListener (this);

    cyclic.setMajorTickSpacing (30); //3
    cyclic.setMinorTickSpacing (10); //1
    cyclic.setPaintTicks (true);
    cyclic.setPaintLabels (true);

    cyclic.addChangeListener (this);

    tail.setMajorTickSpacing (20);
    tail.setMinorTickSpacing (10);

```

```

tail.setPaintTicks (true);
tail.setPaintLabels (true);

tail.addChangeListener (this);

content.add (scale);
content.add (position);

content.add (cyclic);
content.add (cycpos);

content.add (tail);
content.add (tailpos);

content.add (spacer);

content.add (thrusttext);
content.add (powertext);
content.add (torquetext);

content.add (tailtorque);
content.add (tailpower);

content.add (tailroll);

setContentPane (content);
}

//now we must add the calculation of the torque and power...

public void stateChanged (ChangeEvent event)
{
    JSlider src = (JSlider) event.getSource ();
    if (!src.getValueIsAdjusting ())
    {
        rpm = scale.getValue ();
        cycVal = cyclic.getValue ();
        tailCycVal = tail.getValue ();

        double cv = cycVal;
        cv = cv / 10;

        String num1 = Double.toString (cv);
    }
}

```



```

String zeros = "0000";
String num2 = num1 + zeros;
String str1 = num2.substring (0, 4);

double tcv = tailCycVal;
tcv = tcv / 10;

String num3 = Double.toString (tcv);
String num4 = num3 + zeros;
String str2 = num4.substring (0, 4);

position.setText ("Main-rotor is at " + scale.getValue () + " RPM");
cycpos.setText ("Collective is at " + str1 + " degrees");
tailpos.setText ("Tail Collective is at " + str2 + " degrees");

//tailroll.setText("Tail Roll hier");

calculation (rpm, cv);
tailCalcs (rpm, tcv);

}

}

public void calculation (int rpm, double cv)
{

//initialize the aircraft parameters

//System.out.println(cv);

double R = 0.6;           //Main Rotor blade radius
int N = 2;                //number of blades
double c = 0.055;        //chord-length
double a = 5.7;          //2D lift-curve slope
double Cd0 = 0.0011;     //constant drag coeff
double rho = 1.205;      //air density

double A = Math.PI * R * R; // Disk Area
double SR = N * c / (Math.PI * R); //solidity ratio

double Omega = rpm * 2 * Math.PI / 60;

```

```

double cycVal = cv; //hmmm suspect method

double cycValRad = cycVal * Math.PI / 180;

/* THRUST CALCULATIONS COMMENCES HERE */
//initialize integration variables for thrust calculations

double step = 1;
double rmax = 30;
double r = 1;
double counter;

double sum = ((Math.pow ((SR * a), 2) / 32)) * (Math.sqrt (1 + (32 *
cycValRad * r) / (SR * a)) - 1) * r;

for (counter = step ; counter <= (rmax - 1) ; counter = counter + step)
{
    r = (counter / rmax);
    sum = sum + 2 * ((Math.pow ((SR * a), 2) / 32)) * (Math.sqrt (1 +
(32 * cycValRad * r) / (SR * a)) - 1) * r;
}

double h = (step / rmax); //for integration
double int1 = (h / 2) * sum;

double C_T = (SR * a * cycValRad) / 6 - int1; //Thrust Coefficient

double T_bet = rho * A * (Math.pow ((Omega * R), 2)) * C_T; //thrust
produced according to BladeElementTheory

double thr = T_bet;

String thrStr = Double.toString (thr);
String zeros = "00000";
String TS = thrStr + zeros;
String thrustString = TS.substring (0, 5);

thrusttext.setText ("The Amount of Thrust Produced is : " +
thrustString + " N ");

```



```

/** POWER CALCULATIONS COMMENCES HERE */
//initialize integration variables for power calculations

step = 1;
rmax = 30;
r = 1;

// should that be | cycValRad * r |   ?????

double lambda = (SR * a / 16) * (Math.sqrt (1 + (64 * cycValRad) / (3
* SR * a)) - 1);
sum = 0.5 * lambda * SR * a * (cycValRad * r * r - lambda * r);

for (counter = step ; counter <= (rmax - 1) ; counter = counter + step)
{
    r = (counter / rmax);
    lambda = (SR * a / 16) * (Math.sqrt (1 + (64 * cycValRad) / (3 * SR
* a)) - 1);
    sum = sum + lambda * SR * a * (cycValRad * r * r - lambda * r);
}

h = (step / rmax); //for integration
int1 = (h / 2) * sum;

double C_P = 0.125 * SR * Cd0 + int1; //Power Coefficient

double P_bet = rho * A * (Math.pow ((Omega * R), 3)) * C_P; //power
produced according to BladeElementTheory

double pwr = P_bet;

String pwrStr = Double.toString (pwr);
String PS = pwrStr + zeros;
String powerString = PS.substring (0, 5);

powertext.setText ("The Amount of Main-Rotor Power Required is : "
+ powerString + " W ");

/** CALCULATE THE AMOUNT OF TORQUE */

double torque = P_bet / Omega;

```

```

String torqueNum = Double.toString (torque);
String torqueString = torqueNum.substring (0, 5);

torquetext.setText (torqueString + " Nm of torque is generated ");

} //end calculations

//Calculations for torque and power of tail rotor

public void tailCalcs (int rpm, double tcv)
{
    //initialise the aircraft parameters

    double R = 0.108;           //Tail Rotor blade radius
    int N = 2;                  //number of blades
    double c = 0.022;          //chord-length
    double a = 5.7;            //2D lift-curve slope
    double Cd0 = 0.001;        //constant drag coeff
    double rho = 1.205;        //air density

    double lt = 0.725;         //length of "force-arm"
    double ht = 0.07;          //height of tail-rotor ac above cog

    double A = Math.PI * R * R; //Disk Area
    double SR = N * c / (Math.PI * R); //solidity ratio

    double ratio = 5.6;        //ratio of tail-rotor speed to main rotor
    speed
    double Omega = ratio * rpm * 2 * Math.PI / 60;

    double tailCycVal = tcv;

    double cycValRad = tailCycVal * Math.PI / 180;

    /** THRUST CALCULATIONS COMMENCES HERE **/
    //initialise integration variables for thrust calculations

    double step = 1;

```



```

double rmax = 30;
double r = 1;
double counter;

double sum = ((Math.pow ((SR * a), 2) / 32)) * (Math.sqrt (1 + (32 *
cycValRad * r) / (SR * a)) - 1) * r;

for (counter = step ; counter <= (rmax - 1) ; counter = counter + step)
{
    r = (counter / rmax);
    sum = sum + 2 * ((Math.pow ((SR * a), 2) / 32)) * (Math.sqrt (1 +
(32 * cycValRad * r) / (SR * a)) - 1) * r;
}

double h = (step / rmax); //for integration
double int1 = (h / 2) * sum;

double C_T = (SR * a * cycValRad) / 6 - int1; //Thrust Coefficient

double T_bet = rho * A * (Math.pow ((Omega * R), 2)) * C_T; //thrust
produced according to BladeElementTheory

/** POWER CALCULATIONS COMMENCES HERE */
//initialize integration variables for power calculations

step = 1;
rmax = 30;
r = 1;

double lambda = (SR * a / 16) * (Math.sqrt (1 + (64 * cycValRad) / (3
* SR * a)) - 1);
sum = 0.5 * lambda * SR * a * (cycValRad * r * r - lambda * r);

for (counter = step ; counter <= (rmax - 1) ; counter = counter + step)
{
    r = (counter / rmax);
    lambda = (SR * a / 16) * (Math.sqrt (1 + (64 * cycValRad) / (3 * SR
* a)) - 1);
    sum = sum + lambda * SR * a * (cycValRad * r * r - lambda * r);
}

h = (step / rmax); //for integration
int1 = (h / 2) * sum;

```

```

double C_P = 0.125 * SR * Cd0 + int1; //Power Coefficient

double P_bet = rho * A * (Math.pow ((Omega * R), 3)) * C_P; //power
produced according to BladeElementTheory

double thr = P_bet;

String pwrStr = Double.toString (thr);
String zeros = "00000";
String PS = pwrStr + zeros;
String powerString = PS.substring (0, 5);

tailpower.setText ("The Amount of Tail-Power Required is : " +
powerString + " W ");

/* CALCULATE THE AMOUNT OF TORQUE */

double torque = It * T_bet;

String torqueNum = Double.toString (torque);
String torqueString = torqueNum.substring (0, 5);

tailtorque.setText (torqueString + " Nm of counter-torque is
generated ");

double roll = ht * T_bet;

String rollNum = Double.toString (roll);
String rollString = rollNum.substring (0, 5);

tailroll.setText ("Roll moment due to tail-rotor position is : " +
rollString + " Nm ");

} //end tailCalcs

public static void main (String [] args)
{
    Changes4 eg = new Changes4 ();
}
}

```



## **APPENDIX A.2 – VERTICAL CLIMBING FLIGHT**

### **Description**

In order to perform this analysis, a computer program was written in Matlab. This program calculated the incremental power required, incremental collective setting for the main rotor, the main rotor and tail rotor collective settings and the total power required to climb.

All these calculations were performed at three main rotor RPM settings: 1000RPM, 1100RPM and 1200RPM. The calculations were also performed at different climbing speeds.

### **Method**

The program was solved for three different settings of the main rotor rotational velocity. The body of the program was the same for all of these settings.

In order to determine the required information (as specified in Chapter 4):

- the inflow velocity of the helicopter in hover was determined
- the climbing inflow velocity was calculated
- the thrust required to climb was determined
- the effect of the vertical drag was added to the climbing thrust
- the incremental power was calculated
- the incremental collective pitch was calculated
- the hovering components of the collective pitch and power was determined
- the climbing values of collective pitch, thrust and power was calculated
- the amount of torque required to drive the rotor was determined
- the tail rotor power and collective pitch angle was determined.

## The program

```
% Johnny Visagie
%
% Hover analysis - NEW
%
% 13 October 2003
%
% Program to analyze a hovering helicopter with certain inputs.

clear all;
close all;
clc;

% inputs
W = 2.6*9.81;
R = 0.618;
N = 2;
c = 0.044;
a = 5.7;
T0 = 6*pi/180;
Tt = T0;
Cd0 = 0.011;
rho = 1.205;

% Fuselage Characteristics
S = (0.09*0.370);           % Estimated planform area as seen from
above
Cd = 2;                     % Flat-plate drag coeff
z = 0.1;                    % Fuselage location below rotor

% Tail Rotor Characteristics

It = 0.715;                 % Distance from cg to tail rotor [m]
Rt = 0.110;
ct = 0.022;                 % tail rotor chord
At = pi*Rt*Rt;             % Tail rotor area
Nt = 2;
SRt = Nt*ct/(pi*Rt);
at = 5.7;
```



```

A = pi*R*R;           % Disk Area

SR = N*c/(pi*R);     % Solidity Ratio

teller = 0;

% Color Scheme
kleur = ['r';'k';'b'];
Omega = [1000;1100;1200]*(2*pi)/(60);

for t = 1:1:3

    Omega_R = Omega(t);
    Omega_Rt = (Omega_R*R)/Rt;

    teller = 0;

    % Climbing Velocity
    for Vc = 0:0.1:1.5

        teller = teller + 1;

        % Firstly calculate values for hover
        % Calculate Main Rotor Collective

        C_T = W / (rho * A * (Omega_R*R)^2);
        MRCol(teller) = 6*C_T/(SR*a) + 1.5*sqrt(C_T/2);

        % Calculate Main Rotor Power
        K = 1.15; % See Johnson, p.54
        CP = K * (C_T^1.5)/sqrt(2) + 0.125*SR*Cd0;

        % Main Rotor Power
        PowMR(teller) = CP*rho*A*(Omega_R*R)^3;

        % Now calculate values for climbing
        % assume thrust = weight, as in hover
        T = W;
        nu_h = sqrt(T/(2*rho*A));

        % According to Momentum Theory (Johnson, p.95)
        nu = -Vc/2 + sqrt( (Vc/2)^2 + nu_h^2);

```

```

% Adjust thrust to include vertical drag
% Use Johnson, p.117
n = 1 + (z/R) / sqrt(1 + (z/R)^2);
DelT = T * (S/A)*Cd*( (Vc + n*nu)/(2*nu_h))^2;
T = T + DelT;

% Power increase needed for climb
DelP(teller) = (Vc + nu - nu_h)*T;

% Delta P Coeff
DelCP = DelP(teller) / (rho * A * (Omega_R * R)^3);

% Thrust Coeff
CT = T / (rho * A * (Omega_R*R)^2);

% increase in Collective setting
DelCol(teller) = 1.5*DelCP/CT;

% Add Components together
% Collective setting for climb
MRCol(teller) = MRCol(teller) + DelCol(teller);

% Main Rotor Power Required for Climb
PowMR(teller) = PowMR(teller) + DelP(teller);

% Determine the Tail Rotor Settings
% Calculate the Main Rotor Torque
% Main Rotor Torque
Q(teller) = PowMR(teller) / Omega_R;

% Calculate Tail Rotor Collective Setting
Tt = Q(teller) / It; % Tail Rotor Thrust

% Tail Rotor Thrust Coefficient
C_Tt = Tt / (rho*At*(Omega_Rt*Rt)^2);

% Tail Rotor Collective Setting
TRCol(teller) = 6*C_Tt/(SRt*at) + 1.5*sqrt(C_Tt/2);

```



```

% Calculate Tail Rotor Power Required
% Tail Rotor Power Coeff
CPt = K * (C_Tt ^ 1.5)/sqrt(2) + 0.125*SRt*Cd0;
% Tail Rotor Power
PowTR(teller) = CPt*rho*At*(Omega_Rt*Rt)^3;

% Calculate the Total Power
Power(teller) = PowMR(teller) + PowTR(teller);

% Calculate the Torque
Torque(teller) = PowMR(teller) / Omega_R;

end

Vc = 0:0.1:1.5;

figure(1); hold on; grid on;
H = plot(Vc, DelP, kleur(t));
title('\DeltaP Required for Climbing Flight')
xlabel('Climbing Velocity (m/s)');
ylabel('\DeltaP (W)');

figure(2); hold on; grid on;
H2 = plot(Vc, DelCol*180/pi, kleur(t));
title('Increase in Collective Setting for Climbing Flight')
xlabel('Climbing Velocity (m/s)');
ylabel('\Delta\theta (degrees)');

figure(3); hold on; grid on;
H = plot(Vc, MRCol*180/pi, kleur(t));
title('Main Rotor Collective Setting in Climb');
xlabel('Climbing Velocity (m/s)');
ylabel('\theta (degrees)');

figure(4); hold on; grid on;
H = plot(Vc, TRCol*180/pi, kleur(t));
title('Tail Rotor Collective Setting in Climb');
xlabel('Climbing Velocity (m/s)');
ylabel('\theta (degrees)');

```

```
figure(5); hold on; grid on;  
H = plot(Vc, Power, kleur(t));  
title('Total Power Required for Climbing Flight')  
xlabel('Climbing Velocity (m/s)');  
ylabel('Power (W)');
```

```
figure(6); hold on; grid on;  
H = plot(Vc, Torque, kleur(t));  
title('Torque Required for Climbing Flight')  
xlabel('Climbing Velocity (m/s)');  
ylabel('Torque (Nm)');
```

```
end
```

```
figure(1); legend('1000 RPM','1100RPM', '1200RPM',0);  
figure(2); legend('1000 RPM','1100RPM', '1200RPM',0);  
figure(3); legend('1000 RPM','1100RPM', '1200RPM',0);  
figure(4); legend('1000 RPM','1100RPM', '1200RPM',0);  
figure(5); legend('1000 RPM','1100RPM', '1200RPM',0);  
figure(6); legend('1000 RPM','1100RPM', '1200RPM',0);
```



**APPENDIX A.3 – Combined Trim Analysis and calculation of the Stability and Control analysis of a helicopter in forward flight**

```
% Johnny Visagie
%
% TRIM Analysis of H/C combined with the Stability and Control Derivation
% Version 4
% Uncouple longitudinal and lateral motions
%
% 4 November 2003
```

```
% _____
% ASSUMPTIONS MADE
%
% No Blade Stall
% Drag coefficient of blade section constant
% small angle assumption
```

```
clear all;
close all;
clc;
tic
warning off
```

```
% Initialise properties of the Hirobo Shuttle Z
%Mass and Inertia Characteristics
```

```
Mass = 3.25;           % kg
Ixx = 0.04096135;     % kg m^2
Iyy = 0.13653783;     % kg m^2
Izz = 0.13653783;     % kg m^2
Ixz = 0;              % kg m^2
```

```
%Main Rotor characteristics
```

```
R = 0.618;           % m
e = 0.1100;
i = 0;
c = 0.044;           % m
b = 2;               % Amount of Blades
a = 5.7;             % 2D Lift - Curve Slope
C_dr = 0.0110;       % Rotor-blade Drag-coefficient
Omega_R = (1500*2*pi)/60; % rad / s
M_b = 0.0700;        % kg
I_b = 1/3*M_b*R^2;   % kg m^2
Delta_3 = 0;         % rad
rbcg = 0.5*R;        % m to blade cg
```

%Tail Rotor Characteristics

R\_t = 0.11;                   % m  
e\_t = 0;  
c\_t = 0.022;                 % m  
b\_t = 2;                     % Number of Tail-rotor blades  
Omega\_t = 5.6\*Omega\_R;       % rad / s

s\_t = b\_t\*c\_t/(pi \*R\_t);     % Tail solidity  
A\_t = pi \* R\_t^2;            % Tail-rotor disk area

Prod\_t = Omega\_t \* R\_t;

% horizontal stabilizer  
St = 0.012;                 % m^2

% Vertical fin  
Sf = 0.01435 ;             % m^2  
alpha\_f = 0;  
af = 4\*1.2/pi;

%Distances from the H/C c.o.g.  
% l indicates distances in the X direction  
% h denotes distance in the negative Z direction  
% M, T, H and V represent the Main Rotor, Tail Rotor,  
% Horizontal Stabilizer and Vertical Fin respectively  
% all units are m

IM = -0.035;  
hM = 0.255;  
IT = -0.715;  
hT = 0.08;  
IH = -0.40;  
hH = 0.075;  
IV = -0.65;  
hV = 0.065;

f = -IM/R;

% fuselage side area  
S\_B = 0.0703;

% Flight Characteristics & Quantities

% Flight Characteristics



```

g = 9.81;          % Gravitational Acceleration

% Calculate variables that will be used alot
s = b*c / (pi*R);
A = pi * R^2;
D0 = 0.0119;      % equivalent frontal flat-plate area
W = Mass*g;
xg = 0.5;         % estimated

rho = 1.215;

fact = rho * s * A * (Omega_R*R)^2;

Wc = W / fact;    % weight - coefficient

eps = 3*e / (2*(1 - e));

Lock = rho*c*a*(R^4) / I_b; % Lock number

% Specify Flight Trim Conditions

Tau = 0*pi/180;   % Flight Path Angle

% Determine drag

C_D = 2.0;        % flat-plate assumption

d0 = D0 / (s*A);  % Dimensionless drag

Theta_tw = 0*pi/180; % Twist angle in blade

s_b_t = s_t*A_t*(Omega_t*R_t) / (s * A * (Omega_R*R)); % noramlised tail
solidity

% ===== %

%-----%
%      START TRIM ANALYSIS      %
%-----%

% Assume we disconnect Long and lat
% Work out Longitudinal trim
% rotor forces referred to tip-path plane
% small angle assumption

teller = 0;

```

```

for mu = 0.015:0.015:0.133

    teller = teller + 1;

    Vknot = mu*(Omega_R*R)*3.6/1.86;

    test = 1;
    eps = 0.00001;

    % initial estimates
    theta_f = -2.5 * pi / 180;
    B1t = 0.0986;

    while ( test > eps)
        % determine h-force coefficient

        V = Vknot * 1.86/3.6;
        mu = V / (Omega_R*R);

        D = 0.5 * rho * V^2 * D0 * C_D;

        d0 = D0 / (s * A);

        h_cD = 0.25 * mu * C_dr;           % H-force coeff...1st estimate

        % disc incidence
        alpha_d = -(0.5*mu^2*d0*cos(Tau) + h_cD) / Wc - Tau;

        % Estimate Thrust and inflow for main rotor
        Thrust = W;
        U_T = sqrt(Thrust / (2*rho*A));
        V_bar = V / U_T;
        vi_bar = sqrt( 0.5*(- V_bar^2 + sqrt(V_bar^4 + 4) ) );
        vi = vi_bar * U_T;

        Lam_i = vi / (Omega_R*R);

        Lam_d = mu*alpha_d - Lam_i;

        t_cD = Wc + 0.5 * mu ^ 2 * d0 *sin(Tau);

        % Calculate a first estimate of the collective pitch angle - eqn 5.44 in
        % Bramwell
        % This is the pitch-angle at 75% of blade-radius NB

```



```

Theta_0 = 1.5 * ( 4 * t_cD / a - Lam_d * ( 1 - 0.5 * mu ^ 2) / ( 1 + 1.5 *
mu ^ 2) ) * ( ( 1 + 1.5 * mu ^ 2) / (1 - mu ^ 2 + 2.25 * mu ^ 4));

% estimate a0 equation 5.42
a0 = 0.125*Lock * ( Theta_0 * ( 1 - 19 * mu ^ 2 / 18 + 1.5 * mu ^ 4) / (1 +
1.5 * mu ^ 2) + (4/3) * Lam_d * (1 - 0.5 * mu^2) / (1 + 1.5 * mu ^ 2));

% calculate a1 from equation 5.41
a1 = (2 * mu * ( 4 * Theta_0 / 3 + Lam_d) ) / ( 1 + 1.5 * mu ^ 2);

% calculate b1 from Bramwell equation (5.40)
nu = Lock/16;
b1 = 4/3*(mu*a0 + 1.1*sqrt(nu)*Lam_i)/(1 + 0.5*mu^2);

% recalculate a1 to include effect of b1 can I do this (same planes?)
a1 = (2 * mu * ( 4 * Theta_0 / 3 + Lam_d) ) / ( 1 + 1.5 * mu ^ 2) +
(8/Lock)*eps*b1/(1 - 1.5 * mu ^ 2);

% k - value -> due to uneven inflow
k = 0.127;          % estimate, Bramwell, p.139

% Recalculate (new) h_cD
h_cD = 0.25*mu*C_dr - 0.25*a*Lam_d*(0.5*a1 - mu * Theta_0);

% calculate torque - coefficient
q_c = C_dr * (1 + 4.7 * mu ^ 2) / 8 - Lam_d * t_cD - mu * h_cD + k *
Lam_i * t_cD;

Power = q_c * rho * s * A * (Omega_R*R)^3;

Mf = 0;
CMf = Mf / (rho * s * A * (Omega_R*R)^2 * R);

CMs = b * M_b * xg * e / (2 * rho * s * A * R);

S = M_b*rbcg*Omega_R^2;
Ms = 0.5*b*S*e*R; % in-case needed later

C_ms = b*M_b*rbcg*e / (2*rho*s*A*R);

% _____ %
% TAIL CALCS START HERE %
% ***** %

% add tail component

% tail solidity
V_T = St * (-IT/R) / (s * A);

```

```

% tail zero incidence
alpha_s = 2.5*pi/180;

% tail 2d lift-curve slope
at = 3.5;

eps0 = Lam_i / mu;

%      % _____ %
%      % Horse - Shoe vortex model %
%      % ..... %
%
%      s_p = R*pi/4;
%      K0 = W/(rho*V^2*s_p);
%      xtp = sqrt(IH^2 + (hM - hH)^2);
%      ytp = sqrt(s_p^2 + (hM - hH)^2);
%      bet_tp = atan(s_p / (-IH));
%
%      w_tp = 2*K0/(4*pi*xtp)*cos(bet_tp) + 2 * K0 / (4*pi*ytp)*(cos(bet_tp) +
1);
%      eps = atan(w_tp/V);
%
%
B1t = a1 + (CMf + h_cD * (hM/R) - Wc * f - 0.5*mu^2*V_T*at*(alpha_d +
alpha_s - eps0) ) / ( Wc * (hM/R) + C_ms + 0.5 * mu^2 * V_T * at);

D = 0.5 * rho * V^2 * D0 * C_D;

d0 = D0 / (s * A);

alpha_nf = theta_f + B1t;

V_hat = mu / cos(alpha_nf);

alpha_d = -(0.5*mu^2*d0*cos(Tau) + h_cD) / Wc - Tau; % disc
incidence

theta_f_new = alpha_d + B1t - a1 + Tau;

test = abs(theta_f_new - theta_f);

theta_f = theta_f_new;

end %while

```





```

t_ct = Tt / (rho * s_t * A_t * (Prod_t)^2);

mu_t = V / Prod_t;

% Estimate thrust and inflow for Tail rotor
Thrust = Tt;
U_T = sqrt(Thrust / (2*rho*A_t));
V_bar = V / U_T;
vi_bar = sqrt( 0.5*(- V_bar^2 + sqrt(V_bar^4 + 4) ) );
vi = vi_bar * U_T;

Lam_it = vi / (Prod_t);

% Bramwell, p.176
Theta_0t = 1.5/(1 + 1.5*mu^2)*(4/a*t_ct - Lam_it);

% collective pitch setting for tail-rotor
TCol(teller) = Theta_0t;

% _____ %
% _____ %
% START LONGITUDINAL STABILITY CHARACTERISTICS %
% CALCULATIONS HERE %
% _____ %
% .....,..... %

% First determine the derivatives
% names are chosen to indicate how the derivative would have been spoken

alpha_nf = alpha_d - a1;

Lam = mu*alpha_nf - Lam_i;

dlamidmu = (2 * mu * Theta_0 + alpha_nf -
(4*t_cD/(a*Lam_i))*V_bar*vi_bar^3) / (1 + (4/a)*(t_cD/Lam_i)*(1+vi_bar^4));

dlamdmu = alpha_nf - dlamidmu;

dtcdmu = (2*mu*Theta_0 + alpha_nf + V_bar*vi_bar^3/(1+vi_bar^4)) / (4/a
+ (Lam_i/t_cD)/(1 + vi_bar^4));

da1dmu = 2*mu*dlamdmu/(1 - 0.5*mu^2) + (a1/mu) + a1*(mu/(1 -
0.5*mu^2));

dhcddmu = 0.25*C_dr;

dtcdw = 0.25*a/(1 + (a/4)*Lam_i/t_cD + vi_bar^4);

```



```

da1dw = (2*mu) / ( (1 - 0.5*mu^2)*(1 + (a/4)*Lam_i/t_cD + vi_bar^4));

dhcddw = 0.25*a/(1 + (a/4)*Lam_i/t_cD + vi_bar^4)*( 0.5*a1 - mu*Theta_0
+ mu*Lam_d/(1 - 0.5*mu^2));

dtcdq = 0;

da1dq = -(16/Lock)*(1/(1 - 0.5*mu^2));

dhcddq = -0.25*a*( (-a0/3)/(1+0.5*mu^2) + a0/3 - Lam*da1dq/2 -
mu*a1*da1dq + mu^2*Theta_0*da1dq + mu*b1/8);

dlamidw = ( 0.25*a * Lam_i / t_cD + vi_bar^4) / (1 + 0.25*a*Lam_i/t_cD +
vi_bar^4);

% Force derivatives here

xu(teller) = -t_cD*da1dmu - alpha_d*dtcdmu - dhcddmu;
Xu(teller) = xu(teller)*(rho*s*A*Omega_R*R)/(Mass);

zu(teller) = -dtcdmu;
Zu(teller) = zu(teller)*(rho*s*A*Omega_R*R)/(Mass);

xw(teller) = -t_cD*da1dw - alpha_d*dtcdw - dhcddw;
Xw(teller) = xw(teller)*(rho*s*A*Omega_R*R)/(Mass);

zw(teller) = -dtcdw;
Zw(teller) = zw(teller)*(rho*s*A*Omega_R*R)/(Mass);

xq(teller) = -t_cD*da1dq - dhcddq;
Xq(teller) = xq(teller)*(rho*s*A*Omega_R*R^2)/(Mass);

% Calculate necessary numbers
C_Lt = at*(alpha_s - eps0);
h1 = hM/R*cos(theta_f) - f*sin(theta_f);
l1 = f*cos(theta_f) + hM/R*sin(theta_f);

% Moment derivatives
m_u_p(teller) = -h1*xu(teller) + (l1)*zu(teller) + CMs*da1dmu -
mu*V_T*(C_Lt + 0.5*at*(dlamidmu - Lam_i/mu));
M_u(teller) = m_u_p(teller) * (rho*s*A*Omega_R*R^2) / (Iyy);

m_w_p(teller) = -h1*xw(teller) + (l1)*zw(teller) + CMs*da1dw -
0.5*mu*at*V_T*(1 - dlamidmu);
M_w(teller) = m_w_p(teller) *(rho*s*A*Omega_R*R^2) / (Iyy);

```

```

m_q_p(teller) = -h1*xq(teller) + CMs*da1dq - 0.5*mu*at*V_T*(-IT/R);
M_q(teller) = m_q_p(teller) *(rho*s*A*Omega_R*R^3) / (Iyy);

```

```

% Stability quadratic - necessary numbers

```

```

mu_star = W/(g*rho*s*A*R);
t_hat = mu_star / (Omega_R);
ib = Iyy/(W*R^2/g);

```

```

% Determine the values without primes

```

```

m_u(teller) = mu_star/ib*m_u_p(teller);
m_w(teller) = mu_star/ib*m_w_p(teller);
m_q(teller) = mu_star/ib*m_q_p(teller);
m_w_punt(teller) = mu_star/ib*(- 0.5*mu*at*V_T*(-IT/R));

```

```

% More values

```

```

N1(teller) = -xu(teller) - zw(teller);
P1(teller) = xu(teller)*zw(teller) - xw(teller)*zu(teller);
Q1(teller) = -mu*xu(teller) - Wc*sin(Tau);
R1(teller) = -Wc*(zu(teller)*cos(Tau) - xu(teller)*sin(Tau));
S1(teller) = Wc*cos(Tau) - mu*xw(teller);
T1(teller) = -Wc*(zu(teller)*cos(Tau) - xw(teller)*sin(Tau));

```

```

% The values of the quadratic

```

```

qA1(teller) = 1;
qB1(teller) = N1(teller) - m_q(teller) - mu*m_w_punt(teller);
qC1(teller) = P1(teller) - N1(teller)*m_q(teller) - Q1(teller)*m_w_punt(teller)
- mu*m_w(teller);
qD1(teller) = S1(teller)*m_u(teller) - P1(teller)*m_q(teller) -
R1(teller)*m_w_punt(teller) - Q1(teller)*m_w(teller);
qE1(teller) = T1(teller)*m_u(teller) - R1(teller)*m_w(teller);

```

```

% The quadratic

```

```

char_eq = [qA1(teller), qB1(teller), qC1(teller), qD1(teller), qE1(teller)];
L = roots(char_eq);

```

```

% The roots

```

```

r1(teller) = L(1);
r2(teller) = L(2);
r3(teller) = L(3);
r4(teller) = L(4);

```

```

% estimate

```

```

M_w_punt(teller) = 0;

```





```

% Airodynamic derivatives
yv(teller) = -t_cD*a1/mu - 0.25*C_dr - s_b_t*dtcdw - 0.3 * mu * S_B / (s*A);
lv_p(teller) = -( (hM/R)*t_cD + CMs)*a1/mu - ht_p*s_b_t*dtcdw;
lp_p(teller) = -16/Lock*( (hM/R)*(t_cD + a*Lam_d/8) + CMs) / (1 +
0.5*mu^2) - ht_p^2*s_b_t*dtcdw;
lr_p(teller) = ht_p*lt_p*s_b_t*dtcdw;
nv_p(teller) = lt_p*s_b_t*dtcdw;
np_p(teller) = ht_p*lt_p*s_b_t*dtcdw;
nr_p(teller) = -lt_p^2*s_b_t*dtcdw;

```

```

% Re-dimensionalised factors <- ek dink die is dalk verkeerd!!
Yv(teller) = yv(teller)*(rho*s*A*Omega_R*R)/Mass;
Lv(teller) = lv_p(teller)*(rho*s*A*Omega_R*R^2)/lxx;
Lp(teller) = lp_p(teller)*(rho*s*A*Omega_R*R^3)/lxx;
Lr(teller) = lr_p(teller)*(rho*s*A*Omega_R*R^3)/lxx;
Nv(teller) = nv_p(teller)*(rho*s*A*Omega_R*R^2)/lzz;
Np(teller) = np_p(teller)*(rho*s*A*Omega_R*R^3)/lzz;
Nr(teller) = nr_p(teller)*(rho*s*A*Omega_R*R^3)/lzz; %- 0.5*rho*af*Sf*(-
IV)*V/lzz;

```

```

% Bramwell se dom estimates
Yp(teller) = 0;
Yr(teller) = 0;

```

```

L_v_primed = (lzz*Lv + lxx*Nv) / (lxx*lzz - lxx^2);
L_p_primed = (lzz*Lp + lxx*Np) / (lxx*lzz - lxx^2);
L_r_primed = (lzz*Lr + lxx*Nr) / (lxx*lzz - lxx^2);
N_v_primed = (lxx*Nv + lxx*Lv) / (lxx*lzz - lxx^2);
N_p_primed = (lxx*Np + lxx*Lp) / (lxx*lzz - lxx^2);
N_r_primed = (lxx*Nr + lxx*Lr) / (lxx*lzz - lxx^2);

```

```

% These coefficients are for dimensional items

```

```

A2(teller) = sec(phi)*cos(theta_f)*(1 - lxx^2/(lxx*lzz));
B2(teller) = sec(phi)*cos(theta_f)*(-Yv(teller) - Lp(teller) - Nr(teller) +
(lxx^2/(lxx*lzz))*Yv(teller)...
- (lxx/lxx)*Np(teller) - (lxx/lzz)*Lr(teller));
C2(teller) = sec(phi)*cos(theta_f)*(Yv(teller)*Lp(teller) + Yv(teller)*Nr(teller)
+ Lp(teller)*Nr(teller)...
- Lr(teller)*Np(teller) + (lxx/lxx)*Yv(teller)*Np(teller) +
(lxx/lzz)*Yv(teller)*Lr(teller)...
- Lv(teller)*Yp(teller) - (lxx/lxx)*Nv(teller)*Yp(teller) -
(lxx/lzz)*Lv(teller)*(Yr(teller)...
-V) - Nv(teller)*(Yr(teller)-V));

```



```

D2(teller) = sec(phi)*cos(theta_f)*(-Yv(teller)*Lp(teller)*Nr(teller) +
Yv(teller)*Lr(teller)*Np(teller)...
+ Lv(teller)*Nr(teller)*Yp(teller) - Lr(teller)*Nv(teller)*Yp(teller) -
Lv(teller)*Np(teller)...
*(Yr(teller)-V) + Lp(teller)*Nv(teller)*(Yr(teller)-V)) -
g*(cos(theta_f))^2*(Lv(teller) + (lxz/lxx)...
*Nv(teller)) - g*sin(theta_f)*cos(theta_f)*cos(phi)*(Nv(teller) +
(lxz/lzz)*Lv(teller));
E2(teller) = g*sin(theta_f)*cos(theta_f)*cos(phi)*(Nv(teller)*Lp(teller) -
Np(teller)*Lv(teller)) + ...
g*(cos(theta_f))^2*(Nr(teller)*Lv(teller) - Nv(teller)*Lr(teller));

```

```

% set up the stability quadratic

```

```

lat_char_eq = [A2(teller), B2(teller), C2(teller), D2(teller), E2(teller)];
Lat = roots(lat_char_eq);

```

```

% Extract the roots

```

```

lr1(teller) = Lat(1);
lr2(teller) = Lat(2);
lr3(teller) = Lat(3);
lr4(teller) = Lat(4);

```

```

zw_bram =

```

```

[0.60;0.80;0.95;1.03;1.1;1.1375;1.175;1.2;1.225;1.244;1.26;1.27];
lrp_bram(teller) = ht_p*lt_p*s_b_t*zw_bram(teller);
nvp_bram(teller) = s_b_t*zw_bram(teller)*lt_p;
nrp_bram(teller) = -lt_p^2*s_b_t*zw_bram(teller);

```

```

% Dutch roll oscillation

```

```

nv(teller) = nv_p(teller)*mu_star/iC;
T_dutch(teller) = 2*pi*t_hat/sqrt(mu*nv(teller));

```

```

% _____ %
% %
% START CONTROL RESPONSE CALCULATIONS HERE %
% %
% %

```

```

% The B1 derivatives (longitudinal cyclic)

```

```

dtcdb1 = -mu*dtcdw;
dhcddb1 = -mu*dhcddw;
da1db1 = -mu*da1dw;

```

```

xb1(teller) = dtcdb1*alpha_d + t_cD*(1 + mu*da1dw) - dhcddb1;
zb1(teller) = -dtcdb1;
mb1_p(teller) = -h1*xb1(teller) + l1*zb1(teller) - CMs*(1 + mu*da1dw);

% The collective derivatives

dtcdt0 = (a/6)*(1 + 1.5*mu^2) / (1 + (0.25*a*Lam_i/t_cD)/(1 + vi_bar^4));
dlamidt0 = 1/(1 + vi_bar^4)*Lam_i/t_cD*dtcdt0;
da1dt0 = 2*mu/(1 - 0.5*mu^2)*(4/3 - dlamidt0);
dlamddt0 = mu*da1dt0 - dlamidt0;
dhcddt0 = (a/8)*(a1*dlamddt0 + Lam_d*da1dt0 - 2*mu*(Lam_d +
Theta_0*dlamddt0));

xt0(teller) = -t_cD*da1dt0 - alpha_d*dtcdt0 - dhcddt0;
zt0(teller) = -dtcdt0;
mt0_p(teller) = -h1*xt0(teller) + l1*zt0(teller) - CMs*da1dt0;

% initial gust response

w_gust = 10.5;
zwh = -2*a*mu / (8*mu + a*s);
n_init(teller) = -zwh*w_gust/(Wc*Omega_R);

end

mu = 0.015:0.015:0.133;

% Un-comment the graph you would like to see

% Force and Moment derivative comparison
% %
% % Z_w
% figure(1);
% H = plot(mu,-zw,'r*');grid on; hold on;
% legend('Current',4);
% title('Comparison of z_w derivative for the Hirobo Shuttle Z');
% xlabel('\mu');
% ylabel('-z_w');
%
% % Z_u
% figure(2);
% H = plot(mu,-zu,'r*');grid on; hold on;
% legend('Current',1);
% title('Comparison of z_u derivative for the Hirobo Shuttle Z');
% xlabel('\mu');
% ylabel('-z_u');
%
% % X_w

```



```

% figure(3);
% H = plot(mu,xw,'r*');grid on; hold on;
% legend('Current',2);
% title('Comparison of x_w derivative for the Hirobo Shuttle Z');
% xlabel('\mu');
% ylabel('x_w');
%
% % X_u
% figure(4);
% H = plot(mu,-xu,'r*');grid on; hold on;
% legend('Current',2);
% title('Comparison of x_u derivative for the Hirobo Shuttle Z');
% xlabel('\mu');
% ylabel('-x_u');

% % m_w_p
% figure(5);
% H = plot(mu,m_w_p,'r*');grid on; hold on;
% legend('Current',2);
% title('Comparison of m_w^, derivative for the Hirobo Shuttle Z');
% xlabel('\mu');
% ylabel('m_w^,');
% %
% %m_q_p
% figure(6);
% H = plot(mu,m_q_p,'r*');grid on; hold on;
% legend('Current',2);
% title('Comparison of m_q^, derivative for the Hirobo Shuttle Z');
% xlabel('\mu');
% ylabel('m_q^,');
%
% %m_u_p
% figure(7);
% H = plot(mu,m_u_p,'r*');grid on; hold on;
% legend('Current',1);
% title('Comparison of m_u^, derivative for the Hirobo Shuttle Z');
% xlabel('\mu');
% ylabel('m_u^,');
%
% %
% %
% figure(8); grid on; hold on;
% plot(real(r1), imag(r1), 'm*');
% plot(real(r2), imag(r2), 'r*');
% plot(real(r3), imag(r3), 'b*');
% plot(real(r4), imag(r4), 'k*');
% ylabel('Imaginary');
% xlabel('Real');
% title('Root loci of longitudinal mode of motion of the Hirobo Shuttle Z');
%
% %

```

```

% % y_v
% figure(9); grid on; hold on;
% H = plot(mu,yv,'r*');
% xlabel('\mu');
% ylabel('y_v');
% title('y_v derivative of the Hirobo Shuttle Z');
% legend('Current',1);
%
%
% % lv_p
% figure(10); grid on; hold on;
% H = plot(mu,lv_p,'r*');
% xlabel('\mu');
% ylabel('l_v^,');
% title('l_v^, derivative of the Hirobo Shuttle Z');
% legend('Current',1);
%
%
% % lr_p & np_p
% figure(11); grid on; hold on;
% H = plot(mu,lr_p,'r*');
% xlabel('\mu');
% ylabel('l_r^, and n_p^,');
% title('l_r^, and n_p^, derivatives of the Hirobo Shuttle Z');
% legend('Current',4);
%
%
% % nv_p
% figure(12); grid on; hold on;
% H = plot(mu,nv_p,'r*');
% xlabel('\mu');
% ylabel('n_v^,');
% title('n_v^, derivative of the Hirobo Shuttle Z');
% legend('Current',4);
%
%
% %nr_p
% figure(13); grid on; hold on;
% H = plot(mu,nr_p,'r*');
% xlabel('\mu');
% ylabel('n_r^,');
% title('n_r^, derivative of the Hirobo Shuttle Z');
% legend('Current',4);
%
% % lp_p
% figure(14); grid on; hold on;
% H = plot(mu,lp_p,'r*');
% xlabel('\mu');
% ylabel('l_p^,');
% title('l_p^, derivative of the Hirobo Shuttle Z');

```



```

% legend('Current',4);
%
% %
% figure(15); grid on; hold on;
% plot(real(lr1), imag(lr1), 'm*');
% plot(real(lr2), imag(lr2), 'r*');
% plot(real(lr3), imag(lr3), 'b*');
% plot(real(lr4), imag(lr4), 'k*');
% ylabel('Imaginary');
% xlabel('Real');
% title('Root locus of Lateral mode of motion of the Hirobo Shuttle Z');
% % title('Dutch Roll Mode of Hirobo Shuttle Z');
% % title('"Spiral root" of Hirobo Shuttle Z');
% % title('Larger rolling roots of Hirobo Shuttle Z');
%
%
% % approximate dutch roll oscillation
% figure(16); grid on; hold on;
% H = plot(mu,T_dutch,'r-*');
% xlabel('\mu');
% ylabel('time (s)');
% title('Approximate period of "Dutch Roll" oscillation of the Hirobo Shuttle Z');

% figure(17); hold on;
% H = plot(mu,xb1,'b-',mu,-mb1_p,'r--');
% grid on;
% title('Control derivatives for Hirobo Shuttle Z due to cyclic pitch');
% xlabel('\mu');
% legend('x_B_1','-m_B_1',0);
%
% figure(18); hold on;
% H = plot(mu,zb1,'r-');
% grid on;
% title('Control derivatives for Hirobo Shuttle Z due to cyclic pitch');
% xlabel('\mu');
% legend('z_B_1',0);
%
% figure(19); hold on;
% H = plot(mu,xt0,'b-',mu,mt0_p,'r--');
% grid on;
% title('Control derivatives for Hirobo Shuttle Z due to collective pitch');
% xlabel('\mu');
% legend('x_\theta_0','m_\theta_0',0);
%
% figure(20); hold on;
% H = plot(mu,-zt0,'r--');
% grid on;
% title('Control derivatives for Hirobo Shuttle Z due to collective pitch');
% xlabel('\mu');

```

```
% legend('-z_\theta_0',0);  
%  
% figure(21); hold on; grid on;  
% H = plot(mu, n_init,'r-');  
% title('Initial response for Hirobo Shuttle Z in vertical gust of v_G = 10.5 m/s');  
% xlabel('\mu');  
% ylabel('Normal Acceleration (g)');
```

```
warning on  
disp('END');
```



## APPENDIX B – Derivation of the $\frac{\partial a_1}{\partial \mu}$ Derivative

Bramwell (1976) defines as his equation (5.39)

$$a_1 = \frac{2\mu \left( \frac{4}{3}\theta_0 + \lambda \right)}{1 - \mu^2/2} \quad (\text{D.1})$$

Calculating

$$\frac{\partial}{\partial \mu} \left[ 2\mu \left( \frac{4}{3}\theta_0 + \lambda \right) \right] = 2\mu \left( \frac{\partial \lambda}{\partial \mu} \right) + 2 \left( \frac{4}{3}\theta_0 + \lambda \right) \quad (\text{D.2})$$

and

$$\frac{\partial}{\partial \mu} (1 - \mu^2/2) = -\mu \quad (\text{D.3})$$

beforehand is useful in determining

$$\frac{\partial a_1}{\partial \mu} = \frac{\left[ 2\mu \left( \frac{\partial \lambda}{\partial \mu} \right) + 2 \left( \frac{4}{3}\theta_0 + \lambda \right) \right] (1 - \mu^2/2) + \mu \cdot 2\mu \left( \frac{4}{3}\theta_0 + \lambda \right)}{(1 - \mu^2/2)^2} \quad (\text{D.4})$$

$$= \frac{2\mu \left( \frac{\partial \lambda}{\partial \mu} \right) + 2 \left( \frac{4}{3}\theta_0 + \lambda \right)}{(1 - \mu^2/2)} + \frac{\mu \cdot 2\mu \left( \frac{4}{3}\theta_0 + \lambda \right)}{(1 - \mu^2/2)^2} \quad (\text{D.5})$$

$$= \frac{2\mu \frac{\partial \lambda}{\partial \mu}}{(1 - \mu^2/2)} + \frac{a_1}{\mu} + \frac{\mu a_1}{(1 - \mu^2/2)} \quad (\text{D.6})$$

**APPENDIX C.1  
HELICOPTER SPECIFICATIONS: AH1-G Huey Cobra**

Engine Type	unspecified
Main Rotor Diameter	13.4112 m (R = 6.7056m)
Main Rotor Speed	319 RPM
Main Rotor Chord	685.8 mm
Number of Main Rotor Blades	2
Main Rotor Blade Mass	124.99 kg
Main Rotor Blade 2D lift curve slope	6.28
Main Rotor Blade Drag Coefficient	0.0110
Main Rotor Blade Hinge Offset	none – teetering rotor
Tail Rotor Diameter	1.2954 m
Gearing ratio	5.125 : 1
Tail Rotor Chord	213.7 mm
Number of Tail Rotor Blades	2
Tail Rotor Blade Weight	3.325 kg
All Up Mass	3628.74 kg
Horizontal Stabilizer Area	1.3657 m <sup>2</sup>
Distance to Horizontal Stabilizer	5.1562 m
Vertical Stabilizer Area	1.728 m <sup>2</sup>
Distance to Vertical Stabilizer	7.7597 m
Distance to Main Rotor Hub	0.114 m (rearwards)
Height to Main Rotor Hub	2.026 m
Distance to Tail Rotor Hub	8.260 m
Height to Tail Rotor Hub	1.150 m
Frontal Area (equivalent flat plate)	unspecified – estimated at 0.9144 m <sup>2</sup>
Fuselage Length	unspecified
Side Area (equivalent flat plate)	14.5022 m <sup>2</sup> (0.37m x 0.19m)

Note: all distances and heights are referenced to the helicopter centre of gravity position.



**APPENDIX C.2**  
**HELICOPTER SPECIFICATIONS: Bramwell Test Helicopter**

Engine Type	unspecified
Main Rotor Diameter	16 m (R = 8m)
Main Rotor Speed	248 RPM (26 rad / s)
Main Rotor Chord	314 mm
Number of Main Rotor Blades	4
Main Rotor Blade Mass	74.7 kg
Main Rotor Blade 2D lift curve slope	5.7
Main Rotor Blade Drag Coefficient	0.013
Main Rotor Blade Hinge Offset	4%
Tail Rotor Diameter	1.4 m
Gearing ratio	5.714:1
Tail Rotor Chord	220 mm
Number of Tail Rotor Blades	2
Tail Rotor Blade Weight	unspecified
All Up Weight	45000 N
Horizontal Stabilizer Area	0.8378 m <sup>2</sup>
Distance to Horizontal Stabilizer	9.6 m
Vertical Stabilizer Area	unspecified
Distance to Vertical Stabilizer	unspecified
Distance to Main Rotor Hub	0 m (rearwards)
Height to Main Rotor Hub	2 m
Distance to Tail Rotor Hub	11 m
Height to Tail Rotor Hub	1.6 m
Frontal Area (equivalent flat plate)	2.3 m <sup>2</sup>
Fuselage Length	unspecified
Side Area (equivalent flat plate)	11.74 m <sup>2</sup> (0.37m x 0.19m)

Note: all distances and heights are referenced to the helicopter centre of gravity position.

**APPENDIX C.3**  
**HELICOPTER SPECIFICATIONS: Hirobo Shuttle Z**

Engine Type	Methanol
Main Rotor Diameter	1.236 m (R = 0.618m)
Main Rotor Idling Speed	1500 RPM
Main Rotor Chord	44 mm
Number of Main Rotor Blades	2
Main Rotor Blade Mass	70 g
Main Rotor Blade 2D lift curve slope	5.7
Main Rotor Blade Drag Coefficient	0.011
Main Rotor Blade Hinge Offset	0.068m
Tail Rotor Diameter	220 mm
Gearing ratio	5.6 : 1
Tail Rotor Chord	22 mm
Number of Tail Rotor Blades	2
Tail Rotor Blade Weight	8 g
All Up Weight	3.25 kg (includes 250g fuel)
Horizontal Stabilizer Area	0.012 m <sup>2</sup>
Distance to Horizontal Stabilizer	0.4 m
Vertical Stabilizer Area	0.01435 m <sup>2</sup>
Distance to Vertical Stabilizer	0.65 m
Distance to Main Rotor Hub	0.035 m (rearwards)
Height to Main Rotor Hub	0.255 m
Distance to Tail Rotor Hub	0.715 m
Height to Tail Rotor Hub	0.08 m
Frontal Area (equivalent flat plate)	0.0171 m <sup>2</sup> (0.09m x 0.19m)
Fuselage Length	0.370 m
Side Area (equivalent flat plate)	0.0703 m <sup>2</sup> (0.37m x 0.19m)

Note: all distances and heights are referenced to the helicopter centre of gravity position.



**APPENDIX C.4**  
**HELICOPTER SPECIFICATIONS: JR Voyager E**

Engine Type	Electric
Main Rotor Diameter	970 mm
Main Rotor Idling Speed	1600 RPM
Main Rotor Chord	43 mm
Number of Main Rotor Blades	2
Main Rotor Blade Mass	45-50 g
Main Rotor Blade 2D lift curve slope	5.7
Main Rotor Blade Drag Coefficient	0.011
Main Rotor Blade Hinge Offset	55 mm
Tail Rotor Diameter	175 mm
Gearing ratio	23.33:5 => 4.67
Tail Rotor Chord	23 mm
Number of Tail Rotor Blades	2
Tail Rotor Blade Weight	5g
All Up Mass	2.0 kg
Horizontal Stabilizer Area	0
Distance to Horizontal Stabilizer	520 mm
Vertical Stabilizer Area	0.00001
Distance to Vertical Stabilizer	
Distance to Main Rotor Hub	-30 mm
Height to Main Rotor Hub	190 mm
Distance to Tail Rotor Hub	520 mm
Height to Tail Rotor Hub	10 mm
Frontal Area (equivalent flat plate)	170x70 mm <sup>2</sup>
Fuselage Length	300 mm
Side Area (equivalent flat plate)	230x170 mm <sup>2</sup>

Note: all distances and heights are referenced to the helicopter centre of gravity position.

## APPENDIX D – EXAMPLE OF A FULL DYNAMIC MODEL

This appendix contains the equations to describe a fully dimensionalised and non-time scaled dynamic model of a helicopter. The helicopter in this case is the Hirobo Shuttle Z and the non-dimensional speed is  $\mu = 0.105$ . The following table contains the non-dimensional and time-scaled stability and control derivatives as contained in Tables 7.1, 7.2 and 7.7.

**Table D.1 – Non-Dimensional and Time Scaled Derivatives**

LONGITUDINAL DERIVATIVES							
zw	zu	xw	xu	xq	mw'	mq'	mu'
-1.08	-0.09	0.0242	-0.0096	0.1336	-0.0819	-0.4139	0.0335

LATERAL DERIVATIVES					
yv	lv'	lr' & nr'	nv'	nr'	lp'
-0.1481	-0.0387	0.0215	0.11	-0.1262	-0.3587

CONTROL DERIVATIVES						
x <sub>B1</sub>	m <sub>b1</sub> '	z <sub>B1</sub>	X <sub>Theta0</sub>	m <sub>Theta0</sub> '	Z <sub>Theta0</sub>	n <sub>init</sub>
0.0554	-0.1151	0.1134	0.0098	-0.0519	-0.7418	1.4228

Equation (6.25) was derived from the full set of equations of longitudinal motion. These equations are (Bramwell 1976)

$$\begin{aligned}
 (W/g)\dot{u} - X_u u - X_w w - X_q q + W\theta \cos \tau &= X_{B_1} B_1 + X_{\theta_0} \theta_0 \\
 -Z_u u + (W/g)\dot{w} - Z_w w - Z_q q - (W/g)v\dot{\theta} + W\theta \sin \tau &= Z_{B_1} B_1 + Z_{\theta_0} \theta_0 \quad (D.1) \\
 -M_u u - M_w w - M_{\dot{w}} \dot{w} + I_{yy} \ddot{\theta} - M_q q &= M_{B_1} B_1 + M_{v_0} \theta_0
 \end{aligned}$$

In this equation, stability and control derivatives are indicated by capital letters with subscripts. The capital letter indicates the aerodynamic force or moment and the subscript



indicates the origin of this particular force or moment. The aerodynamic force in the longitudinal direction due to velocity in the longitudinal direction is indicated by the symbol  $X_u$ . These derivatives are then non-dimensionalised by dividing them with a certain function of the helicopter parameters as in

$$x_u = X_u / (\rho s A \Omega R^2 / M) \quad (D.2)$$

The value of  $X_u$  can thus be determined from equation (D.2) and Table D.1 by calculating (refer to Appendix C.3):

$$\begin{aligned} X_u &= -0.0096 \times (1.215 \times 0.04533 \times 1.19985 \times 157.078 \times 0.618 / 3.25) \\ &= -0.0189 \end{aligned} \quad (D.3)$$

The non-dimensionalization of the force and moment derivatives is illustrated in Bramwell (1976) on page 192. It must be remembered that Bramwell (1976) defines the non-dimensional force coefficients as being normalised by the mass of the helicopter (the moment coefficients are normalized by the appropriate inertia). This is not explicitly stated in the text, but can be found by performing the required calculations. The same steps as in equations (D.2) and (D.3) were followed to construct Table D.2.

**Table D.2 – Dimensional and Real Time Force and Moment Coefficients**

LONGITUDINAL DERIVATIVES							
Zw	Zu	Xw	Xu	Xq	Mw	Mq	Mu
-2.1316	-0.1777	0.0479	-0.0189	0.163	-2.3785	-7.4257	0.9739

LATERAL DERIVATIVES						
Yv	Lv	Lr	Np	Nv	Nr	Lp
-0.2924	-3.7466	1.2849	0.3855	3.1923	-2.2642	-21.4506

CONTROL DERIVATIVES					
X_B1	M_B1	Z_B1	X_thet0	M_thet0	Z_thet0
10.6088	-324.448	21.7271	1.8831	-146.383	-142.128

The full dynamic model of the Hirobo Shuttle Z at a non-dimensional speed of 0.105 (10.2 m/s or 36.7 kph) can now be written as:

$$\begin{aligned}
 3.25\dot{u} + 0.0189u - 0.0479w - 0.163q + 31.88\theta \cos \tau &= 10.6088B_1 - 142.128\theta_0 \\
 0.1777u + 3.25\dot{w} + 2.1316w - 3.25v\dot{\theta} + 31.8825\theta \sin \tau &= 27.7271B_1 - 142.128\theta_0 \\
 -0.9739u + 2.3785w + 0.136538\ddot{\theta} + 7.4257q &= -324.448B_1 - 146.383\theta_0
 \end{aligned}$$

The fully dimensional and non-time scaled equations of lateral motion were given by Bramwell (1976) as:

$$\begin{aligned}
 (W/g)\dot{v} - Y_v v - Y_p p + (W/g)Vr - Y_r r - W\phi \cos \tau - W\psi \sin \tau &= Y_{A_1} A_1 + Y_{\theta_t} \theta_t \\
 -L_v v + I_{xx} \dot{p} - L_p p - I_{xz} \dot{r} - L_r r &= L_{A_1} A_1 + L_{\theta_t} \theta_t \\
 -N_v v - I_{xz} \dot{p} - N_p p + I_{zz} \dot{r} - N_r r &= N_{A_1} A_1 + N_{\theta_t} \theta_t
 \end{aligned} \tag{D.4}$$

It is pointed out that this thesis only accounted for stick-fixed control in the lateral direction. All the lateral control variables are thus set to zero. Some of the insignificant stability derivatives (those that were found to be very small) were also left out of the model. This results in the following dynamic model:

$$\begin{aligned}
 3.25\dot{v} - 0.2924v + 3.25Vr - 31.8825\phi \cos \tau - 31.8825\psi \sin \tau &= 0 \\
 3.7466v + I_{xx} \dot{p} + 21.4506p - I_{xz} \dot{r} - 1.2849r &= 0 \\
 -3.1923v - I_{xz} \dot{p} - 0.3855p + I_{zz} \dot{r} + 2.2642r &= 0
 \end{aligned} \tag{D.5}$$

Equations (D.4) and (D.5) represent a dynamic model of the hirobo Shuttle Z at a speed of 36.7 k/hour. These equations can now be used in a program like “Matlab Simulink” in order to simulate the physical reaction of the helicopter.